EXPERIMENTAL TESTING OF BIMETALLIC AND REACTIVE SHAPED CHARGE LINERS

BY

JEFFREY SCOTT MASON

THESIS

Submitted in partial fulfillment of the requirements
for the degree of Master of Science in Mechanical Engineering
in the Graduate College of the
University of Illinois at Urbana-Champaign, 2010

Urbana, Illinois

Adviser:

Professor Nick Glumac

ABSTRACT

A series of 13 shaped charge tests was conducted. The primary objectives were to investigate small scale bimetallic and reactive liners and to record the target deformation characteristics of larger scale reactive liners. Tests 1 - 9 used liners of 20.02 mm diameter and were conducted in either a containment tube that housed an array of target plates or in a large blast tank without target plates. The liners in tests 1 - 9 were either solid copper, solid aluminum, or a bimetallic design consisting of a copper cone with an aluminum insert. The bimetallic liners showed some light emission that indicated hydroreaction, but their depth of penetration was 56% less than the solid copper liners. Peak pressures for each liner were measured in the containment tube at various depths. Peak pressures were also measured in the blast tank at 203 mm and 368 mm below the base of the liner. The peak pressures of the solid copper liners and the composite liners were not significantly different.

Tests 10 - 13 used larger scale, 50.75 mm liners and were fired into large tanks. Test 10 fired a copper liner into water, tests 11 and 12 fired an aluminum liner into water with a target plate array, and test 13 fired an aluminum liner into a non-reactive oil with a target plate array. Tests 11 and 12 showed large plate deformations in the unpenetrated target plates, while test 13 showed very little plate deformation in unpenetrated plates. For example, the maximum deformation of the first unpenetrated plate in test 12 was 10.6 mm below its original position. The maximum deformation of the first unpenetrated plate in test 13 was 0.42 mm below its original position. An optical system was used to determine the jet tip velocity of tests 11 - 13. Jet tip velocity varied by 14.0% across the three tests.

In loving memory of my mom

ACKNOWLEDGMENTS

I would like to thank Prof. Nick Glumac and Prof. Herman Krier for guiding this project and assisting with the shaped charge tests. Thanks to both of you for making my graduate experience a true education.

I would also like to give a heartfelt thanks to my research group, including John Rudolphi, Lance Kingston, Patrick Lynch, Drew Coverdill, Jennifer Peuker, David Chonowski, and Bradley Horn. It has been a pleasure working with you and developing friendships with you outside of work. Best wishes to you all!

Special thanks need to be given to John Rudolphi and Lance Kingston for assisting with many shaped charge tests. If you both had not helped me subdue and clean up the remains of the oil test, my hopes of graduating on time would have been lost.

I cannot express my gratitude to my family (Jim, Phillip, and Anna Mason) deeply enough. You have all played a monumental role in shaping my life. For that, I am eternally grateful.

Finally, I'd like to thank Jesus Christ for providing life itself and the reason to do something worthwhile with that life.

This project was supported by the Office of Naval Research under contract numbers N00014-01-1-0899, N00014-03-1-0788, and N0001408-01-0072. The program managers are Dr. Judah Goldwasser and Mr. Daniel Tam.

TABLE OF CONTENTS

LIST OF FIGURES

LIST OF TABLES

CHAPTER 1

INTRODUCTION

1.1 Brief History and Application of Shaped Charges

The concept of a shaped charge, or an explosive fill with a shaped cavity, lined or unlined, in one end of the explosive and the detonation source in the opposite end, is a concept that has origins as early as the late 1700's. The modern use of the term "shaped charge" most often refers to a charge with a cavity lined with some material. The idea that, by removing some portion of the explosive charge, the damage in a target could be increased is generally attributed to Charles E. Munroe in 1888. A very nice summary of shaped charge development is given by Walters [4]. For a more complete history of the discovery and development of shaped charges, the reader is referred to Kennedy [5]. Their work will not be reproduced here, but it is noted that shaped charge research dramatically increased just before and during WWII because of its potential for military applications. Walters attributes the discovery of modern lined shaped charges to Henry Hans Mohaupt and Franz Rudolf Thomanek, who independently developed the first effective lined shaped charge penetrators in the late 1930s [4].

Lined shaped charges are used most extensively for perforation of geological formations in the oil industry. They are also used for military applications and for demolition (both military and industrial). The current research is conducted with military applications in mind.

1.2 Shaped Charge Geometry and Nomenclature

A typical lined shaped charge of cylindrical geometry is shown with a target in Figure 1.1. Subsequently, a reference to the term "shaped charge" should be meant as referring to a lined shaped charge assembly as shown in Figure 1.1.

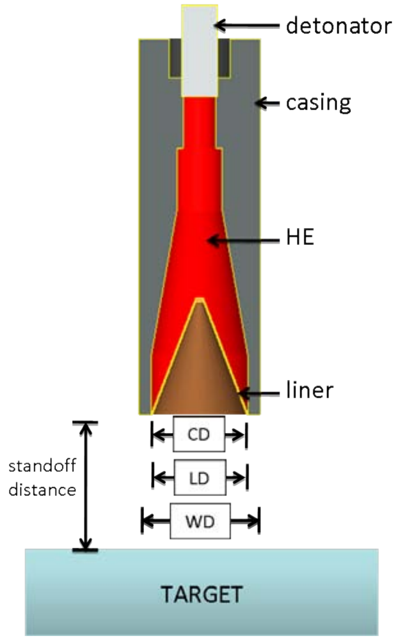

Figure 1.1: Components and nomenclature of a shaped charge assembly (cross sectional view)

As shown in Figure 1.1, the basic shaped charge consists of four elements: a high explosive, a detonator, a liner and a casing. The high explosive (HE) provides the main energy of the charge and must be initiated by a detonator (or sometimes a detonator and a booster). The liner can be made of a variety of materials and is shown as a cone for this cylindrical shaped charge. If the shaped charge were linear or circular, the liner could be wedge shaped or semi-circular. Even in the context of cylindrical charges, which are of greatest interest in the current study, the liner geometry can vary greatly, and although conical liners are very common, trumpet shaped, hemispherical, and multi-angle conical liners are also used. The casing provides containment for the other components. The overall diameter of the charge is referred to as the warhead diameter (WD). The diameter of the

HE is referred to as the charge diameter (CD) and the diameter of the liner is the liner diameter (LD). As depicted in Figure 1.1, the "top" of the charge will refer in this report to the end of the charge where detonation is initiated with the detonator, and the "bottom" of the charge will be the opposite end, containing the liner. The distance from the base of the liner to the target is known as the standoff distance.

Figure 1.2 shows only the conical liner from a cylindrical shaped charge. As noted in the figure, the included angle of the cone is called the apex angle. This angle, in addition to the liner thickness and liner material, is critical to the behavior of the shaped charge.

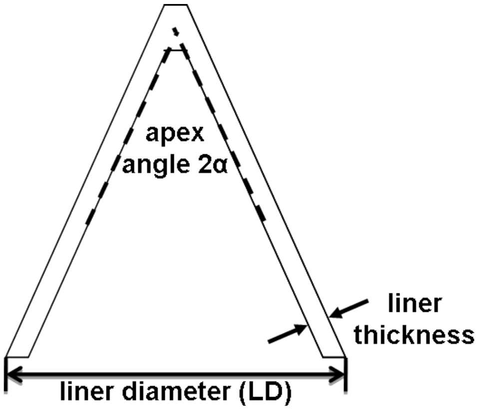

Figure 1.2: Basic liner geometry

1.3 Behavior of the Shaped Charge after Detonation

Though varying geometries will be discussed in subsequent sections of this report, the basic conical charge suffices nicely to demonstrate the general behavior of a shaped charge during its use. Fundamental work on the topic of shaped charge behavior was completed by Pugh, Eichelberger, and Rostoker [6] and Birkhoff et al. [7]. Figure 1.3 shows the collapse and formation stages of the shaped charge.

After initiation, a detonation wave passes through the HE from top to bottom at very high speeds, with the actual speed being dependent on the type of HE used in the charge. Typical speeds may be approximately 8 km/s [4] but can decrease to 6.2 km/s

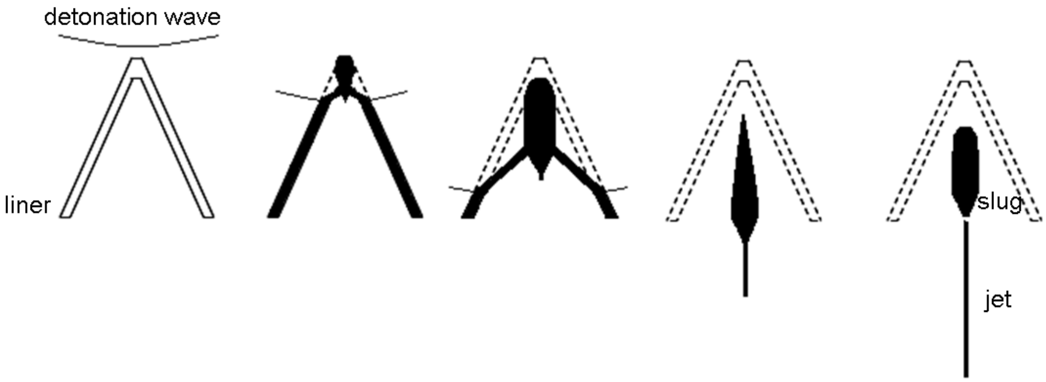

Figure 1.3: Liner collapse and formation of jet and slug

for less energetic high explosives such as sensitized nitromethane [8]. When the detonation wave impacts the apex of the liner, the liner is deformed and begins to collapse towards the central axis of the charge. Strain rates of the liner material can be as high as 10^4 - 10^7/s, and pressures can reach as high as 200 GPa during the collapse. Because of the very large strain rates of the liner material, the liner collapses in the hydrodynamic regime, behaving as an inviscid, incompressible fluid [6, 7, 4]. It is important to note, however, that the liner is still a solid, as no evidence for melting is seen in the microstructure of the liner post-detonation [9]. When the liner material reaches the central axis of the charge, it collides with itself and forces a portion of the liner material out the bottom of the charge as a long, thin, very high speed jet. The tip of the jet can travel faster than the detonation wave, with speeds higher than 10 km/s being achievable [10]. Because portions of the liner closer to the apex have a smaller collapse angle than those portions near the base, there is a velocity gradient in the outflowing jet. The tip of the jet has the highest velocity, and the velocity decreases to the rear of the jet. This velocity gradient is often assumed linear and creates a stretching jet whose diameter will decrease and which will ultimately fragment [11]. The time from the initiation of the charge to the fragmentation of the jet is referred to as the breakup time, t_b. Interestingly, Carleone has shown that the upper 40% of the height of the cone contributes significantly to a massive tip particle rather than to the stretching jet [12]. The liner material that does not enter into the jet forms a slower, more massive portion called the slug. The slug moves on the order of one tenth the speed of the jet, although speeds of both the jet and the slug are very dependent on the geometry of the liner.

This jet is able to penetrate a target due to the high pressures created between the jet tip and the target. During the penetration event into a metal plate, peak pressures can reach as high as 100-200 GPa, average temperatures are 20-50% of the target melt temperature, and strains in the target of 0.1 - 0.5 are common [4]. Therefore, it is clear that the jet does not melt the target or burn through the target, but rather displaces the target material as the mechanism of penetration.

1.4 Basic Liner and Charge Design

It should be noted here that there are many parameters of the liner and charge that can be varied by a shaped charge designer to achieve the desired properties of the jet and slug. With regard to the liner design only, parameters that are often varied are the liner material, liner thickness, and apex angle. As previously mentioned, the liner could also be manufactured to have multiple angles, or could be a trumpet-like shape, or could even be fluted to produce liner spin. The charge parameters that are varied are the standoff distance, type of HE, method of detonation (whether point or plane detonation), use of a wave shaper inside the charge, material of confinement, thickness of confinement, and use of boattailing to decrease the amount of HE used [4]. In all situations where the desired result includes penetration of a target, it is necessary that the shaped charge produce a well formed jet as depicted in Figure 1.3 rather than a discontinuous, fragmented jet or no jet at all. A continuous stretching jet results in the greatest penetration. It is certainly not within the scope of this report to discuss the influence of all parameters upon the performance of the liner, partly because absolute maximum penetration is not the goal of the current study. If it were, a variable angle, variable thickness charge (VAVT) would have been chosen, as VAVT charges have been known to increase penetration tens of percent over standard chargers [13].

However, the parameters of greatest importance to the current goal will be discussed here, and further mentions of parameters in shaped charge design will be discussed as required for full understanding of the current objectives.

1.4.1 Liner thickness

Walters states that typical liner thicknesses range from 1 to 4% of the CD and that thin liners can typically be accelerated to higher speeds than can thick liners simply due to the effect of decreasing the ratio of liner mass to explosive energy [4]. Chanteret completed a study in which the thickness of a 45 mm diameter 60° copper liner was varied from 0.2 mm to 3.0 mm (or from 0.44 to 6.6% of the CD) [14]. His results indicated a minimum wall thickness of about 0.25 mm that seemed to be independent of charge diameter (but may vary based on apex angle). Below this limit, no compact jet was formed. For a thickness of 0.4 mm, the jet tip velocity was 7.7 km/s, and as the liner thickness increased to 3.0 mm, the jet tip velocity decreased to 4.2 km/s. Although tapering of the liner thickness can be used to change the division of jet and slug material, tapered liners will not be considered in this report.

1.4.2 Liner material

It is well known that the liner material plays a large role in the performance of the shaped charge. Again, Walters gives a concise summary of appropriate liner material characteristics [4]. He states that materials having a high melting temperature, high density, high bulk speed of sound, and high dynamic strength are most likely to result in good penetration due to a well formed jet. For any material that is chosen, fine grain structure, proper grain orientation, and good elongation are important. In addition, practical considerations generally restrict the use of expensive or toxic materials.

Although there has been significant discussion regarding jet coherence criteria, it is well-known that if all other factors are equal, an increase in the sound speed of the liner material will result in an increase in the maximum velocity of a coherent jet [2]. This sound speed is to be taken as the bulk speed of sound in the material rather than the longitudinal or transverse shear speed of sound. However, the appropriate speed of sound is not well-known under conditions of high pressures and temperatures [4].

1.4.3 Apex angle

The apex angle of a liner influences the collapse behavior and therefore many characteristics of the resulting jet. In general, a smaller apex angle results in a faster jet tip velocity as well as a lower jet mass [4]. A larger apex angle slows the jet tip but adds more mass to the jet. As the apex angle continues to increase, eventually the liners have a shape that behaves much like a hemisphere or dish, which are typically associated with explosively formed penetrators (EFPs, also called self-forging fragments) rather than shaped charges. EFPs operate on similar principles as shaped charges but are in a separate category because instead of forming a distinct jet and slug, an EFP results in a massive slug only. They do not penetrate as well as shaped charges because of the lack of a high speed jet (EFP slugs typically travel about 2-3 km/s), but their massive slug carries a very large amount of momentum and they are generally consistent over long standoff ranges due to their higher stability in air travel. The most common apex angles for shaped charges are between 40° and 60°. 42° apex angles are used by the Ballistics Research Laboratory for their standard charges, and this angle is emulated elsewhere quite often.

1.4.4 Precision required

To ensure round-to-round consistency of shaped charges, a high level of precision must be maintained in the fabrication of the individual components and their assembly. The Ballistics Research Laboratory's precision shaped charge, with a diameter of 81 mm (3.189

in.), maintains tolerances of +/- 0.0051 mm (0.0002 in.) for wall thickness variation on a transverse plane and +/- 0.051 mm (0.002 in.) for a longitudinal plane parallel to the liner axis [15]. For non-precision charges of the same diameter, the transverse and longitudinal thickness variations are relaxed slightly to +/- 0.051 mm (0.002 in.) and +/- .102 mm (0.004 in.) respectively [4]. It should be noted that tapered liners are often used to enhance shaped charge performance, so the requirements for longitudinal thickness are likely given to simply characterize a standard charge and should not be interpreted as affecting the straightness of the jet. Aseltine gives mathematical relations to show that asymmetries in the liner fabrication will result in components of jet velocity in the radial direction, and specifically notes that thickness variations in the top $\frac{1}{3}$ to $\frac{1}{2}$ of the cone result in the largest radial velocities. Therefore, special care should be taken when fabricating the top of the cone [15]. He also indicates that variations in the explosive fill that result in an asymmetrical impact of the shock wave upon the cone can be a large reason for poorly performing shaped charges. He states that a variation of less than 2% in explosive composition can affect the jet straightness more than a variation in liner thickness that encompasses the entire tolerance limit. This explosive variation could result from voids in the explosive fill, heterogeneous composition of the explosive, poor contact of the explosive on the liner, or eccentricities in the explosive in reference to the liner orientation [15]. Straightness of the jet is imperative for a high performing jet. Leidel also stresses the importance of concentricity of the liner [16]. When introducing .0508 mm (0.002 in.) of eccentricity into a 63.5 mm (2.5 in.) diameter charge, the resultant penetration was less than 50% of a precision charge and could be noted by the off-axis jet penetration hole [16].

1.4.5 Standoff distance

It is well-known that as the standoff distance of a shaped charge increases, the penetration performance increases up to a peak at some optimal standoff, then begins to decrease. The reason for this variation in penetration is simply that if the standoff distance is too short, the jet will not have enough space to form and elongate properly before reaching the target. Penetration depth is highly dependent on jet length, so by increasing the standoff distance, the jet, which has a velocity gradient, is given more time to elongate. This effect increases the penetration depth. However, if the standoff distance is too great the jet has an increased propensity to particulate due to necking and stretching. If the jet has some radial component of the velocity, a larger standoff distance will make this flaw more apparent, causing the jet to veer off axis and further decrease the penetration. In addition, small jet fragments have an increased propensity to tumble in flight and thereby not impact the target with the same precision as a linear, continuous jet.

1.4.6 Charge design

Various aspects of the casing and explosive components of the charge should also be taken into account for a successful shaped charge design. The casing should be manufactured with sufficient precision to avoid eccentricity of the explosive during the process of filling the casing [16]. In addition, the charge diameter combined with the charge length give the amount of HE used and therefore the amount of energy available for the charge. The amount of energy release should be sized for individual applications. For a military application, the charge should be designed in such a way as to give sufficient energy to penetrate a target. For a laboratory test, it may be more important to insure that the charge does not have enough energy to inflict unwanted damage on the test facilities. Boattailing is a simple technique that can be used to minimize the amount of explosive for a given CD as seen in Figure 1.4. Walters recommends care in choosing the break point, the point at which the discontinuity in the casing wall occurs. Generally this point is just below the apex of the liner and thereby avoids rarefaction waves interfering with the liner collapse [4]. The distance between the apex of the cone and the initiation point is termed the head height and is the parameter of interest in the direction of the charge axis (rather than the overall charge length). Walters gives rules of thumb that a 1 CD head height will show slight improvements in jet velocity, penetration, and kinetic energy over a $\frac{5}{8}$ CD head height, but very little additional improvement is shown by increasing the head height to $\frac{3}{2}$ CD [4]. Understandably, this rule of thumb could be affected by casing design. Sufficient space should be given for the detonation wave to become approximately planar, rather than highly spherical. Leidel also experimentally showed that for a 63.5 mm (2.5 in.) liner diameter, a charge with a head height of 49.5 mm (1.95 in.) showed equivalent penetration performance to the same charge with a 33.5 mm (1.32 in.) head height [16]. Boattailing was not used in Leidel's experiments.

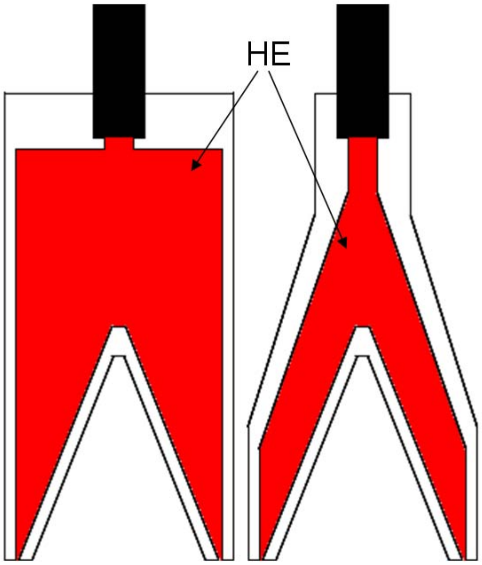

Figure 1.4: Use of boattailing to remove HE mass for a given charge diameter

The casing material and thickness can also be important in the performance of the shaped charge. A highly constrained charge will help apply pressure to the liner throughout its collapse process and thereby facilitate good jet formation. Walters refers to Evans who recommended a practical maximum wall thickness for the casing at of $\frac{1}{10}$ CD in steel. Further increases make the charge heavier, but not any more effective [17]. Thinner casing walls may release explosive energy too early and thus negatively affect the pressures experienced by the liner during liner collapse [4].

CHAPTER 2

OBJECTIVE OF CURRENT RESEARCH AND LITERATURE REVIEW

2.1 Objective of Current Research

Based upon the shaped charge design criteria explained above and previous work on reactive shaped charges completed here at the University of Illinois at Urbana-Champaign, it is postulated that a shaped charge could be designed for an underwater environment that results in a high level of penetration, but incorporates energetic materials to increase the energy output of the shaped charge. The primary objective of this research was to design and test a shaped charge liner, made of multiple materials and hereby referred to as a composite liner, that would increase damage to the target without increasing either the amount of explosive used or the mass of the liner and without sacrificing penetration capability versus a single material liner. A dense, ductile material that performs well as a penetrating liner should be incorporated into the liner design such that this material perforates the target to an acceptable depth. A material that is reactive with water (under the correct conditions) should be incorporated into the design of the liner such that this material, upon reaction, increases the total energy release of the liner versus a liner without a reactive material. A shaped charge that incorporates a reactive material in the liner is referred to as a reactive shaped charge. The energy released by the energetic material upon reaction should be delivered to the target in the form of increased damage to a target versus a single material liner. It was a second objective to measure the results of the composite charge tests and quantifiably demonstrate its performance versus a baseline, single material liner. It was a still further objective that the tests of composite liners should form a baseline for evaluation of subsequent composite liners that differ in geometric design, materials used, or method of fabrication and assembly. Finally, another objective of this research was to scale up the current shaped charge setup to incorporate larger liners. In this way, the damage production performance of larger scaled reactive shaped charges could be documented.

2.2 Previous Work

2.2.1 Reactive shaped charges

Dyna East Technologies

Over a period from 1998 to 2003, Dyna East Technologies (DET) performed a series of studies on reactive shaped charges. These charges were fired into water and resulted in bright illumination of the shaped charge jet tip when the liner consisted of aluminum or aluminum-titanium. The tests were instrumented with high speed video cameras, x-ray flash radiography, and pressure transducers. Their conclusions, as early as 1999, were that, when compared with a copper liner:

1. Penetration rate is not enhanced with a titanium-aluminum jet
2. Larger penetration cavities are produced by a titanium-aluminum jet
3. Faster cavity growth rates are achieved with a titanium-aluminum jet
4. Pressure and impulse in the water are enhanced with a titanium-aluminum jet

The above conclusions, quoted from DET [18], were expanded upon further in the test series. DET analyzed bubble size and cavity growth from various copper, aluminum, and titanium-aluminum shaped charge tests and remarked that a significant increase in gas cavity volume and duration of the gas bubble was seen for reactive jet materials. For the same materials, some increase in shock pressure, impulse, and energy was seen. These increases meant that there was an additional energy release from the jet/water reaction [19]. It should be noted that the titanium-aluminum liners were powder metallurgy compositions. DET also performed some cavity growth correlations using CTH code.

Felts

A significant amount of work in the field of shaped charges and energetic materials has been completed by the research group of Nick Glumac and Herman Krier at the University of Illinois at Urbana-Champaign (UIUC) of which the author is now a part. A review of relevant work completed within this group follows.

The earliest work on reactive shaped charges at UIUC was completed by Joshua Felts, who essentially duplicated the results of Dyna East Technologies' tests on a smaller scale. Felts obtained high speed video images of aluminum liners 12.2 mm in diameter that showed illumination when fired into water, but not into oil (spindle oil, with specific gravity .906 was used), suggesting that the high levels of oxygen available in water allowed a combustion event to occur. Felts also used spectroscopy to attempt to determine species present during the light emission event. He saw no signs of AlO, Al_2O, or AlO_2 [20]. Prof. Nick Glumac, who collaborated with Felts on the spectroscopic work, states that Felts' collection geometry precluded access to light from both AlO_2, which emits in the IR range, or Al_2O, which emits in the UV range. Both UV and IR were out of range for these tests. AlO would have been seen if it was present with a strong signal.

Felts also performed shaped charge experiments seeking to compare the dynamic pressures in the water tank of various liners by examining the resultant deformation of thin walled aluminum cans that were placed just beneath the incoming jet. Felts found that the thin walled aluminum cans were deformed significantly more by the aluminum lined charges than they were by the copper lined charges.

Finally, in order to approximate an aluminum-titanium liner, a titanium plate was placed just below the surface of the water. An aluminum liner was then fired into the water, impacting the plate, and was observed via high speed video and spectroscopy. The aluminum liner, when fired through the titanium plate, exhibited brighter light emission, and for a longer duration, than a copper liner fired through the titanium plate. Spectroscopic measurements were taken to determine the species present and some tests showed a resemblance to the absorption spectrum of TiO. Felts hypothesized that this resemblance could be due to TiO formation during the event, or, more likely, to TiO existing on the plate before the event occured.

Bill

Randall Bill fired shaped charges made from titanium, aluminum, tantalum-aluminum, hafnium, titanium-aluminum, tantalum-boron, and copper into water and recorded time resolved pressure data and spectroscopy, as well as high speed video images. He observed significant light emission from the interaction of the titanium-aluminum, aluminum, and hafnium liners with water. He also observed some light emission from the tantalum-boron and tantalum-aluminum liners' interaction with water. The solid copper liner exhibited only light emission attributable to the detonation event itself. Bill's spectroscopic results, in contrast to Felts', indicate clearly the presence of combustion intermediates from the reactive charges from early time spectra (approximately 30-50 μs after detonation for the aluminum liner). His spectra show peaks indicating AlO from aluminum combustion in the aluminum charge, HfO from hafnium combustion in the hafnium charge, and BO_2 for the tantalum-boron charge. Late time spectra (approximately 120 μs after detonation for the aluminum liner) showed continuum emission that lent itself to a blackbody temperature fit. These late time blackbody temperature fits for the aluminum charge showed temperatures of 2700 to 3100 K, which is consistent with aluminum combustion temperatures in H_2O reactions seen at higher ambient temperatures [21]. Bill recorded data for peak pressures and integrated impulse for these charges that demonstrated the ability of reactive shaped charges to deliver increased pressure impulses compared to non-reactive charges. Titanium-aluminum and tantalum-aluminum liners produced pressure impulses higher than aluminum, copper, hafnium, and tantalum-boron [22]. Of note here, in regards to Bill's thesis, is that the aluminum and some of the copper charges were the only charges in which nitromethane, sensitized with DETA, was used as the high explosive. For all other charges tested, PBXN-9 was used as the high explosive. Bill also used various methods including X-ray diffraction, $NaOH$ dissolution, and pycnometry to assist in calculating the amount of aluminum reacted. A relevant result of this work is that for an aluminum charge fired using nitromethane, 46% of the liner mass was said to react, as indicated by X-ray diffraction and the appearance of combustion products. An identical liner was fired into a solution of 27% H_2O_2 (a more oxygen rich environment) and showed 68% of the mass reacted to form Al_2O_3 [22]. It should be noted that Fant refined these mass percentages of reaction in a more detailed analysis (below).

Fant

Brian Fant added to reactive shaped charge research by firing aluminum liners into water, spindle oil, and 27% H_2O_2 solution. He completed penetration tests into each of these mediums with a series of steel plates spaced in the medium, as well as completing penetration tests into each medium without steel plates. The data he collected involved high speed video images, time resolved pressure measurements, and quantification of deformation and damage to the steel plate targets. He again utilized ex-situ X-ray diffraction, $NaOH$ dissolution, and pycnometry to determine the amount of Al_2O_3 that had presumably reacted from aluminum in the liner, indicating that aluminum combustion had occurred during the penetration event. A significant result of this was that approximately 16%, 35%, and 75% of the original mass of the aluminum liner reacted in spindle oil, water, and 27% H_2O_2 respectively. Fant's conclusion was then that 16% of the reaction must come from reaction of the liner with detonation products, an additional 19% from reaction with water, and a further 40% when water is replaced by 27% H_2O_2. Furthermore, deformation of steel plates was greatest in the

27% H_2O_2 solution, and least in the spindle oil. Fant referred to the sum of the maximum deformation value for each plate in a given test as the “total deformation.” The average total deformations of the spindle oil tests, water tests, and 27% H_2O_2 tests were 29.85 mm, 37.5 mm, and 54.18 mm respectively. Especially in unpenetrated plates, minimal deformation was seen in the spindle oil tests, more deformation was seen in the water tests, and much more deformation was seen in the 27% H_2O_2 tests. Maximum penetration of the liner was significantly reduced in 27% H_2O_2 (2.5 +/- .7 plates) when compared to water (4.5 +/- .7 plates) and oil (4 plates). The hypothesis for this effect is that a violent reaction of the 27% H_2O_2 may have halted the penetration of the aluminum jet. This reaction could result in decreased penetration but increased damage as the tests showed [23].

Rudolphi

John Rudolphi built upon the research of Fant, Bill, and Felts as he conducted shaped charge tests using aluminum alloys as the liner materials. A baseline aluminum liner (6061 aluminum) was compared to aluminum-lithium and aluminum-gallium liners. These liners were fired through a series of alternating steel plates and water-filled cavities contained in a steel tube. Rudolphi added the capability of this facility to measure time resolved pressure and light emission inside the cavities of the steel tube. In addition, he used silicone to attach copper foil on each of the first five plates and applied a voltage that changed when the jet perforated the foil and the steel plate, connecting the circuit. These simple gauges showed the time when the jet impacted each successive plate and could be used to draw conclusions about the penetration velocity of the jet. Using this experimental apparatus, Rudolphi demonstrated that by alloying the aluminum liner with lithium or gallium, approximately 25% more aluminum was caused to react with the water. In addition, both the aluminum-lithium and aluminum-gallium liners had a smaller average penetration depth when compared to the baseline aluminum liners. This result, as noted above from Fant, could indicate a more violent reaction from the alloyed liners. Seven of Rudolphi’s nine tests with reactive liners exhibited a greater deformation in the first unpenetrated plate than the last penetrated plate. Pressure results, however, were inconclusive [24].

Moore

At the Naval Postgraduate School, Joseph Moore carried out research that involved the simulation of long rod penetrator, made of aluminum, under a hypervelocity (approximately 4 km/s) impact into a water tank. He used AUTODYN$^{\text{TM}}$ software to investigate material erosion of the rod, cavity formation, and areas of high temperature and pressure that might lend themselves to hydroreaction. He also worked with the Ernst Mach Institute (EMI) to carry out experiments using a light gas gun to accelerate an aluminum rod to 3.25 km/s before impacting an expendable water tank. The speed range of 3-5 km/s was chosen because it best approximates the velocity of the tail of a modern high speed shaped charge jet. Moore was able to demonstrate that his simulations of erosion front, bow shock geometry, cavity formation, penetration depth, and penetration velocity had good qualitative and quantitative agreement with the experimental results from EMI (although the simulations slightly over predicted penetration depth and velocity). He showed that areas around the erosion front at the cavity-water interface encountered high pressures and temperatures that warranted further study of methods to incorporate reactive materials into shaped charge liners so that they might not hamper line of sight penetration performance, but could release additional chemical energy to the target. The experiments at EMI demonstrated some luminosity at the cavity-water interface that could indicate combustion of aluminum [25].

Craig

William Craig built upon the numerical and experimental studies completed by Moore. He utilized a 2-D simulation of a long rod penetrator fired into water at 3250 m/s, as in Moore's work. Craig's results allowed him to develop a mass flux relation for the revealing of virgin aluminum at the erosion front of this aluminum rod that might be useful for investigating or calculating potential reaction energy release. He also estimated (albeit loosely) that while partial vaporization of the water at the erosion interface was very likely, fusion of the aluminum was much less common. His estimates only predicted that the aluminum at this interface would reach 400° C. However, he noted that shaped charge jets, due to the high explosive required to initiate them and the high pressures reached during their formation, often reach these temperatures before they reach their target.

Craig also performed variations of Moore's tests with EMI, firing a long aluminum rod into a tank at approximately 3250 m/s using EMI's two-stage light gas gun. His first test fired the rod through an N_2 atmosphere before entering a tank filled with spindle oil, with density 80% that of water. No illumination was observed during the test, indicating that the illumination seen in Moore's test was the result of the water medium rather than the air in the atmosphere around the water tank or any other effects. The next phase of Craig's experiments involved firing the aluminum rod at an oblique steel target submerged first in water (reactive), then spindle oil (unreactive), then peroxide (most reactive). Unfortunately, during the test in water, the light gas gun was damaged and the tests in spindle oil and peroxide were not able to be completed. Craig proceeded in creating a 3D simulation of the event, again in AUTODYN$^{\text{TM}}$, to compare hole sizes of the experiment and the simulation. Since the simulation did not take into account reactivity of the rod with the water, the implication of similar hole sizes between the simulation and the experiment would imply that the reaction event in the experiment did not augment the hole size in the target. Craig's results showed that even after accounting for coarse zoning and possible differences in penetrator orientation, the hole diameter from the simulation and the hole diameter of the experiment agreed within 10%. He postulated that perhaps the reaction kinetic speed was not on the same order of the penetration event, and therefore did not augment damage production in the target [26].

Belnap

Paul Belnap conducted an experimental exploration of the energy release of reacting and non-reacting shaped charge events. He used a calorimeter tube to determine the chemical, kinetic, and thermal energy of aluminum liners fired into oil, water, and hydrogen peroxide and copper liners fired into oil and water. He measured total energy releases for the aluminum-oil case (7.9 kJ), for the copper-water case (8.8 kJ), for the aluminum-water case (16.9 kJ) and the aluminum-hydrogen peroxide case (35.5 kJ). He also performed numerical analysis of the kinetic energy and thermal energy release during these events, but asserts that only due to offsetting errors do the thermal energy release results from the simulation compare favorably to the experiments. Belnap concluded from his calorimetry experiments that approximately half of the liner can be assumed to react with the water or hydrogen peroxide [27].

Other researchers

The reader is referred to the following sources for further examples of reactive liners.

- Liu suggested that the reaction between molten aluminum and water could be used to do useful work. He suggested that this work could be done by using an aluminum shaped charge liner or a liner formed from powdered aluminum and a metal oxide. Liu, L. (2003). Use of aluminum in perforating and stimulating a subterranean formation and other engineering applications (102/301 ed.). Alberta/CA: F42B 3/00.

- Langan et al. used thermal spraying of reactive materials to form liners of low porosity. These reactive materials were intended to react with each other upon detonation. Langan, T., Riley, M. A., and Buchta, W. M. (2007). In Surface Treatment Technologies I. (Ed.), Reactive shaped charges and thermal spray methods of making same (102/306 ed.). MD/United States: F42B 1/032.

- An extension of the previous Langan et al. patent. Langan, T., Riley, M. A., and

Buchta, W. M. (2010). In Surface Treatment Technologies I. (Ed.), Reactive shaped charges comprising thermal sprayed reactive components (102/306 ed.) F42B 1/032.

2.2.2 Composite shaped charges

Experimental

Kolsky The first documented experimentation of a composite shaped charge was performed by Kolsky in an attempt to understand jet formation. He used 1.0 cm diameter bimetallic liners and fired them into polyethylene rods and water. These charges consisted of a 0.37 mm thick copper layer and 0.37 mm thick steel layer. When he fired these charges with the steel inside and the copper outside (copper layer in contact with the explosive), he found a fragment at the bottom of the penetration hole that was entirely steel. Another fragment, about $\frac{2}{3}$ of the way down the hole, was found to be steel on the outside and copper on the inside. Finally, the plug was shown to be copper on the outside with a steel core. When the liner material order was reversed (copper on the inside and steel on the outside), the composition of the fragments was correspondingly reversed as well. Kolsky makes no mention of his bonding method or assembly process [28].

Walters and Golaski Walters and Golaski published a report of experimentation and numerical simulation of a stratified copper and nickel liner. They used a diffusion bonding technique to attach the copper and nickel and, presumably, completed at least one final machining step after the bonding was finished. Walters remarks, "note that the jet collapses and forms as expected, probably due to the similar behavior of copper and nickel under shock loading conditions as well as the identical densities of copper and nickel." Three figures from Walters and Golaski, 1987, reproduced in Figures 2.1, 2.2, and 2.3 as well as in The Fundamentals of Shaped Charge Liners [4], are helpful in understanding the movement of the stratified materials during the jet formation process [1].

Figure 2.1: Stratified Ni/Cu liner formed by Walters and Golaski [1]

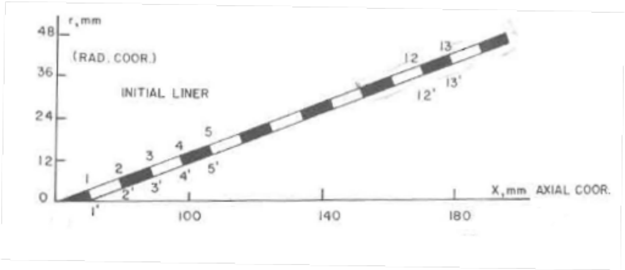

Figure 2.2: Initial conditions of HELP code simulation of stratified Ni/Cu liner, Walters and Golaski [1]

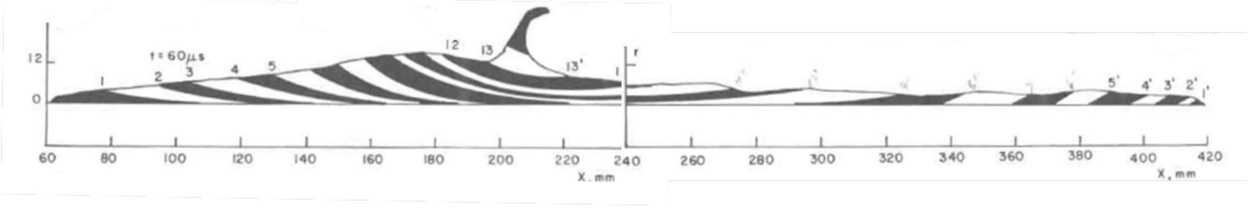

Figure 2.3: Final conditions of HELP code simulation of stratified Ni/Cu liner, Walters and Golaski [1]

Chanteret and Lichtenberger Chanteret and Lichtenberger completed testing of liners of two layers, the inner layer (here meaning the layer not in contact with the explosive) being made of a lower sound speed material, and the outer layer being made of a material with a higher sound speed. The intention of this test was to determine whether the classical subsonic coherence criteria could be bypassed for a material if another material with higher sound speed acted as a buffer to the high explosive. Chanteret referenced an experiment at ISL (French-German Research Institute of Saint-Louis) that successfully tested a Cu/Au liner where a 0.6 mm Cu layer was the buffer material for a 0.18 mm Au layer. This charge resulted in a jet with the same jet tip velocity (6.6 km/s) as a 1 mm copper liner. However, from the X-ray pictures that were taken of this jet, a disturbance can be seen when some copper begins to flow into the jet. Bimetallic liners were made in a second, similar configuration using a copper cone of varying thickness, from 0.45 mm to 1.4 mm and a buffer layer of constant thickness of either nickel (0.4 mm thickness) or aluminum (1.3mm thickness). These liners had 20° apex angles so they would produce very high speed jets, approximately 11.2 km/s at the jet tip. Again, the objective was that the high sound speed buffer material would allow the copper jet to remain coherent at higher speeds than a copper jet alone. Chanteret's results showed that the bimaterial jets were as divergent as jets formed by solid copper liners, despite the fact that liners made solely out of nickel remained coherent [29]. Finally, Chanteret completed a test with nickel and copper trumpet shaped liners in a top/bottom approach where nickel formed the top 55% of the liner (nearest the detonator end of the charger) and the copper formed the bottom 45% of the liner. Because of the identical densities of these materials, discontinuities in liner thickness are not required at the junction of the two materials. Chanteret supposed that a uniform thickness would decrease the chances of discontinuities or disturbances in the collapse and jet formation stage of the liner. However, upon testing the charge, X-ray evidence showed a separation between the nickel front part of the jet and the copper rear part of the jet as shown in Figure 2.4. He then used a laser welding technique to bond the two materials early in the liner manufacturing process (allowing finish machining of the already bonded materials). This liner resulted in a jet in which the material junction was hardly noticeable in the X-ray evidence before jet breakup 2.5. This laser welded composite liner compared favorably against a similar solid nickel liner in that the composite had the same jet tip velocity but the rear of the jet was seen to be more ductile because of the copper [2].

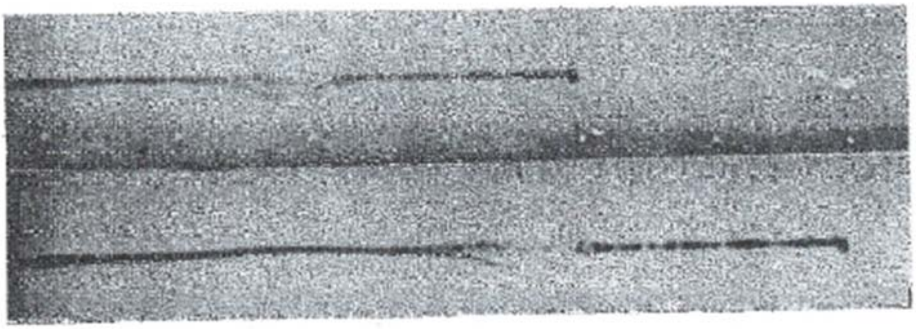

Figure 2.4: Bimetallic 20° liner with nickel apex (60 mm) and copper base (50 mm). (Top) 37.8 μs. (Bottom) 44.6 μs.[2]

Figure 2.5: Laser welded bimetallic 20° liner with nickel apex (60 mm) and copper base (50 mm). (Top) 37.8 μs. (Bottom) 44.6 μs.[2]

Schilling Thomas Schilling performed tests with a similar top/bottom approach as Chanteret's final experiment, but with the objective of investigating penetration performance. He refers to this configuration as "sequent-material." Schilling used liners with a 6.371 cm CD, wall thickness of 3.77% CD, apex angle of 42° and overall height of 8.7 cm. Schilling also notes that the machined surfaces of the liners had at least a 0.4 μm finish and that tolerances were held to +/- 0.004 cm. Schilling used OFHC copper for the top section of his liners and

1100-aluminum alloy for the bottom section. He used two methods of joining the materials: explosive welding (placing the joint at 4.097 cm from the bottom of the liner) and a tenon-mortise joint with epoxy (placing the interior joint at 4.097 cm from the bottom of the liner). He machined the explosively welded liners after bonding them, and also finish machined the inside of the tenon-mortise joint liner after the sections were bonded. In penetration tests that were conducted vertically in an air environment, he found that the optimal standoff for all charges was 8 CD and that the explosively welded liner penetrated 70% of the depth of the solid copper liner, while the tenon-mortise joined liner penetrated 58% the depth of the solid copper liner. This decrease in penetration capability was accompanied by an increase in beyond penetration pressurization. Namely, the average initial peak pressure of the sequent material liners was approximately twice that of the copper liners [30].

Other researchers The reader is referred to the following sources for further examples of multi-material liners.

- The oil industry produces liners with the slug being zinc so that it evaporates during the penetration process and does not plug the perforation hole. (Lebourg, M. P., and Fagan, H. C. (1962). In Schlumberger Well Surv Corp (Ed.), Perforating apparatus (102/306 ed.) F42B 1/032.)

- Regan and Jonas used gold inner plating on a copper outer liner to improve penetration versus a solid copper liner. This performance increase resulted from the formation of a gold jet and occured without increasing the amount of explosive used. Regan, J.M. and G. H. Jonas, The Generation and Penetration Characteristics of High Density Shaped Charge Jets, BRL Memorandum Report, AD370730, 1965. (this report was not obtained by the author, summary notes obtained from [3])

- Skolnick et al. obtained a patent for the use of a multi-layer shaped charge where layers were selected based on impedance in order to reduce the loss of explosive energy across the interface between materials. Skolnick, S., and Goodman, A. (1985). In Southwest Energy Group L. (Ed.), Energy transfer through a multi-layer liner for shaped charges (86/1 R ed.). NM/United States: C06B 21/00.

- Faibish and Mayseless were able to create bimetallic liners by explosive welding of tantalum and copper. Faibish, E. and M. Mayseless, A Double-Layered Conical Liner Manufactured by Explosive Welding, Proceedings 8th International Symposium on Ballistics, Orlando, Florida, 1984, pp. W-1 - W-6.

Modeling

Robinson Allen C. Robinson (Sandia National Laboratories) published a report detailing an analytical prediction of material segmentation for a bimaterial jet. He applied the model to the steady state case of two materials flowing beside each other, as they would in a bimaterial shaped charge jet, into a line of symmetry and determined the locations where the materials would be partitioned into the jet and slug for varying collapse angles and density ratios between the materials. Robinson then input this model into a two-dimensional wave propagation code to analyze cases of two-dimensional impact of a flat plate on a plane of symmetry and axisymmetric collapse of a disk. An important result of this work is that when Robinson used copper for the inner liner and aluminum for the outer liner in proportions appropriate to result in a bimaterial jet, as shown in Figure 2.6, he observed that there was a delay in the response of the high density, high impedance material (here copper). This delay caused there to be a single material jet of copper until steady state conditions were reached at which point the jet was indeed copper and aluminum. Robinson noted that this delay could be increased by using a higher density or higher impedance material, resulting in a larger portion of the jet being of a single material before the bimaterial jet was formed.

Next, Robinson used a shaped charge modeling code that he developed called SCAP to perform a 1-D analysis of bimaterial liner collapse. His results for the copper-gold liner (gold was the inner material) agree well with published data points (the published data consists of seven tests). The results for the aluminum-copper (copper was the inner material) liners agree with published data at both extremes (entirely copper and entirely aluminum) but no experimental data is referenced for any aluminum-copper composite liners. Of the most interest to the current study is the aluminum-copper modeling. Robinson varied the composition of the liners from entirely copper to entirely aluminum and included many ratios between these extremes. SCAP's results indicated that the optimal thickness of aluminum for the aluminum copper charge was 20% of the total liner thickness. He used constant breakup times for all Al/Cu liners of 63.9 μs and imposed a minimum penetration velocity of 1.6 mm/μs for the jet into steel. Using these parameters, the 20% aluminum liner penetrated approximately 30% more into armored steel than did the solid copper jet. A similar effect was seen for the copper-gold liners where the optimal thickness of gold was 15% of the total liner thickness. Robinson states that for an all gold liner, the explosive cannot drive the metal fast enough to produce a high jet tip velocity. As the amount of copper is increased, the jet velocity increases because the total mass of the liner decreases, and deeper penetration is achieved. The experimental data seem to reflect this conclusion (see Figure 2.7 from Robinson's paper). It is interesting, however, that classically, the jet tip velocity, provided it is fast enough to behave in the hydrodynamic regime, is seen to have little to no effect on penetration. Rather, the length of the jet is the primary indication of the maximum penetration achievable by a jet. It is the thought of this author that the increase in jet tip velocity that Robinson notes actually stretches the jet further before the assigned breakup time, and therefore increases the penetration depth [3].

Curtis and Cornish J.P. Curtis and R. Cornish published an article that developed an analytical treatment of a shaped charge consisting of multiple layers of different materials. The geometry investigated is similar to the front/back liner design discussed in section 3.2 of this report. The model is inteded to be a precursor to hydrocode simulations in the design

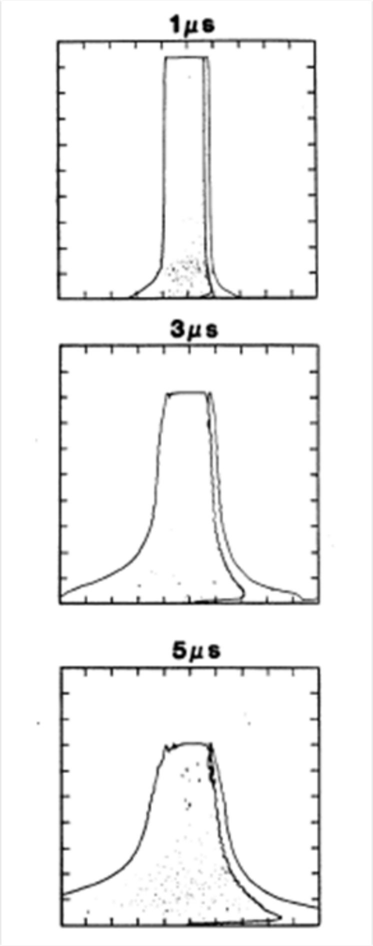

Figure 2.6: Axisymmetric CSQ simulations for an incoming jet where 10% of the thickness is copper. The left plate is aluminum, the right is copper. Note the delay time required to have a multimaterial jet. Adapted from [3]

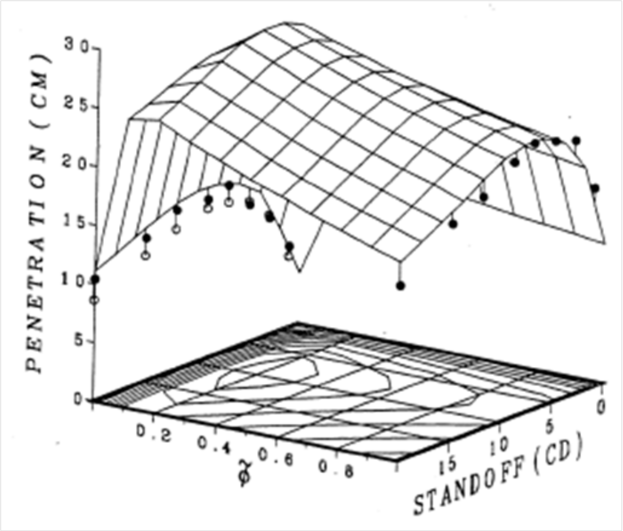

Figure 2.7: Cu-Al penetration curve, dependent on the thickness of the copper portion of the jet, and the charge standoff. $\phi = 1$ represents a solid copper liner and $\phi = 0$ represents a solid aluminum liner. Adapted from [3]

stage of multiple material, multiple layer shaped charge liners. For a given liner of multiple layers, the model is able to predict the critical collapse angle that is required for a layer to begin to enter the jet. Using the model a different way, one could determine the appropriate thicknesses of layers based on desired characteristics of the jet and slug. One key prerequisite for this analysis is the a priori knowledge of the collapse angle, β, which is common to all layers. It is also assumed that the velocity of all layers toward the conical axis are equal, and that no energy is lost in the formation process [31]. This model could be used by future researchers in the Glumac group as a multilayer shaped charge design aid.

CHAPTER 3

LINER DESIGN

3.1 Material Selection (Copper and Aluminum)

Copper has long been known as an effective liner material due to its relatively high density and ductility. These properties lead to formations of a long stretching jet that penetrates quite well. Fant and Rudolphi have concisely summarized the justification of aluminum to be studied as a reactive material for use in underwater shaped charges [23, 24]. Aluminum undergoes a highly exothermic reaction with water under conditions of high temperatures and pressures according to

$$Al_{(s)} + \frac{3}{2}H_2O_{(l)} \rightarrow \frac{1}{2}Al_2O_{3(s)} + \frac{3}{2}H_{2(g)} + 409.1kJ \tag{3.1}$$

Because this energetic release is on the same order as the kinetic energy of the jet, reactivity of the liner has potential to enhance damage production of a shaped charge [24].

3.2 Design of Composite Liner

Several different designs of bimetallic composite liners were pursued throughout the course of the current research. For the reasons mentioned above, aluminum was chosen as the reactive material of choice, while copper was chosen as the dense, ductile, highly penetrating material. The materials were kept consistent throughout the project. Without exception, copper alloy 145, also known as tellurium copper or machinable copper, was used in the liners. Also without exception, aluminum alloy 6061 was used as the aluminum of choice. For optimal performance of shaped charge liners, pure materials would have been slightly better because they have a homogenous atomic make up [32]. By introducing alloying materials into pure aluminum or copper, it increases the likelihood of small disturbances as a stress wave propagates through the material. However, the Glumac and Krier research group has had good results using liners made of various alloys in the past [24]. Also, aluminum alloy 6061 and copper alloy 145 are significantly easier to machine than the corresponding pure metals, which can tend to gum up machine tools and cause loss of precision in the fabrication stage. Sacrificing a small amount of penetration or reactive performance in favor of creating high precision liners was determined to be a good trade-off for this project.

The subsequent composite liner designs were based on the material presented above in the literature review. Of primary importance was the diagram from Walters and Golaski [1] depicting starting and ending locations of various sections of the liner (Figures 2.1, 2.2, and 2.3) and a diagram from Dr. Ron Brown at the Naval Postgraduate School indicating the jet and slug partioning of a solid liner (Figure 3.1). From all this information, hypotheses were made to suggest the appropriate places to introduce aluminum into the liner design in order to have the best chance of reaction during the penetration event. Additionally, the liner designs needed to be generally conventional in shape and operation. Material substitutions might change the performance of the liner, but retaining the shape and mechanism of the liner would allow it to be retrofitted into existing applications if desired.

The first composite liner design that was pursued was a front/back approach. This design is shown in Figure 3.2 and involves fabricating two separate liners, one of aluminum and one of copper. Each of these liners is half the desired thickness of the final liner so that when the copper liner is stacked on top of the aluminum liner, the final desired thickness is obtained. Alternatively, the materials could be machined from one composite piece of stock if that stock contained the conical interface between the two materials. For example, if a conical cavity was machined in one end of a copper bar, that cavity could then be plated

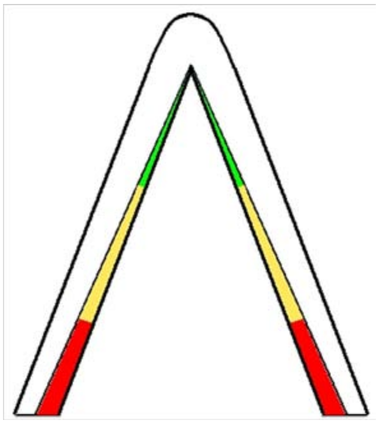

Figure 3.1: Partitioning of liner into leading section of jet (green), middle section of jet (yellow), and trailing section of jet (red). From Dr. Ron Brown (private communication).

with aluminum before doing a final machining step to create a two part liner with a bond between the copper and aluminum.

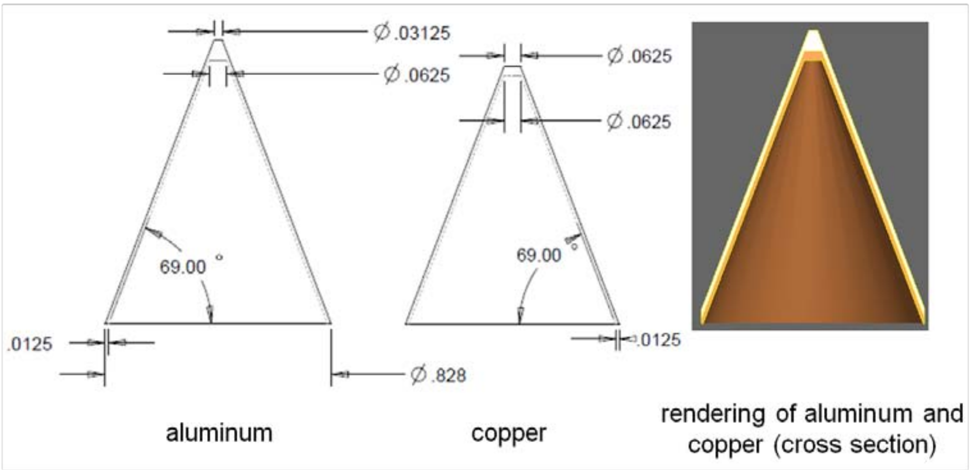

Figure 3.2: Schematic and rendering of front/back liner design

The intention of the front/back approach was to create a liner in which the jet was formed of the penetrating material (copper) while the slug was made of the reactive material (aluminum). This design was intended to place the dense, ductile material in the jet so that penetration performance will be similar to a solid liner made of a highly penetrating material. After the copper had penetrated the target, the reactive material would be delivered to the target, increasing the damage due to the energetic reaction of the aluminum with the

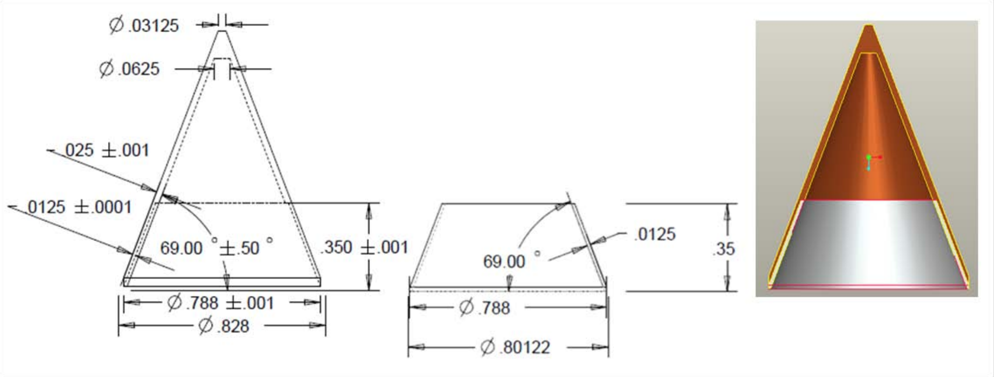

Figure 3.3: Schematic and rendering of Cu/Al insert design

surrounding materials.

The second liner design that was explored was a solid copper liner with a cutout so that an aluminum insert could be fit in the inside bottom of the liner (Figure 3.3). This design was suggested by Dr. Ron Brown at the Naval Postgraduate School as a way to retain some of the penetration ability of copper and the reactive potential of aluminum. It was hypothesized that the jet tip and front of the jet from this liner would be made of copper while the back portion of the jet would be made of aluminum. Finally, the slug would be made almost entirely of copper. Although the aluminum in the back of the jet has a lower velocity than the tip of the jet, it is still significantly faster than the slug. This liner design will henceforth be referred to as the "Cu/Al insert" design in this report. The Cu/Al insert design was the only composite design that was actually tested.

A third liner design that was explored briefly was a top/bottom approach, shown in Figure 3.4. This design was given more consideration after initial difficulties were encountered with the Cu/Al insert design. This design was intended to place copper in the front of the jet and aluminum in the back of the jet. In this way it would be similar to the Cu/Al insert design. However, the top/bottom design has additional aluminum that would end up in the slug.

Finally, a larger scale composite liner was explored. This liner had a diameter of 50.75 mm (1.998 in.) and was of interest due to the relaxation of tolerances for larger liners. As

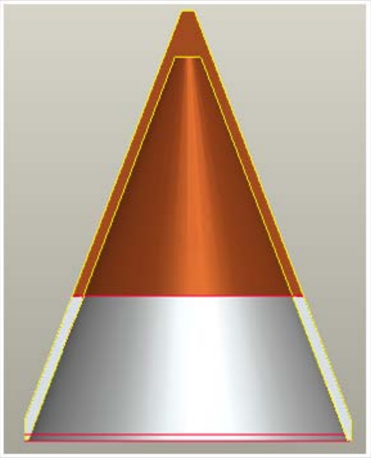

Figure 3.4: Rendering of top/bottom approach

mentioned previously, fabrication tolerances of liners are very tight and scaling from 20.02 mm (0.788 in.) diameter liner to a 50.75 mm diameter liner should relax the tolerances by the scaling factor of 2.54. This liner design is shown in Figure 3.5. It is essentially the same design as the 20.02 mm Cu/Al insert design, but all dimensions are scaled by 2.54. The only exceptions to this photographic enlargement are the wall thickness, the height of the aluminum insert, and the diameter at the inside apex of the cone. These changes were added based on feedback from Dr. Ron Brown at the Naval Postgraduate School.

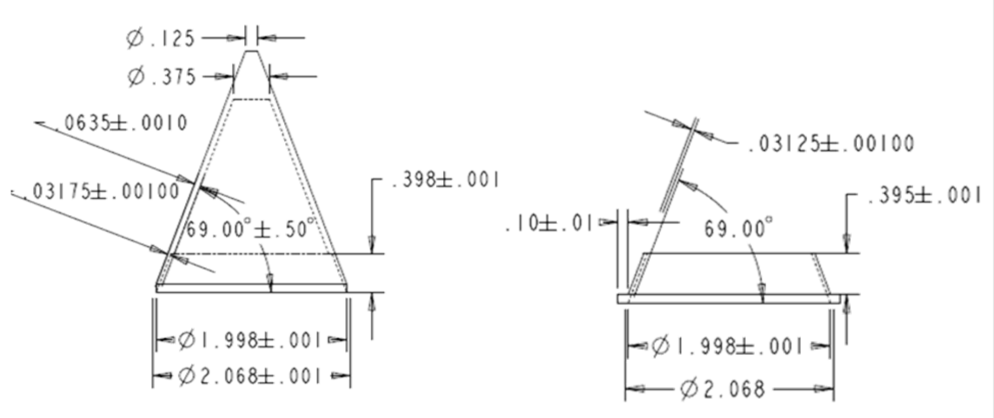

Figure 3.5: Schematic of Cu/Al insert large scale liner

3.3 Fabrication of Bimetallic Liners

Numerous methods were explored to create these bimetallic liners. Fabrication of the liners needed to be cost effective, capable of producing liners with high precision and accuracy, and allow for future experimentation with a wide variety of liner materials. Cost effectiveness had to be considered for both the research phase of this project and a potential production phase that could occur if the results from the short runs were sufficiently promising. Some fabrication techniques that could be viable for long runs or production had startup costs that were deemed too high for an experimental run of ten parts or less. These constraints eliminated a significant number of fabrication techniques. The fabrication methods explored will be described below in regards to their feasibility for the project.

3.3.1 Hot dipping

Due to the choice of copper and aluminum for the liner design, the first method explored was a simple hot dip. Aluminum has a melting temperature of 660° C or 1220° F while copper has a melting temperature of 1084° C or 1983° F. Aluminum's significantly lower melting temperature allows for the dip of a solid copper piece into a molten aluminum mass. On site at the Mechanical Engineering Laboratory (MEL) there is a furnace that is used primarily for the instruction of casting techniques to undergraduate students. This furnace was utilized to conduct the melting of aluminum necessary for the hot dip. The first trials were conducted using standard copper piping and were seen to achieve poor results in thickness uniformity and repeatability. Although results were poor, some improvement was seen by increasing the furnace temperature to 816° C or 1500° F and including a pre-dip chemical cleaning of the copper instead of using a lower furnace temperature (704° C or 1300° F) and no chemical cleaning. The chemical cleaning performed during these tests used a 10% by volume (2.29M) solution of HNO_3 and the copper pipe was immersed in the solution for two minutes. HNO_3

reacts with copper according to

$$Cu_{(s)} + 4HNO_{3(aq)} \rightarrow Cu(NO_3)_{2(aq)} + 2NO_{2(g)} + 2H_2O_{(l)} \tag{3.2}$$

thereby etching away a small amount of the surface of the copper, leaving an oxide free surface with which the aluminum can bind [33].

3.3.2 Casting of aluminum around a copper core

It was hypothesized that a bond with a more uniform thickness and higher geometrical precision could be formed through the pouring of molten aluminum around a copper core. It was clear that if this process was to be successful in forming a precision shaped charge liner, there must be a bond formed between the copper and aluminum materials with sufficient strength that it could be finished machined. At this point in the project, the front/back liner design was being pursued. An illustration of the process of the pouring, casting, and finish machining necessary to create the front/back liner design is shown in Figure 3.6.

Prof. Nick Glumac machined the solid copper cone with a center post at the base of the cone. A mold was designed to create a cavity around the copper cone, and this mold was fabricated on an Eden 350 Objet machine owned by the Mechanical Science and Engineering department. The mold was glued to a wooden block, and sand was packed around it to create the cope and drag for the sand casting form. The form was designed so that the copper cone could be sunk into the drag and the cope would be placed on top, leaving a cavity around the copper cone. Aluminum would be poured into a channel that was connected to the cavity in order to increase control of the aluminum introduction around the copper. This cone was cleaned by immersion in a 20% by volume (4.6M) solution of HNO_3 for one minute. The copper cone was placed into the form, and the aluminum was heated above the melting point to 843° C. Approximately 1.5 hours passed between the cleaning of the copper and the pouring of aluminum around the copper. After the aluminum was poured, the part

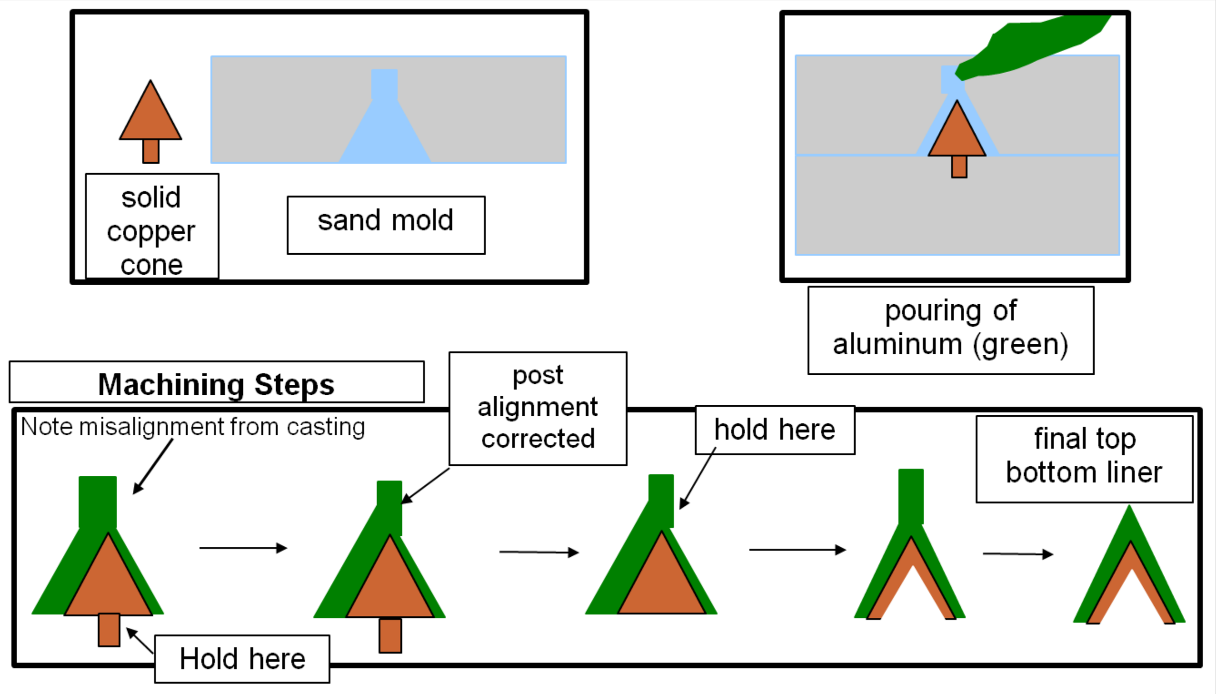

Figure 3.6: Steps of pouring aluminum around a copper piece, then machining to correct misalignments and produce a top bottom liner

was allowed to cool in air for approximately 20 minutes before being extracted from the mold. Excess material was removed using a bandsaw. In order to increase the strength of the copper to aluminum bond, annealing was performed for 14 hours at 454° C. According to Manna et al., annealing allows the copper and aluminum interface to undergo significantly more diffusion bonding than would occur through a simple hot dip or casting process alone [34]. After the annealing was complete, the part was quenched in water and then cut in half with a bandsaw. Adhesion was seen to be fairly good in that the aluminum and copper did not separate during the bandsaw cutting. However, a few voids were noticed at the interface that could cause significant problems for a precision shaped charge liner. At this point, it was decided to continue to experiment with the casting process but to also explore other methods of fabrication that would require the work to be completed by a contracted company.

Further casting experiments were performed using the Cu/Al insert liner design. The casting setup was changed due to the need to just place aluminum inside a portion of the copper cone rather than creating a front/back design. The copper piece before casting is shown in Figure 3.7. The copper piece was machined to its desired final thickness including the step where the aluminum insert was to be placed. Also, four notches were machined into the base of the copper cone to enhance the strength of the composite piece while final machining on a lathe took place. In this casting process, the same cleaning process was used to etch the outer layer of the copper piece. A similar annealing process was also completed with this configuration. Final machining on a lathe was required to remove excess aluminum, leaving only the insert showing in the Cu/Al insert drawing (Figure 3.3). Results after final machining are shown in Figure 3.7 for trial one and trial two of this configuration. Note that both trials exhibited cracking, voids, and asymmetries that were deemed too significant for proper jet formation.

Figure 3.7: (Left) Copper piece before pouring (Center) Trial 1 after machining (Right) Trial 2 after machining

3.3.3 Cold spraying and plating

Cold spraying was investigated for the production of the front/back liner design. Although cold spraying of aluminum onto a thin copper cone promised good adhesion between the materials, low porosity of the aluminum, and the possibility to spray many materials other than aluminum, there were difficulties with the technique that were of significant concern. Namely, during the cold spraying process, aluminum particles would be impacting the .3172 mm (0.0125 in.) thick copper cone with pressures up to 300 psi, likely causing deformation of the copper cone. Additionally, cold spraying would be conducted by placing the copper cone on a mandrel and spinning it while the aluminum was sprayed onto the copper surface. Because the diameter of the cone changes with height, the rate of delivery of aluminum would need to be extremely well controlled. The cost associated with cold spraying became prohibitively expensive for a short run of parts, but may be pursued further for production level quantities of parts.

Plating is a fairly attractive option for fabrication and was explored in multiple capacities. The plating of copper onto aluminum or plating of aluminum onto copper could, in principle, be used to create the front/back design. For the Cu/Al insert design, aluminum plated onto copper would be more logical. Plating at a thickness of .3175 mm (.0125 in.) is a fairly time consuming procedure and is therefore quite expensive. It would offer low porosity and a nice uniform thickness, but was deemed too expensive for a short run of parts.

3.3.4 Hydroforming, spinning, and friction welding

Stamping is a technique that has been used to create shaped charge liners for past experiments at the University of Illinois at Urbana-Champaign [22]. Hydroforming is similar to stamping but in some cases can offer greater thickness uniformity [35]. For this reason, hydroforming was explored. However, hydroforming is generally used to create parts larger than the desired 20.02 mm cones, and companies were unwilling to attempt the liners. A similar obstacle was encountered when attempting to identify a company that would spin form the liners.

Friction welding is a means to join dissimilar metal rods under high pressures and temperatures. This technique was investigated as a bond forming step in the liner fabrication process. After friction welding, the composite metal rod could be finish machined. This technique is most feasible for the top/bottom liner design because the copper aluminum interface is on a single plane perpendicular to the axis of the cone. The front/back and

Cu/Al insert designs have geometrically more complex material interfaces and would thus be significantly harder to accomplish with friction welding. The small diameter rods that would be used in the friction welding process for the liners added additional experimental cost. This process was deemed too costly for a short run of parts.

3.3.5 Machining

Machining the liners allows for a wide variety of materials to be used, and the cost to produce a part was not anticipated to be prohibitive. However, there are two potential concerns with machining of the liners. First, the precision of the part depends primarily upon the skill of the machinist. Secondly, machining does not allow for a bond to be created between the materials. Although the research group of Prof. Glumac and Krier does a significant amount of their own lathe work, the precision required for a composite liner justified contracting the job to a professional shop. When locating a machine shop, the major requirement for precision was to hold the thickness of the liner to +/- 0.0254 mm (0.001 in.) at any spot on the liner wall. Due to the nature of turning a part on the lathe, if completed carefully, the variation on any given transverse plane perpendicular to the cone axis should be very small indeed. If the standards for the BRL precision charge of 81 mm were scaled to the 20.02 mm liner, the transverse and longitudinal thickness tolerances would be +/- .00128 mm (.00005 in.) and +/- .0128 mm (.0005 in.) respectively. It is unlikely that this precision could be obtained. However, if the standards for the BRL "non-precision" charge of 81 mm were scaled to the 20.02 mm liner, the transverse and longitudinal thickness tolerances would be +/- .0128 mm (.0005 in.) and +/- .0254 mm (.001 in.) respectively. It is much more likely that the precision of the "non-precision" BRL liner could be matched. The bond between the two materials was deemed unnecessary due to the extremely high rate of deformation present during jet formation. Since the materials deform in the hydrodynamic regime, an assumption was made that they would flow together during jet formation and elongation.

Wagner Machine Co. in Champaign, IL accepted the job of machining the front/back liner design. They machined one .3175 mm thick 6061 aluminum cone and one .3175 mm thick copper cone that could be stacked to form the front/back liner. The parts exhibited very nice surface finish and precision. Not long after this first front/back liner was produced, the focus of the project shifted to the Cu/Al insert design, as it was deemed more likely to place aluminum only in the back of the jet. Wagner Machine Co. again accepted this task and produced seven Cu/Al insert liners (14 pieces). They also produced several solid copper liners of the same geometry for use as a comparative baseline.

Some experimentation was completed on the group's lathe in pursuit of the top/bottom design. The objective was to use glue or a bonding agent to secure one copper rod to one aluminum rod with sufficient strength that they could be finish machined. Although bonding created by 5 minute epoxy was not of sufficient strength to machine close to the final liner shape, the bonding formed from JB Weld® was much more promising. After the JB Weld® cured, the material was loaded into the lathe and very light passes (only 0.0254 mm depth) were used to remove material. A liner of thickness 0.635 mm (0.025 in.) was produced but the aluminum and copper separated as the part was cut off. The JB Weld® liner is shown in Figure 3.8. Since this process was nearly successful for a liner of 20.02 mm diameter, it is very likely that by increasing either the diameter or the wall thickness of the charge (and therefore the effective bonded area between the materials) this liner could be a viable option for testing.

Figure 3.8: (L) Composite liner created using JB Weld® adhesive (R) Liner separated on the lathe just before achieving the desired thickness

CHAPTER 4

EXPERIMENTAL METHODS

4.1 Overview

Throughout this project, a series of liner designs were tested in a variety of testing apparatuses. The tests completed will be summarized and categorized here in order to aid in understanding throughout the discussion of the testing facilities. Each test will be discussed in further detail in Chapter 5 of this report. A total of 13 tests were completed. The first five tests were conducted in a steel containment tube designed and built for the purpose of diagnostic shaped charge tests. These five tests included two tests of solid copper liners and three tests of composite Cu/Al insert liners. All five liners were 20.02 mm in diameter. After the completion of the five initial tests, four tests were conducted in a larger open water tank, also designed and built for this purpose. Of these four tests, one solid copper liner, one solid aluminum liner, one Cu/Al insert liner, and one liner of the Cu/Al insert design, but with the aluminum insert removed, were tested. All four of these liners were 20.02 mm in diameter. After the completion of these four tests, three further tests were conducted in the open water tank with liners of 50.75 mm diameter. These three tests included one solid copper liner and two solid aluminum liners. Finally, one test was completed in a disposable container set inside the open water tank. This final test was the only one in which oil was used as the target fluid. This test used a 50.75 mm solid aluminum liner. The test number, test dates, liner material, liner diameter, test fluid, and test facility are summarized in Tables 4.1 and 4.2. Further details pertaining to each test will be referenced as needed and can be found in the appendices. With these tests in mind, the testing facilities, diagnostics, and charge assemblies will now be described in further detail.

4.2 Test Facilities

4.2.1 Laboratory and sound enclosure

All tests conducted were performed in the College of Engineering Student Projects Laboratory (ESPL) Annex, 1013 W. Western Avenue, Urbana, IL. ESPL has been used in the past by members of the Glumac-Krier research group to conduct shaped charge tests. Randall Bill was the first student to use ESPL for shaped charge experiments that were deemed excessively loud to perform inside the Mechanical Engineering Laboratory [22]. As such, Bill is responsible for the initial outfitting of the laboratory. Evolution of the tests and testing equipment has occurred due to continued work in this area by subsequent members of the Glumac-Krier research group. Namely, Brian Fant and John Rudolphi have made significant contributions to the testing facilities and safety precautions necessary to conduct these tests [23, 24]. The contributions to the facility from Bill, Fant, and Rudolphi will be covered on a component level basis in the descriptions that follow.

Inside ESPL, a sound enclosure was constructed by Bill, and further detail of the enclosure can be found in Bill's thesis [22]. The sound enclosure is intended to provide a secure area that deadens sound from the explosive events and also houses the test itself and the immediately surrounding safety measures. All tests were conducted inside the sound enclosure. Before testing of the 50.75 mm (1.988 in.) diameter charges, a significant update of the sound enclosure was performed by Rudolphi with assistance from the author. The method of construction remained with same: a frame of 1.5 in. (38.1 mm) schedule 40 steel pipe and appropriate fittings with a shell made of $\frac{3}{4}$ in. (19 mm) thick medium density fiber board. The length and width of the sound enclosure were maintained at 8 ft by 8 ft (2.44 m by 2.44 m), but the height of the sound enclosure was increased from 8 ft (2.44 m) to 10 ft.

Table 4.1: Test summary

Test Summary

Test No.	*Date*	*Liner Design/Material*	*Fluid Used*	*Diameter (mm)*	*Liner Mass (g)*	*Liner Thickness (mm)*
1	4/20/2009	solid copper	water	20.02	*	0.635^n
2	5/4/2009	solid copper	water	20.02	*	0.635^n
3	5/15/2009	Cu/Al insert	water	20.02	3.8995	0.635^n
4	5/28/2009	Cu/Al insert	water	20.02	3.9719	0.635^n
5	6/22/2009	Cu/Al insert	water	20.02	**	0.635^n
6	7/2/2009	Cu/Al insert	water	20.02	4.0353	0.635^n
7	7/15/2009	Cu/Al without Al insert	water	20.02	**	0.635^n
8	7/20/2009	solid aluminum	water	20.02	1.567	0.635^n
9	7/20/2009	solid copper	water	20.02	5.176	0.635^n
10	10/13/2009	solid copper	water	50.75	**	1.61^n
11	3/25/2010	solid aluminum	water	50.75	22.3077	1.50^F
12	4/9/2010	solid aluminum	water	50.75	22.7448	1.52^F
13	6/21/2010	solid aluminum	Hygold L-750 oil	50.75	22.8576	1.55^F

*mass not recorded, estimate 4.7 - 5.1 g **mass not recorded ^{n}nominal thickness ^{F}more detail in Appendix F

Table 4.2: Test diagnostics

Diagnostics Used						
Test No.	*Plate Penetration*	*Light Emission*	*Time of Arrival*	*Pressure*	*HSV*	*Laser Velocity*
1	X	X	X	X		
2	X	X	X	X		
3	X	X	X	X		
4	X	X	X	X		
5	X	X	X	X		
6				X	X	
7					X	
8				X	X	
9				X	X	
10				X	X	
11	X				X	X
12	X				X	X
13	X				X	X

(3.05 m). Additionally, efforts were made to increase the sound deadening performance of the sound enclosure. Previously, fiberglass insulation was tacked to the inside walls of the sound enclosure and held there by light fabric. This method was not sufficiently quieting or sufficiently robust to hold up to multiple shaped charge tests. During the remodeling of the sound enclosure, AcoustiBlok® was installed in place of the fiberglass and fabric. Additionally, air gaps between the walls of the enclosure and the cement floor and air gaps between adjacent fiberboard panels were sealed with caulk or wood to further contain noise from the blast. Figure 4.1 shows the outside of the sound enclosure (the addition to the height can be noted) and the inside of the sound enclosure, including the AcoustiBlok® material. These efforts were effective in reducing the noise of the experiments to a level appropriate for tests on campus, even for the large diameter charges.

Figure 4.1: Sound enclosure with AcoustiBlok® sound deadening material

4.2.2 Steel containment tube

Five of the thirteen tests conducted were performed in the shaped charge steel containment tube (henceforth referred to as the containment tube). This tube was designed by Rudolphi and used without revision by the author. While a general description will be given here, the reader is referred to Rudolphi's thesis for further design details [24]. The containment tube is constructed of A530 steel and is 60.96 cm (24 in.) in length with an outer diameter of 15.24 cm (6 in.) and wall thickness of 19.05 mm (0.75 in.). The containment tube is used exclusively for liners with diameters of 20.02 mm. During a shaped charge test, the containment tube is used in a vertical orientation and sealed on the bottom by a steel plate. This seal allows the tube to be filled with a fluid and fitted with an array of target plates, separated by steel spacers. Another steel plate is then fitted to the top of the tube. This plate contains a hole through which the shaped charge jet and slug pass. The entire tube is bolted to a base plate that retains the shaped charge liner assembly before the firing event. Finally, this entire assembly is bolted into a larger tank (the open water tank described below) to restrict movement of the containment tube during a test. This setup results in the 20.02 mm liner having an air standoff distance of 5.08 cm (2 in.). The first target plate is covered with 2.54 cm (1 in.) of water. A cross sectional illustration of the containment tube, top and bottom sealing plates, target plate and spacer array, and base plate is shown in Figure 4.2. The shaped charge liner assembly would be inserted into the hole in the base plate as indicated. The containment tube is also outfitted with numerous ports to allow data collection from various diagnostic sensors during the test.

Plate and spacer array

All five tests completed in the containment tube for this study used ten target plates. Rudolpi used eight target plates for his study but additional plates were added due to the increased penetration depth of a copper liner compared an aluminum liner. The plates were fabricated

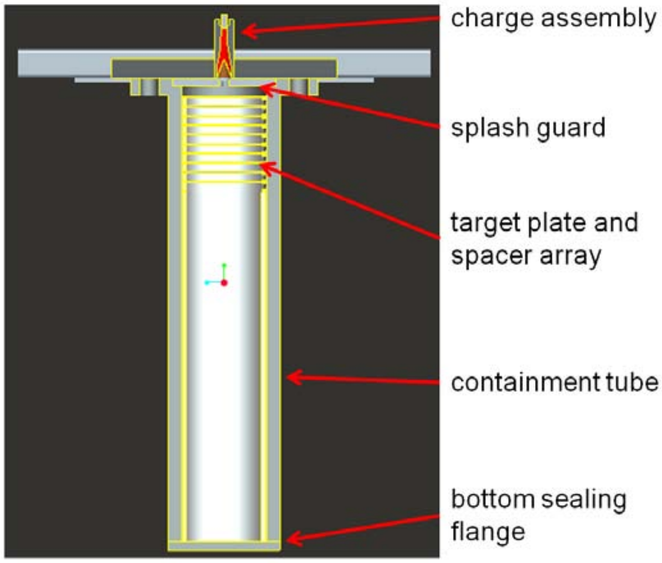

Figure 4.2: Containment tube test setup components

using a wire EDM process to cut 11.30 cm (4.45 in.) diameter circular plates from a 1.22 m by 2.44 m (4 ft. by 8 ft.) plate of 14 gauge A1011 hot rolled steel. The steel was obtained from Kurland's Steel in Urbana, IL and the wire EDM process was performed by the in-house machine shop at the Mechanical Engineering Laboratory. Despite the nominal thickness of 14 gauge steel to be 0.0747 in (1.90 mm), plates used throughout the five tests in the containment tube were either 0.0735 in. (1.87 mm) (for tests 1,2, and 3) or 0.0785 in. (1.99 mm) (for tests 4 and 5). Rudolphi has completed tensile tests of the same plate material with a thickness of 0.0747 in. (1.90 mm) and found the average elastic modulus to be 180 - 200 GPa, the average 0.2% yield strength to be 200 MPa, and the average ultimate strength to be 330 MPa [24]. These values could be used to correlate numerical simulations of the event if desired.

The spacers used were designed by Rudolphi, and the reader is again referred to his thesis for detailed drawings and descriptions [24]. For the purposes of this report, it will suffice to note that the spacers have an inner diameter of 10.23 cm (4.026 in.), a height of 12.7 mm (0.500 in.), and were machined from low carbon alloy steel tubing. Each cavity is therefore 10.23 cm in diameter and 12.7 mm high, bounded by a target plate on the top and bottom, and the spacer forms the walls of the cavity. The spacers had additional holes machined in the sides to allow the diagnostic sensors to be inserted through the containment tube and through the spacer into the cavity.

Diagnostics used with the containment tube

As mentioned above, the containment tube was filled with water and fitted with an array of alternating target plates and water filled cavities. Sensors were fitted to various locations in the tube that are denoted henceforth by their cavity number. For example, the water filled cavity above the fourth target plate is called "cavity 4." There are also two ports on the bottom sealing plate of the tube. One port goes entirely through the plate and can be fitted with a pressure transducer. The second port can also be fitted with a pressure transducer, but this port is not open to the water inside the tube because the depth of the hole is less than the thickness of the plate. Rudolphi used this port to verify that the vibration of the pressure transducers caused by the translation of stress waves through the tube was not contributing significantly to the pressure measured by the transducers [24]. Light emission and pressure measurements were obtained via sensors connected to the tube's diagnostic ports. Time of arrival of the jets to each of the first five target plates was measured using gauges on the plates connected to a data acquisition system through additional ports in the tube. Figure 4.3 shows the locations of each possible diagnostic inside the containment tube. It should be noted that not every port was used in every shaped charge test. The data acquisition was limited by the number of sensors available rather than the number of ports available. In regards to diagnostics for the containment tube, no significant changes were made from Rudolphi's setup, but brief descriptions of each diagnostic follow for the clarity of the reader.

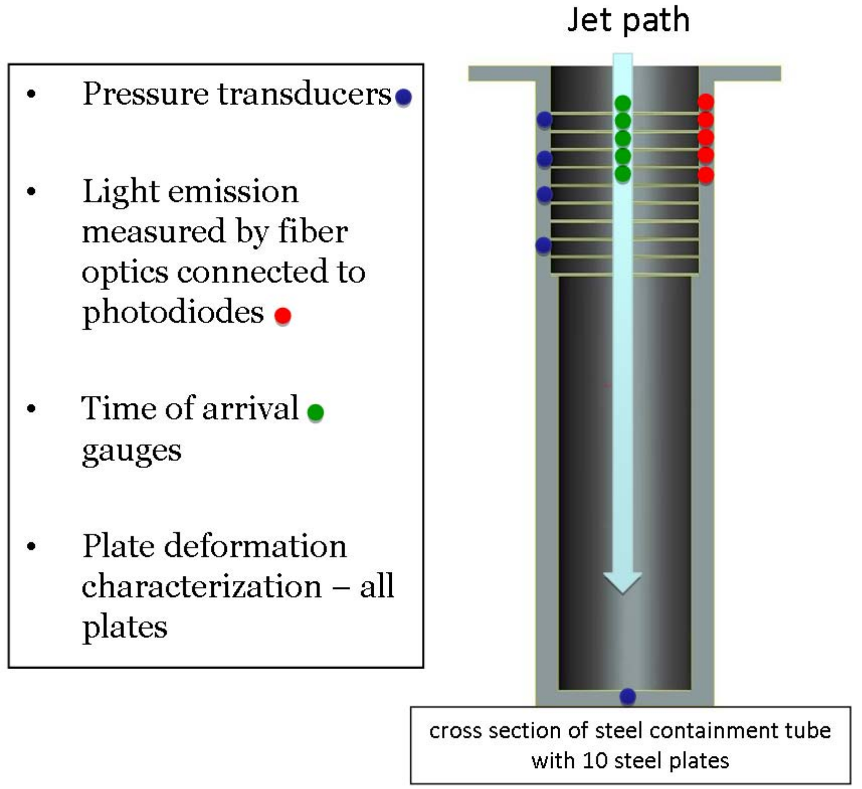

Figure 4.3: Possible sensor locations for containment tube tests

Light emission As noted previously, when a reactive jet enters the water, a luminous reaction may occur. Spatially and temporally resolved light emission data can assist in demonstrating the location, time, and intensity of the reaction and can aid in the fundamental understanding of the process. Time resolved light emission data on a per cavity basis was collected via a fiber optic system connected to the data acquisition system. For each of the five tests in the containment tube, light emission data were collected for cavities 1-5. A self-sealing bolt with a hole drilled down the axis was fitted with a polymer fiber optic cable (AnchorOptics part no. AX02545) and a sapphire window (Edmund Optics part no. NT43-365) as shown in cross section in Figure 4.4. This fiber optic cable was coupled to a Thorlabs photodiode (part no. PDA55) to monitor the light emission. This photodiode was used with a 0dB gain setting and therefore had a response time of 35 ns.

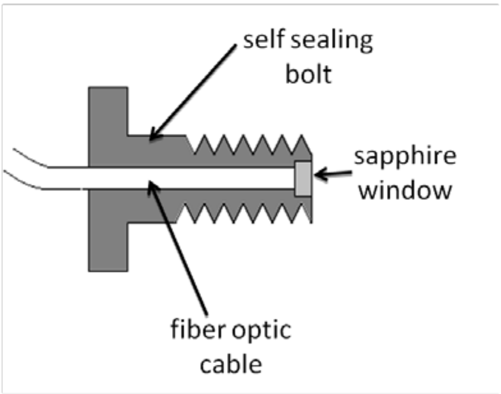

Figure 4.4: Cross section of bolt with contained fiber optic

Pressure Time resolved pressure data also provide indication of the event intensity and therefore the damage production potential of each liner. Ports were available on the containment tube to attach pressure transducers at cavities 2, 4, 6, and 9, as well as on the bottom of the tube. The pressure transducers used for these tests were either Kistler 603B1 or Kistler 607M140. The specifications of these sensors are tabulated in Table 4.3 using information provided by the manufacturer. These gauges are not designed for underwater usage, so the gauges were fit into Delrin housings, and the sensing end of the gauge was covered with a light coating of vacuum grease. Additionally, the sensing ends of the transducers were mounted flush with the inside diameter of the containment tube, not flush with the inside diameter of the spacer. This mounting style was done to assure that no damage to the transducer would occur if there was movement of the spacer during an event. Before a shaped charge test, each pressure transducer was placed in a pressure testing vessel built by John Rudolphi that provided a dynamic load to the transducer. However, it should be noted that the pressures reached in this vessel were generally less than 500 psi, while pressures recorded during the shaped charge event reached up to 25,000 psi or greater. This goal of this pressure vessel testing was not to calibrate the transducers but to simply verify that they were working properly. Kistler 5004 charge amplifiers were used with the transducers, and the output of the amplifiers was routed to the data acquisition system.

Table 4.3: Pressure transducer specifications

Pressure Transducer Specifications from Manufacturer's Websites			
	Kistler 603B1	*PCB 138A26*	Units
Measuring range	15000	50000	psi
Overload	18000		psi
Sensitivity	-0.35 pC/psi	0.2 mV/psi	
Rise time	1	< 1.5	μs
Shock resistance	20000	20000	g
Acceleration sensitivity	0.002		psi/g

Time of arrival data In order to obtain information about the penetration velocity of the shaped charge jet, the first five target plates were fitted with time of arrival gauges that recorded the time, in relation to the initial detonation signal sent by the fire set, that the jet reached the top surface of the each plate. These gauges were very similar to those used previously by Rudolphi, and a schematic of a single gauge is shown in Figure 4.5. As shown, the gauge works by separating a thin metal foil (for these tests, Alfa Aesar 0.001 in (0.0254 mm) thick silver foil, part no. 12190, was used) from the plate by an insulator (either silicone adhesive or electrical tape) and applying a voltage across the insulator. This voltage

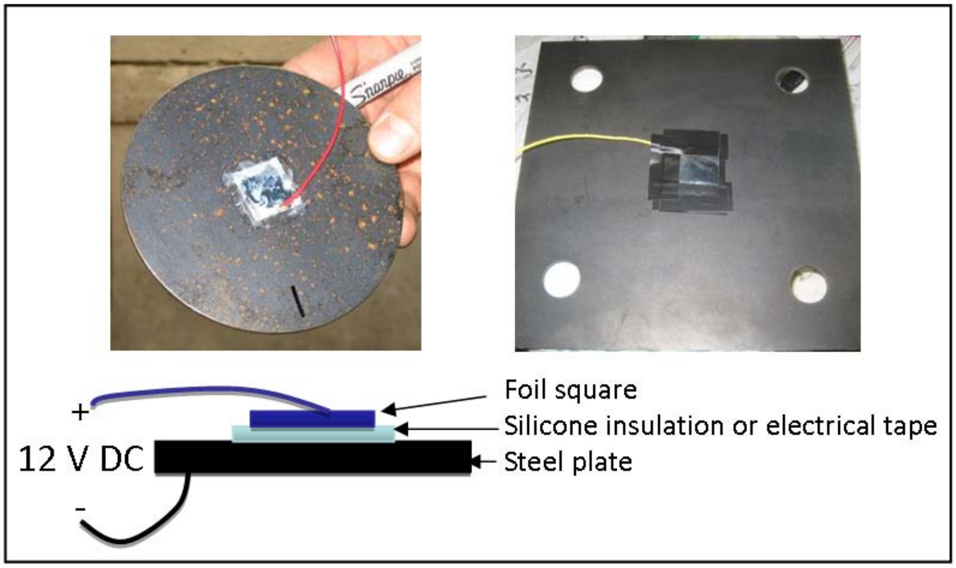

Figure 4.5: Schematic and examples of time of arrival gauges used in plate penetration tests. The circular plate was used in the containment tube, while the square plate was used in the blast tank.

is continuously monitored by the data acquisition system. While the insulator remains intact, a non-zero voltage is maintained. However, when the jet impacts the foil, it is pushed through the insulator and contacts the steel plate. When this contact occurs, the voltage difference between the plate and the foil goes to zero, indicating that the jet has struck the top surface of the plate.

Plate deformation The final diagnostic that was obtained from the containment tube setup was the measurement of plate deformation. After the completion of a test, the plates were extracted from the containment tube, and their deformation data was quantified. Calipers were used to measure hole diameter (if a hole existed in the plate), and a measuring apparatus was designed by the author to measure the displacement of the plate from its original flat shape. This measuring apparatus is shown in Figure 4.6. Figure 4.7 shows an illustration of one deformed plate that was encountered often. In all cases, a positive deformation indicates deformation of the plate toward the top of the tube (where the jet originated), and a negative deformation indicates deformation of the plate in the direction of the bottom of the tube. These displacements were plotted for visualization purposes and can be found in the complete test results given in Appendix E.

Figure 4.6: Measuring apparatus used to quantify plate deformation for plates from containment tube

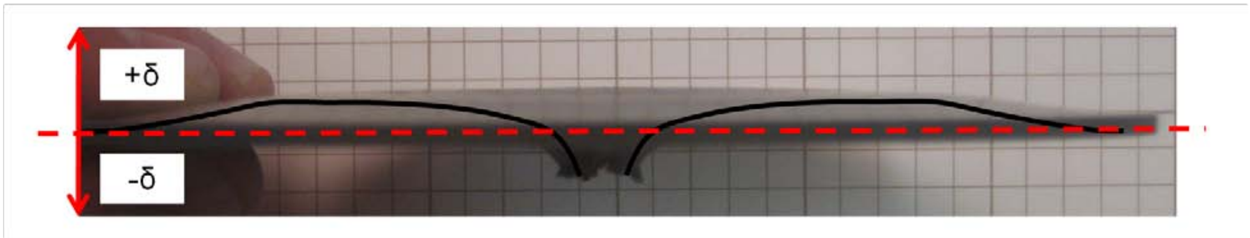

Figure 4.7: Example of deformed plate from containment tube, showing positive and negative deformation conventions

4.2.3 Blast tank

The same tank into which the steel containment tube was bolted to control its movement during a shaped charge test could also be used without the containment tube to allow variation on the diagnostics used. The charge assembly was still retained by the base plate which was bolted to the blast tank. The tank was then filled with water, and the liner

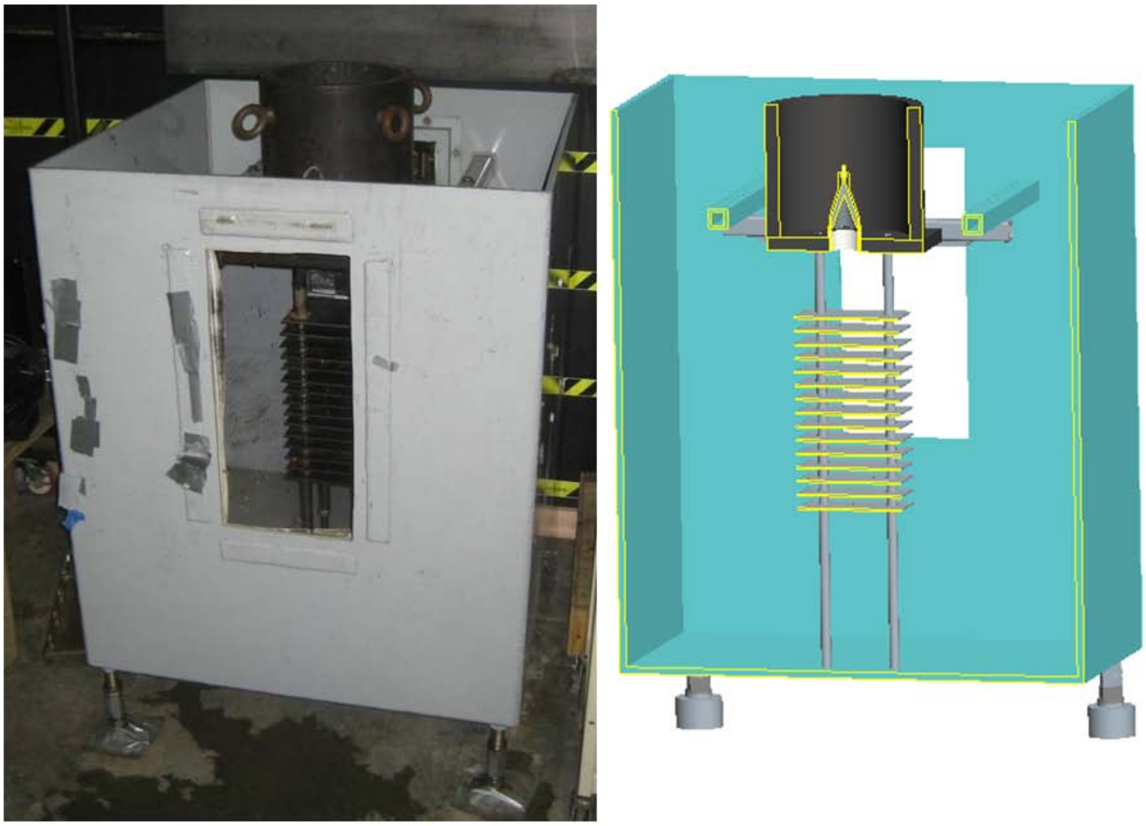

Figure 4.8: (L)Photo of blast tank with base plate, target array, and shroud installed (R)Rendering of cross section of the blast tank with base plate, target array, shroud, and charge assembly intalled

was fired vertically down into the water. This tank will be referred to as the blast tank. A rendering and a photograph of the blast tank are shown in Figure 4.8. This tank was designed by a group of senior mechanical engineering students for a senior design project and has been used by Bill, Fant, Rudolphi, and the author [36]. The 1.0 in. (25.4 mm) thick polycarbonate windows on the front and back of the tank allowed optical access to the event that the containment tube did not afford. Bill and Fant demonstrated the use of high speed cameras to record the penetration of the shaped charges into this tank after it had been filled with water [22, 23]. Fant also designed a plate array that could be used in this tank to test for penetration characteristics. The author conducted similar experiments with different liner designs.

As noted previously, tests 6 - 13 were conducted in this tank. Tests 6 - 9 were of liners with 20.02 mm diameters and tests 10 - 12 were of liners with 50.75 mm diameters. Test 6 - 10 incorporated pressure measurements and high speed video imaging. Tests 11 - 13 incorporated high speed video imaging, plate deformation quantification, time of arrival data, and a velocity measurement of the jet tip in air. Pressure transducers used during tests 11 and 12 did not give any usable signal. A discussion of each diagnostic follows.

Diagnostics in the blast tank

Pressure A maximum of two pressure sensors were used in the blast tank tests. These sensors were PCB 138A26 tourmaline sensors designed for underwater blast applications. They were used with a PCB 482A22 signal conditioner which output data to the data acquisition system. The sensors were mounted on a pole attached inside the blast tank. Because they were mounted against a surface rather than being exposed to pressure on all sides, the pressure recorded was twice the actual free stream pressure in the tank. This multiplier is used to account for the fact that the pressure wave is reflected off the surface of the pole and contributes to the measured pressure. All pressure data presented for these tests has been corrected to reflect the actual free stream pressure. The mounting height of each transducer on the pole is given for each test in Table 4.4 as a depth from the base of the liner to the measuring element of the transducer. All transducers in the blast tank were also 26.7 cm (10.5 in.) away from the axis of penetration. The total distance of the measuring element of the transducer from the liner base could be computed using these two distances.

Table 4.4: Pressure transducer depths from liner base for tests 6 - 13

Pressure Transducer Depths								
	Test 6	*Test 7*	*Test 8*	*Test 9*	*Test 10*	*Test 11*	*Test 12*	*Test 13*
Depth1 (cm)	20.3	*	20.3	20.3	*	*	*	*
Depth2 (cm)	36.8	*	36.8	36.8	36.8	*	*	*
*pressure data was not recorded								

High speed video imaging In order to gain understanding of the behavior of the liners during formation and penetration, a high speed video camera was used to record the events. Of specific interest were the penetration characteristics of the Cu/Al insert liner, but this case was compared to a solid copper liner, a solid aluminum liner, and a Cu/Al insert design without the aluminum insert. Tests 6 - 9 were recorded using the VisionResearch Phantom v5.2 camera placed approximately 1.52 m (5 ft.) from the charge axis. With incandescent backlighting consisting of three 500 W work lights, the Phantom v5.2 could be used to resolve features of the shaped charge event at an exposure time of 3.00 μs and a frame rate of 61538.462 frames per second (16.25 μs frame interval). It accomplished this image acquisition with a resolution of 40 x 192 pixels using an 8 mm lens with f/# 1.3. Test 7 used slightly different settings. The frame rate was 59701.493 fps (16.75 μs frame interval), the exposure time was 3.00 μs and the resolution was 32 x 208 pixels. Tests 10 - 13 utilized the VisionResearch Phantom v7.0 camera. This camera has a more sensitive sensor than the Phantom v5.2, so the exposure time could be significantly decreased. Likewise, the resolution was refined to allow for maximum frame rate while still capturing the interesting portion of the event. During tests 10 and 11, the Phantom v7.2 was able to capture the event with the same backlighting but with an exposure time of 1 μs, a frame rate of 105263.158 frames per second (9.50 μs frame interval), and a resolution of 128 x 56 pixels. During these tests, the same 8 mm lens was used, and the camera was placed approximately 1.52 m (5 ft.) from the charge axis. Test 12 placed the camera approximately 3.7 m (12 ft.) away from the charge axis and used a 1 μs exposure and a 25 mm lens. The lens f/# was set to 3.8 and the resolution of the image was 40 x 144 pixels, which allowed a frame rate of 117647.059 fps (8.5 μs frame interval). No backlighting was used for test 12 as it was determined that the event itself produced more than enough light to resolve the plate setup and details of the penetration event. Test 13 used the same lens as test 12, but the f/# was set to 5.6. The camera was again placed approximately 3.7 m (12 ft.) away from the event. Test 13 was fired into oil and was therefore not expected to be self-illuminating. Therefore, two Photogenics

PL2500DR flashes were fired during the event to provide backlighting for this test. Table 4.5 summarizes the camera settings, mm per pixel at the event plane, and distance of the camera from the event plane for each test.

Plate penetration Plate penetration in the blast tank was only completed for tests 11 - 13. These scaled up 50.75 mm diameter liners were new ventures for the Glumac-Krier group. Therefore, a new target plate and spacer array needed to be designed. When designing the plate array, several considerations were taken into account. The long term objective of this design was to compare the penetration depth and damage production of a composite liner against the penetration depth and damage production of a solid copper or solid aluminum liner of the same geometry. With this goal in mind, the plate array needed to be able to offer sufficient plate resolution to compare relatively small differences in penetration depth accurately. To increase resolution of the plate array, a large number of thin plates should be used. However, the plate array also needed to accommodate the penetration depth of a solid copper liner up to 50.75 mm in diameter without allowing the jet to perforate the bottom of the blast tank. Thicker plates can accommodate a more deeply penetrating charge. Also, a large number of plates and spacers require a long downtime between tests to fabricate and assemble the target array.

The objective of test 10 was primarily to demonstrate that the 50.75 mm diameter solid copper charge (the most deeply penetrating charge that would be tested) could be safely fired in the blast tank without either perforating the bottom of the tank or damaging test equipment. This test was conducted without a plate array but with additional safety precautions. Tests 11 - 13 were 50.75 mm diameter aluminum liners that were tested for penetration using the target plate array.

Obtaining an estimate of the depth of penetration for 50.75 mm diameter liners was of primary importance in the design of the plate array. In order to determine the depth of penetration for a 50.75 mm liner through a multi-layered target, a significant effort was

Table 4.5: Relevant camera settings and parameters for high speed video adquisition, tests 6 - 13

High Speed Video Camera Parameters									
Test no.	*Camera used*	*Lens*	*f/#*	*Exposure (s)*	*Frame rate (fps)*	*Frame interval (s)*	*mm/pixel*	*Array size*	*Camera distance (m)*
6	Phantom 5	8 mm	1.3	3	61538.46	16.25	2.12	40 x 192	1.5
7	Phantom 5	8 mm	1.3	3	59701.49	16.74	2.07	32 x 208	1.5
8	Phantom 5	8 mm	1.3	3	61538.46	16.25	2.12	40 x 192	1.5
9	Phantom 5	8 mm	1.3	3	61538.64	16.25	2.12	40 x 192	1.5
10	Phantom 7	8 mm	1.3	1	105263.2	9.5	3.63	56 x 128	1.5
11	Phantom 7	8 mm	1.3	1	105263.2	9.5	3.63	56 x 128	1.5
12	Phantom 7	25 mm	3.8	1	117647.1	8.5	2.54	40 x 144	3.7
13	Phantom 7	25 mm	5.6	1	102564.1	9.75	2.54	32 x 120	3.7

given to investigation of analytical models. It was found that models capable of predicting with reasonable accuracy the depth of penetration through a multilayered target required knowledge of the liner's break-up time and velocity prior to penetration. Neither of these factors were known about the 50.75 mm diameter liner. Prediction of the penetration depth through alternating layers of two materials as dissimilar as steel and water added to the complexity. Due to these obstacles and our lack of experience with shaped charge analytical modeling to this project, alternate means were pursued to obtain an estimate of penetration.

Using the results from tests performed by the Glumac-Krier research group in the containment tube, a plate and spacer array was designed that maintained similar characteristics. Foremost in the design was the scaling behavior of shaped charges as described by Walters and Zukas (originally published by Baker et al. [37]). For the photographic enlargement of a shaped charge by a scaling factor (increasing the liner diameter, charge diameter, charge length, confinement wall thickness, liner wall thickness, and standoff distance by a scaling factor while maintaining the same geometry for all parts involved), the following relationships should hold:

- The jet tip velocity remains constant
- The jet diameter, jet length, penetration depth, and jet breakup time increase by the linear scaling factor
- The jet mass, total jet kinetic energy, and hole volume increase by the cube of the scaling factor

Despite concerns that these scaling relationships had only been demonstrated for liners from 40 mm to 178 mm charge diameter, an assumption was made that the scaling in question (liners scaled from 20.02 mm to 50.75 mm), would hold at least approximately to these relationships. Literature exists on this topic [38] but was unavailable to the author. A second concern was that the liners in question were not precise photographic enlargements of each other. Note the difference in tip geometry of the liners in Figure 4.9. Finally, the casing design used for the 50.75 mm liners was certainly not a photographic enlargement of the previous casing used for the 20.02 mm liners. Significant changes had been made to decrease the amount of high explosive needed for the event and to remove portions of the casing that would only contribute to fragmentation. However, rather than rigorously address these concerns in an analytical or computational solution, it was assumed that these changes would not affect penetration depth significantly more than simple round-to-round variation. Walters estimates that the jet velocity gradient, jet diameter, jet mass, and breakup time can show round-to-round variation of as much as +/- 20% [4]. In order to account for this variation and the assumptions that were made about scaling relationships, the most highly penetrating liner, a solid copper liner of 50.75 mm diameter, was fired into the tank with additional safety precautions. These precautions will be discussed in Section 4.5 below. After ascertaining that the solid copper charge would not create a perforation in the bottom of the test tank, the design of the plate array was resumed. Data from past tests in the Glumac-Krier research group showed that 50.75 mm aluminum liners typically penetrated through 8.9 mm (0.35 in.) of steel and 84 mm (3.3 in.) of water. The data from the author's two solid copper 20.02 mm liners showed an average penetration of 14.9 mm (0.588 in.) of steel and 114 mm (4.50 in.) of water. Using a scaling factor of 2.54 (the ratio of 50.75:20.02), the large diameter aluminum and copper liners were expected to penetrate 23 mm (0.90) in of steel and 214 mm (8.41 in.) of water and 38 mm (1.5 in.) of steel and 290 mm (11.43 in.) of water respectively.

The plate thickness and spacing parameters were chosen in order replicate the percentages of steel and water from the containment tube tests on a per inch basis. For the containment tube tests, the water-filled cavities were 12.7 mm (0.500 in.), thick and the target plates were either 1.87 mm thick or 1.99 mm thick. Taking one cavity and one 1.87 mm thick plate as a metric, the resulting calculation shows that for a jet that penetrates 25.4 mm (1 in.), 12.8% of the penetration is through steel and 87.2% of the penetration is through water. However, if the 2.54 cm of water above the first plate is added to these

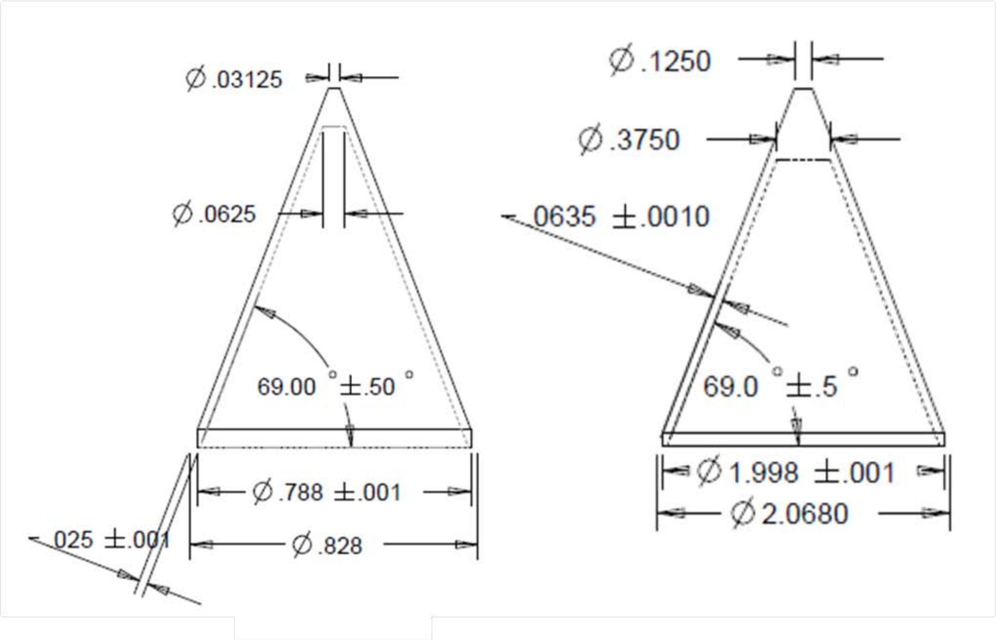

Figure 4.9: Note the differences in tip geometry between (L)the small scale liner and (R)the design used for the large scale copper test

calculations the percentage becomes dependent on the total number of plates penetrated for a given test. As a jet penetrates more deeply the percentage of steel and water penetrated per inch approaches the limiting case of one cavity and one plate. For a depth dependent case, the material penetration percentages can be calculated by:

$$\%SP = \frac{L_S}{L_W + L_S} \tag{4.1}$$

where $\% \, SP$ is the percentage of the total penetration distance that was through steel, L_S is the total thickness of steel penetrated, and L_W is the total thickness of water penetrated. L_S and L_W are calculated as

$$L_S = P_P t_P \tag{4.2}$$

$$L_W = t_{W1} + (P_P - 1)t_S + t_{S,h} \tag{4.3}$$

where P_P is the number of plates fully penetrated, t_P is the plate thickness, t_{W1} is the height of water above the first plate, t_S is the spacer thickness, and $t_{S,h}$ is an additional spacer thickness added only if there is evidence that the jet hit the next plate. As an example, if a liner were to penetrate only three plates and just strike the fourth, the percentage of steel per inch penetrated would be only 8.82% compared to the 12.8% found using one plate and one cavity as a test case. The plate array was therefore designed to replicate the percentage of steel penetrated per inch at the expected depth of penetration based on the scaling relationships. Ten gauge steel (nominal thickness of 0.1345 in. or 3.416 mm) was chosen to form the plates, and 0.900 in. (22.9 mm) thick spacers were used to separate the plates. These choices meant that, based on the predictions about the thickness of steel that the liners would penetrate, the 50.75 mm diameter aluminum liner would be predicted to stop in plate 7 and the 50.75 diameter copper liner would be predicted to stop in plate 12. After the steel was purchased, it was determined that the thickness of the plates was actually 0.1290 in. (3.277 mm) rather than the nominal thickness of 0.1345 in. (3.416 mm). This change in thickness did not change the number of plates predicted to be penetrated, but it did suggest that the jet would be stopped at a deeper position in the final plate. Tensile tests were completed on three specimens cut as shown in Figure A.10. The specimens were cut from the same sheet of steel as the target plates. An example of the data obtained from the tensile tests is shown in Figure 4.10. Figure 4.11 shows an example of the upper and lower yield behavior of the specimens. Figure 4.12 shows an example of the linear fit used to determine the elastic modulus of the specimen. Table 4.6 shows the results of the tensile tests. Note that both the yield strength and the tensile strength is given in terms of the engineering stress on the specimen.

Table 4.6: Properties of steel target plates used in 50.75 mm diameter tests, based on three tensile tests

Properties of Steel Target Plates Used with 50.75 mm Diameter Liners					
	%EL (1 in. gauge length)	Lower yield (MPa)	Tensile strength (MPa)	Elastic modulus (GPa)	Hardness (HRB)
mean	48.8	321.7	419.7	224.1	76.0
std dev.	2.63	3.79	4.04	4.19	0.76

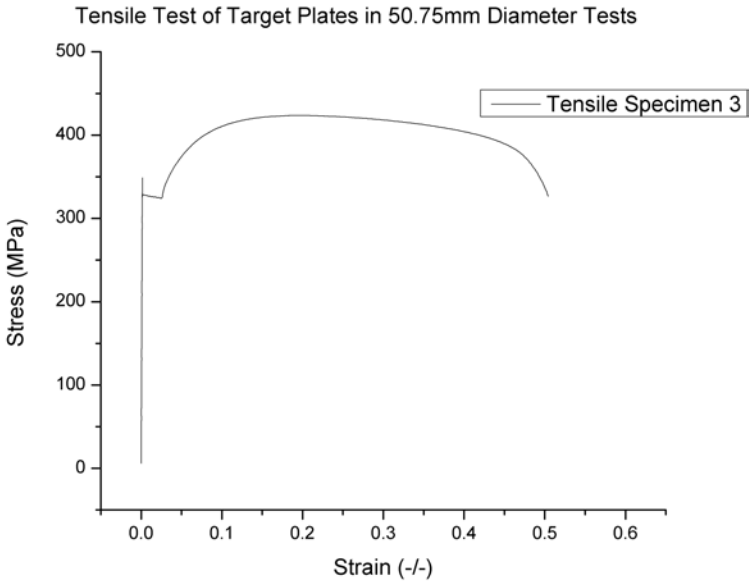

Figure 4.10: Example of the behavior of the target steel under load

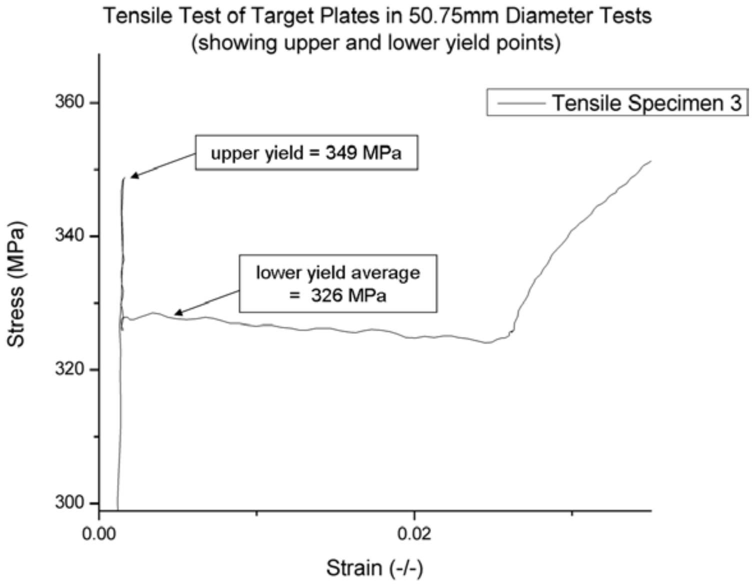

Figure 4.11: Example of the upper and lower yield behavior of the target steel

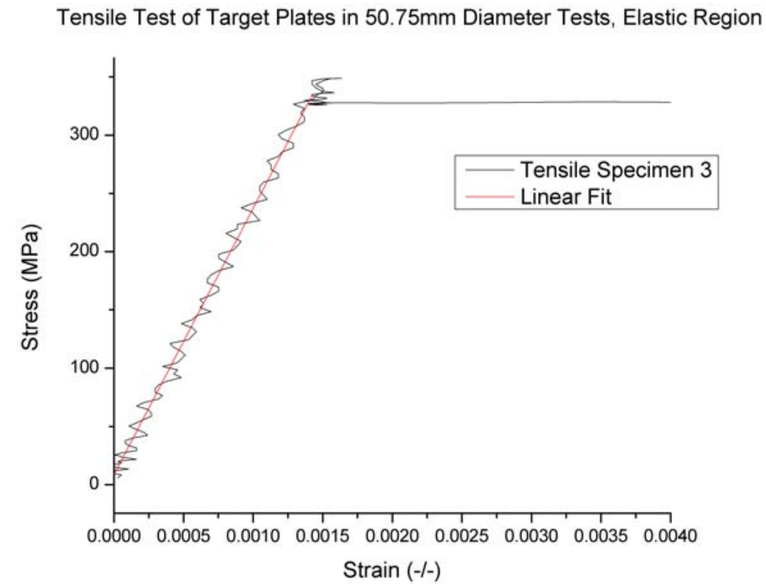

Figure 4.12: Example of the linear fit used to determine the elastic modulus of the target steel

Once the parameters had been established for the desired thickness of steel plates and spacers between plates, the plate array needed to be fit in the blast tank. The design of the plate array for these tests was based on the plate penetration experiments conducted by Fant in the blast tank [23], but all components were sized and fitted by the author. A photo of the plate array attached to the base plate is shown in Figure 4.13, showing the series of steel plates mounted on threaded rods with spacers separating the plates. The threaded rod was 3/4”-10 steel rod, grade B7 (McMaster-Carr part no. 98957A738) cut to four lengths of 31 5/8 in. (80.3 cm) by the author. The spacers were cut from steel tubing, 0.87 in. interior diameter, 1.00 in. outer diameter (McMaster-Carr part no. 7767T23). The tubing was first cut into sections slightly longer than 0.90 in. (22.9 mm) in length using a bandsaw. Next, the spacers were loaded onto the lathe and finished machined to 0.900 +/- 0.005 in (22.9 mm +/- 0.13mm). The spacers closest to 0.900 in. (22.9 mm) were used to separate the plates near the top of the plate array. Fourteen of these spacers were required for each threaded rod. Two additional spacers for each rod were cut from the steel tubing. One of these spacers was cut to 120.4 mm (4.740 in.) to assure that the first plate was located 19.1 cm (7.50 in.) below the base of the liner. This 7.50 in. gap was necessary to allow for 12.7 cm (5.00 in.) of air standoff and 6.35 cm (2.50 in.) of water above the first target plate. The second spacer was cut to 16.5 cm (6.5 in.) and used below the last plate. The length of this spacer was not critical. Two 3/4"-10 grade 5 nuts (McMaster-Carr part no. 95462A538) were used to secure each threaded rod to base plate as shown in Figure 4.14. An additional nut was used to tighten the assembly on each rod. This nut provided compression of the spacer below the last target plate and therefore compressed the entire assembly. One 3/4"-10 coupler nut, 2.25 in. (57.15 mm) in length was used at the bottom of each threaded rod to allow for adjustable height of the assembly (McMaster-Carr part no. 90264A241). After the plate array was entirely assembled and attached to the baseplate, it could be bolted into the blast tank. The coupler nuts would then be extended to contact the bottom of the blast tank, providing added rigidity to the system. The plates themselves were obtained from Kurland's Steel in Champaign in the form of a 1.22 m by 2.44 m (4 ft. by 8 ft.) sheet of hot rolled A1011 low carbon steel. The author then used a bandsaw to slice this sheet into smaller 20.3 cm by 20.3 cm (8 in. by 8 in.) sections and a drill press owned by the group to drill 13/16 in. (20.64 mm) diameter holes in the corner of each plate to allow it to slide onto the four threaded rods.

Time of arrival The time of arrival gauges for the blast tank operated on the same principal as the time of arrival gauges in the containment tube (Figure 4.15). The only difference was in the wire routing. Instead of routing the lead wires through ports as in the case of the steel containment tube, the lead wires emerging from the silver foil were made to simply pass out of the tank through a small hole in the polyethylene cover that is placed over the tank during a test. The ground wire in this test setup was taped to the plate array using aluminum tape. For tests 11 and 12, five time of arrival gauges were used. For test 13, 12 gauges were used. In each test, the ground wire was taped to a plate deep in the plate array so that the wire would not become dislodged before it registered the arrival of the jet

Figure 4.13: Photo showing base plate with attached threaded rods, target plates, spacers, and nuts

Figure 4.14: (L)Photo showing base plate with threaded rods attached by two 3/4”-10 nuts (R)Bottom of plate array showing compressing spacer, compressing nut, and coupling nut

through the last gauged plate.

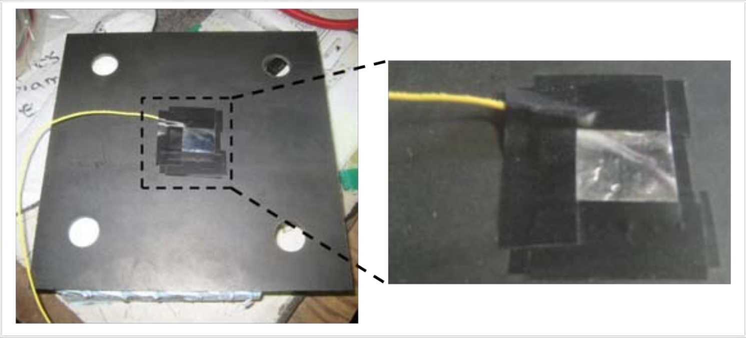

Figure 4.15: Time of arrival gauge as used in the blast tank. Inset shows detail of electrical tape attachment.

Velocity in air As mentioned previously, the Glumac-Krier research group had never obtained data regarding the jet tip velocity of any liner before it began to penetrate a target. The time of arrival gauges and high speed video images are useful for determining a penetration velocity, but cannot act as a measure of the true jet tip velocity. While the jet is penetrating a target, it has some penetration speed that is in fact the jet tip speed minus the speed at which the jet is being shortened due to erosion.

$$U = V - V_E \tag{4.4}$$

where U is the visually apparent penetration velocity gleaned from the high speed video results or the measured penetration velocity taken from the time of arrival data, V is the jet tip velocity, and V_E is the velocity of erosion of the jet. The penetration velocity, U, can be used to estimate V, the jet tip velocity using the following relationship derived from Bernoulli's equation as:

$$\rho_j (V - U)^2 = \rho_t U^2 \tag{4.5}$$

where ρ_j is the jet density and ρ_t is the target density. In order to experimentally determine the jet velocity in air before penetration of the water, a laser-based velocity measurement system was designed. Using the same principal as chronographs use to measure muzzle velocities, the laser system was designed to send two laser beams through the blast tank windows and into two photodiodes. When the jet passes through the laser beams, the photodiodes register the intensity drop. To find the velocity, all that is needed is the distance between the two laser beams and the time the jet crosses each beam. This system was implemented for tests 11 - 13.

There were several predicted difficulties with the system that were taken into account with the design. First, best estimates of the jet diameter predicted that it would be 1.5 to 2.5 mm. The laser beam was also on the order of 2 mm, and striking a 2 mm target with a 2 mm shaped charge jet was deemed very unlikely. Secondly, there were concerns that vibrations from the explosive event would disrupt the measurement system before the jet passed through the two beams. Finally, there were concerns about the amount of light that would be produced during the explosive event. The high speed camera images that had been obtained had in every case been saturated around the event during the early times, until at least 60 μs (Figure 4.16). If too much light entered the photodiodes from the event, it would be possible that the drop in intensity due to the jet's obstruction would be lost in the rising intensities of the event. It was also possible that the photodiodes could become saturated. After saturation, there is a small time taken to recover to normal operation. If the jet passed through the laser beam during the time the photodiode was saturated or recovering from saturation, the data would be lost. Each of these concerns was addressed in the design of the system.

In order to increase the likelihood that the jet would pass through the laser beam, an optical setup was prepared to expand the beam from a point into a line with a width of approximately 12.7 mm. The development of the laser beam shape as it passed through the optics is shown in Figure 4.17. The beam expander used two positive focal length cylindrical lenses from AnchorOptics to form a Keplerian style beam expander. The lenses were placed apart at a distance equal to the sum of the focal lengths of the individual lenses. The

Figure 4.16: Early image from the copper 50.75 mm test, showing large numbers of saturated pixels

expansion ratio was simply the ratio of the focal lengths. The laser chosen was a Helium-Neon laser from Melles-Griot (part no. 05-LHR-991). The manufacturer provided data for this laser is shown in Table 4.7. This laser had a beam diameter of 0.65 mm +/- 5% and divergence of 1.24 mR. It was estimated that the laser would be placed approximately 1.5 m from the event. At 1.5 m, the divergence of the beam creates a beam diameter of .836 mm. In order to expand that beam diameter to 12.7 mm, an expansion ratio of 15.2 was required. However, due to the constraints of the lenses available and the flexibility of the 12.7 mm desired beam width, the lenses chosen for the expander gave an expansion ratio of 9.2, resulting in a theoretical line width at the event of 7.7 mm (3/10 in.). The lenses were AnchorOptics part nos. AX27178 and AX27144. In addition to a 7.7 mm width, this laser line would have some height due to divergence of the beam in the vertical direction. A third cylindrical lens, AnchorOptics part no. 27148, was used during test 11 to attempt to minimize this line height without affecting the width. This lens was not used for tests 12 or 13 as it was not seen to be effective. A 25.4 mm (1.00 in.) diameter 50% beam splitter was used in combination with a 25.4 mm (1.00 in.) square mirror to split the laser into two parallel lines. The optical setup for test 11 is shown in Figure 4.18. It should be noted that after assembling the optics, the actual line width was much closer to 12.7 mm (0.5 in.) as desired (see Figure 4.17). This may have been due to the laser beam diameter not matching the manufacturer's specifications or due to visibility of the laser beam outside the $\frac{1}{e^2}$ diameter. Figure 4.17 shows the laser lines after they have passed entirely through the blast tank where they will be measured by the photodiodes.

Table 4.7: Specifications for the laser used in velocity measurements

Melles-Griot 05-LHR-991 Specifications	
Beam diameter ($\frac{1}{e^2}$)	.65 mm +/- 5%
Divergence	1.24 mR +/- 5%
Minimum output	10 mW
C/2L mode spacing	341 MHz
Nominal tube current	6.5 mA
Tube diameter	37 mm
Tube length	440 mm

The concern that vibrations from the event would change the alignment of the system before the jet passed through the laser beams was addressed using a simple vibrational analysis based on material sound speeds. As a worst-case scenario, analysis was performed on a hypothetical elastic wave that would begin at the instant of the detonation signal and originate at the base of the detonator. The time required for this wave to propagate through the tank to the tank windows was calculated. Figure 4.20 shows the path the wave is required to travel before reaching the window of the tank, divided into 5 stages. Table 4.8 tabulates the speeds the wave will travel through each stage, the distance of travel, and the time required for each stage. The required time for the sound wave to reach the edge of the window on the side of the blast tank is 208.7 μs, taking 6 km/s as the longitudinal sound speed of steel, 3.1 km/s as the transverse sound speed in steel, and 6.2 km/s as the detonation speed in sensitized nitromethane [8].

It is important that the jet passes through the laser lines before the sound waves reach the blast tank window. Table 4.9 describes the time required for formation of jets from 20.02

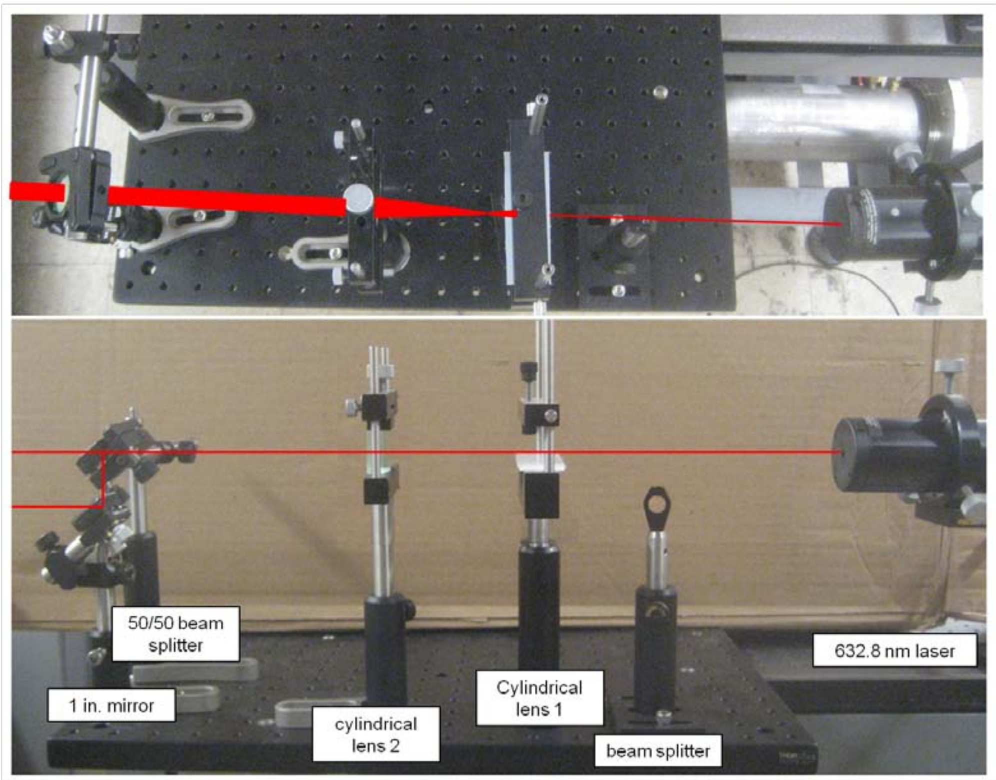

Figure 4.17: (Top) Top view of the optical setup for the laser velocity diagnostic (Bottom) Side view of the optical setup for the laser velocity diagnostic

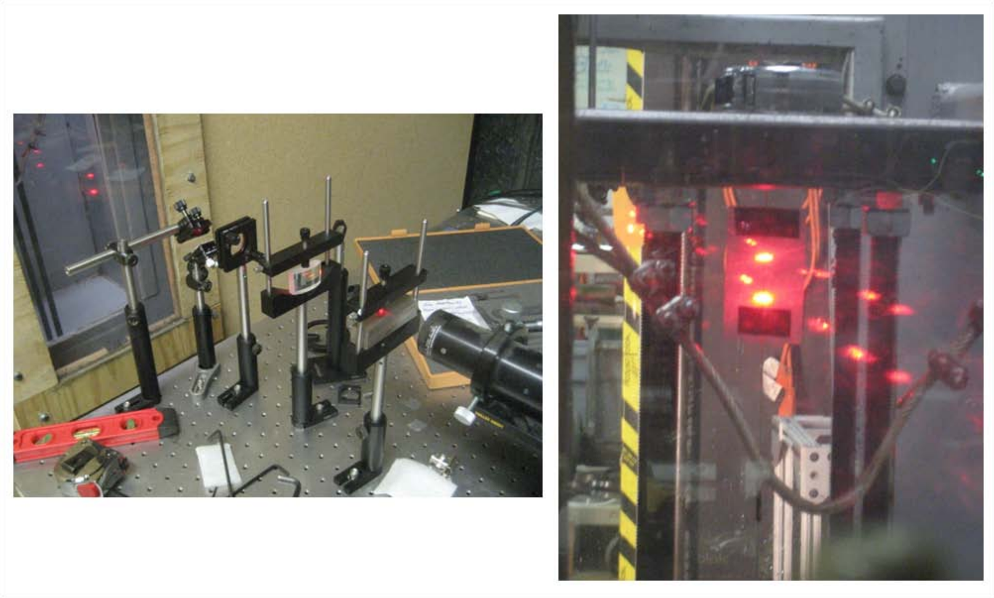

Figure 4.18: (L) Laser velocity diagnostic used for tests 11 - 13 (R) Multiple reflections as the laser passes through the sound enclosure and tank windows

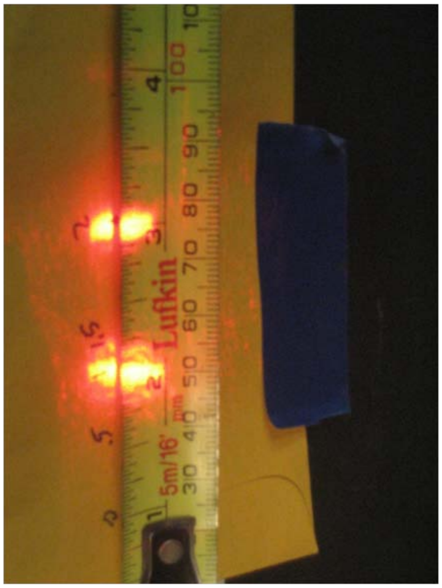

Figure 4.19: Laser line spacing, width, and thickness for test 11

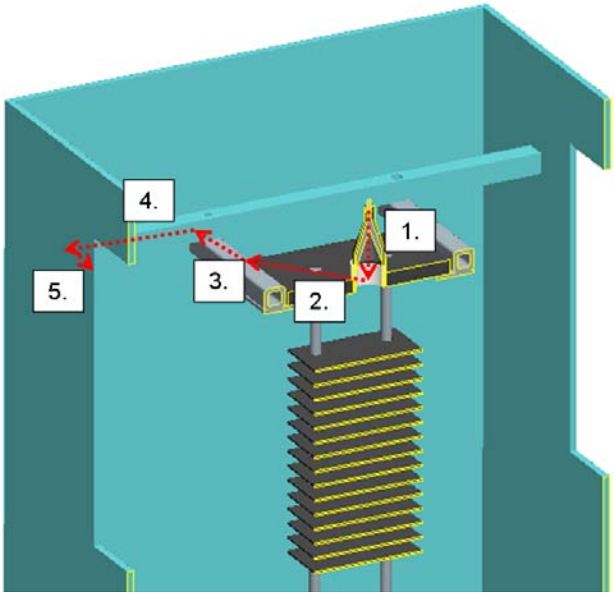

Figure 4.20: Path that waves must travel from detonator to tank window in order to potentially cause disturbances in laser velocity diagnostic

Table 4.8: Times required for waves to travel from detonator to blast tank window

Wave path to disrupt laser velocity diagnostic and required times				
Description	Distance Travelled (cm)	Wave Propagation - Material	Wave Speed (mm/s)	Time Required (μs)
detonator to base plate	10.7	nitromethane	6.20	17.2
center to edge of base plate	18.7	transverse wave - steel	3.10	60.3
base plate tube to tank tubes	7.8	transverse wave - steel	3.10	25.2
tank tube to outer wall	24.4	transverse wave - steel	3.10	78.7
down wall to window	16.4	longitudinal wave - steel	6.00	27.3
TOTAL				208.7

mm aluminum liners based on measurements from Rudolphi [24]. After the fireset sends the initiation signal to the detonator (Teledyne RISI Inc. RP-81) the function of the detonator is quoted by the manufacturer to last 5.38 μs. From Rudolphi's data, the average time of arrival at the first gauged plate was 29.50 μs after the initiating signal. Therefore, the detonation wave travelled through the high explosive, the jet formed, and the jet travelled through 76.2 mm (3.00 in.) of air and 25.4 mm (1.00 in.) of water in approximately 24.12 μs. This calculation assumes that the apex of the cone becomes the jet tip and hence has to travel 25.4 mm (1.00 in.) to reach the base of the cone and an additional 50.8 mm (2.00 in.) of air for the standoff distance. In the casing for the 20.02 mm. charge the distance from the end of the detonator to the apex of the cone is 42.2 mm (1.66 in.). Using 6.2 km/s as the detonation wave speed of nitromethane sensitized with DETA [8], this 42.2 mm (1.66 in.) distance would require 6.80 μs. 17.32 μs is left for the apex of the cone (where the jet tip is formed) to travel four inches (one inch to reach the base of the charge, two inches through the air standoff distance and one inch through the water on top of the first plate). The average velocity of the jet over this time is then 4.40 km/s. It should also be noted that the solid copper liner would have a slower average velocity than the solid aluminum liner due to its larger liner mass to charge mass ratio. Therefore, a solid copper liner is the worst case scenario when considering whether the jet will reach the water before the vibrations do. The same calculations are shown in Table 4.10 for the 20.02 mm copper liners fired by the author.

Table 4.9: Estimation of jet speed in air from Rudolphi's 20.02 mm solid Al liners

Estimation of Jet Speed in Air for 20.02 mm Aluminum Liner		
RP-81 Operation Time	5.38	μs
Distance from detonator to cone apex	42.2	mm
Detonation speed of nitromethane	6.20	km/s
Time required for HE propagation to cone apex	6.80	μs
Distance from cone apex to plate 1	76.2	mm
Time of arrival at plate 1	29.50	μs
Time for jet formation, travel through air and water	17.32	μs
Average velocity through air and water	4.40	km/s

Table 4.10: Estimation of jet speed in air from author's 20.02 mm Cu liners

Estimation of Jet Speed in Air for 20.02 mm Copper Liner		
RP-81 Operation Time	5.38	μs
Distance from detonator to cone apex	42.2	mm
Detonation speed of nitromethane	6.20	km/s
Time required for HE propagation to cone apex	6.80	μs
Distance from cone apex to plate 1	76.2	mm
Time of arrival at plate 1	32.60	μs
Time for jet formation, travel through air and water	20.42	μs
Average velocity through air and water	3.73	km/s

These data can be used to predict the time of arrival of a 50.75 mm aluminum or copper liner at the surface of the water in order to assure that it will strike the water before the vibrations of the tank will disrupt the optical measurement system. According to scaling relations, the tip velocity of the jet formed by the 20.02 mm diameter liner and the 50.75 mm diameter should be the same, or at least quite similar. Again, 5.38 μs are allowed for operation of the detonator. In the casing for the 50.75 mm charge, the distance from the end of the detonator to the apex of the cone is 37.3 mm (1.47 in.). Using a 6.2 km/s detonation wave speed, 6.20 μs is allowed for the detonation wave to reach the apex of the liner. At an average speed of 4.40 km/s the apex of the cone must travel 190.5 mm (7.50 in.), including 64.3 mm (2.53 in.) to reach base of cone and 127 mm (5.00 in.) through the air standoff distance, to reach the surface of the water in the blast tank. This travel will take approximately 43.47 μs. The total time after detonation for the jet tip to reach the surface of the water is therefore predicted to be 54.87 μs. Tables 4.11 and 4.12 show the pertinent information for the aluminum and copper liners respectively, including a further prediction of the time required to reach the first target plate and comparison with the first plate strike times of tests 11 and 12.

Since the jet is predicted to hit the water 154 μs before the time that the sound waves will reach the level of the water in the blast tank, it is safe to say that no disruption of the optical system will occur. Intuitively, a second argument for this same conclusion can

Table 4.11: Estimation of jet speed for 50.75 mm solid Al liners

Estimation of Jet Speed in Air for 50.75 mm Aluminum Liner Using Data from Table 4.9		
RP-81 Operation Time	5.38	μs
Distance from detonator to cone apex	37.3	mm
Detonation speed of nitromethane	6.20	km/s
Time required for HE propagation to cone apex	6.02	μs
Distance from cone apex to plate 1	191	mm
Average velocity through air and water	4.40	km/s
Time for jet formation, travel through air and water	43.47	μs
Time of arrival at water level (predicted)	54.87	μs
Time of arrival at plate 1 (predicted)	69.30	μs
Time of arrival at plate 1 (actual)	63.5, 65.3	μs

Table 4.12: Estimation of jet speed for 50.75 mm solid Cu liners

Estimation of Jet Speed in Air for 50.75 mm Copper Liner Using Data from Table 4.10		
RP-81 Operation Time	5.38	μs
Distance from detonator to cone apex	37.3	mm
Detonation speed of nitromethane	6.20	km/s
Time required for HE propagation to cone apex	6.02	μs
Distance from cone apex to plate 1	191	mm
Average velocity through air and water	3.73	km/s
Time for jet formation, travel through air and water	51.25	μs
Time of arrival at water level	62.65	μs
Time of arrival at plate 1	79.67	μs

be made. Based on the literature, solid copper liners of similar geometry accelerated by nitromethane have shown jet tip velocities on the order of 6 km/s. This is very close to both the detonation speed of nitromethane and the longitudinal sound speed of steel. Because the elastic waves must propagate out to the sides of the blast tank before propagating down to the level of the water, while the jet travels directly down to the water surface, it can be said with some certainty that the jet will reach the water before the sound waves do, as long as the formation of the jet occurs more quickly than the sound waves reaching the side of the tank.

Finally, to address the issue of the photodiode being exposed to large amounts of light during the event, an effort was made to estimate the light intensity of the event, and care was taken to reduce this amount of light. Since this optical system was designed after the first 50.75 mm diameter copper liner was fired, the high speed video images from this test were used to help estimate the amount of light the even produced. During that test, a significant number of the camera pixels were saturated at early times as shown in Figure 4.16. This saturation was recreated via a more controllable event using a professional photography flash. The blast tank was first filled with water and fitted with the plate array. The photodiodes that would monitor the laser intensity levels were placed next to the window in the blast tank in positions similar to those they would occupy during the shaped charge event. Attached to each Thorlabs PDA55 photodiode was a lens tube containing a 25.4 mm (1.00 in.) diameter PCX lens from AnchorOptics (part no. AX27694) that would be used to focus the laser line back onto the detector of the photodiode. Also in the lens tube was a 632.8 nm interference filter with 4 OD average out of band rejection. This bandpass filter allows 45% intensity of the helium-neon laser line, but has a 10 nm full width half maximum bandwidth to reject much of the broadband spectrum. Figure 4.21 shows the placement of the lenses within the lens tubes for tests 11 - 13. Only the placement of the PCX lens is critical to the operation of the photodiode. A Photogenic PL2500DR flash was used to model the light emission during the shaped charge event. The flash was oriented along an axis parallel to the jet penetration axis, but it was not placed in the middle of the tank. The setup of these flash recreations is shown in Figure 4.22. It was assumed that during a shaped charge test, the photodiodes would be seeing only incoherent light sources. Since the flash bulb was surrounded by a reflector and was directed straight down at the surface of the water, the photodiodes would also only receive incoherent light during the lighting simulations.

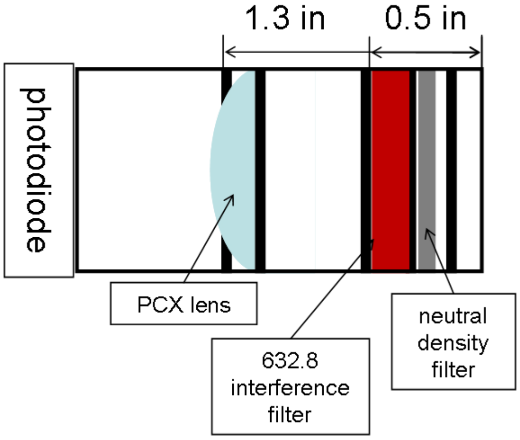

Figure 4.21: Placement of lenses within the lens tube

The PL2500DR was set at maximum intensity to give a worst case scenario. According to Photogenic Professional Lighting, the PL2500DR emits broadband light at a color temperature between 5800 and 6000K, as stated by a company representative. Pyrometry data from the literature suggests that early time nitromethane detonation temperatures can appear to achieve greater than 5500 K (the temperature of the shocked air rather than the adiabatic flame temperature of nitromethane), so this flash is a nice comparison [39]. The flash was able to completely saturate the entire sensor on the Phantom v7.0 when its settings were the same as were used in the solid copper 50.75 mm liner test. During this test, the PDA55 photodiodes reached only 2.06 V of their 0 to 10.8 V range. It was therefore deemed that the light emission from the event would not be a significant problem if the baseline intensity of the laser for each photo diode was kept sufficiently low. With all the concerns about the laser velocity measurement system addressed, the system was implemented for

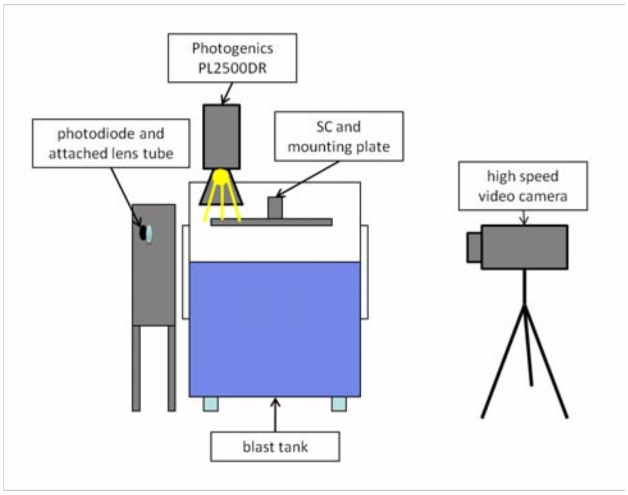

Figure 4.22: Experimental setup used to test camera saturation levels

tests 11 - 13. Accurate measurement of the distance between the laser lines was completed using a depth micrometer with a magnetically attached plate (see Figure 4.23. This plate contained a 100 μm wide slit, machined by fellow mechanical engineering master's student Ken Heinz using a Microlution micro machining machine. The depth micrometer was inserted into the charge retaining hole in the base plate, using clamped stock to hold it in place as shown in Figure 4.24. A pole on the underside of the base plate kept the slit from turning as the micrometer was extended. The micrometer was then extended until the most intense portion of the laser passed through the slit (this location was measured by reading the intensity on the photodiode). The same procedure was completed for the second laser line, and the distance between them was recorded. The accuracy of this method is estimated to be +/- .102 mm (0.004 in.) on the distance between the two lines.

4.2.4 Oil test

After noting that plates surrounding the last penetrated plate were significantly deformed in tests 11 and 12, a test was designed in a fluid that would not exhibit a reaction with the alumium liner. It was deemed that substituting water with a non-reacting fluid of similar density was the most achievable way to determine if the deep plate deformation was

Figure 4.23: (L) Laser line measuring attachment with 100 μm slit (R) Magnetic attachment to depth micrometer

Figure 4.24: Depth micrometer and slit attachment measuring depth of laser lines below base plate

attributable to the reaction of the liner with the fluid into which it was fired. Oil had been effectively used by Fant to prevent liner reaction in his work, and oil was chosen again as the non-reacting fluid here [23]. However, changes were made in both the experimental setup and the type of oil used.

To fire a 50.75 mm liner, the blast tank was again employed. In order to avoid filling the entire blast tank with oil, a new tank was made that was placed inside the blast tank. This tank was created using a polyethylene 55 gallon drum (obtained from Rural King) and two sheets of $\frac{3}{32}$ in. polycarbonate (McMaster part no. 8574K52). The drum was cut so that the polycarbonate sheets could be attached as windows, allowing viewing of the event. A schematic of the drum is shown in Figure 4.25. Adhesive backed silicone rubber strips (McMaster part no. 93755K33) were used with numerous 1/4”-20 bolts to create a mechanical seal that was effective in preventing most leaks. Bolts were required approximately every 2 inches (50 mm) along the joint between the polyethylene tank and the polycarbonate windows. Both rubber sealing washers (McMaster part no. 90130A027) and steel washers were used on both the inside and outside of the tank. Clear siliconized acrylic latex caulk (obtained from Doit Best) was used to build up the depressions on the inside of the plastic drum so that the rubber strips would seal well. The $\frac{3}{32}$ in. (2.38 mm) thick polycarbonate windows’ corners were rounded to allow easier bending into place.

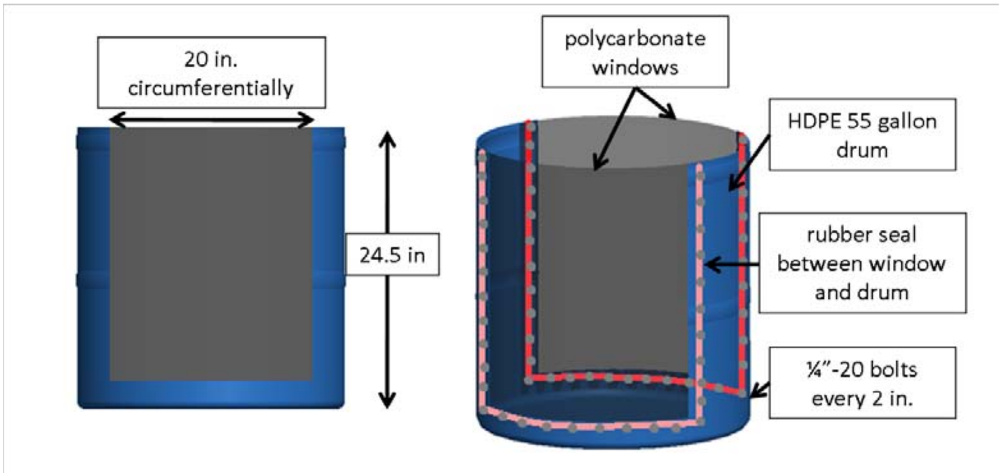

Figure 4.25: (L) Oil test tank dimensions (R) Oil test tank components

After the tank had been assembled and leak tested with water twice (both times exhibiting leaks slow enough to allow its use for testing), it was disassembled and placed into the blast tank. Due to size constraints, the oil tank could not be placed in the blast tank in its assembled form. Figure 4.26 gives an indication of the method used to slide the portion of the drum around the bars in the blast tank. When it was reassembled in the blast tank, a copious amount of siliconized caulk was used around the rubber seals and on each bolt. Aluminum tape further sealed the joints between the windows and the drum. The tank, when filled with oil, was entirely leak-free. Due to the high bending stiffness of the polycarbonate compared to the polyethylene, the tank was oblong when assembly was complete. Braces were cut from wood to place between the wall of the blast tank and the wall of the oil testing tank. These braces returned the oil test tank to a circular shape. Also, the oil test tank had to be raised 114 mm (4.5 in.) off the bottom of the blast tank to accomodate the necessary height of oil. After the oil test tank was raised, the top of the drum was 73.7 cm (29 in.) above the bottom of the blast tank. In a typical open water test, the water was filled to 73.3 mm ($28\frac{7}{8}$ in.) above the bottom of the blast tank. Figure 4.27 shows the oil test tank after being assembled inside the blast tank and a picture of the bolts and rubber strips used to seal the tank.

The inside diameter of the oil test tank was approximately 60 cm (23.5 in.). At its closest point, the corner of a target plate was only 15 cm (6.0 in) from the inside of the oil test tank. It was important to verify that this would allow sufficient time for the deformation of the plates to be completed before any shocks were able to reflect off the tank and return to the plate array. If the shock could reflect back to the plate array and contribute to plate deformation, the oil tank test would not accurately model the “unconfined” nature of the blast tank.

A prediction of the time of impact of the jet upon each plate and a prediction of penetration depth was therefore required. This prediction was accomplished via a somewhat unconventional method because time contraints did not allow a complete analytical or nu-

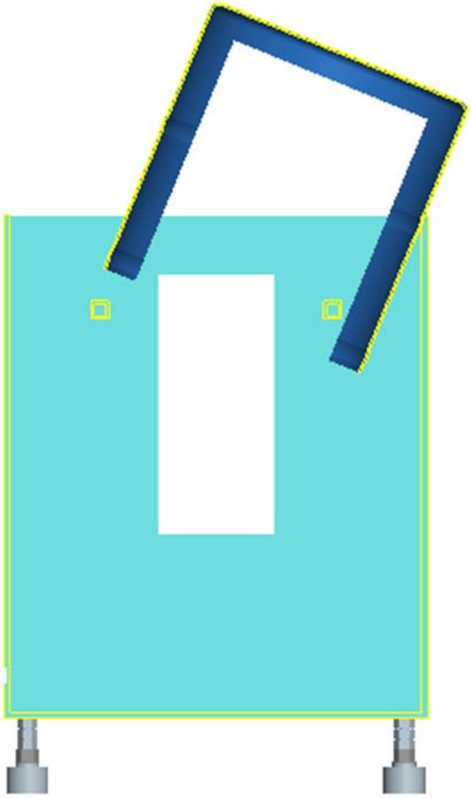

Figure 4.26: Working the oil test tank around the bars inside the blast tank

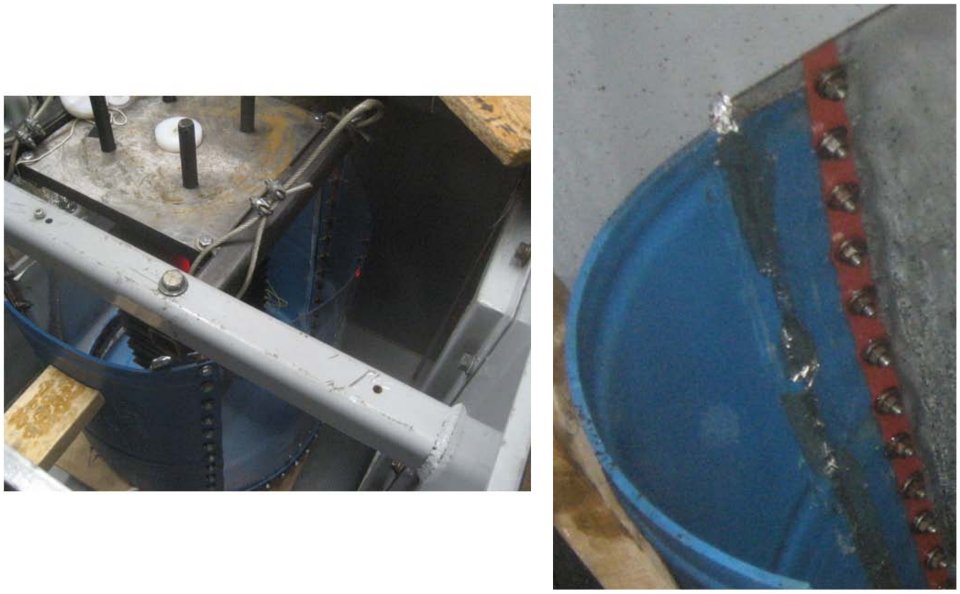

Figure 4.27: (L) Oil test tank assembled inside blast tank (R) Oil test tank seals

merical calculation. Drawing on the time of arrival and high speed video results of test 12, a fictional jet was assumed with a constant length of 20.3 cm (8 in.). This jet was given a tip velocity, a tail velocity, and a linear velocity gradient between tip and tail. Eqn. 4.6 shows that for a given depth of penetration, P, and known target and jet densities, ρ_T and ρ_j respectively, the length of erosion, l, of the jet can be calculated using Eqn. 4.6 [4].

$$l = P\sqrt{\frac{\rho_T}{\rho_j}} \tag{4.6}$$

It was assumed then that a given length of the jet was eroded for each plate penetrated, and a given length was eroded for each water (or oil) cavity penetrated. If one knows the velocity distribution along the jet, after a length is eroded away, the effective new "jet tip" velocity can be found. This prediction is merely a back of the envelope estimate, and does not reflect real jet characteristics such as the stretching jet or the break-up time. In addition, it cannot be used to estimate penetration for alternate geometries of liner or casing. However, fairly good agreement was found between this method and the tests performed by the author. It was predicted that the jet in oil would penetrate into or through plate 9 (in an oil of specific gravity .92). It was also predicted that the jet would hit plate 9 at 199 μs. After the test, it was seen that the jet in the oil test penetrated through plate 9 but did not strike plate 10. Plate 9 was struck at 189 μs, a deviation of only 5.0% from the predicted value.

It was next necessary to determine the time required for the shock wave to reflect from the oil test tank and reach the target plate array. The shock scenario most likely to contribute to target plate damage was that of the bow shock detaching from the jet (after the jet tip has slowed below the oil's sound speed), reflecting from the oil test tank wall or window, and reaching the target plates. It was estimated that, for an oil with a speed of sound of 1.26 km/s, the time required for a shock to move from the center of a target plate to the wall of the tank and back to the edge of the target plate would be approximately

360 μs. This time was nearly twice the predicted duration of the penetration event. The duration of the plate deformation process was still unknown, but because the oil test tank design was as large as was reasonable, it was decided to proceed with the test.

The selection of oil for the test was critical. It was desirable that the oil closely match the properties of water but remove the chance for the reaction of the aluminum liner to occur. Due to the dependence of penetration depth upon the density of the target, the density of the oil was the key property being matched to that of water. The oil that was chosen was Hygold L750 naphthenic base oil, and it was obtained from Mullen Circle Brand, Inc. Hygold L750 has a specific gravity of .92 and, according to a company representative, contains carbon, hydrogen, and nitrogen at 88 %, 12.8 %, and 0.3 % respectively. Very little oxygen content was desirable to prevent the combustion of the aluminum. Approximately 35 gallons of Hygold L750 were used during the test.

4.3 Charge Assemblies

Six distinct parts make up the charge assembly, as shown in Figure 4.28. The six parts are the casing, the liner, the high explosive, the detonator, the detonator retaining nut, and the polyethylene spacer. The detonators used for all tests were Teledyne RISI part no. RP-81, a PETN and RDX based detonator. The detonator was held in place using a polymer retaining nut for all tests. The high explosive used was for all tests was nitromethane (NM) sensitized with diethylenetriamene (DETA). The mixing ratio used for all tests was approximately 99% by volume NM and 1% by volume DETA. The amount of mixture used by the 20.02 mm tests was approximately 12 g (10.5 mL). The 50.75 mm diameter liner tests used approximately 67.8 g (60 mL).

The function of the polyethylene spacer was primarily to retain the liner and casing and locate it in the steel base plate. It also provided some disposable protection between the charge and the base plate so that the base plate was not damaged during the event.

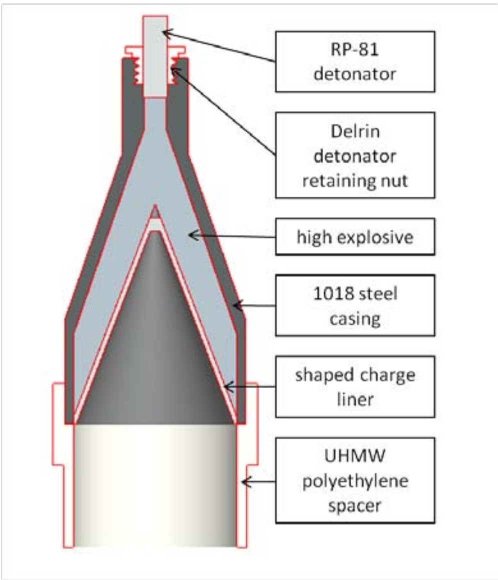

Figure 4.28: Charge assembly and components (1.998 in. liner design shown)

Drawings for the polyethylene spacers (both for the 20.02 mm diameter liner and the 50.75 mm diameter liner) are shown in Figures A.1 and A.2. Out of convenience, ultra high molecular weight polyethylene was used for all 1.998 in. diameter tests.

Four distinct geometries of liners were tested:

1. Solid liner of either copper or aluminum, 20.02 mm diameter (complete dimensions shown in Figure A.3) - tests 1, 2, 8, and 9
2. Cu/Al insert design, 20.02 mm diameter (complete dimensions shown in Figures A.4 and A.5) - tests 3, 4, 5, 6, and 7 *note that test 7 used this geometry without an aluminum insert
3. Solid copper liner, 50.75 mm diameter (complete dimensions shown in Figure A.6) - test 10
4. Solid aluminum liner, 50.75 mm diameter (complete dimensions shown in Figure A.7) - tests 11, 12, and 13

Note that the wall thickness and apex geometry of the 50.75 mm solid copper liner and 50.75

mm solid aluminum liner are different.

The casing design for the 20.02 mm diameter liners is shown with full dimensions in Figure A.8. This design is unchanged from Rudolphi's tests [24]. The casing design for the 50.75 mm charge is a product of the author, and it is shown with full dimensions in Figure A.9. This casing is heavily boattailed to keep the amount of high explosive to a minimum. This interior boattailing is followed on the exterior of the casing to minimize the amount of steel that will fragment and create damage during the event. The minimum head height requirements and casing thickness requirements are met. Dr. Ron Brown provided guidance regarding the appropriate height of the boattailed section.

4.4 Triggering and Data Acquisition

For tests 1 - 5, a RISI fire set (part no. FS61-B) was used to send a high voltage signal through twin leads to the detonator. Clamped around the twin leads was an inductive trigger that sent a signal to trigger the data acquisition systems. For tests 6 - 13, a pulse generator was used (either a Berkeley Nucleonics Corp. Model 500 or a Stanford Research Systems, Inc. Model DG535) to simultaneously trigger a RISI FS-43 fire set and the data acquisition systems and cameras. Generally, one triggering signal was sent to a given oscilloscope, and this signal was routed to each oscilloscope in turn through T-connectors in the BNC wires so that all oscilloscopes triggered simultaneously. If applicable, that trigger signal was also routed to the high speed camera.

The majority of the data acquisition for these tests was performed using a product of Pico Technology, Picoscope 3424. However, time of arrival data for tests 1 - 5 and test 13 was recorded through use of a Scope4PC (# SE420 + SE420ps). Example settings used in each test for the data acquisition system are given in Appendix B. Sample electrical connection diagrams are also seen in Appendix B for tests 12 and 13.

4.5 Safety Precautions

During a shaped charge test, numerous safety precautions are implemented. Most importantly, only Professor Nick Glumac and Professor Herman Krier are allowed to mix the NM and DETA, handle the mixture, or handle the detonator. For each test, a standard operating procedure (SOP) is followed. An example of the SOPs can be found in Appendix C for test 12. Physical safety devices are described in detail by Bill, Fant, and Rudolphi [22, 23, 24]. These devices include a 25.4 mm (1.0 in.) thick steel shroud surrounding the charge. This shroud is secured to the baseplate and lined with sacrificial plates that absorb the fragmentation of the casing so that the shroud is not damaged. A polyethylene cover is placed over the blast tank and around the shroud. This cover is secured with four tie down straps. A 6.35 mm ($\frac{1}{4}$ in.) thick steel plate is laid over the top of the shroud. On top of this plate is placed a rubber mat which is covered and retained by five sand bags, which are covered with a rope blast mat. The test area is then surrounded by 6.35 mm ($\frac{1}{4}$ in.) thick steel plates on all four sides within the sound enclosure.

A few additional safety precautions were added during the test of the 50.75 mm diameter copper liner. On the bottom of the blast tank, an alternating structure of three 2.54 cm thick, 45.7 cm by 45.7 cm square (1 in. thick, 18 in by 18 in.) square steel plates and 3 layers of 2-by-4s were placed, as shown in Figure 4.29. This steel and wood was added to prevent the liner from perforating the bottom of the blast tank. Also, the sacrificial plates used to protect the shroud from casing fragments were increased in thickness from 3.18 mm ($\frac{1}{8}$ in.) to 6.35 mm ($\frac{1}{4}$ in.) These 6.35 mm ($\frac{1}{4}$ in) sacrificial plates were used for tests 11 - 13 as well.

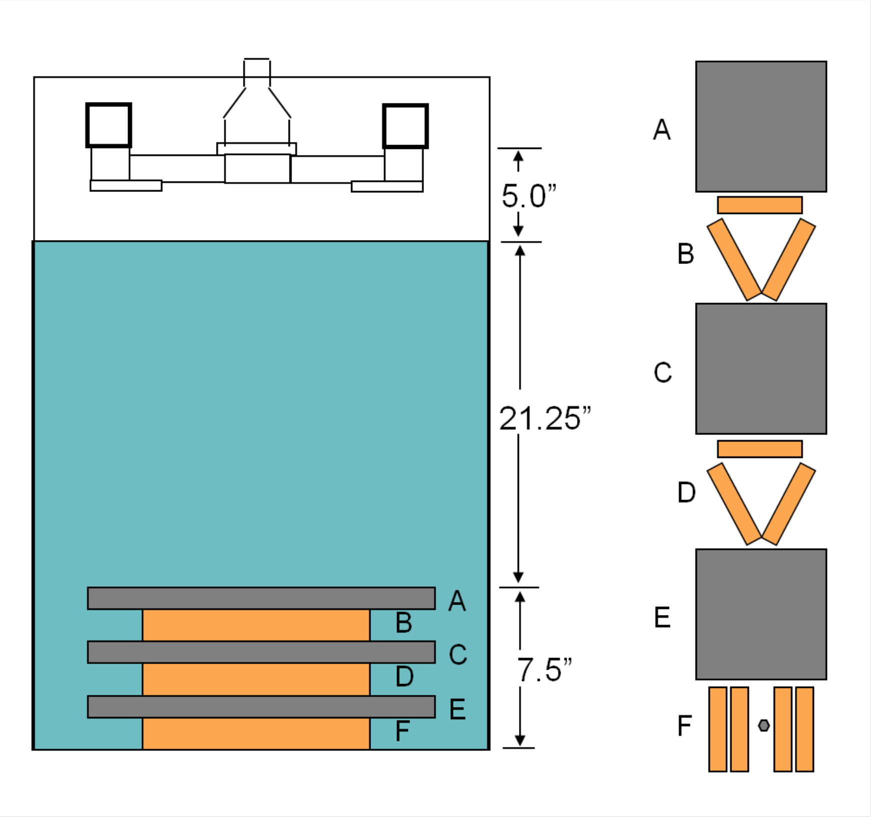

Figure 4.29: Setup for test 10 showing alternating layers of steel and 2 x 4 ’s

CHAPTER 5

RESULTS AND DISCUSSION

Results from the shaped charge tests are presented below, grouped by category of similar tests. Tests 1 - 5, because they involved liners of 20.02 mm diameter and were conducted in the steel containment tube, will be discussed first. Secondly, tests 6 - 9 will be discussed as they involved liners of 20.02 mm diameter and were fired into open water in the blast tank. Thirdly, tests 10 - 13 will be discussed as they involved liners of 50.75 mm diameter and were fired in the blast tank. Tests 10 - 12 were fired into water while test 13 was fired into oil. Within each test grouping, results will be segmented by diagnostic. More complete results exist in the appendices and are referenced as required.

5.1 Tests 1 - 5: 20.02 mm Diameter Liners Fired in the Containment Tube

5.1.1 Light emission

Test 1 and test 2 showed significant light emission only in cavity one, above the first target plate in the steel containment tube (Figures E.1 and E.6). This light is likely emission from the detonation event only. No light is seen from the liner itself or the penetration of the liner through the target plates. Indeed, no luminosity of the liner is expected for solid copper liners since an exothermic reaction does not occur with water at these conditions. Tests 3, 4, and 5, however, show significant light emission in cavity one and deeper cavities (Figures E.11, E.16, and E.21 respectively). Luminosity is seen in the deepest cavity reached by the jet for Tests 3, 4, and 5. Test 3 penetrated through target plate 3 and into cavity four. Test 3 exhibited light emission in each cavity reached, although the light emission in cavity four is quite small, suggesting that a significant portion of aluminum did not react in this cavity. Test 3 also exhibits a sustained light emission event in cavity 3 that continues for 1.25 ms. Test 4 penetrated to cavity 5 and exhibited light emission in cavities 1 through 5. Cavity 4 showed the longest light emission event with a duration of 0.75 ms. Finally, test 5 penetrated to cavity 4 and exhibited luminosity in cavities 1 through 4. Test 5, similar to test 3, showed two light emission peaks for cavities 2 and 3. The reason for this double peak is not known and requires further investigation. It is feasible that this effect could be the reaction of the slug. Stronger than expected light emission was typically seen in cavity 3.

These results demonstrate that the Cu/Al insert design allows the aluminum to reach sufficiently high velocities to undergo the energetic reaction seen by previous University of Illinois researchers. In addition, it is evident that the aluminum from each composite liner reached a similar penetration depth, and achieved hydroreaction at that depth, as the maximum depth penetrated by the liner.

5.1.2 Pressure

Pressure data recorded during tests 1 - 5 can be seen in Figures E.4, E.9, E.14, E.19, and E.24 respectively. Due to the ability to record pressures at various cavities in the steel containment tube or at the bottom flange of the steel containment tube, few direct comparisons can be made between tests 1 - 5. Table 5.1 shows the maximum pressure recorded at each location for each test. Test 1 shows the highest pressure recorded during any of the first five tests. However, this pressure (cavity 2) may not be completely trusted. The pressure of 27432 psi was recorded by a pressure transducer with a maximum rated range of 25000 psi (a Kistler 603B1). In tests 3, 4, and 5, the Cu/Al insert liners penetrated through 3 plates, 4 plates, and 3 plates respectively. Since each of these liners penetrated into cavity 4, it is of interest to compare pressures in cavity 4 across all tests. Test 5 exhibited a pressure of 24010 psi in cavity 4, the highest seen in any test. This pressure is significantly higher than the pressures produced by other Cu/Al insert liners. The reasons for this high pressure are not clear. Peak pressures in tests 2 - 4, in cavity 4, differ by only 11.8%.

It should be noted here that an increase in pressure does not necessarily mean that the shaped charge would perform better in a given application or that it is more desirable overall. From the view of maximization of penetration, unless the pressure comes from a hydroreaction, it is wasted energy. Hydroreaction, however, is a largely separate mechanism from penetration. Pressure from hydroreaction is therefore seen as an enhancement to the charge behavior.

Table 5.1: Maximum pressures recorded by location, tests 1 - 5

Peak Pressures Recorded by Test No. and Location (psi)					
	Test 1	*Test 2*	*Test 3*	*Test 4*	*Test 5*
Cavity 2	27432*	**	**	**	**
Cavity 4	**	18910	19070	17058	24010
Cavity 6	14158	13762	**	**	9512
Cavity 9	**	**	7709	**	5747
Tube Bottom	8068	6084	7826	**	5464
**transcducer exceeded rated range of 25,000 psi*					
*** pressure data was not recorded*					

5.1.3 Depth of penetration, plate deformation, and hole size

Depth of penetration for tests 1 - 5 are shown in Table 5.2. Note that each test 1 - 5 had an air standoff distance of 50.8 mm, a spacer thickness of 12.7 mm, and used water as the target fluid. Tests 1 and 2, those of solid copper liners, penetrated through eight target plates and the water between these plates. However, tests 3 - 5 exhibited significantly lower penetration. The average distance of steel penetrated by the Cu/Al insert liners was 6.6 mm (0.26 in.) while the average distance of steel penetrated by the solid copper liners was 14.9 mm (0.588 in.). The decreased penetration distance indicates clearly that the introduction of the aluminum insert in these tests was a large factor in decreasing total penetration depth.

Deformation plots were constructed for tests 1 - 5 and can be seen in Figures E.5, E.10, E.15, E.20, and E.25 respectively. Note that the maximum positive deformation (due to overpressure in cavity 2) of plate 1 is definitively higher in tests 3 - 5 than tests 1 and 2. Test 3 exhibited a high level of deformation in plates 7, 8, and 9 compared to tests 1, 2, 4, or 5 even though the jet did not penetrate past plate 4 in this test. Test 4 showed similarly high levels of deformation in plates 4 and 5. Plate 5 shows an off-center bulging that seems to indicate that the jet impacted this plate off-center. However, the jet impact, although slightly off center, is not off center in the direction of maximum deformation of the plate.

Three measurements were taken using calipers to determine the hole size of penetrated plates and the impact size of partially penetrated plates. These three measurements help to reflect the often oblong shape of the holes and should not be interpreted to be three measurements of the same distance. Hole size data is shown in Figures E.3, E.8, E.13, E.18, and E.23 for tests 1 - 5 respectively and summarized as average hole sizes in Tables 5.3, 5.4, 5.5, 5.6, and 5.7. Test 4 showed the smallest average hole diameter in plate 1 for any test 1 - 5. Tests 3 and 5, of the same liner design, had average plate 1 hole sizes 170% and 214% larger than test 4. Interestingly, test 4 was also the deepest penetrating Cu/Al liner. In these series of tests, it appears that the average hole diameter in plate 1 is a relatively good indicator of penetration performance. A poorly formed jet can result in a large hole size, because the jet is not long and/or thin, and does not exhibit axial precision. However, a large hole size can also be an indication of enhanced damage due to hydroreaction. In this series of tests, the hole diameter at the final plate penetrated is not larger than expected for the Cu/Al insert liners. A consistent hole size between the Cu/Al insert liners and the solid Cu liners may indicate that the reaction undergone by the aluminum is not significantly contributing to the average hole size.

Table 5.2: Penetration results, tests 1 - 5

Penetration Summary by Test							
	Liner design/material	*Plates completely penetrated*	*Next plate struck*	*Plate thickness (mm)*	*Distance of fluid Penetrated (mm)*	*Distance of steel penetrated (mm)*	*Total penetration depth (mm)*
Test 1	solid Cu	8	no	1.87	114.3	14.94	129.24
Test 2	solid Cu	8	no	1.87	114.3	14.94	129.24
Test 3	Cu/Al Insert	3	no	1.87	50.8	5.60	56.40
Test 4	Cu/Al Insert	4	yes	1.99	76.2	7.98	84.18
Test 5	Cu/Al Insert	3	yes	1.99	63.5	5.98	69.48

Table 5.3: Hole size data for penetrated plates, test 1

Test 1				
Plate No.	*Measurement 1*	*Measurement 2*	*Measurement 3*	*Avg hole diameter (mm)*
1	8.46	6.96	4.52	6.65
2	8.46	4.98	3.89	5.78
3	3.7	3.69	2.1	3.16
4	2.14	2.64	2.31	2.36
5	2.35	2.46	2.36	2.39
6	2.84	2.58	3.12	2.85
7	3.2	3.04	2.88	3.04
8	1.84	1.82	2.28	1.98

Table 5.4: Hole size data for penetrated plates, test 2

Test 2				
Plate No.	*Measurement 1*	*Measurement 2*	*Measurement 3*	*Avg hole diameter (mm)*
1	11	6.35	5.76	7.70
2	8	4.87	3.88	5.58
3	10.34	5.52	2.89	6.25
4	4.08	3.2	1.5	2.93
5	4.16	2.12	2.22	2.83
6	4.34	2.48	2.92	3.25
7	3.2	2.66	2.6	2.82
8	3.84	1.88	2.18	2.63

Table 5.5: Hole size data for penetrated plates, test 3

Test 3				
Plate No.	*Measurement 1*	*Measurement 2*	*Measurement 3*	*Avg hole diameter (mm)*
1	19.82	8.56	6.44	11.61
2	5.25	6.5	5.28	5.28
3	< 1.00			< 1.00

Table 5.6: Hole size data for penetrated plates, test 4

Test 4				
Plate No.	*Measurement 1*	*Measurement 2*	*Measurement 3*	*Avg hole diameter (mm)*
1	6.39	4.88	5.03	5.43
2	5.17	4.78	5.17	5.04
3	3.94	2.91	3.63	3.49
4	< 2.00			< 2.00

Table 5.7: Hole size data for penetrated plates, test 5

Test 5				
Plate No.	*Measurement 1*	*Measurement 2*	*Measurement 3*	*Avg hole diameter (mm)*
1	13.81	7.68	6.24	9.24
2	5.82	3.46	4.56	4.61
3	3.05	4.05	3.23	3.44
*4**	1.99	2.28	1.26	1.84
*plate not completely penetrated				

5.1.4 Velocity from time of arrival gauges

Tables 5.8, 5.9, 5.10, 5.11, and 5.12 show the time of arrival of each liner at the target plates reached for tests 1 - 5 and the calculated penetration velocity of the liners based on the distance between subsequent target plates. The solid copper liners, tests 1 and 2, have higher velocities through each of the first five cavities than the Cu/Al insert liners have through any cavity. Repeatability of the measured speeds of test 1 and 2 is fair. Cavity 4 shows the largest disagreement (34.0%) between tests 1 and 2. Repeatability of the Cu/Al insert liners is good in the cavities 2 and 3, the only cavities where velocity could be measured for all three tests. The largest discrepancy is seen in cavity 2 between tests 3 and 4 (17.8%).

Table 5.8: Time of arrival data, test 1

Time of Arrival - Test 1		
Plate #	*Time of Impact (μs)*	*Velocity (km/s)*
1	35.45	
2	39.80	3.35
3	44.50	3.10
4	50.25	2.53
5	56.65	2.28

The absolute time of arrival (or the time elapsed between the fire signal from the fire set and the time the jet first impacts a plate) for plate 1 is quite consistent across all 5 tests. The largest difference is between tests 1 and 2 (35.45 μs and 31.76 μs respectively) giving a difference of 11.6%.

Table 5.9: Time of arrival data, test 2

Time of Arrival - Test 2		
Plate #	*Time of Impact (μs)*	*Velocity (km/s)*
1	31.76	
2	36.06	3.39
3	40.41	3.35
4	44.71	3.39
5	49.81	2.86

Table 5.10: Time of arrival data, test 3

Time of Arrival - Test 3		
Plate #	*Time of Impact (μs)*	*Velocity (km/s)*
1	34.55	
2	43.50	1.63
3	51.5*	1.82
4	NA	
5	NA	
*difficult to distinguish		

Table 5.11: Time of arrival data, test 4

Time of Arrival - Test 4		
Plate #	*Time of Impact (μs)*	*Velocity (km/s)*
1	35.10	
2	42.75	1.92
3	52.55	1.50
4	69.35	0.87
5	105.40	0.41

Table 5.12: Time of arrival data, test 5

Time of Arrival - Test 5		
Plate #	*Time of Impact (μs)*	*Velocity (km/s)*
1	33.30	
2	42.25	1.64
3	51.25	1.63
4	inconclusive	
5	NA	

5.1.5 Discussion

The most important results of tests 1 - 5 primarily related to the poor performance of the bimetallic liners when compared to the solid copper liners. By introducing the aluminum insert into the copper geometry, the total penetration distance through steel decreased by an average of 55.8%, and the average peak penetration velocities decreased by 48.7%. In fact, the Cu/Al insert liners did not achieve penetration equal to the solid aluminum liners fired by Rudolphi [24]. Peak pressures of the Cu/Al insert were very similar to the solid copper liners, and deformation and hole size data did not conclusively indicate an increase in damage production.

Light emission data clearly indicated evidence of hydroreaction in the deepest penetrated cavities for all Cu/Al tests, an indication that sufficient velocities were being achieved by the aluminum insert to undergo the hydroreaction. However, the causes of poor performance were unclear. A need was therefore identified for testing of these liners with optical access to further investigate their behavior. This need led the project to tests 6 - 9 which involved liners fired into the open water tank.

5.2 Tests 6 - 9: 20.02 mm Diameter Liners Fired into Open Water

5.2.1 Pressure

Pressure data was recorded for tests 6, 8 and 9, and results are shown in Figures E.26, E.29, and E.31 respectively. Pressure data was not recorded for test 7. Table 5.13 shows the maximum pressure recorded by each pressure transducer during the tests. Table 5.13 also indicates the depth at which the transducers were mounted relative to the base of the liner. Transducers at all depths were mounted 26.7 cm (10.5 in.) off the penetration axis of the charge. Test 6, that of the Cu/Al insert design, showed the lowest peak pressures of this series of tests in both transducer locations which corroborates results from tests 1 - 5 in that the addition of the aluminum insert did not increase the peak pressure delivered to the surrounding environment. The highest peak pressures were recorded during the test of the solid aluminum liner, test 8. During this test, transducer 1 had a peak pressure 39.5% higher than the solid copper liner. Transducer 2 recorded a peak pressure 48.0% higher than the solid copper liner. These differences are evident even though the solid copper liner penetrated more quickly and more deeply than the solid aluminum liner (see Figure D.4 for solid copper penetration images and Figure D.3 for solid aluminum penetration images).

5.2.2 High speed video images

High speed video images in this report are labeled by the time that the image was taken after the first light emission is seen in the frame. This light emission is due to the high explosive detonation. However, because the exact time of first light emission cannot be determined (it could actually appear between frames), there is an uncertainty inherent in the time measurement equal to the frame interval time. Images sequences for tests 6 - 9 are given in Figures D.1, D.2, D.3, and D.4 in Appendix D. Figure 5.1 shows a comparison of images from each test at approximately 81 μs after the first light emission is seen from the high explosive. It shows the relative depth of penetration of each liner. Test 9 has the most highly penetrating jet, followed first by test 8, then by test 7, and finally by test 6. The view of these images does not show the jet, but the cavity surrounding the jet. This cavity is opaque due to material from the jet that is eroding. Some indication of jet formation may be able to be deduced from the shape of the cavity in concert with the depth and speed of penetration. The copper liner from test 9 forms a thin cavity and quickly penetrates through the majority of the viewing frame. Conversely, the composite liner designs (tests 6 and 7) have wider cavities and penetrate slowly. A wider cavity could also indicate a release of energy due to hydroreaction. Test 7 shows features indicating fragmentation of the jet as

Table 5.13: Peak pressures recorded by test no. and location, tests 6 - 13

<table>
<tr><th colspan="9">Peak Pressures Recorded by Test No. and Location</th></tr>
<tr><th></th><th><i>Test 6</i></th><th><i>Test 7</i></th><th><i>Test 8</i></th><th><i>Test 9</i></th><th><i>Test 10</i></th><th><i>Test 11</i></th><th><i>Test 12</i></th><th><i>Test 13</i></th></tr>
<tr><td><i>Transducer 1 (psi)</i></td><td>618</td><td>*</td><td>1080</td><td>774</td><td>*</td><td>*</td><td>*</td><td>*</td></tr>
<tr><td><i>Depth of transducer 1 below liner base (mm)</i></td><td>203</td><td></td><td>203</td><td>203</td><td></td><td></td><td></td><td></td></tr>
<tr><td><i>Transducer 2 (psi)</i></td><td>772</td><td>*</td><td>1209</td><td>817</td><td>3103</td><td>*</td><td>*</td><td>*</td></tr>
<tr><td><i>Depth of transducer 2 below liner base (mm)</i></td><td>368</td><td></td><td>368</td><td>368</td><td>368.3</td><td></td><td></td><td></td></tr>
<tr><td colspan="9">*pressure data was not recorded</td></tr>
</table>

early as 100.50 μs after initial light emission.

The aluminum containing liners exhibit luminosity as expected, while the liners without aluminum do not exhibit luminosity. Test 6 shows early luminosity at the jet tip. This tip luminosity was a surprising result contrary to the objective of placing the reactive aluminum in the back of the jet. However, persistent luminosity does manifest itself approximately midway down the depth of the cavity (see times 113.75 μs - 211.25 μs, Figure D.1).

5.2.3 Velocity

Velocities for tests 6 - 9 were calculated from high speed video images using a calibration grid to determine the number of pixels per mm at the event plane. These velocities are shown in Figures E.27, E.28, E.30, and E.32 respectively. Velocities were calculated until the jet either reached the bottom of the viewing plane or until sufficiently low velocities were achieved. The solid aluminum liner, test 8, achieved a maximum velocity of 3.78 km/s, slightly higher than the solid copper liner (3.65 km/s) and significantly higher than both the Cu/Al insert liner (1.17 km/s) and the Cu/Al liner without the aluminum insert (2.22 km/s). Note that due to the intense light emission of the high explosive initially, the position of the jet tip in test 6 could not be determined until the 2nd frame after initial light emission. Test 7 and 9 could be resolved during the first frame after initial light emission, and test 8 could be resolved during the first frame of light emission. Since the velocity of the jet drops so quickly, it is safe to assume that test 6, had the jet tip been able to be resolved, would have had a significantly higher peak penetration velocity. Likewise, the peak velocities for test 7 and 9 would increase. The liners of tests 6 and 7 exhibited not a single, coherent penetration event, but multiple penetration stages. It is likely that the primary stage indicates penetration of the jet tip while subsequent stages indicate either movement of the slug or movement of jet fragments after breakup of the jet.

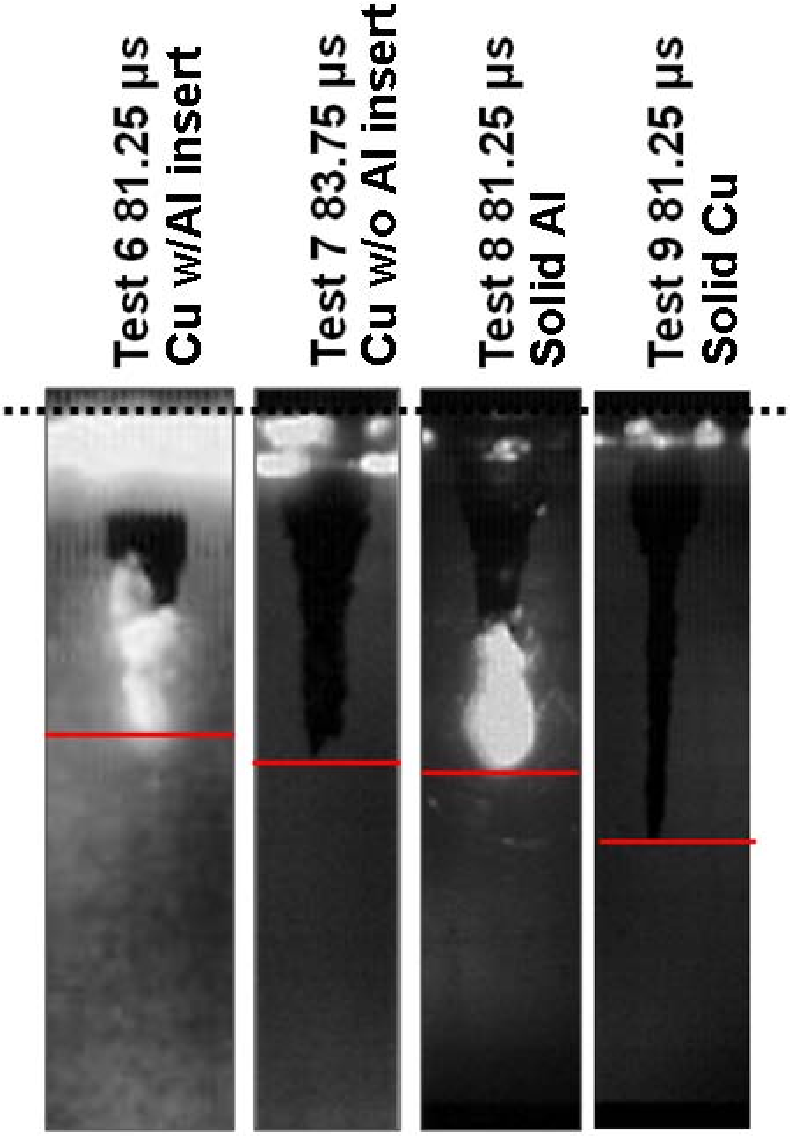

Figure 5.1: Comparison of high speed video images close to 81 μs. (Note that images have been scaled equally). The dashed line denotes the bottom of the base plate. The red line denotes the current penetration level.

5.2.4 Discussion

The high speed video images of tests 6 - 9 demonstrated conclusively that the Cu/Al insert design was not creating a well-formed jet. In fact, the Cu/Al penetrated more slowly than the solid aluminum liner. It is also important the Cu/Al liner without the aluminum insert performed poorly (slow penetration and apparent fragmentation). In this case, there were no bimetallic interactions and no impedance mismatches in the liner, but poor performance persisted. Several theories could explain this behavior. First, there could be an inherent flaw in the liner design. Perhaps the liner collapse cannot occur adequately with a significant step in the liner wall that creates a harsh transition in wall thickness. Alternatively, the machining required to create this step may have introduced small asymmetries in the liner. At this small scale, as noted previously in this report, small asymmetries can cause a large effect on liner performance. Both the assumption about the precision required and the assumption that bonding was not required between the materials in the liner deserve to be revisited.

5.3 Tests 10 - 13: 50.75 mm Diameter Liners Fired into the Blast Tank

Test 10 of a solid copper liner was conducted to verify the ability of the facilities to handle larger scale liners of 50.75 mm diameter. The test was lightly instrumented, using only high speed video imaging and a single pressure transducer mounted 36.8 cm (14.5 in.) below the base of the liner. Three 2.54 cm (1.0 in.) thick steel plates were placed at the bottom of the test tank to prevent the jet from perforating the test tank. After the facilities had been shown to safely handle this larger charge, three tests of 50.75 mm diameter solid aluminum liners were fired through target plate arrays. These tests, 11 - 13, also included time of arrival gauges, high speed video imagaing, and an optical measuring system to determine jet tip velocity before the jet began to penetrate the water. Pressure transducers were used for tests 11 and 12, but they did not record any data. Test 10 and tests 11 - 13 will be discussed separately due to the difference in the diagnostics accompanying the tests.

5.3.1 Test 10 - Pressure

As mentioned previously, test 10 is the only 50.75 mm diameter liner test in which a pressure transducer successfully recorded data. The pressure data are shown in Figure E.33 and the peak pressure recorded was 3103 psi. This pressure is 380% greater than the peak pressure of the solid copper charge of 20.02 mm diameter recorded at the same depth. Evidence of the reflected shock returning to the transducer from the tank walls can easily be seen as well.

5.3.2 Test 10 - Velocity from high speed video images

Velocity calculations showed a peak penetration velocity of 4.20 km/s. Again, the tip position could not be resolved until the fifth frame after initial light emission was seen, so it is likely the tip velocity was higher earlier in the penetration event (Figures D.5, D.6). The penetration velocity during test 10 was significantly higher than the smaller scale solid copper liner, test 9, at comparable times (Figure 5.2). At 66.5 μs a very well formed jet can be seen emerging from a previously wider cavity (Figure D.5).

5.3.3 Tests 11 - 13 - High speed video images

Velocity data were not extracted from the high speed video images for these tests. Test 11 was highly saturated even through late times (Figures D.7, D.8). Test 12 also showed saturation through late times although the saturated areas of the images were much smaller than test 11 (Figures D.9, D.10). This reduction in saturation was achieved by using an f/# of 3.8 for test 12 while f/# 1.3 was used for test 11. For test 13, Figure D.11 shows one image of the plate array taken prior to the event, but using the same lighting conditions

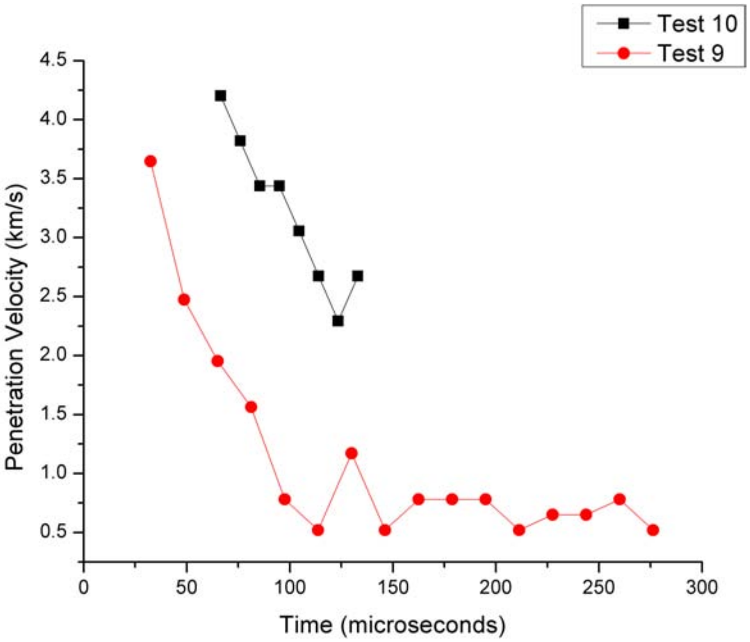

Figure 5.2: Comparison of small scale (test 9) and large scale (test 10) solid copper penetration velocities

as the event: two Photogenics PL2500DR flashes. These flashes have a slight delay after triggering to reach a maximum lighting level. The flashes were set at an intensity value of 500 for this test, while the f/# on the high speed camera lens was set to 5.6. This provided enough light to resolve the plates in the dark oil and saturated very few pixels. Test 11 used an 8 mm camera lens and was situated approximately 1.5 m (5 ft.) from the charge axis. Tests 12 and 13 used a 25 mm camera lens that was situated approximately 3.7 m (12 ft.) from the charge axis. Both tests used the VisionResearch Phantom 7.0 high speed camera.

5.3.4 Tests 11 - 13 - Velocity from time of arrival gauges

The time of impact of the jet upon each of the gauged plates for tests 11 - 13 are shown in Tables 5.14, 5.15, and 5.16 respectively with the velocities calculated from the time of arrival gauges. Repeatability is seen to be fairly good, with impact of the first plate occurring at 65.30 μs for test 11, 63.51 μs for test 12, and 60.86 μs for test 13. Peak penetration velocity of test 11 was 2.84 km/s, while test 12 showed 2.90 km/s, and test 13 showed 2.56 km/s.

These peak penetration velocities are in agreement with velocities measured for aluminum and aluminum alloy liners with a 20.02 mm diameter liner measured by Rudolphi to be between 2.1 and 2.9 km/s [24].

Table 5.14: Time of arrival data and calculated velocity, test 11

Time of Arrival - Test 11		
Plate #	*Time of Impact (μs)*	*Velocity (km/s)*
1	65.30	
2	74.54	2.84
3	87.94	1.96
4	101.18	1.98
5	119.38	1.44

Table 5.15: Time of arrival data and calculated velocity, test 12

Time of Arrival - Test 12		
Plate #	*Time of Impact (μs)*	*Velocity (km/s)*
1	63.51	
2	72.51	2.90
3	84.31	2.21
4	97.91	1.92
5	112.31	1.82

The method used to predict the time of arrival for the aluminum jet in oil (test 13) is evaluated in Table 5.17. This method used data from tests 11 and 12 to determine that an effective jet length was approximately 203 cm. This jet was assigned a linear velocity gradient from the tip (6.43 km/s) to the tail (0.76 km/s) but was not allowed to stretch. The jet was assumed to cease penetration of steel plates when the penetration velocity dropped below 0.4 km/s. The length of jet eroded for each plate or each fluid cavity penetrated was determined using eqn. 4.6. Very nice comparison is seen in Table 5.17. Again, the reader is cautioned that this predictive method was based on specific experimental data and was only developed to observe the results when the target fluid was changed from water to oil.

Table 5.16: Time of arrival data and calculated velocity, test 13

Time of Arrival - Test 13		
Plate #	*Time of Impact (μs)*	*Velocity (km/s)*
1	60.86	
2	71.06	2.56
3	84.26	1.98
4	97.30	2.01
5	110.25	2.02
6	126.65	1.59
7	143.20	1.58
8	166.10	1.14
9	189.00	1.14
10	262.35*	0.36*
*it is unclear whether the jet hit plate 10		

Table 5.17: Experimental vs. predicted times of arrival for test 13

Time of Arrival - Test 13		
Plate #	*Experimental Time of Impact (μs)*	*Predicted Time of Impact (μs)*
1	60.86	67.20
2	71.06	76.04
3	84.26	85.91
4	97.30	97.07
5	110.25	109.92
6	126.65	125.05
7	143.20	143.45
8	166.10	166.94
9	189.00	199.42
10	262.35*	
*it is unclear whether the jet hit plate 10		

5.3.5 Tests 11 - 13 - Velocity from optical system

A parallel laser line diagnostic system was implemented for test 11 and refined for tests 12 and 13 to measure the velocity of the jet before beginning penetration into the water. This method is described in detail in Chapter 4 above. The output of the photodiodes for tests 11 - 13 are shown in Figures E.37, E.45, and E.53 respectively. Figure E.37 indicates a large amount of background light emission that began at 40 μs after the detonation signal and that was collected and recorded by the photodiodes. This background light emission evidently came through the window of the blast tank and was not rejected by the single aperture or laser line interference filter. The light was intense enough to saturate photodiode 1 (closer to the base of the charge) but not intense enough to saturate photodiode 2 (closer to the water). Despite this rise in background intensity, a distinct drop can clearly be deciphered for each photodiode that corresponds to the time in which the jet obstructed a portion of the laser line (Figure E.38). It should be noted that this amount of light intensity was unexpected. Corrective measures were taken for tests 12 and 13 in the form of secondary aperturing to reject significantly more light from the event.

Table 5.18 summarizes the relevant data for test 11. The calculated jet tip velocity through the laser beams in test 11 was 6.18 km/s. Also in Table 5.18, this data was correlated to the time of arrival of the jet tip at the first plate. Based on the distance between the lower laser line and the surface of the first plate, an average velocity can be calculated in this region. For test 11, this velocity is 6.00 km/s. This velocity lies between the measured velocity in air (6.18 km/s) and the measured penetration velocity through cavity 2 (2.84 km/s) which lends some credence to the measurement. For this test, the duration of the intensity drop read by the photodiodes correlated well with the measured thickness of the laser lines. The top and bottom laser line thicknesses were measured to be approximately 2.67 mm (.1047 in) and 2.35 mm (.0924 in) respectively. The jet, moving at 6.18 km/s should have crossed the top and bottom lines in 0.43 μs and 0.38 μs respectively. The top photodiode showed a decrease in intensity for 0.4 μs and the bottom photodiode showed a decrease in intensity for 0.8 μs. The reason for the longer duration of intensity decrease for the bottom photodiode is unknown. The line thicknesses of the laser lines for tests 12 and 13 were not measured. The durations of the intensity drops were:

- Test 12, top photodiode: 2.4 μs
- Test 12, bottom photodiode: 2.6 μs
- Test 13, top photodiode: 1.4 μs
- Test 13, bottom photodiode: *unable to discern accurately*

Table 5.18: Test 11 laser velocity data

Test 11 Laser Velocity Data		
Photodiode 1	45.25	μs
Photodiode 2	49.65	μs
Distance of photodiode 1 from base of liner	69.47	mm
Distance travelled	27.18	mm
Calculated velocity	6.18	km/s
Plate 1 impact	65.3	μs
Time of arrival speed in cavity 2	2.84	km/s
Average velocity between photodiode 2 and plate 1	6.00	km/s

During test 12, a variety of factors contributed to the diminishing of background light intensity (Figure E.45). During test 11, water condensed on the blast tank window after the charge was ready to fire. This significantly attenuated the laser intensity. In test 12, the condensation was avoided so the full power of the laser could be used. This increased intensity allowed for the introduction of further filtering of all light using a neutral density filter with 30% transmission in front of each of the lens tubes. In addition, greater care was taken to properly aperture the blast tank window using black tape and to add an aperture on the front of the lens tube to only allow the photodiode to sense the laser light. These factors resulted in a large reduction of background light sensed by the photodiodes. The photodiodes both showed clear drops in intensity (Figure E.46). For test 12, the measured velocity was 6.43 km/s. The average velocity between the second laser line and the surface of the first plate was 5.24 km/s which falls between the measured jet tip velocity and the measured penetration velocity through cavity 2 (2.9 km/s). Relevant data are summarized in Table 5.19.

Table 5.19: Test 12 laser velocity data

Test 12 Laser Velocity Data		
Photodiode 1	40.50	μs
Photodiode 2	45.16	μs
Distance of photodiode 1 from base of liner	64.45	mm
Distance travelled	29.96	mm
Calculated velocity	6.43	km/s
Plate 1 impact	63.51	μs
Time of arrival speed in cavity 2	2.9	km/s
Average velocity between photodiode 2 and plate 1	5.24	km/s

In test 13, Photodiode 1 showed a very clear drop in intensity while photodiode 2 showed a sharp drop followed by a slow decrease (Figures E.53 and E.54). The reasons for this slow decrease are unclear. The measured velocity was 7.04 km/s. The average velocity between the second laser line and the surface of the first plate was 6.08 km/s which falls between the measured jet tip velocity and the penetration velocity through cavity 2 (2.6 km/s). Relevant data are summarized in Table 5.20.

Table 5.20: Test 13 Laser Velocity Data

Test 13 Laser Velocity Data		
Photodiode 1	41.35	μs
Photodiode 2	45.15	μs
Distance of photodiode 1 from base of liner	68.20	mm
Distance travelled	26.76	mm
Calculated velocity	7.04	km/s
Plate 1 impact	60.862	μs
Time of arrival speed in cavity 2	2.562	km/s
Average velocity between photodiode 2 and plate 1	6.08	km/s

5.3.6 Tests 11 - 13 - Plate penetration, deformation, and hole size

A summary of the penetration results for tests 10 - 13 is given in Table 5.21. Note that the air standoff distance for each test 10 - 13 was 127 mm. Plate deformation for tests 11 - 13 was measured by use of a Brown and Sharpe coordinate measuring machine. Each plate was measured in two paths. The “diagonal” path is a path from one corner of plate to the opposite corner, diagonally across the plate. This orientation quantifies the deformation of the plate between support rods. Secondly, each plate was measured in a “horizontal” path from the middle left side of the plate to the middle right side. This measurement quantifies the deformation where less support is given by the threaded rods. Measurement paths are indicated in Figure 5.3.

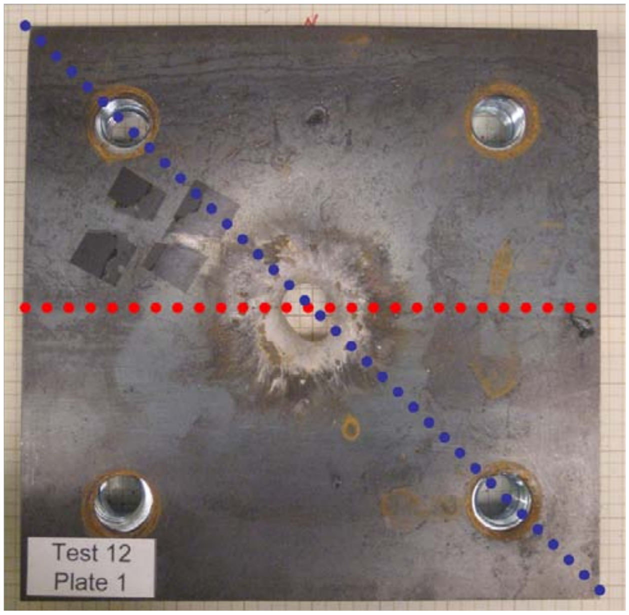

Figure 5.3: Diagonal and horizontal measuring paths for plates from tests 11 - 13

Results are shown for:

- Test 11, diagonal path, plates 1 - 8 Figure E.39
- Test 11, diagonal path, plates 9 - 15 Figure E.40

Table 5.21: Penetration results, tests 10 - 13

Penetration Summary by Test									
	Liner material	*Plates completely penetrated*	*Next plate struck*	*Water above plate 1 (mm)*	*Plate thickness (mm)*	*Spacer thickness (mm)*	*Distance of fluid penetrated (mm)*	*Fluid used*	*Distance of steel penetrated (mm)*	*Total penetration depth (mm)*
Test 10	*solid Cu*	1 steel plate used		543.6	25.4	NA	543.6	water	12.7	556.3
Test 11	*solid Al*	7	yes	63.5	3.3	22.9	223.5	water	25.5	249.0
Test 12	*solid Al*	9	no	63.5	3.3	22.9	246.4	water	29.5	275.9
Test 13	*solid Al*	9	no	63.5	3.3	22.9	246.4	Hygold L-750 oil	29.5	275.9

- Test 11, horizontal path, plates 1 - 8 Figure E.41
- Test 11, horizontal path, plates 9 - 15 Figure E.42
- Test 12, diagonal path, plates 1 - 8 Figure E.47
- Test 12, diagonal path, plates 9 - 15 Figure E.48
- Test 12, horizontal path, plates 1 - 8 Figure E.49
- Test 12, horizontal path, plates 9 - 15 Figure E.50
- Test 13, diagonal path, plates 1 - 8 Figure E.55
- Test 13, diagonal path, plates 9 - 15 Figure E.56
- Test 13, horizontal path, plates 1 - 8 Figure E.57
- Test 13, horizontal path, plates 9 - 15 Figure E.58

The most important conclusion from these plots is that the plates surrounding the last plate impacted by the jet were significantly deformed for the tests in water. In test 11, the jet penetrated through plate 7 and struck plate 8. Plates 8 and 9 were significantly deformed (Figures E.39, E.42, and 5.4). In test 12, the jet penetrated plate 9 but did not strike plate 10. Plates 9 and 10 were significantly deformed. It was suspected that the large deformation at these depths could provide evidence that the hydroreaction of the aluminum had increased the damage to the target. Alternatively, this increased deformation could have been due to a large amount of kinetic energy being delivered to the target plate as the jet was stopped. In order to further evaluate the deformation mechanism, test 13 was conducted in oil, a fluid that does not react with the aluminum liner. In both tests 12 and 13, plate 9 was penetrated entirely but plate 10 was not struck. Therefore, it is most instructive to compare plate deformations between tests 12 and 13. It is seen clearly by the graphs in Figures E.48 and E.56 and the pictures in Figures 5.5 and 5.6 that very little plate deformation was seen from test 13. As an example, the maximum deformation in plate 10 was 10.6 mm for test 12 and 0.42 mm for test 13. Average hole diameter compared fairly well between tests 11 and 12. Hole size in test 13 was larger than test 12 in plates 7, 8, and 9. However, since only one comparison is available, caution should be used in drawing any definitive conclusions.

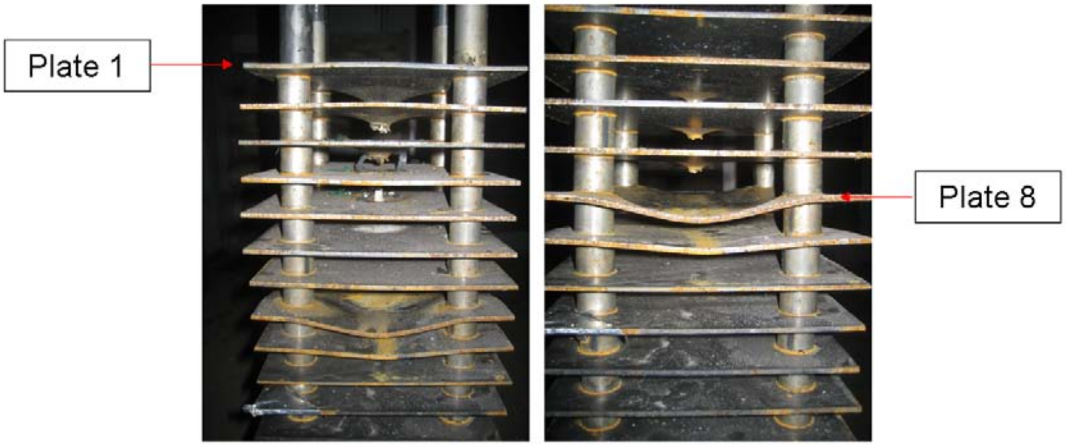

Figure 5.4: Deformation of plates from test 11. In both pictures the plates at the top were nearest the base plate.

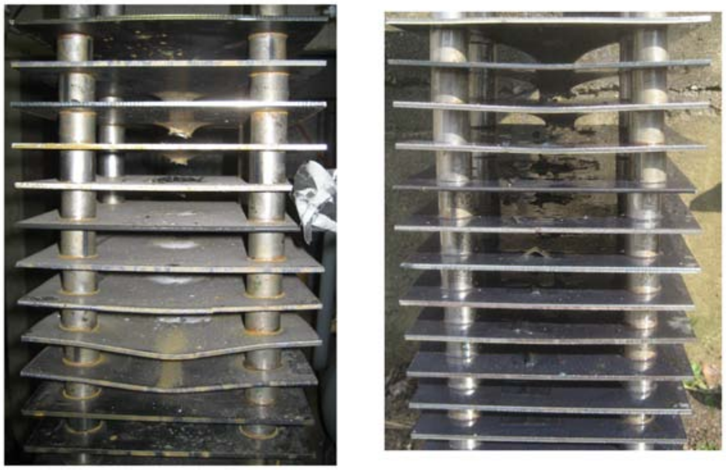

Figure 5.5: Comparison of plate deformation between test 12 (L) and test 13 (R). Top plate is plate 1 in both photos.

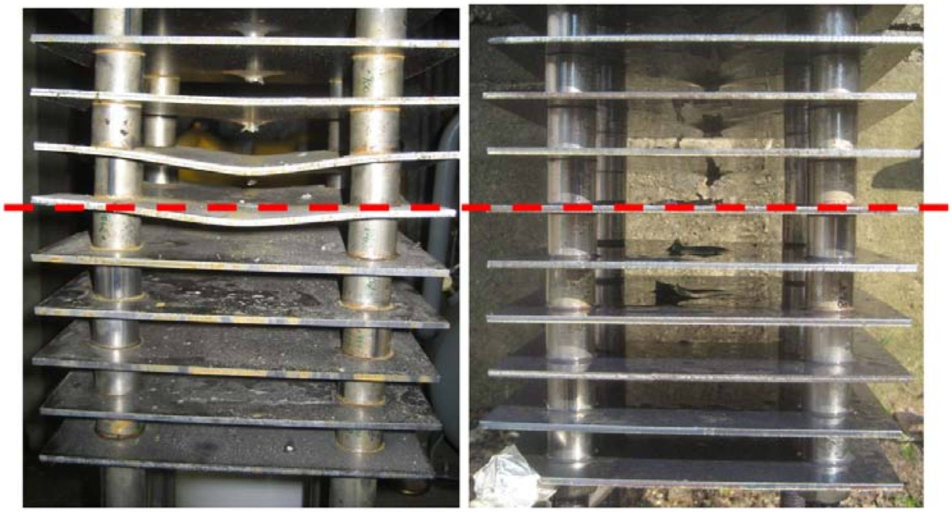

Figure 5.6: Comparison of plate deformation between test 12 (L) and test 13 (R). Red line indicates plate 10, the first unpenetrated plate in both tests.

5.3.7 Discussion

Significant results of tests 10 - 13 include the successful demonstration of the parallel laser line velocity diagnostic and the successful scaling of liner diameters from 20.02 mm to 50.75 mm. The velocities recorded by the laser diagnostic differed by only 4.0 % between tests 11 and 12. The measured velocity of test 13 (the highest measured velocity) is 14.0 % higher than test 11 (the lowest measured velocity). Secondly, the production of significant plate deformation near the bottom of the jet penetration region is significant. Tests 11 and 12 that exhibited hydroreaction also exhibited significantly more deformation in the deep plates than test 13, which showed no hydroreaction due to the use of oil instead of water. This result leads to the hypothesis that the hydroreaction of aluminum could be a contributor to damage production in this area.

CHAPTER 6

CONCLUSIONS AND RECOMMENDATIONS

Several important conclusions can be drawn from the 13 tests discussed in the above report. The author set out to test bimetallic liners to determine if a bimetallic liner could be demonstrated that retained the penetration characteristics of a dense non-reactive liner while providing additional pressure due to hydroreaction of the reactive material. Although the Cu/Al insert liners never exhibited a well formed, deeply penetrating jet, much can be gleaned from the efforts. Insufficient machining precision, lack of bonding between the two materials, or dissimilarities between the properties of the two materials (namely density and sound speed) could have resulted in the liners' poor performance.

It was an important accomplishment of the present study to design the larger scale 50.75 mm diameter liners, their accompanying casings, and to demonstrate four successful tests of such liners with minimal changes to the experimental setup. The foundation is now laid for future researchers to continue testing at this scale. With tests of this scale, this report has demonstrated the ability to perform a non-invasive, accurate measurement of the true jet tip velocity in air using the laser velocity diagnostic. The repeatability of these measurements appears to be good (when considering the well-known variability of seemingly identical charges), with the three data points agreeing within 14.0%.

Perhaps the most important work of the present study was the comparison of test 12, a large aluminum liner in water, to test 13, a large aluminum liner in oil. In both tests 12 and 13, the jet penetrated 9 plates but did not conclusively strike plate 10. High speed video images show that the lack of oxygen in the oil prevented the reaction of the aluminum liner during test 13. The target plates from test 12 exhibited large deformation in the unpenetrated plates. In contrast, the target plates from test 13 exhibited very little deformation in the unpenetrated plates. This is an important result that merits futher study of the usefulness of hydroreaction for underwater warhead applications.

It is recommended that the research group of Glumac and Krier support their experimental data with in-house hydrocode simulations. These simulations would be extremely useful in determining the causes of poor performance in the case of the Cu/Al insert liners. Another diagnostic that could offer convincing documentation of the behavior of all the liners tested is flash X-ray radiography. The possibility of adding this diagnostic should be investigated. If further tests are completed using the laser velocity diagnostic it is recommended that a more robust solution to the alignment of the laser and lenses be developed. The time required to set up the optics, align the laser, align the lenses, align the photodiodes, and measure the distance between laser lines was extensive. The time required to fabricate the target plates and spacers for each test was also extensive. Plate and spacer fabrication should be outsourced to a machine shop for future test runs. Finally, it is recommended that, as much as possible, the shaped charge lab in ESPL transition to an autonomous lab. The time wasted transporting equipment back and forth from ESPL should not be ignored. An autonomous lab would allow more frequent testing and likely result in more consistent data.

APPENDIX A

ENGINEERING DRAWINGS OF SPACERS, LINERS, CASINGS, AND TENSILE TEST SPECIMENS

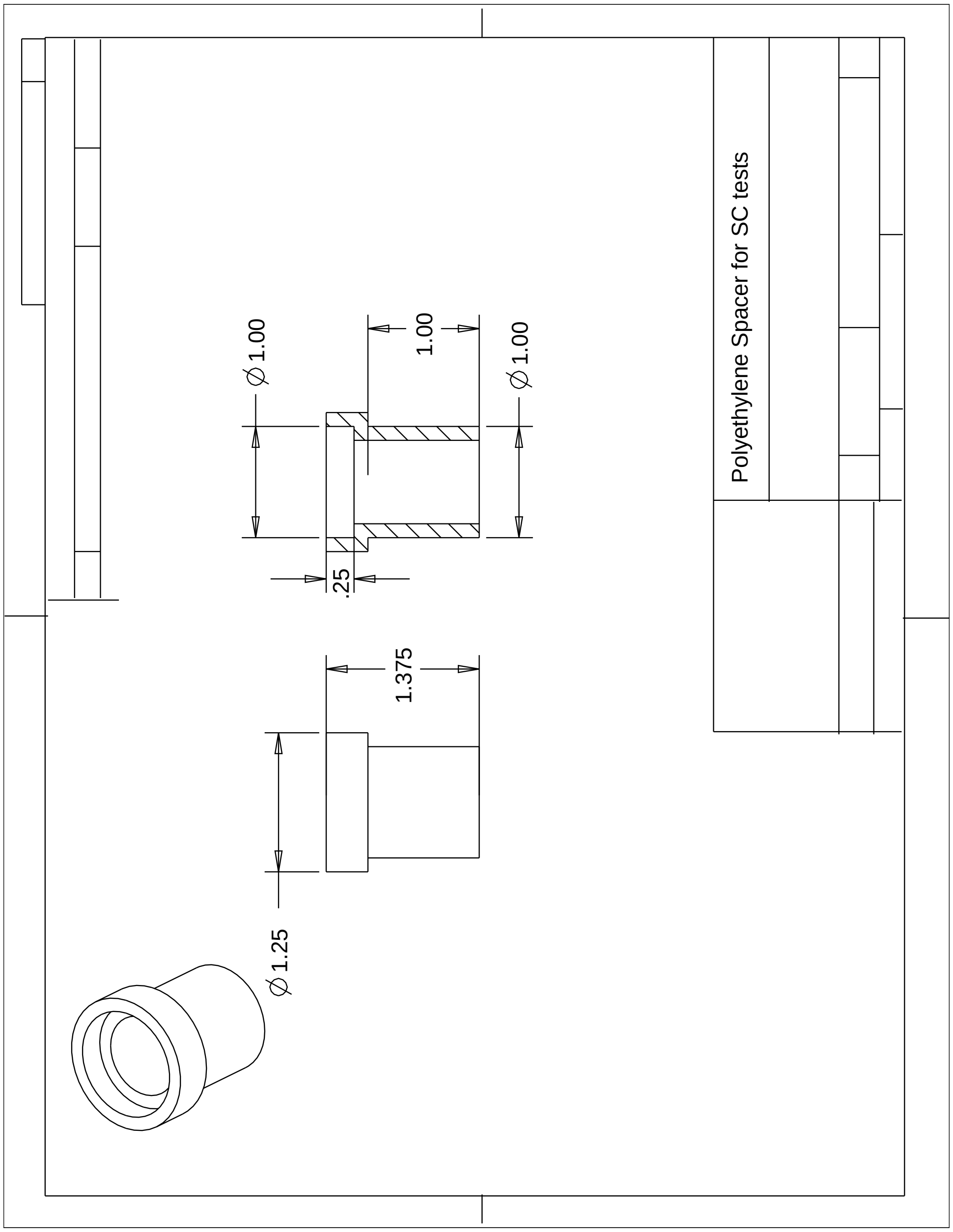

Figure A.1: Polyethylene spacer used for 20.02 mm tests

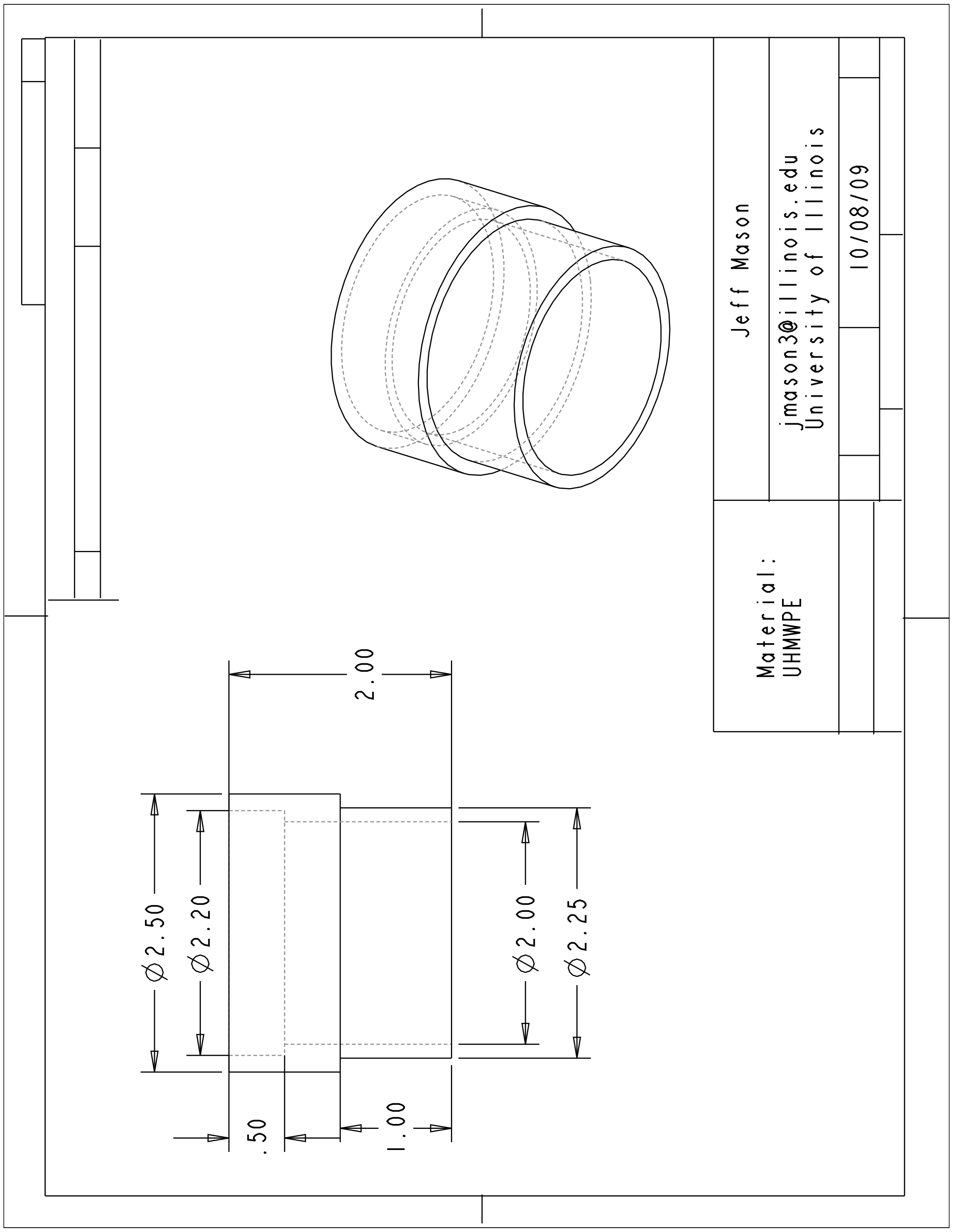

Figure A.2: Polyethylene spacer used for 50.75 mm tests

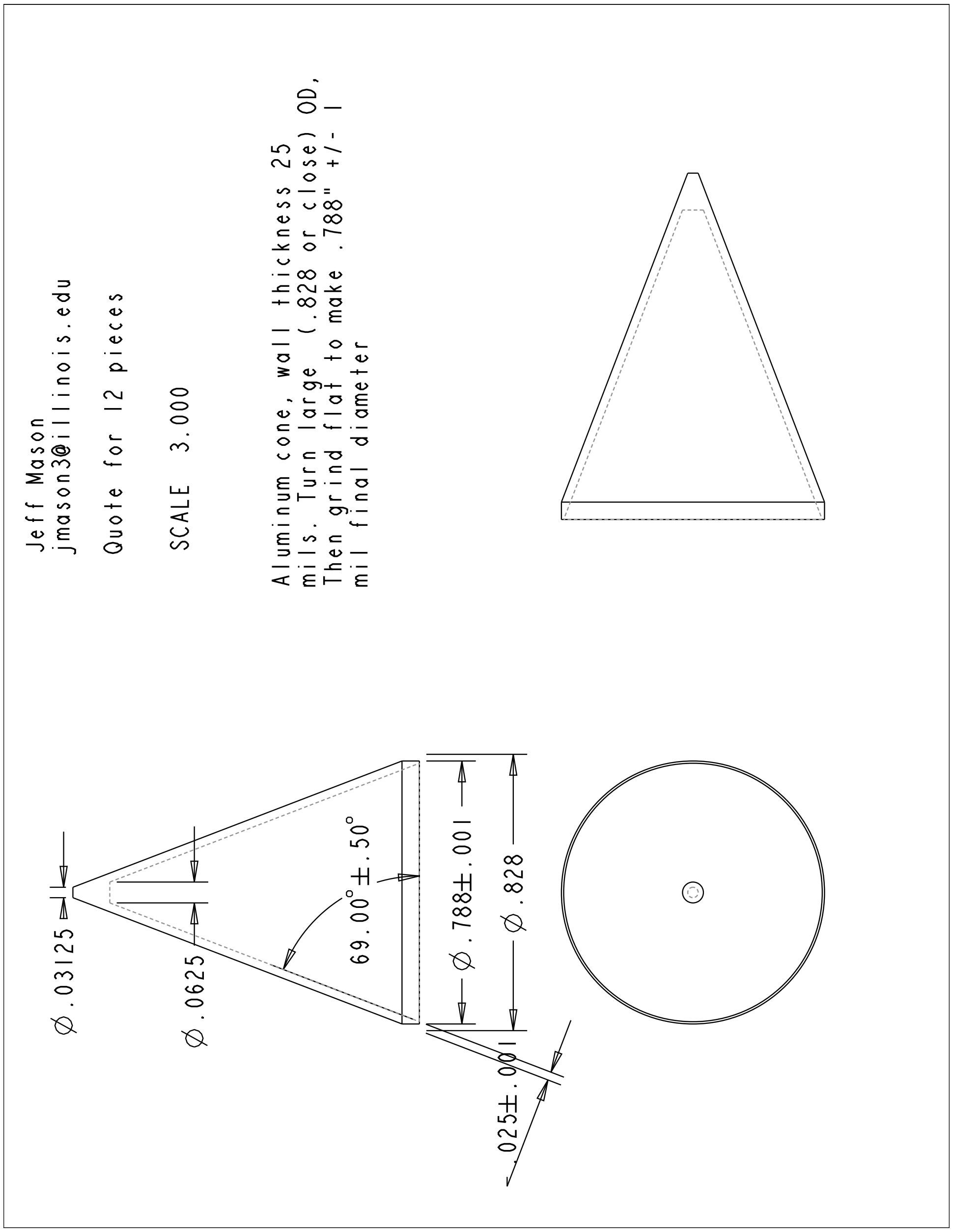

Aluminum cone, wall thickness 25 mils. Turn large (.828 or close) OD, Then grind flat to make .788" +/- 1 mil final diameter

Figure A.3: Small scale liner design (aluminum or copper)

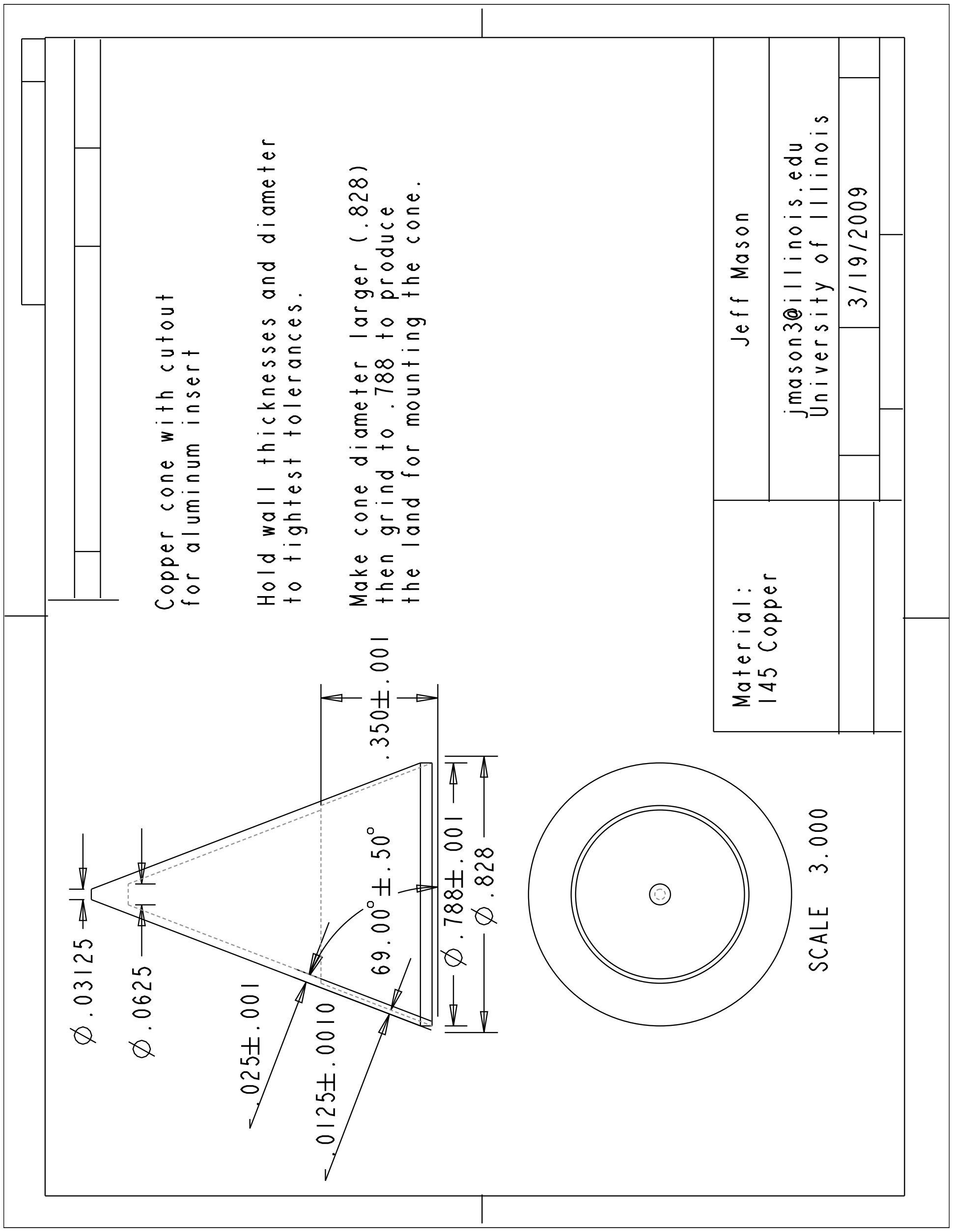

Copper cone with cutout for aluminum insert

Hold wall thicknesses and diameter to tightest tolerances.

Make cone diameter larger (.828) then grind to .788 to produce the land for mounting the cone.

Figure A.4: Composite liner design part 1, copper cone with cutout

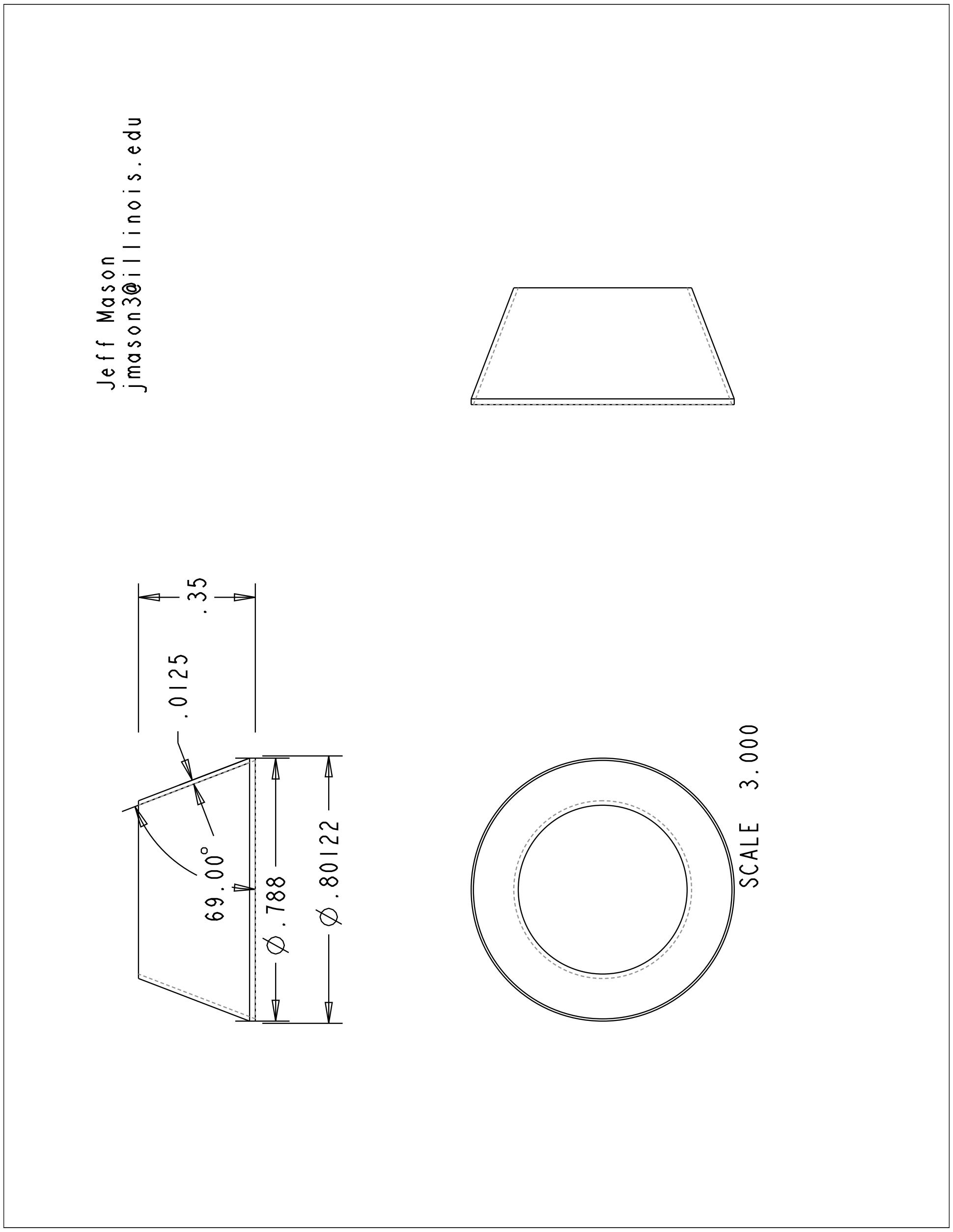

Figure A.5: Composite liner design part 2, aluminum insert

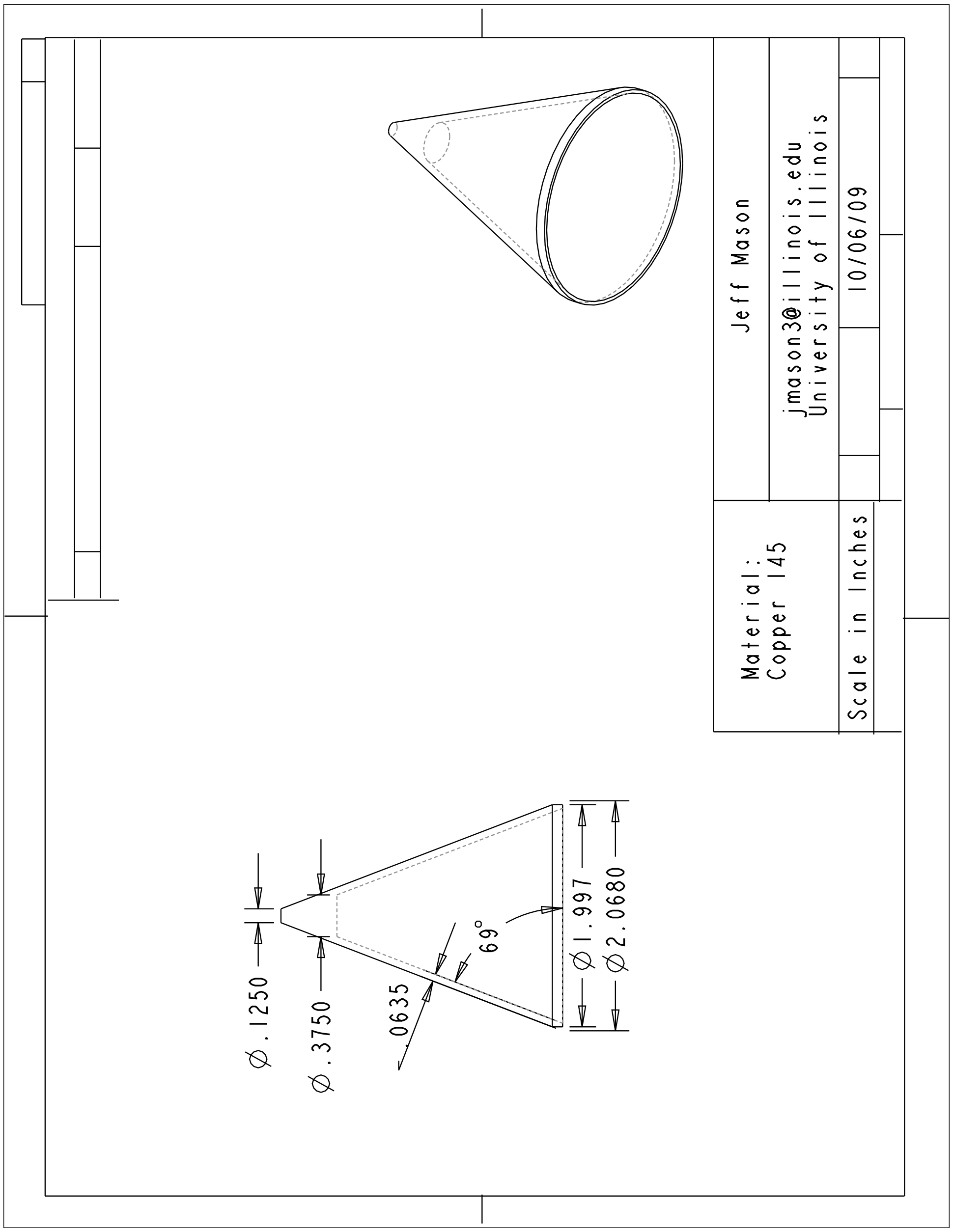

Figure A.6: Large copper liner design (test 10)

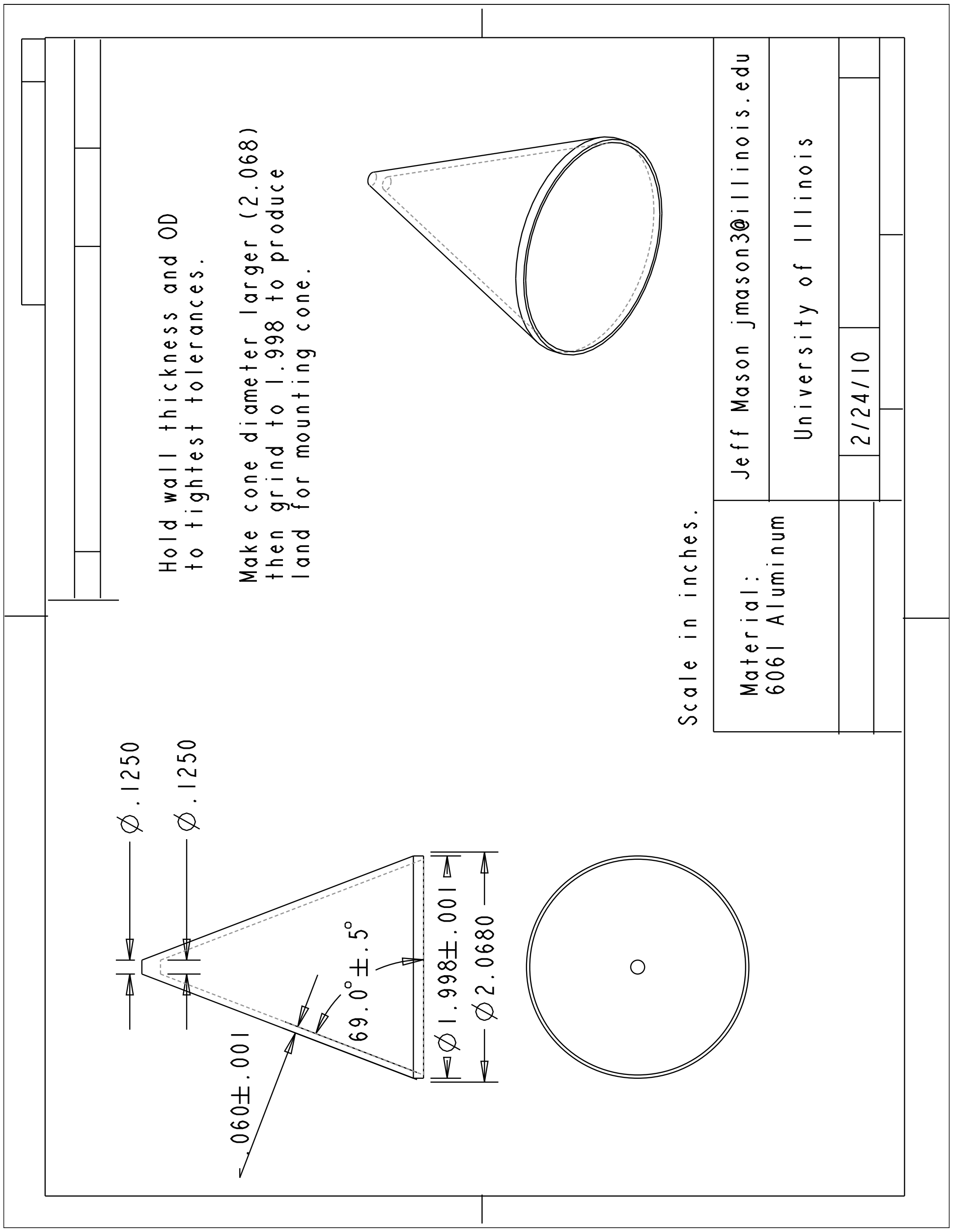

Figure A.7: Large aluminum liner design (tests 11-13)

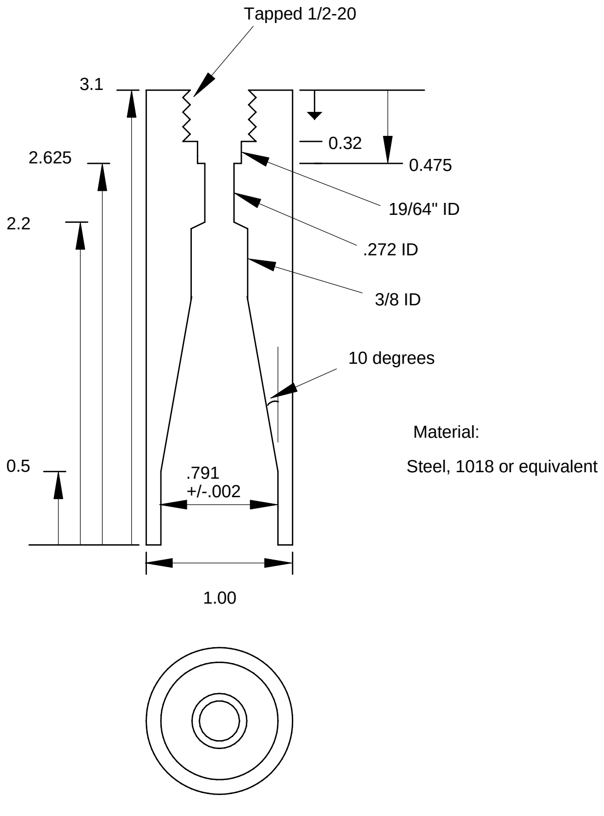

Figure A.8: Casing design for small diameter liners (tests 1- 9)

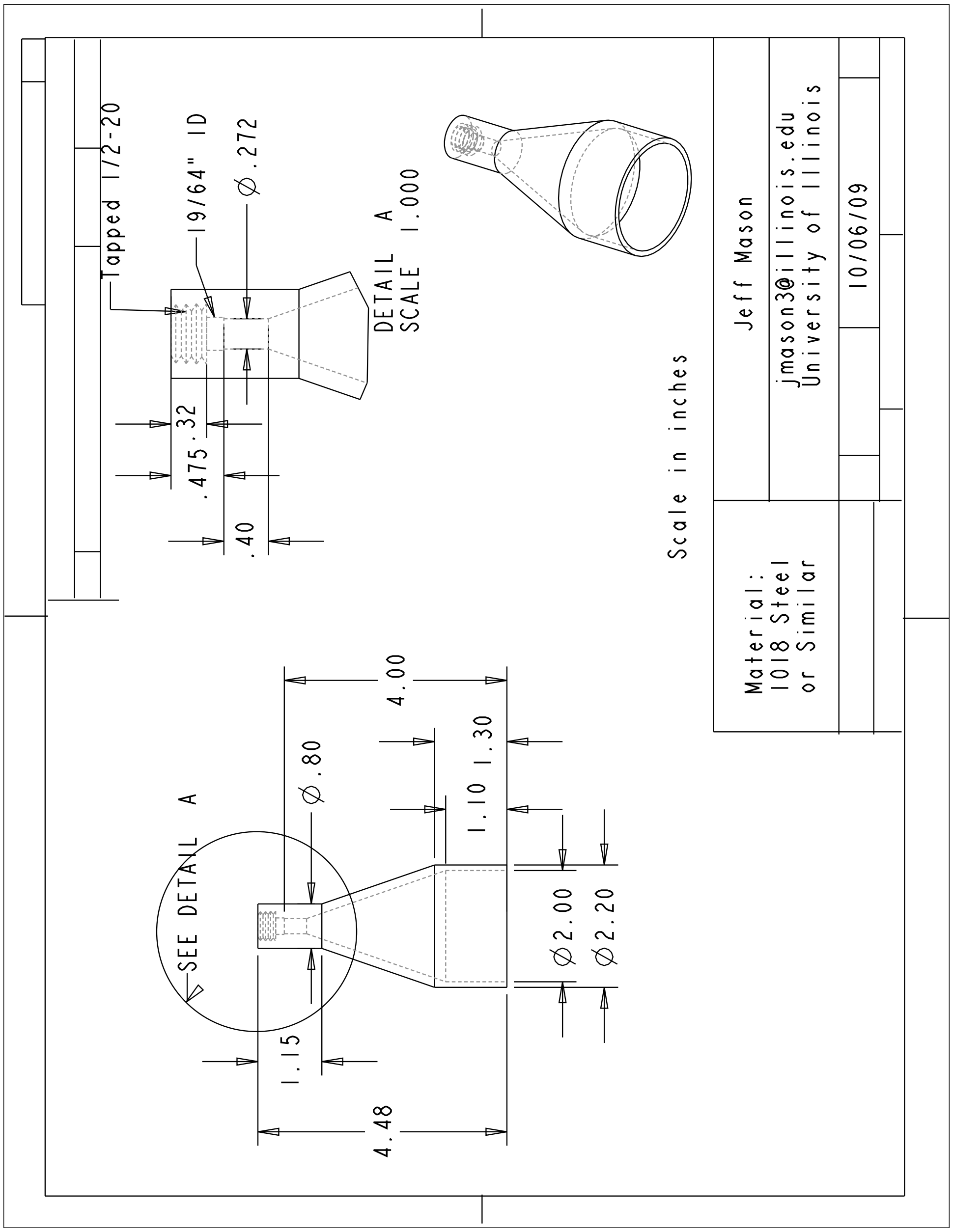

Figure A.9: Casing design for large scale liners (tests 10-13)

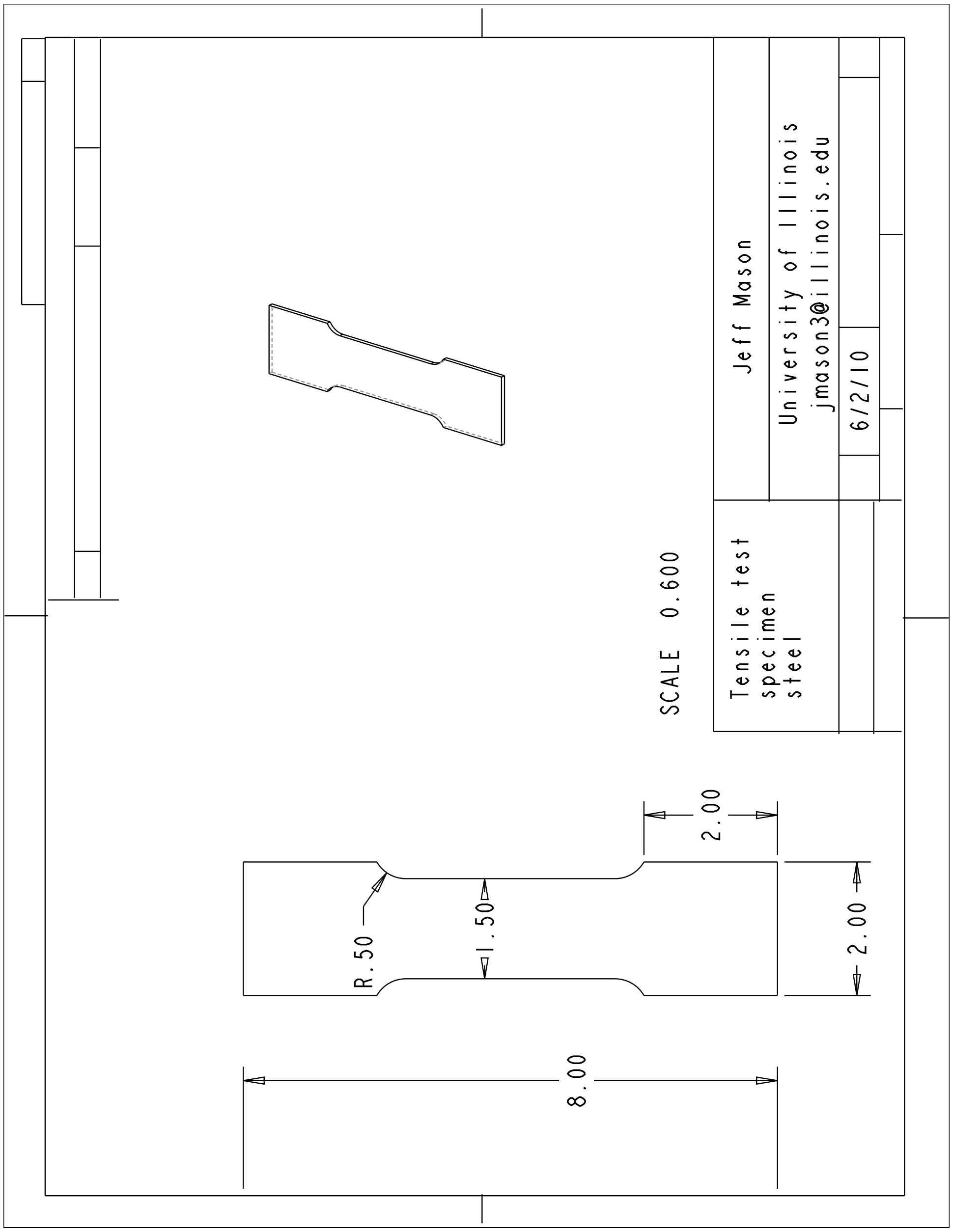

Figure A.10: Tensile specimen design used to test target plate material for 50.75 mm diameter liners

APPENDIX B

DATA ACQUISITION SETTINGS AND SAMPLE ELECTRICAL CONNECTION DIAGRAMS

Table B.1: Example data channel settings

Data Channel Settings		
Measurement	*AC/DC*	*Voltage (+/-)*
Time of arrival (1-5) in water	*DC*	*10*
Time of arrival (1-5) in oil	DC	20
Time of arrival (6-12) in oil	DC	20
Pressure - Kistler	AC	20
Pressure - PCB	DC	5
Light emission photodiode	DC	10
Laser velocity photodiode	DC	10
Trigger - inductive	AC	20
Trigger - signal generator	DC	5
most data was recorded for 2 ms		

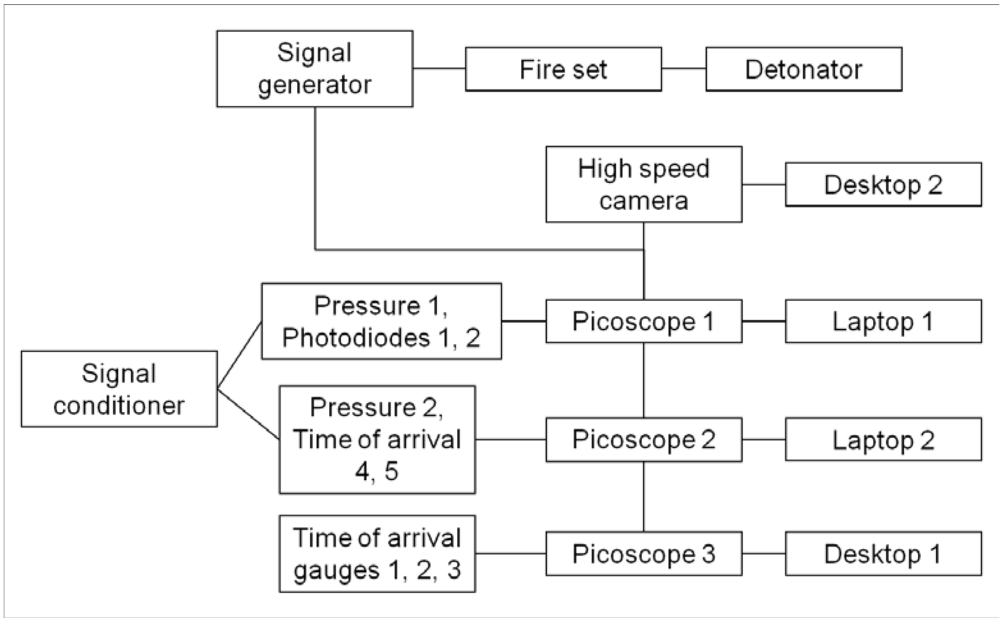

Figure B.1: Diagram of electrical connections, test 12

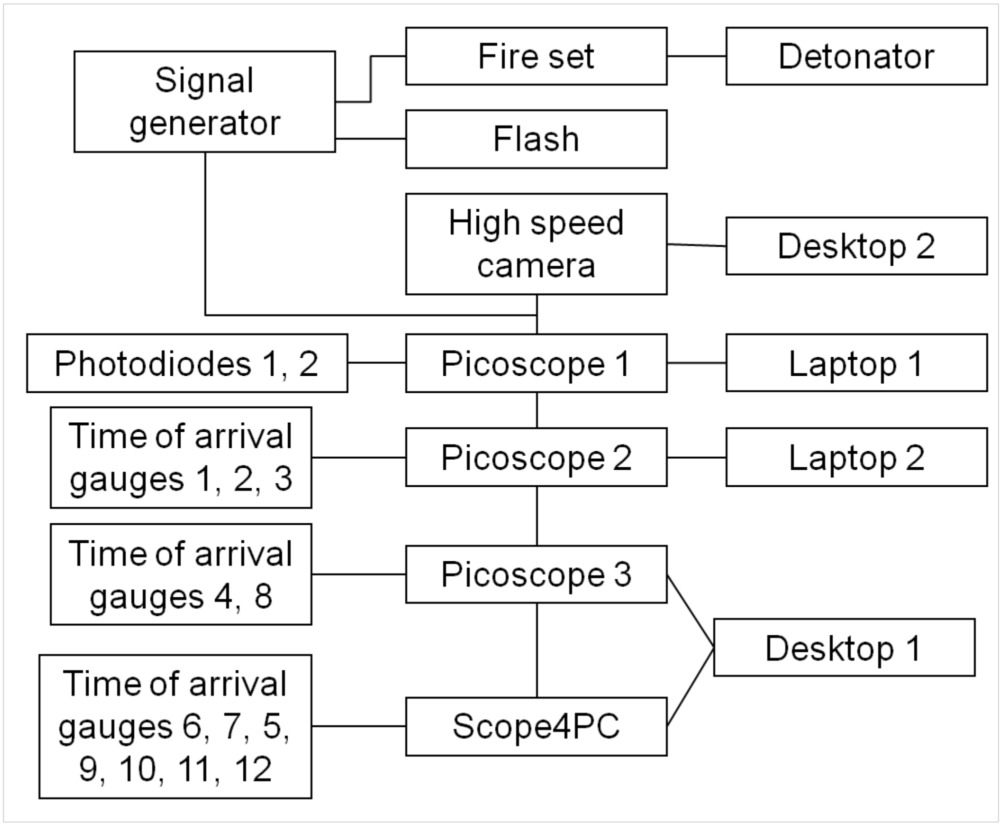

Figure B.2: Diagram of electrical connections, test 13

APPENDIX C

STANDARD OPERATING PROCEDURES

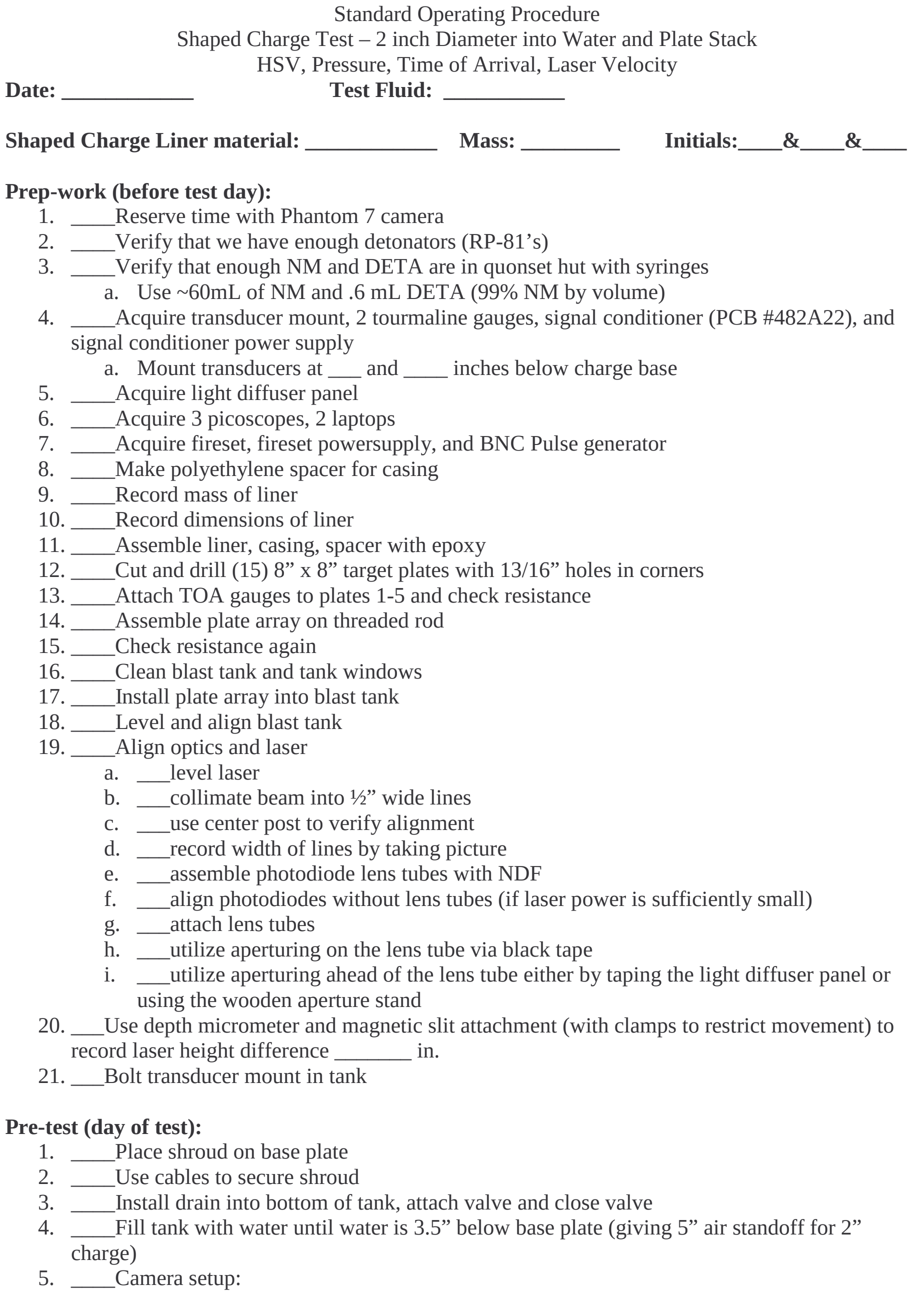

Standard Operating Procedure
Shaped Charge Test – 2 inch Diameter into Water and Plate Stack
HSV, Pressure, Time of Arrival, Laser Velocity

Date: ____________ **Test Fluid:** ___________

Shaped Charge Liner material: ____________ **Mass:** _________ **Initials:**____&____&____

Prep-work (before test day):

1. ____Reserve time with Phantom 7 camera
2. ____Verify that we have enough detonators (RP-81's)
3. ____Verify that enough NM and DETA are in quonset hut with syringes
   a. Use ~60mL of NM and .6 mL DETA (99% NM by volume)
4. ____Acquire transducer mount, 2 tourmaline gauges, signal conditioner (PCB #482A22), and signal conditioner power supply
   a. Mount transducers at ___ and ____ inches below charge base
5. ____Acquire light diffuser panel
6. ____Acquire 3 picoscopes, 2 laptops
7. ____Acquire fireset, fireset powersupply, and BNC Pulse generator
8. ____Make polyethylene spacer for casing
9. ____Record mass of liner
10. ____Record dimensions of liner
11. ____Assemble liner, casing, spacer with epoxy
12. ____Cut and drill (15) 8" x 8" target plates with 13/16" holes in corners
13. ____Attach TOA gauges to plates 1-5 and check resistance
14. ____Assemble plate array on threaded rod
15. ____Check resistance again
16. ____Clean blast tank and tank windows
17. ____Install plate array into blast tank
18. ____Level and align blast tank
19. ____Align optics and laser
    a. ___level laser
    b. ___collimate beam into ½" wide lines
    c. ___use center post to verify alignment
    d. ___record width of lines by taking picture
    e. ___assemble photodiode lens tubes with NDF
    f. ___align photodiodes without lens tubes (if laser power is sufficiently small)
    g. ___attach lens tubes
    h. ___utilize aperturing on the lens tube via black tape
    i. ___utilize aperturing ahead of the lens tube either by taping the light diffuser panel or using the wooden aperture stand
20. ___Use depth micrometer and magnetic slit attachment (with clamps to restrict movement) to record laser height difference _______ in.
21. ___Bolt transducer mount in tank

Pre-test (day of test):

1. ____Place shroud on base plate
2. ____Use cables to secure shroud
3. ____Install drain into bottom of tank, attach valve and close valve
4. ____Fill tank with water until water is 3.5" below base plate (giving 5" air standoff for 2" charge)
5. ____Camera setup:

Figure C.1: Standard Operating Procedure for test 12, part 1

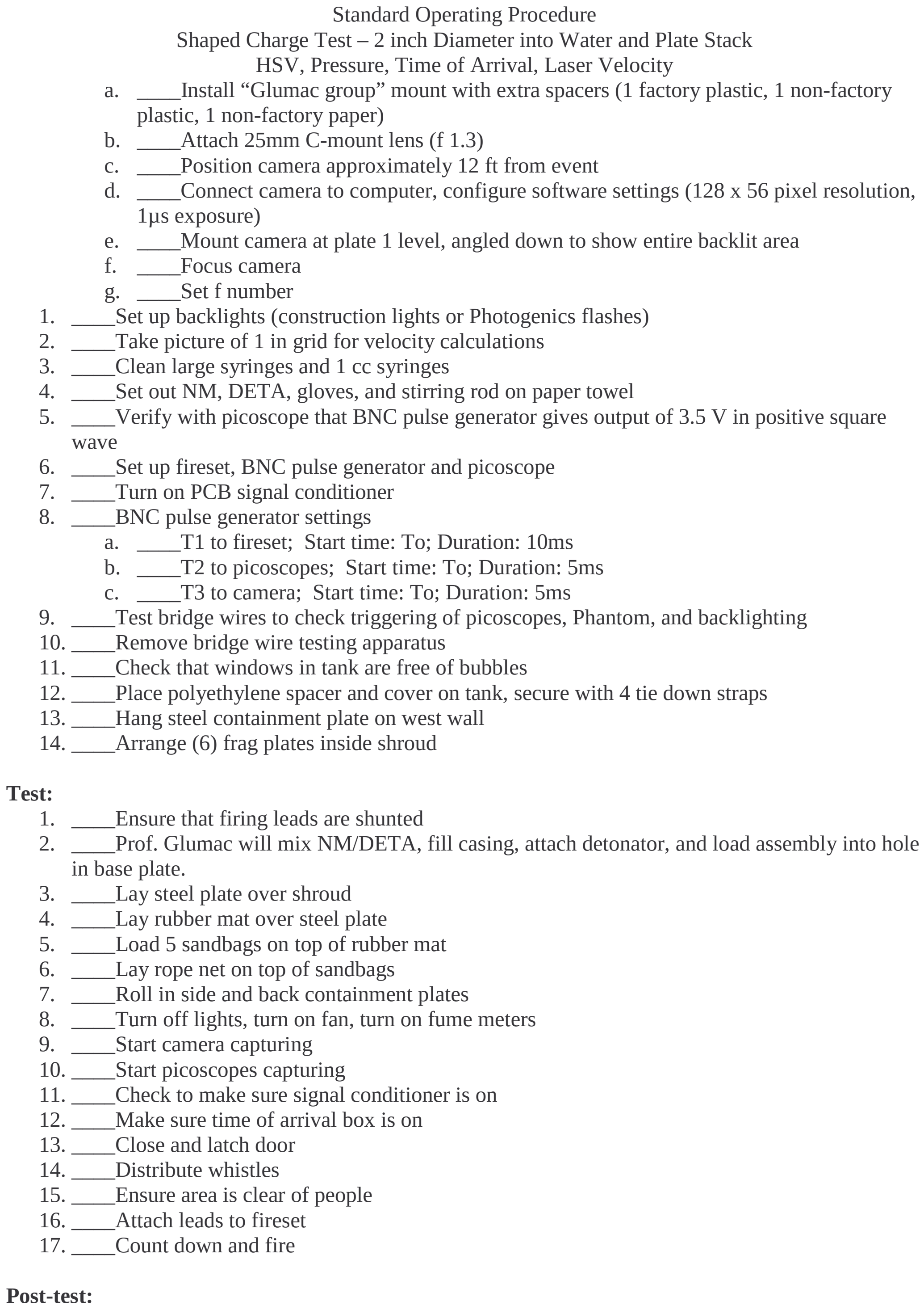

Standard Operating Procedure
Shaped Charge Test – 2 inch Diameter into Water and Plate Stack
HSV, Pressure, Time of Arrival, Laser Velocity

    a. ____Install “Glumac group” mount with extra spacers (1 factory plastic, 1 non-factory plastic, 1 non-factory paper)
    b. ____Attach 25mm C-mount lens (f 1.3)
    c. ____Position camera approximately 12 ft from event
    d. ____Connect camera to computer, configure software settings (128 x 56 pixel resolution, 1µs exposure)
    e. ____Mount camera at plate 1 level, angled down to show entire backlit area
    f. ____Focus camera
    g. ____Set f number

1. ____Set up backlights (construction lights or Photogenics flashes)
2. ____Take picture of 1 in grid for velocity calculations
3. ____Clean large syringes and 1 cc syringes
4. ____Set out NM, DETA, gloves, and stirring rod on paper towel
5. ____Verify with picoscope that BNC pulse generator gives output of 3.5 V in positive square wave
6. ____Set up fireset, BNC pulse generator and picoscope
7. ____Turn on PCB signal conditioner
8. ____BNC pulse generator settings
    a. ____T1 to fireset; Start time: To; Duration: 10ms
    b. ____T2 to picoscopes; Start time: To; Duration: 5ms
    c. ____T3 to camera; Start time: To; Duration: 5ms
9. ____Test bridge wires to check triggering of picoscopes, Phantom, and backlighting
10. ____Remove bridge wire testing apparatus
11. ____Check that windows in tank are free of bubbles
12. ____Place polyethylene spacer and cover on tank, secure with 4 tie down straps
13. ____Hang steel containment plate on west wall
14. ____Arrange (6) frag plates inside shroud

Test:

1. ____Ensure that firing leads are shunted
2. ____Prof. Glumac will mix NM/DETA, fill casing, attach detonator, and load assembly into hole in base plate.
3. ____Lay steel plate over shroud
4. ____Lay rubber mat over steel plate
5. ____Load 5 sandbags on top of rubber mat
6. ____Lay rope net on top of sandbags
7. ____Roll in side and back containment plates
8. ____Turn off lights, turn on fan, turn on fume meters
9. ____Start camera capturing
10. ____Start picoscopes capturing
11. ____Check to make sure signal conditioner is on
12. ____Make sure time of arrival box is on
13. ____Close and latch door
14. ____Distribute whistles
15. ____Ensure area is clear of people
16. ____Attach leads to fireset
17. ____Count down and fire

Post-test:

Figure C.2: Standard Operating Procedure for test 12, part 2

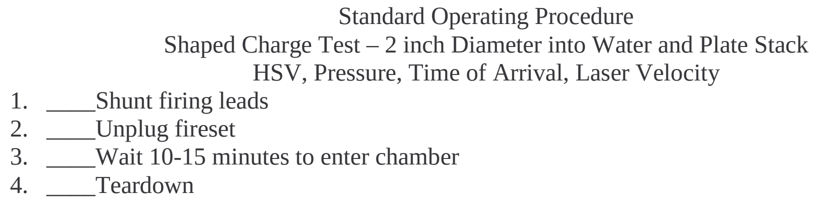

Standard Operating Procedure
Shaped Charge Test – 2 inch Diameter into Water and Plate Stack
HSV, Pressure, Time of Arrival, Laser Velocity

1. ____Shunt firing leads
2. ____Unplug fireset
3. ____Wait 10-15 minutes to enter chamber
4. ____Teardown

Figure C.3: Standard Operating Procedure for test 12, part 3

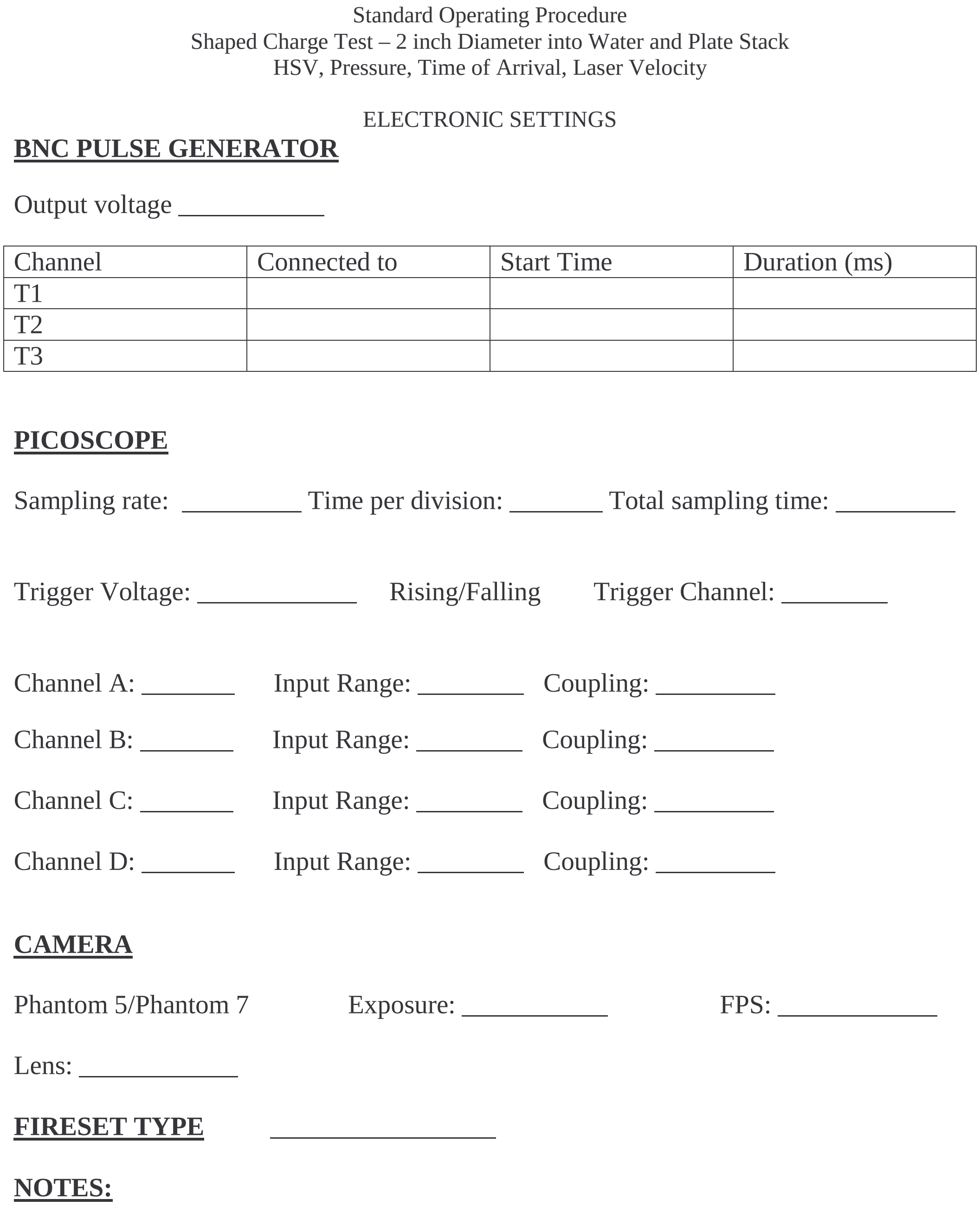

Standard Operating Procedure
Shaped Charge Test – 2 inch Diameter into Water and Plate Stack
HSV, Pressure, Time of Arrival, Laser Velocity

ELECTRONIC SETTINGS

BNC PULSE GENERATOR

Output voltage ___________

Channel	Connected to	Start Time	Duration (ms)
T1			
T2			
T3			

PICOSCOPE

Sampling rate: _________ Time per division: _______ Total sampling time: _________

Trigger Voltage: ____________ Rising/Falling Trigger Channel: ________

Channel A: _______ Input Range: ________ Coupling: _________

Channel B: _______ Input Range: ________ Coupling: _________

Channel C: _______ Input Range: ________ Coupling: _________

Channel D: _______ Input Range: ________ Coupling: _________

CAMERA

Phantom 5/Phantom 7 Exposure: ___________ FPS: ____________

Lens: ____________

FIRESET TYPE _________________

NOTES:

Figure C.4: Example of electronics settings record sheet

APPENDIX D

COMPLETE IMAGE SEQUENCES

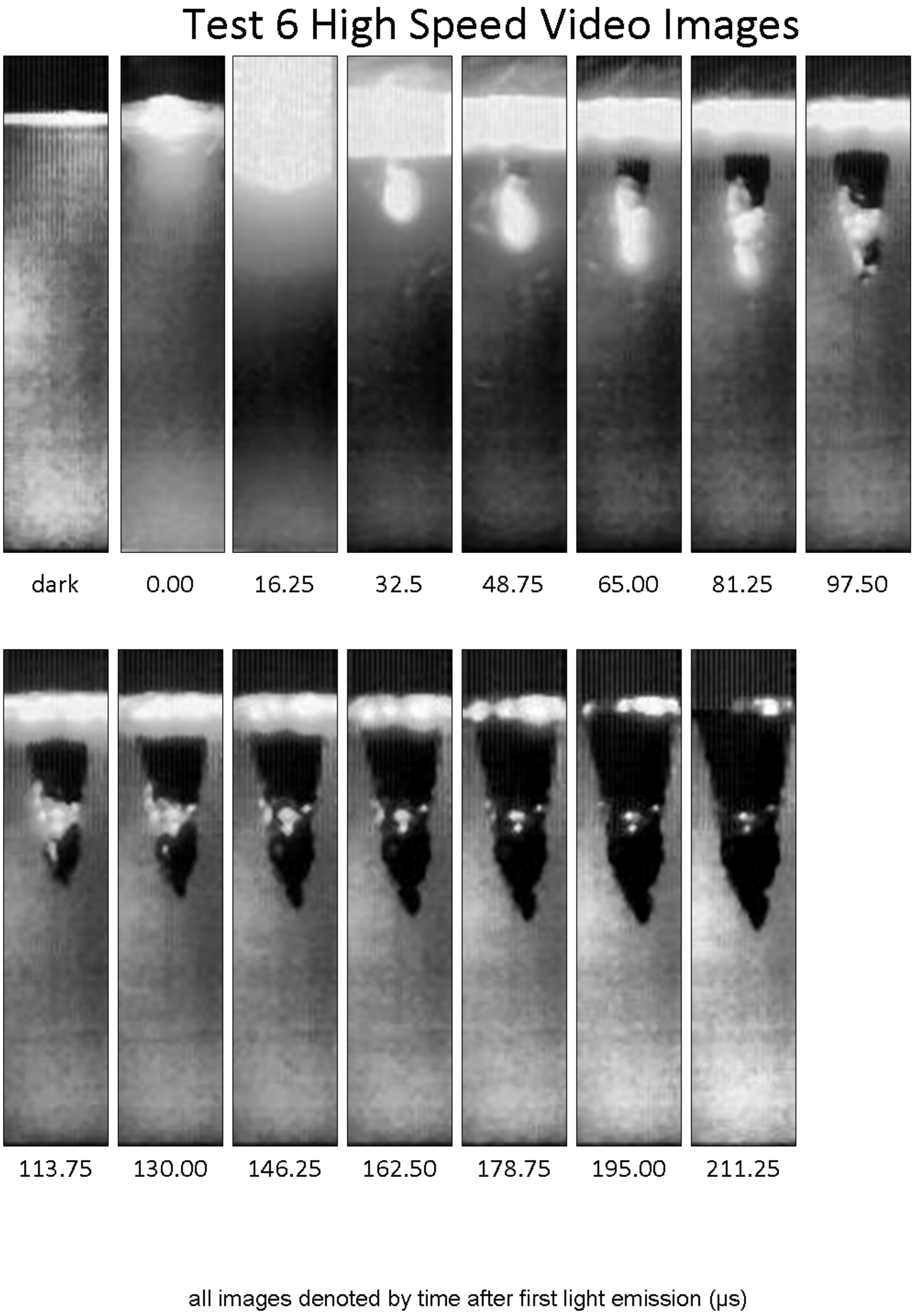

Figure D.1: Image sequence from test 6, Cu/Al insert design, 20.02 mm

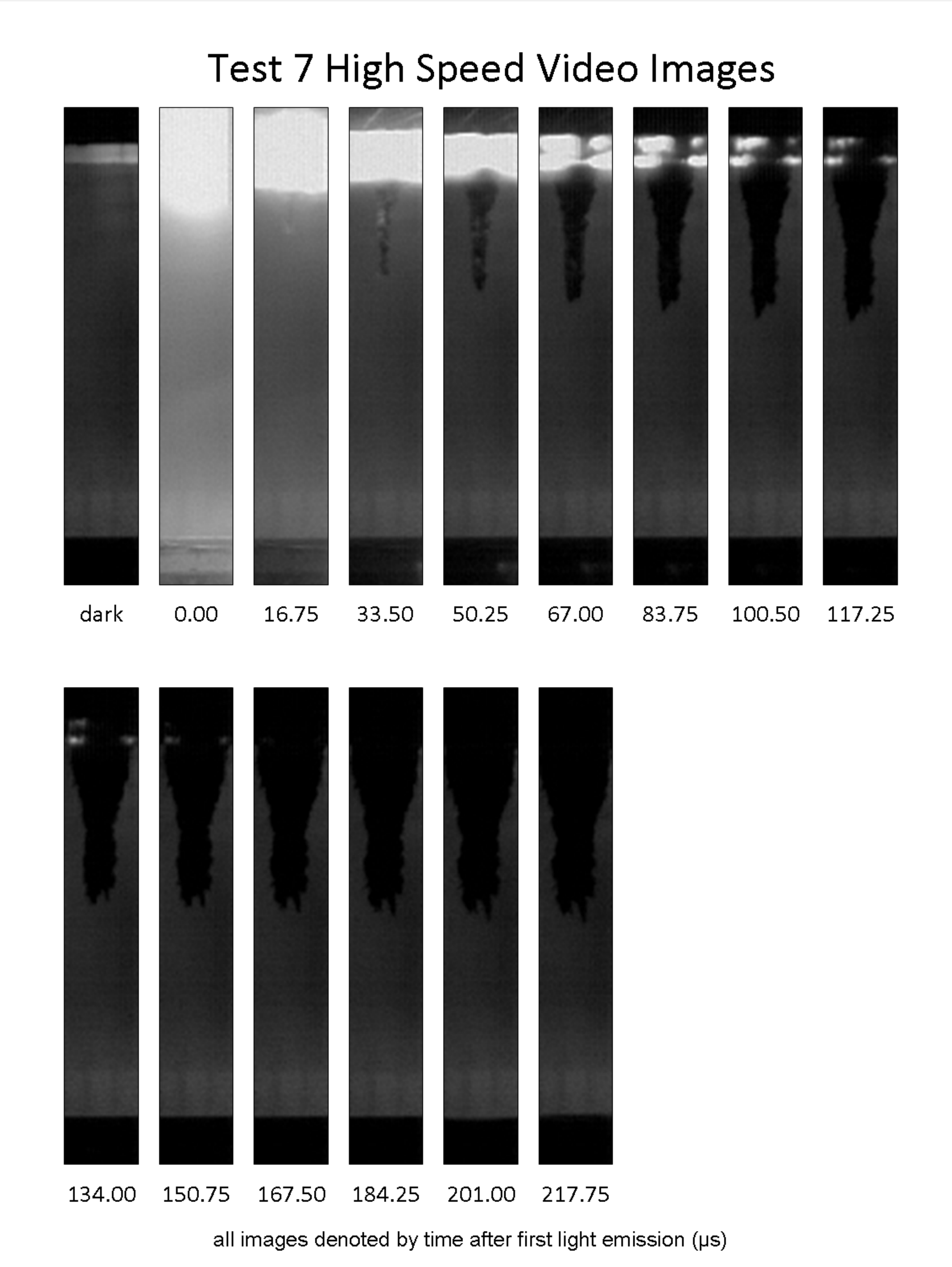

Figure D.2: Image sequence from test 7, Cu/Al insert design without aluminum insert, 20.02 mm

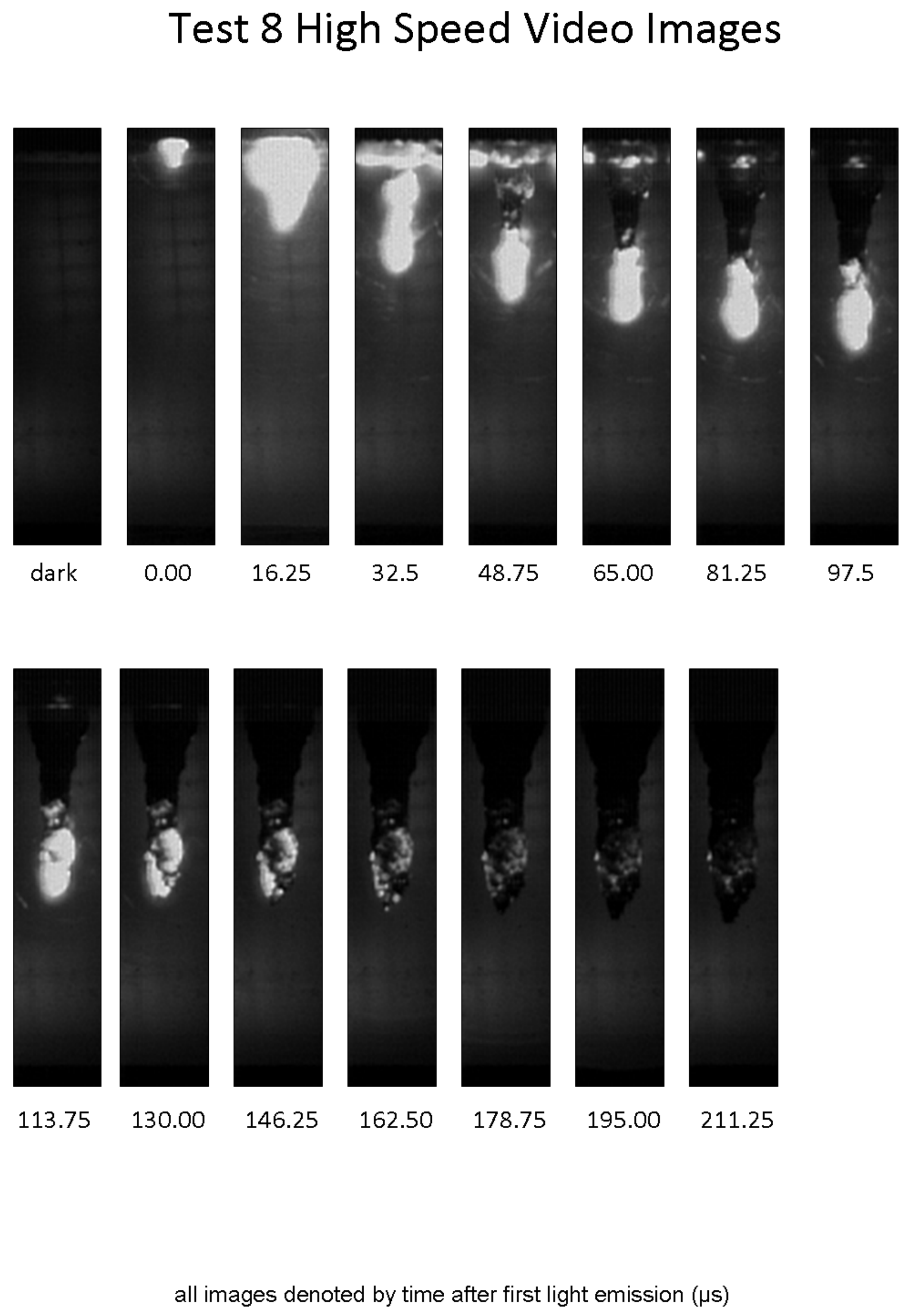

Figure D.3: Image sequence from test 8, solid Al liner, 20.02 mm

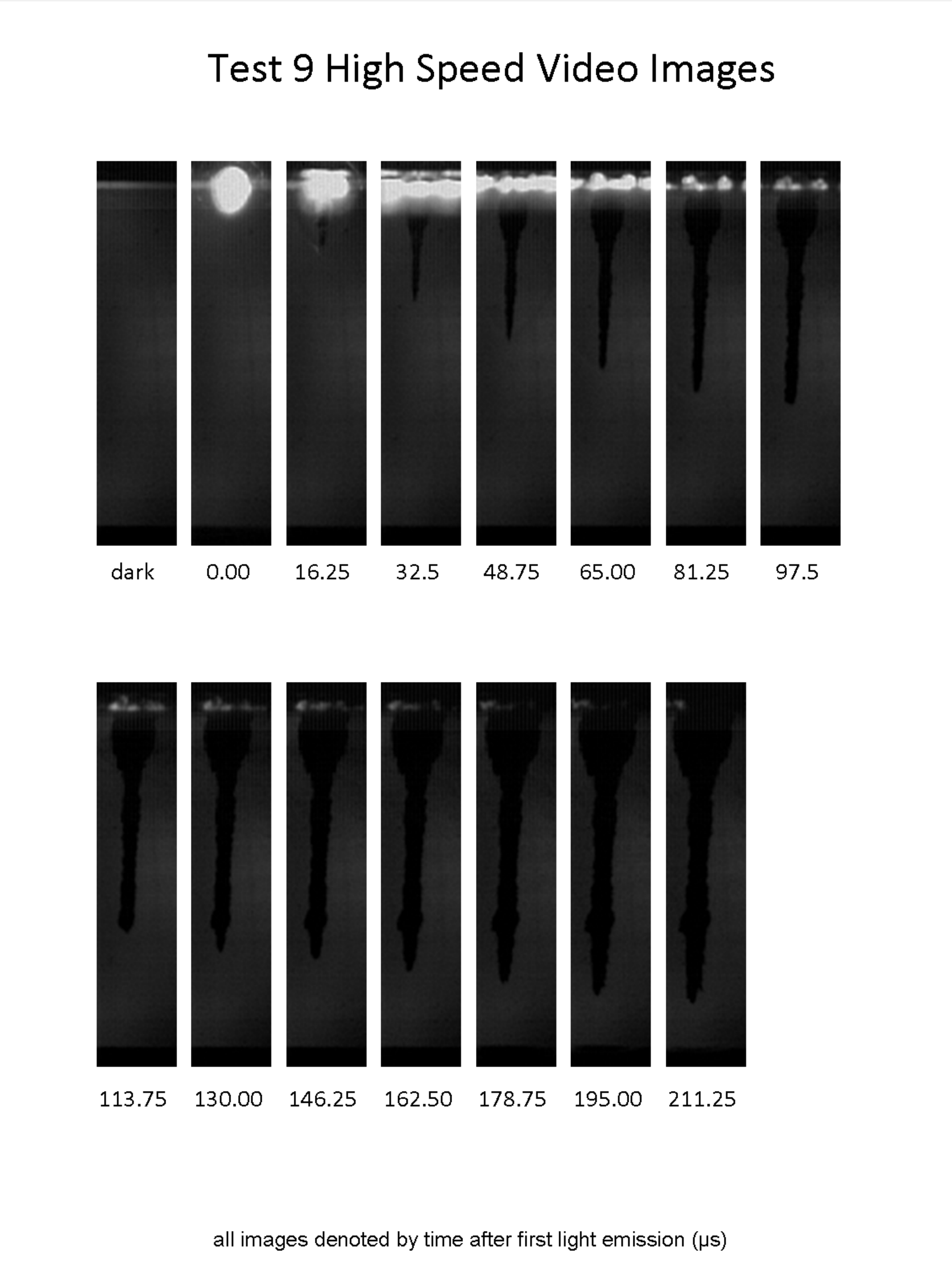

Figure D.4: Image sequence from test 9, solid Cu liner, 20.02 mm

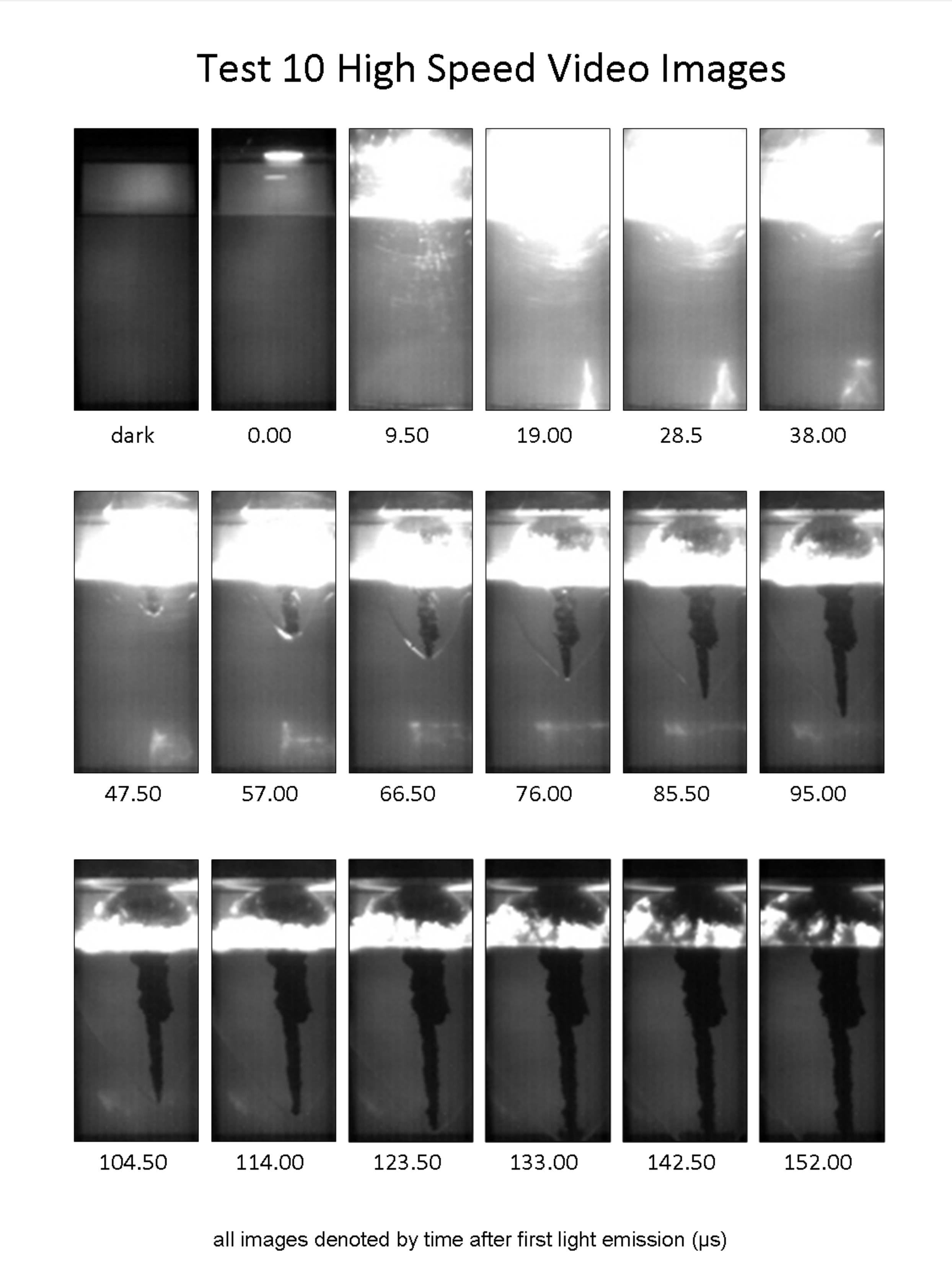

Figure D.5: Image sequence from test 10, solid Cu liner, 50.75 mm

Test 10 High Speed Video Images

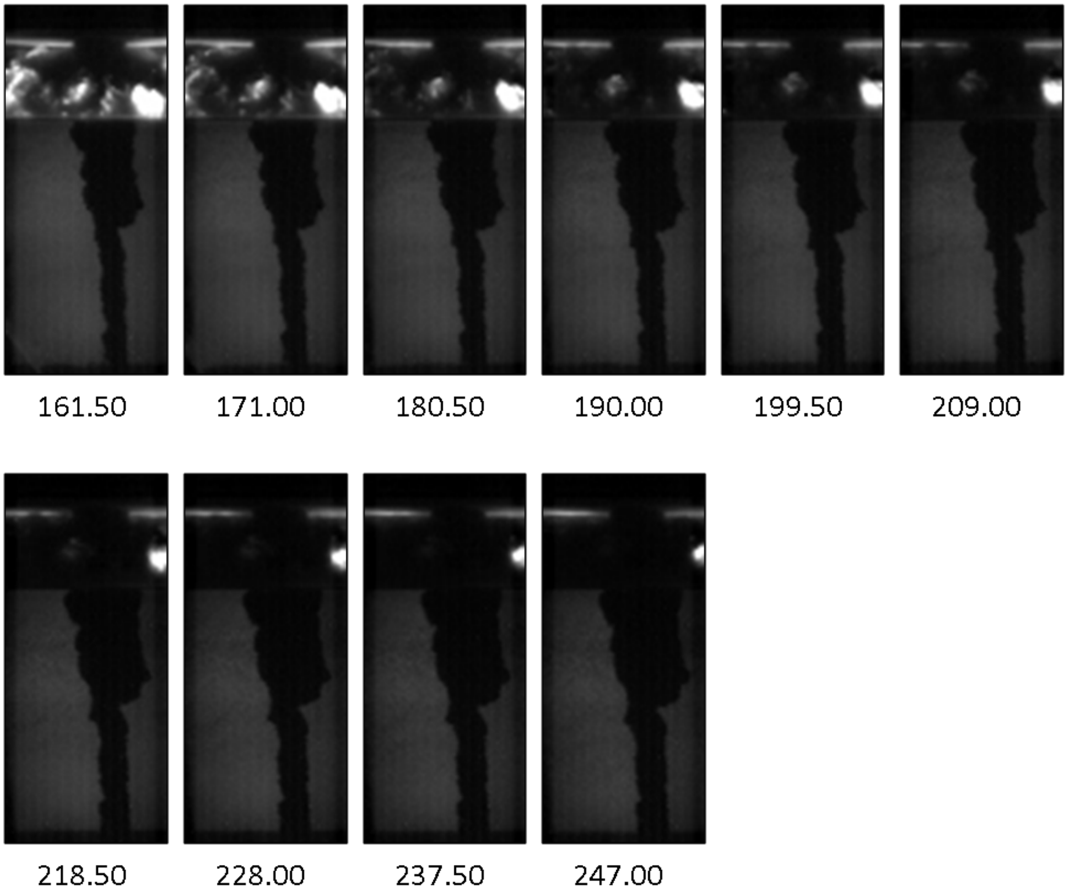

all images denoted by time after first light emission (μs)

Figure D.6: Image sequence from test 10, solid Cu liner, 50.75 mm, cont.

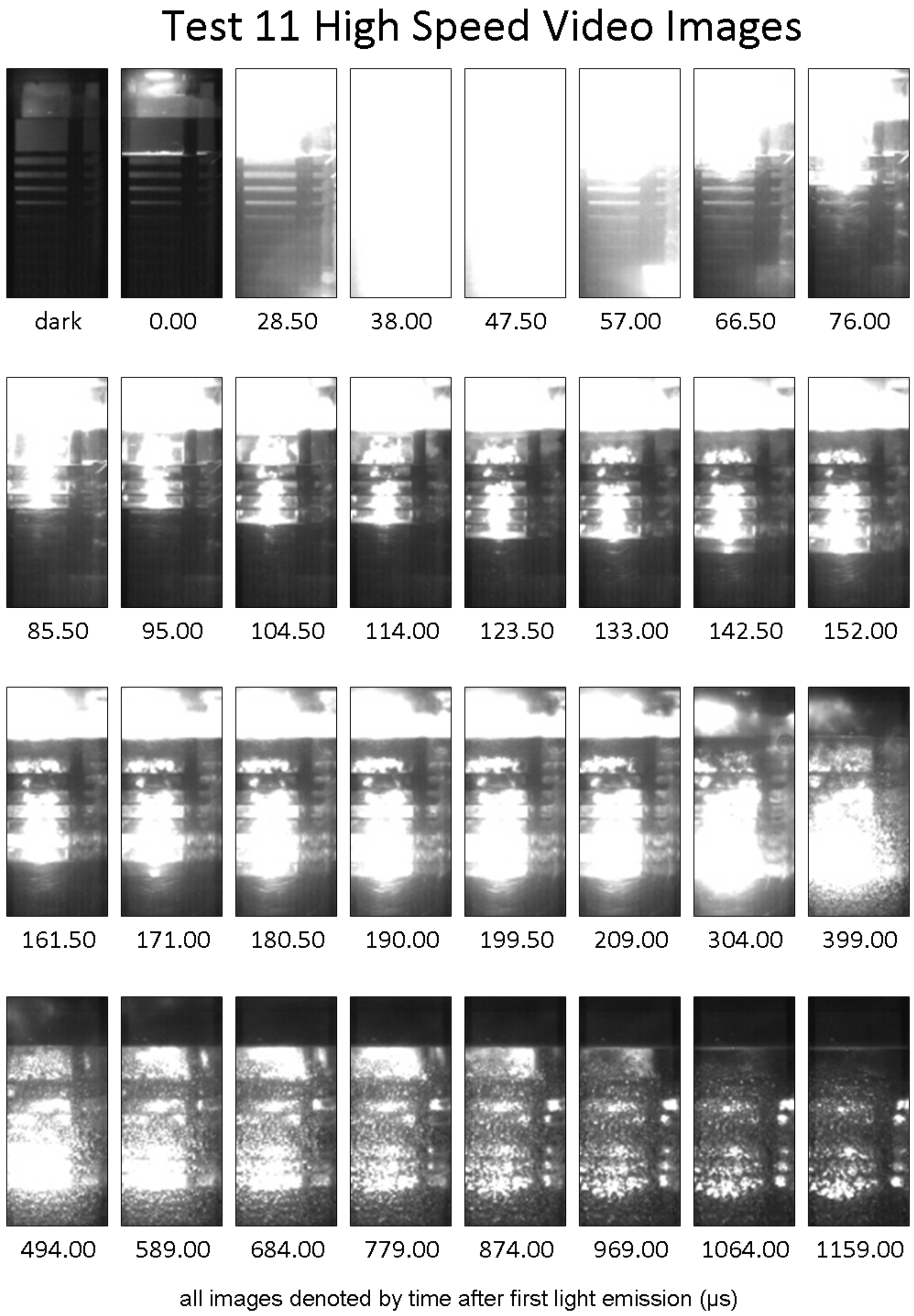

Figure D.7: Image sequence from test 11, solid Al liner, 50.75 mm

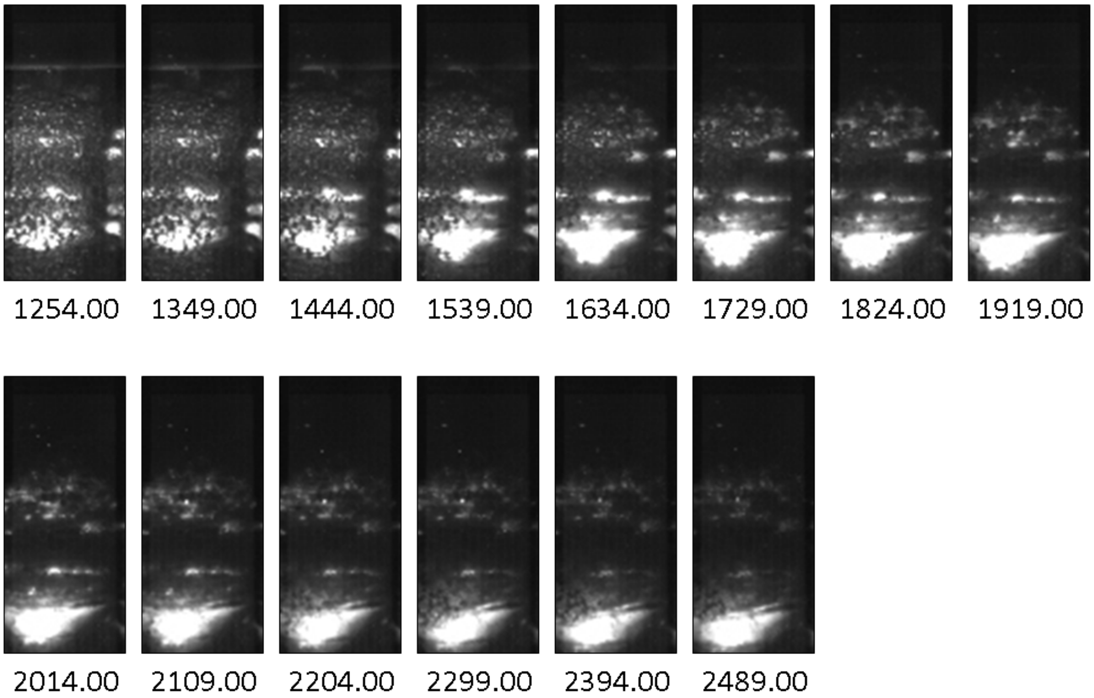
Test 11 High Speed Video Images, Continued.

all images denoted by time after first light emission (μs)

Figure D.8: Image sequence from test 11, solid Al liner, 50.75 mm, cont.

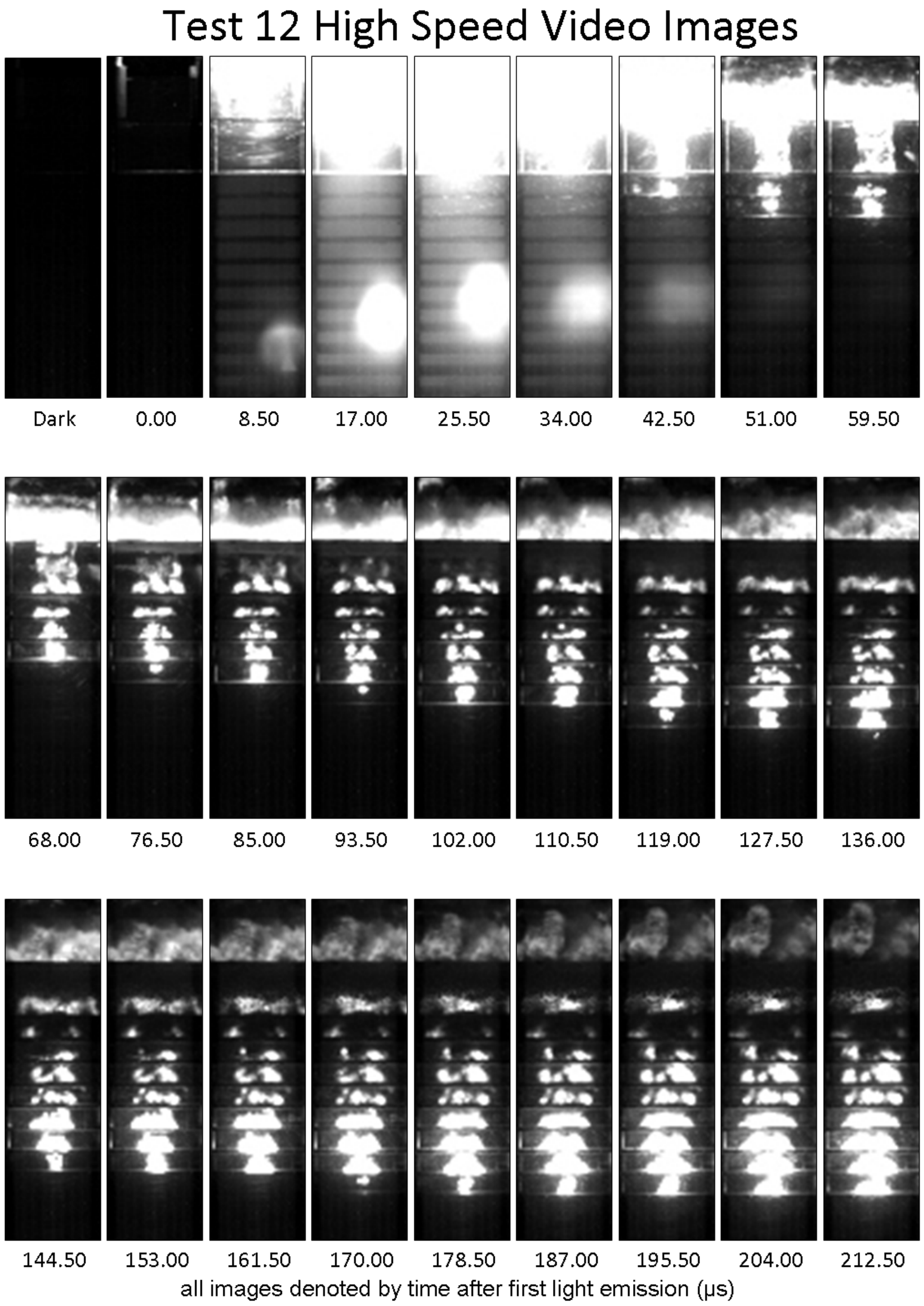

Figure D.9: Image sequence from test 12, solid Al liner, 50.75 mm

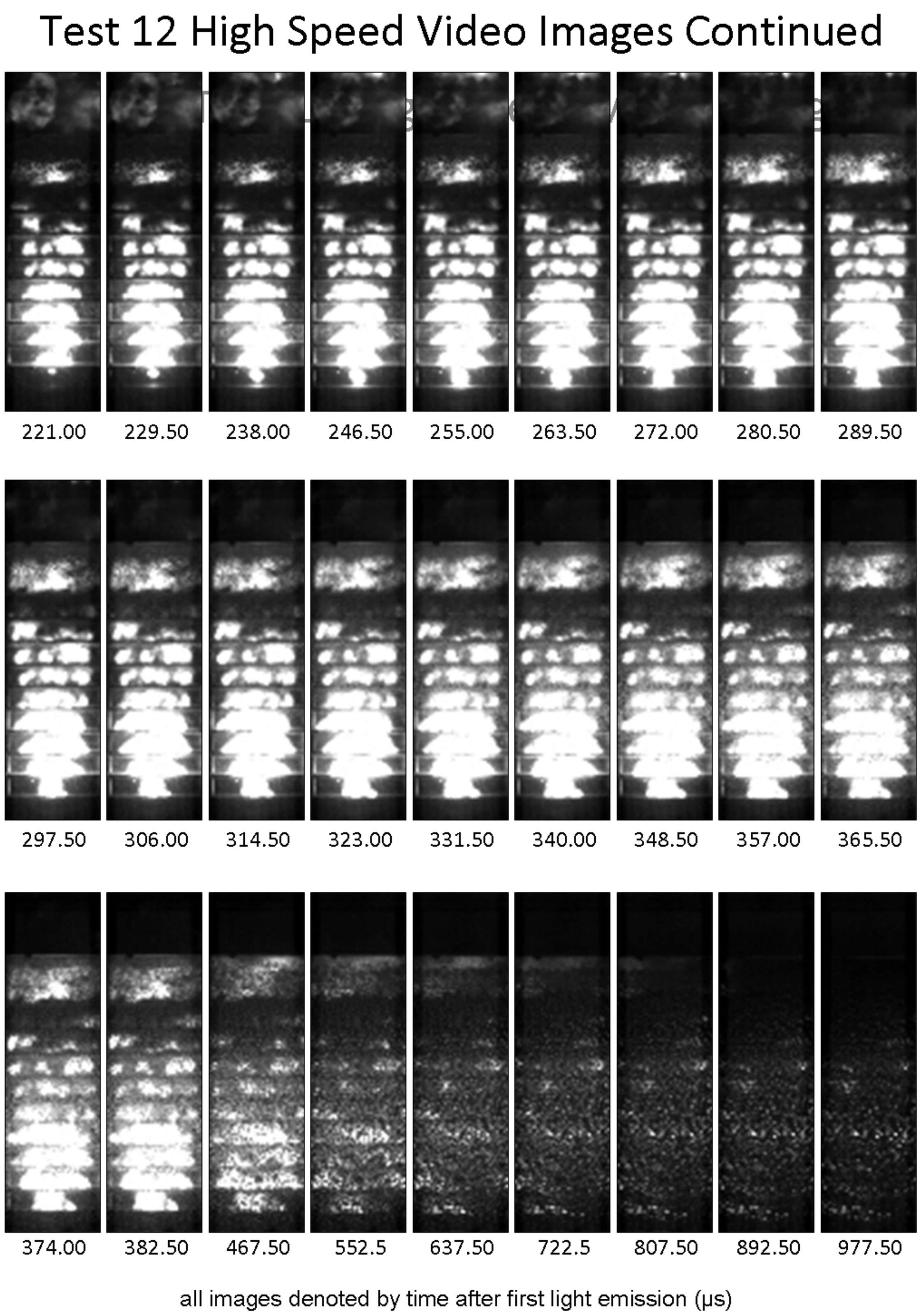

Test 12 High Speed Video Images Continued

all images denoted by time after first light emission (μs)

Figure D.10: Image sequence from test 12, solid Al liner, 50.75 mm, cont.

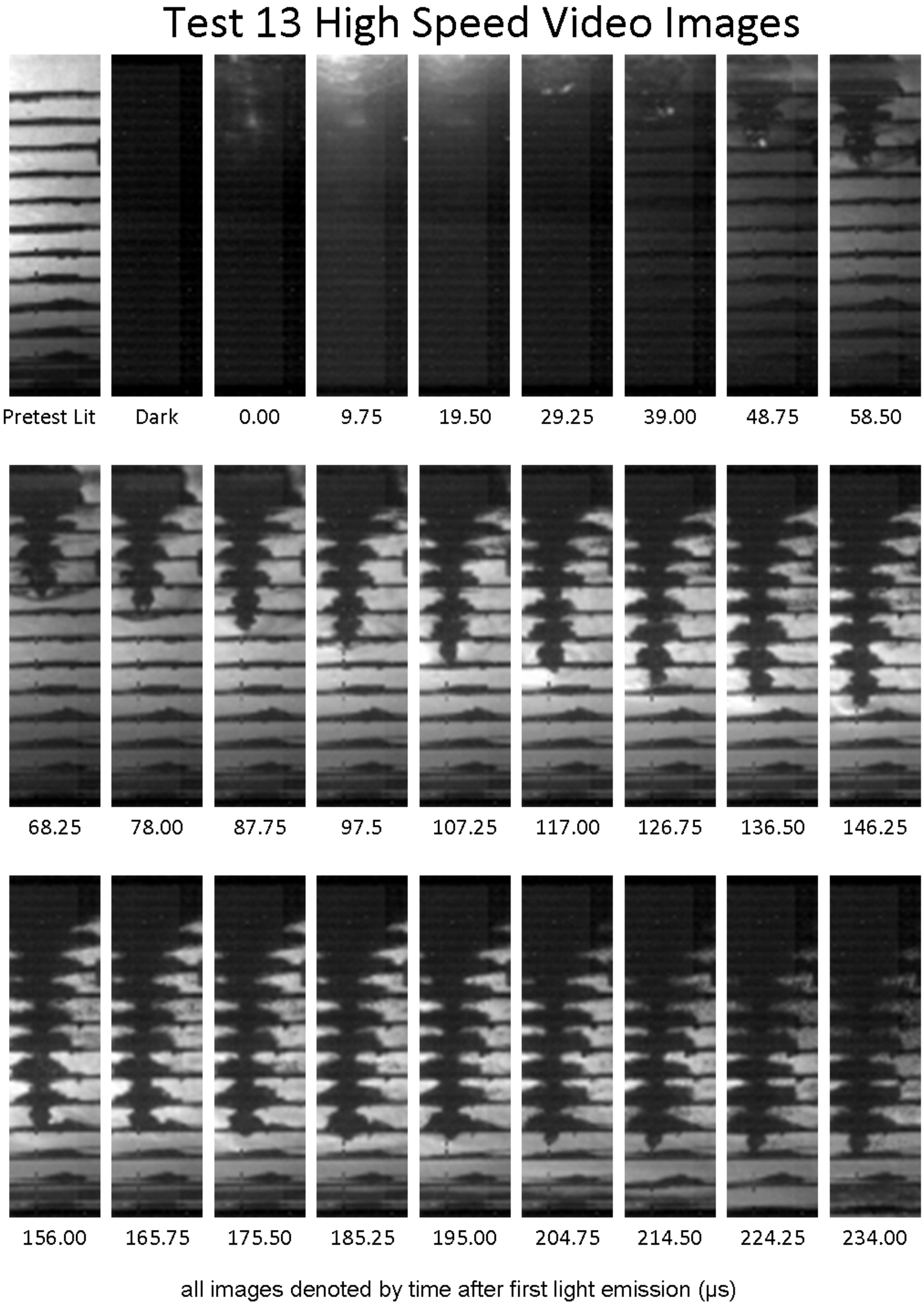

Figure D.11: Image sequence from test 13, solid Al liner into oil, 50.75 mm

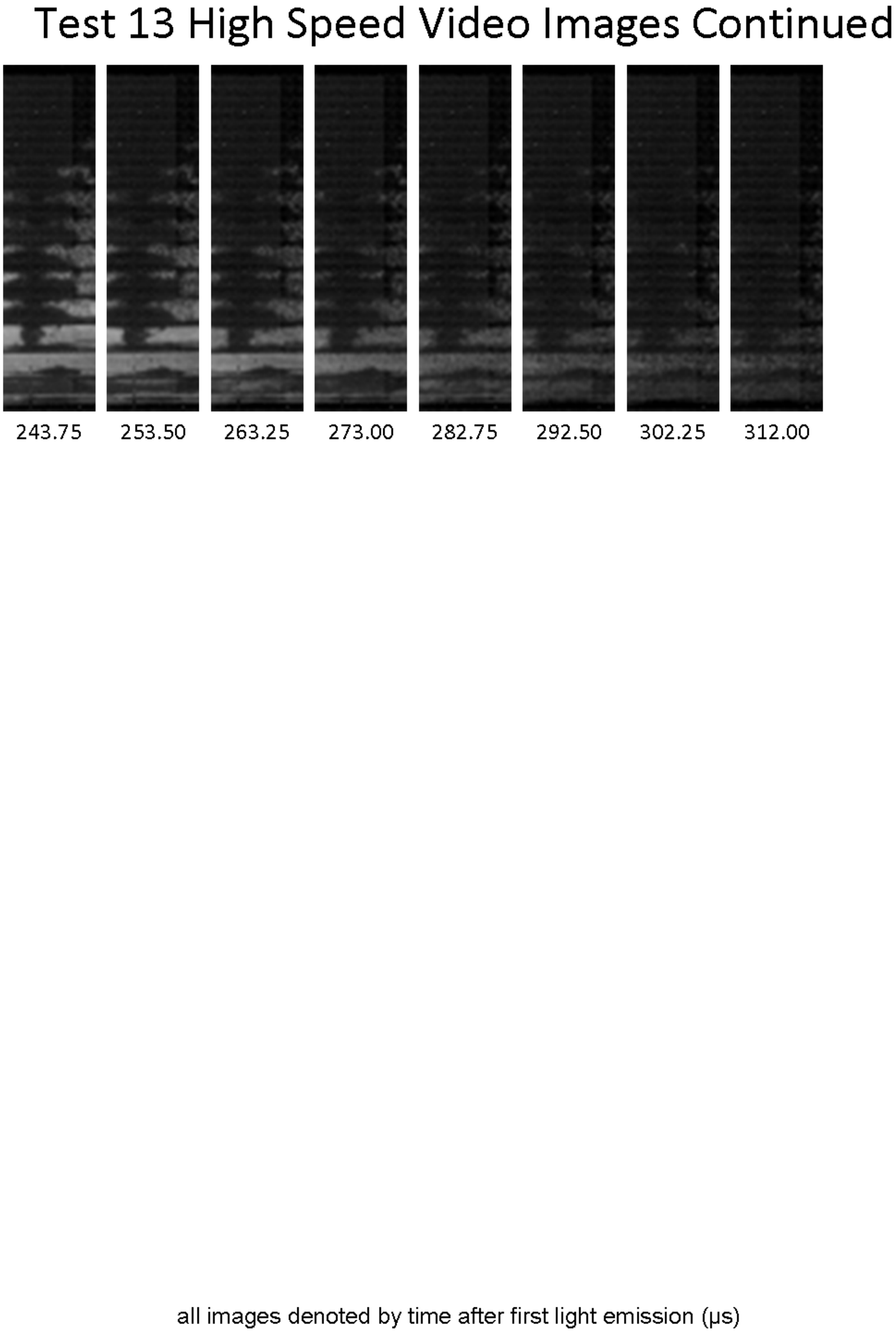

Figure D.12: Image sequence from test 13, solid Al liner into oil, 50.75 mm, cont.

APPENDIX E

COMPLETE TESTS RESULTS

E.1 Test 1

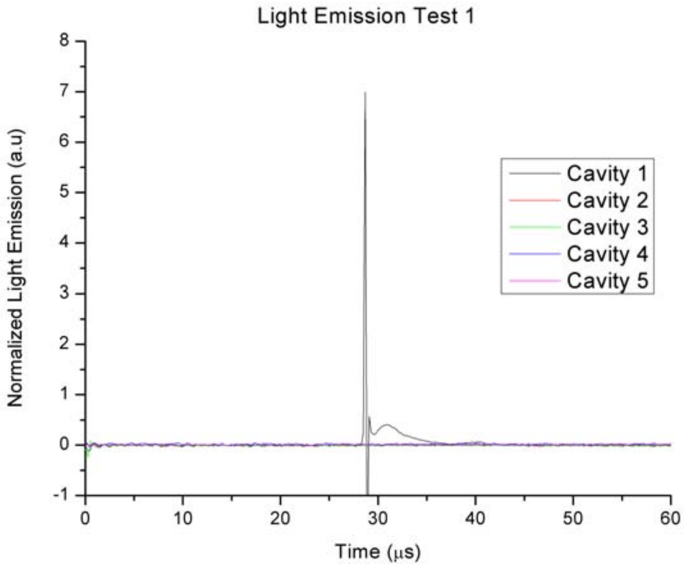

Figure E.1: Test 1 light emission

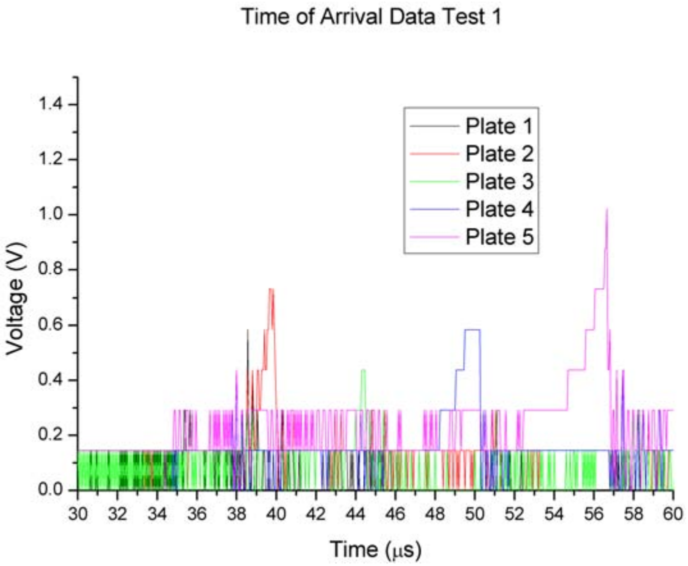

Figure E.2: Test 1 time of arrival

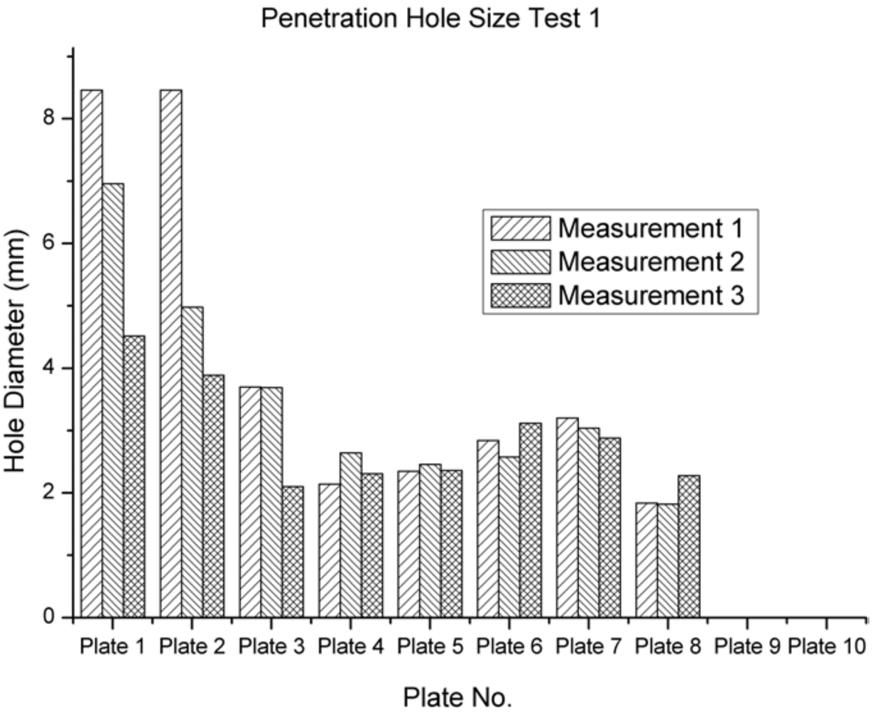

Figure E.3: Test 1 hole size

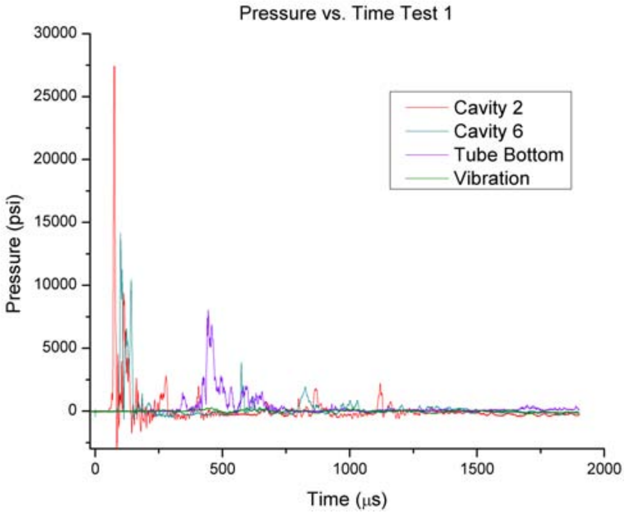

Figure E.4: Test 1 pressure data

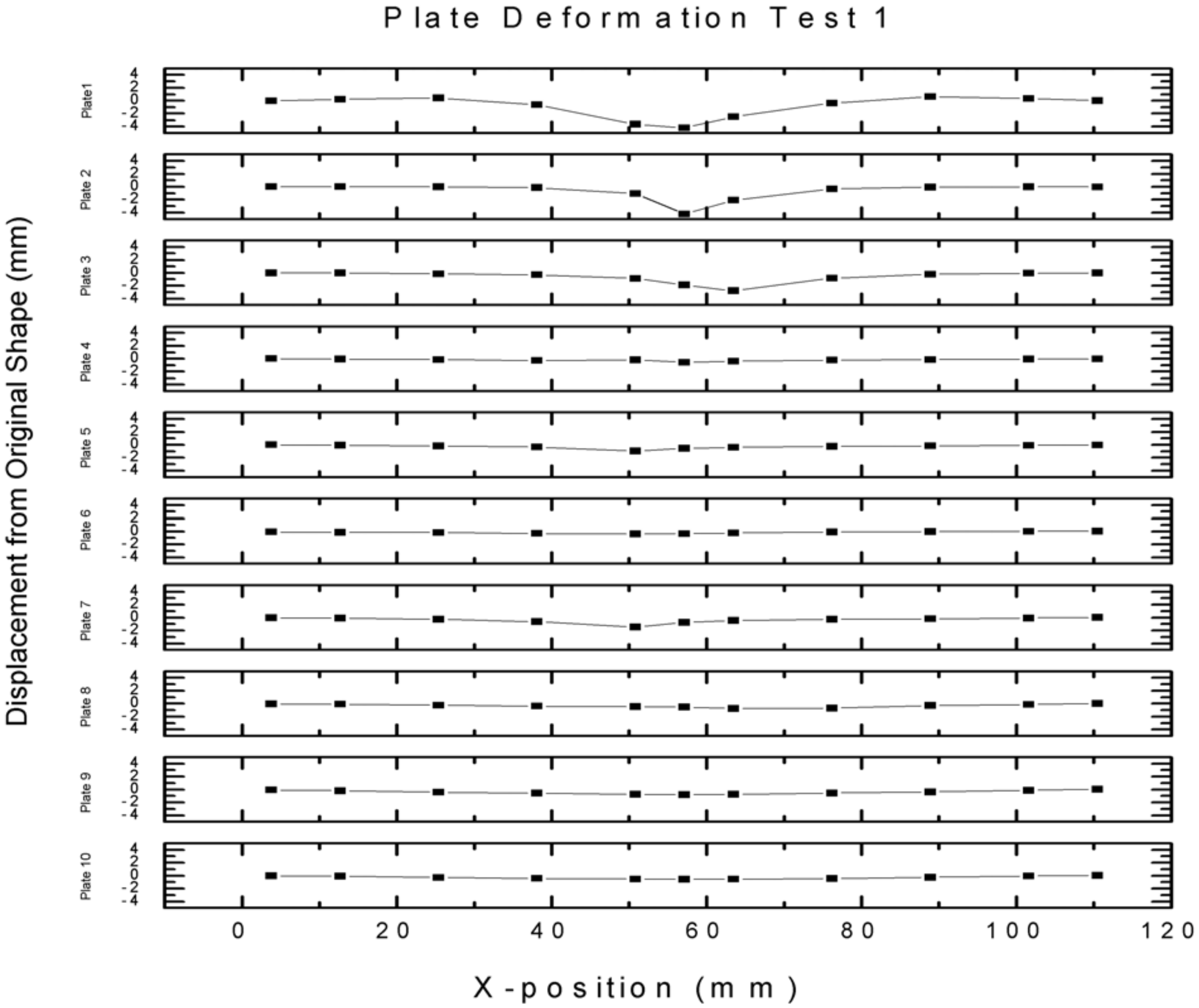

Figure E.5: Test 1 plate deformation

E.2 Test 2

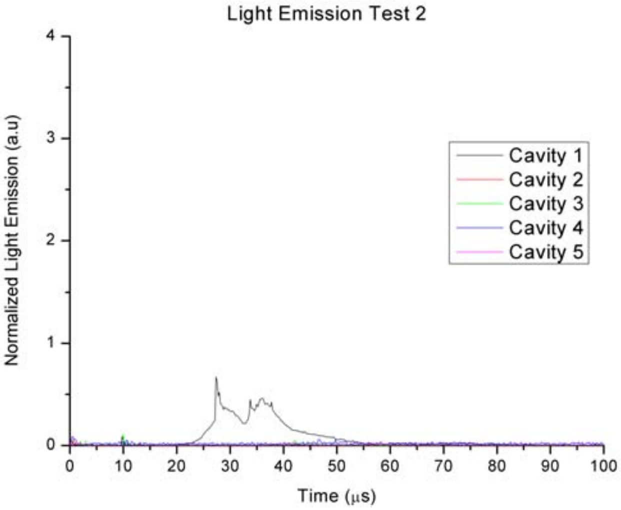

Figure E.6: Test 2 light emission

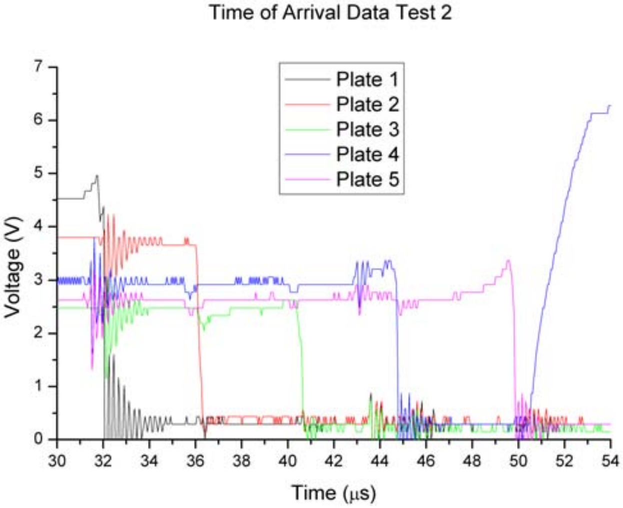

Figure E.7: Test 2 time of arrival

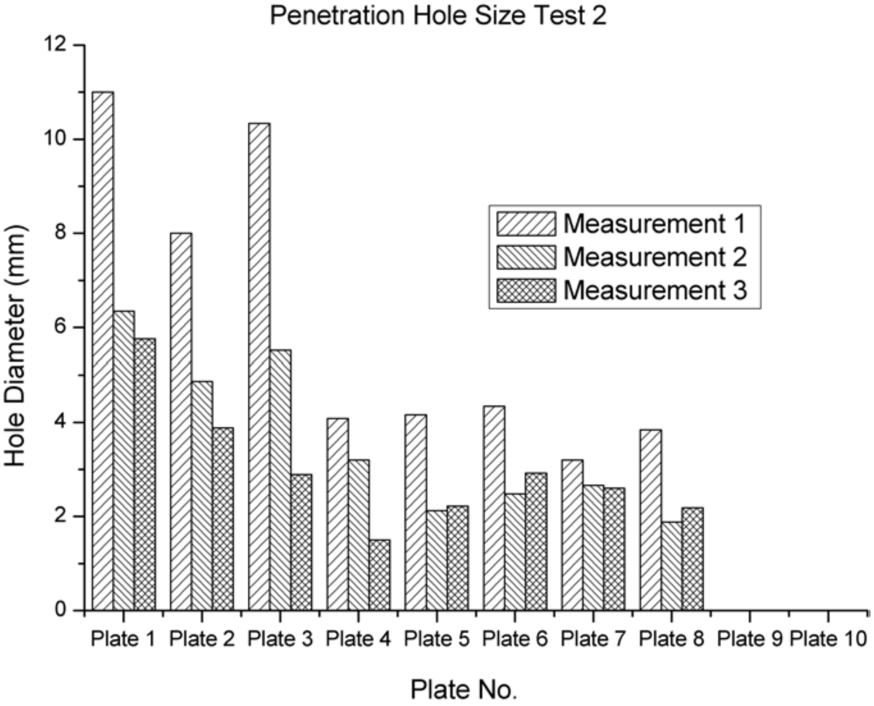

Figure E.8: Test 2 hole size

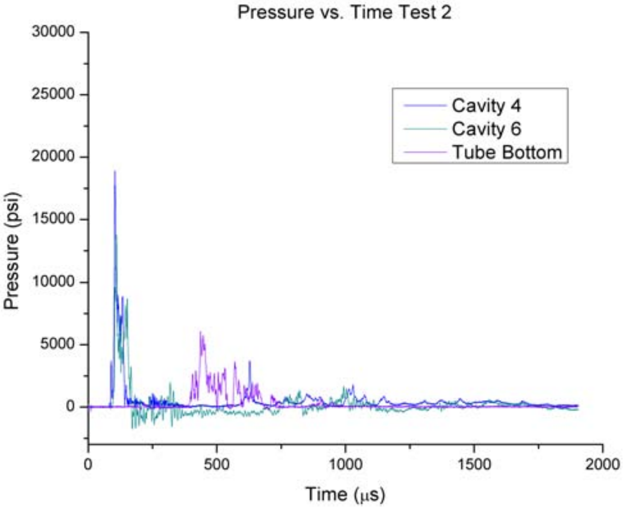

Figure E.9: Test 2 pressure data

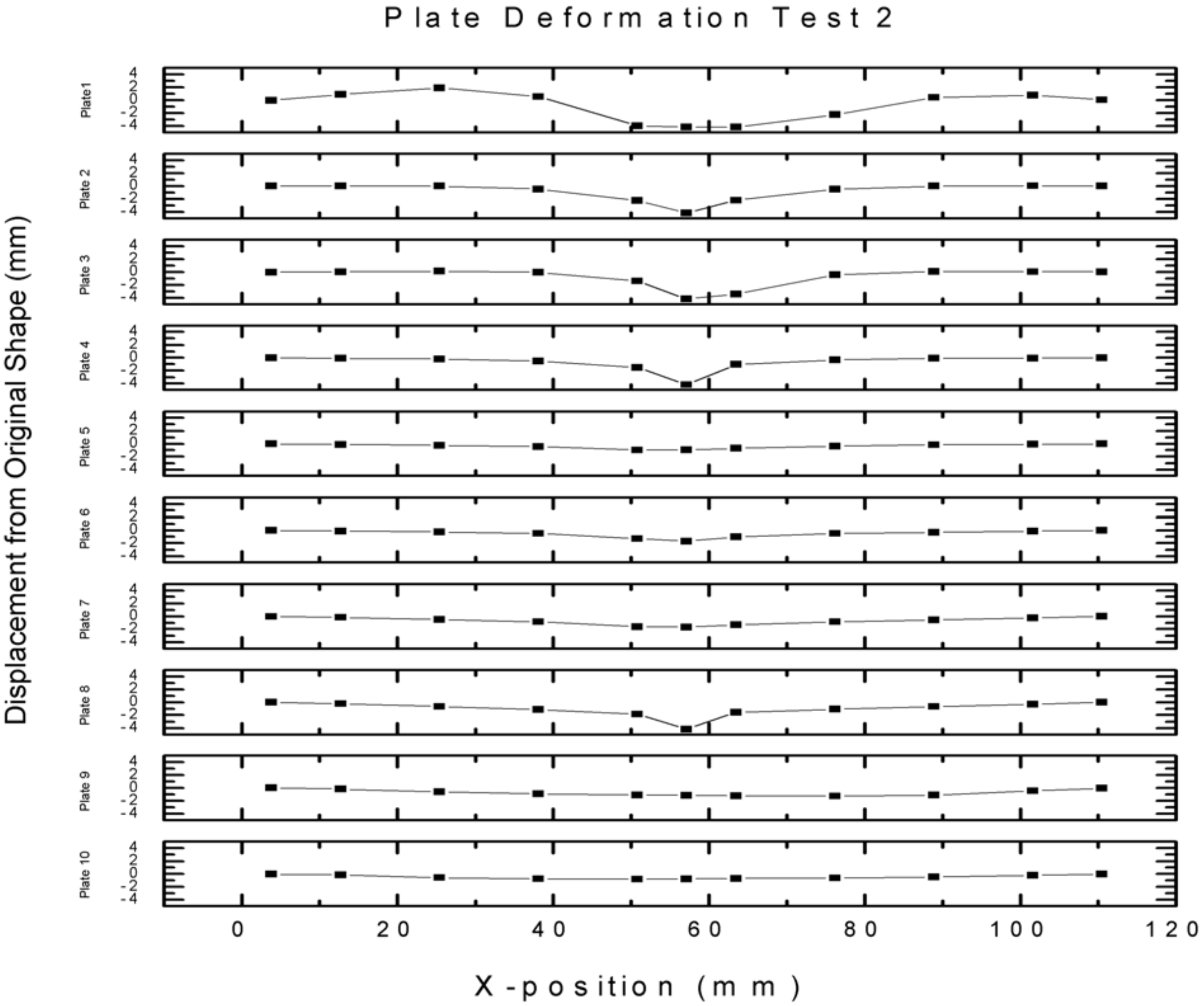

Figure E.10: Test 2 plate deformation

E.3 Test 3

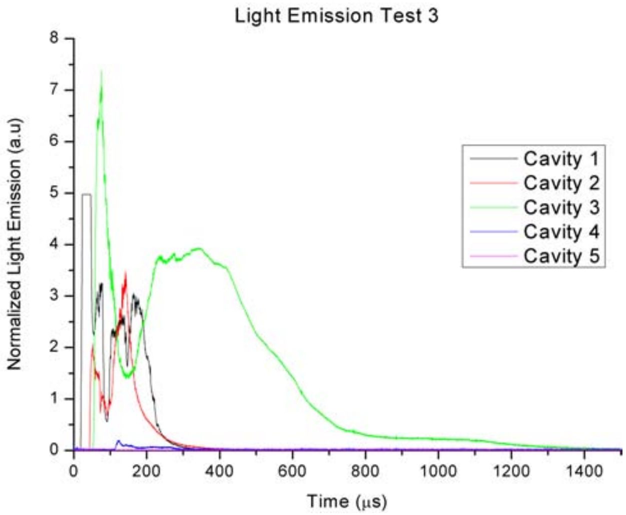

Figure E.11: Test 3 light emission

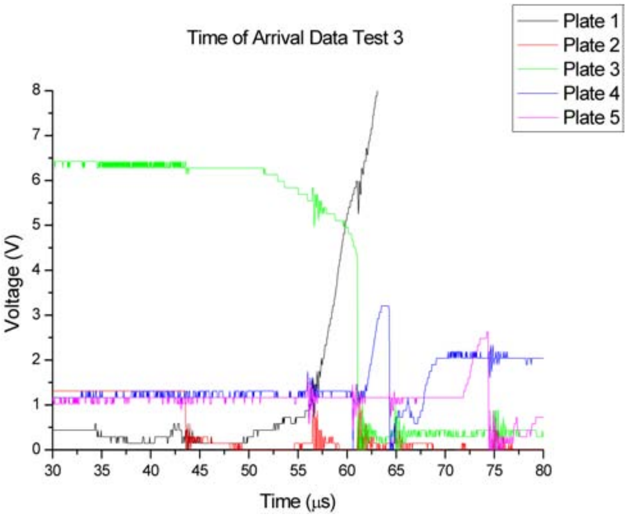

Figure E.12: Test 3 time of arrival

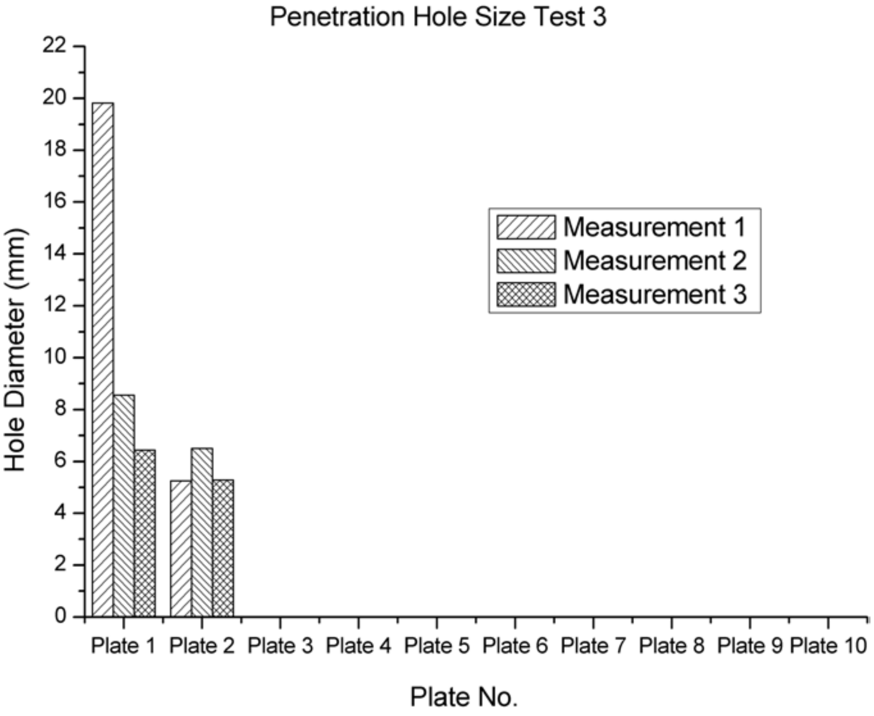

Figure E.13: Test 3 hole size

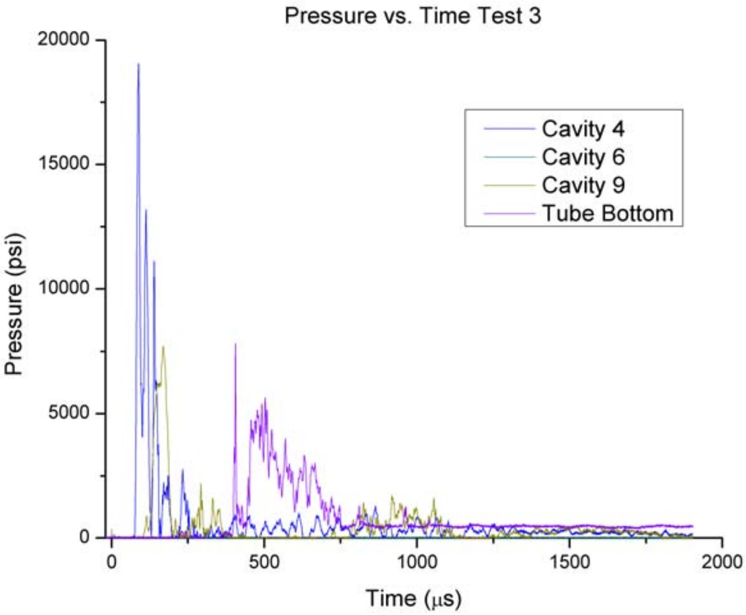

Figure E.14: Test 3 pressure data

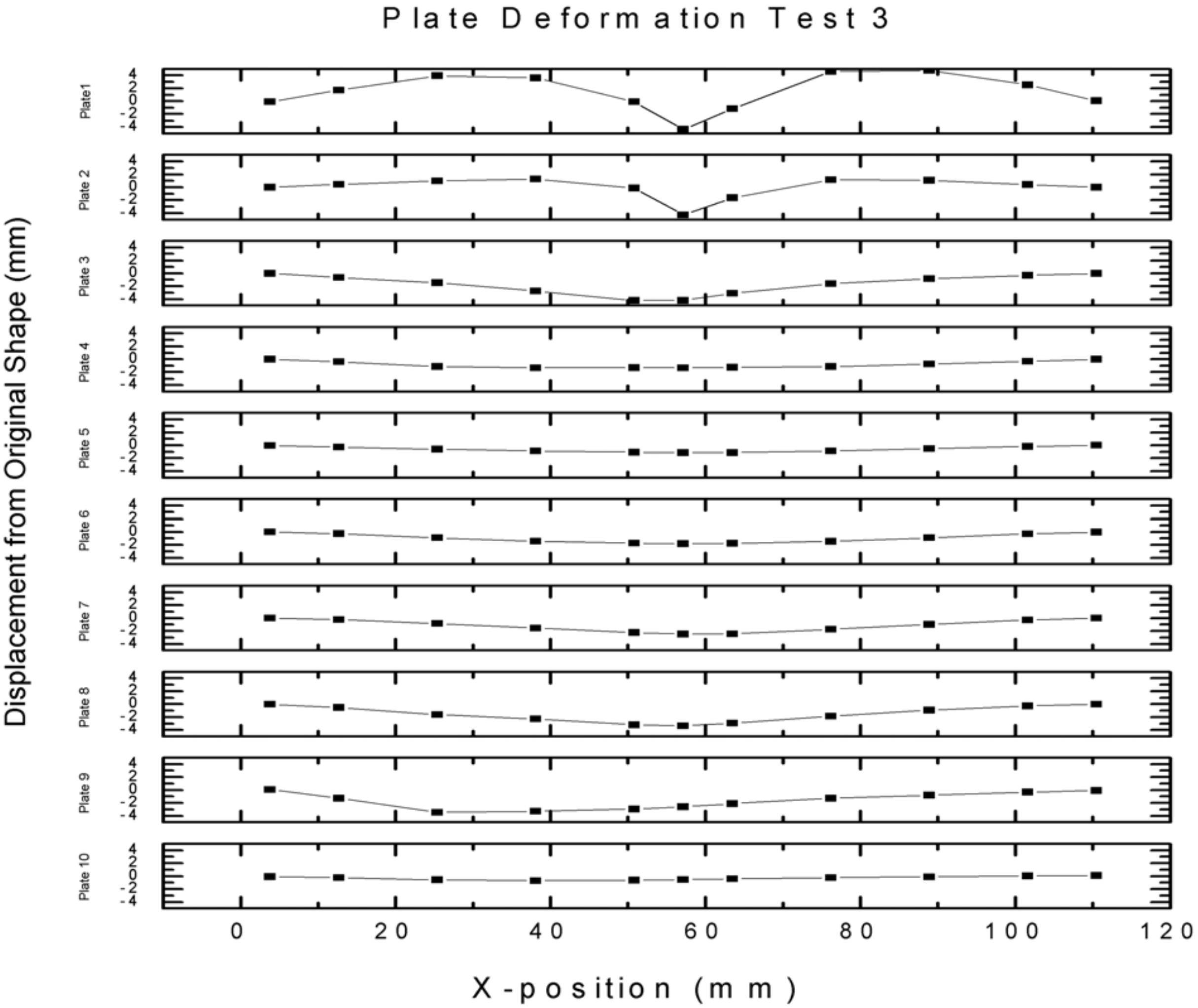

Figure E.15: Test 3 plate deformation

E.4 Test 4

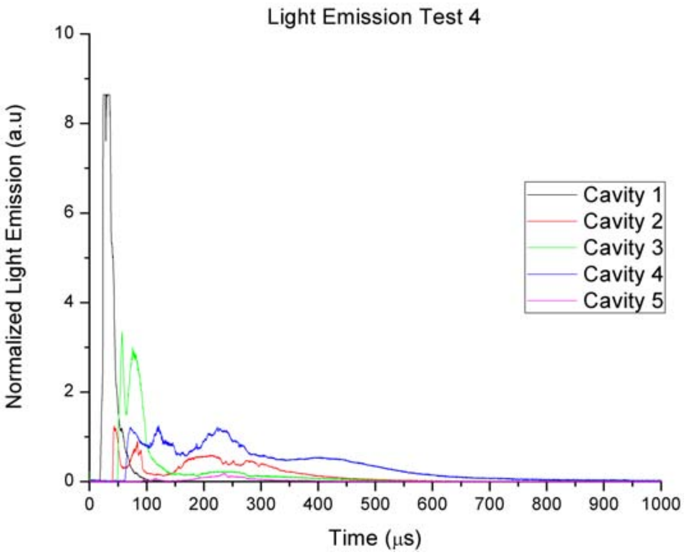

Figure E.16: Test 4 light emission

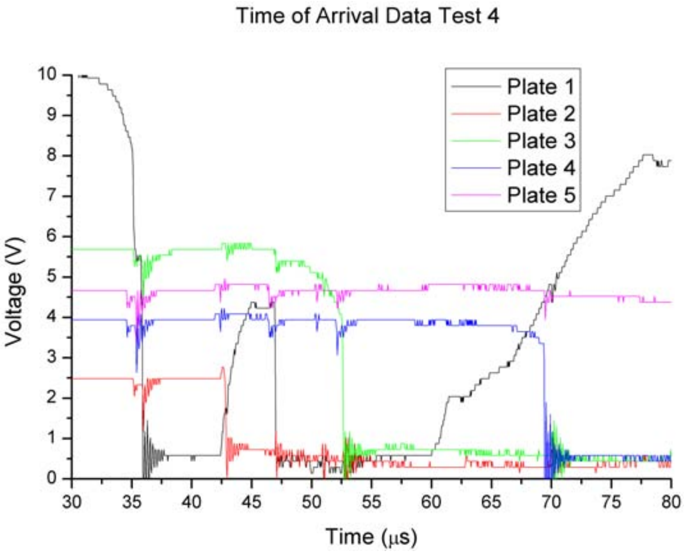

Figure E.17: Test 4 time of arrival

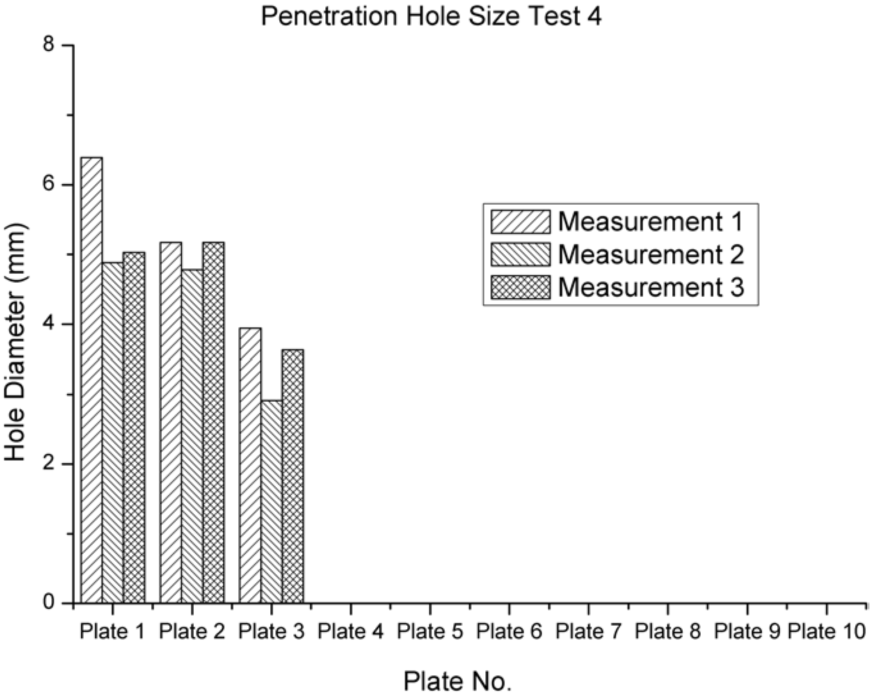

Figure E.18: Test 4 hole size

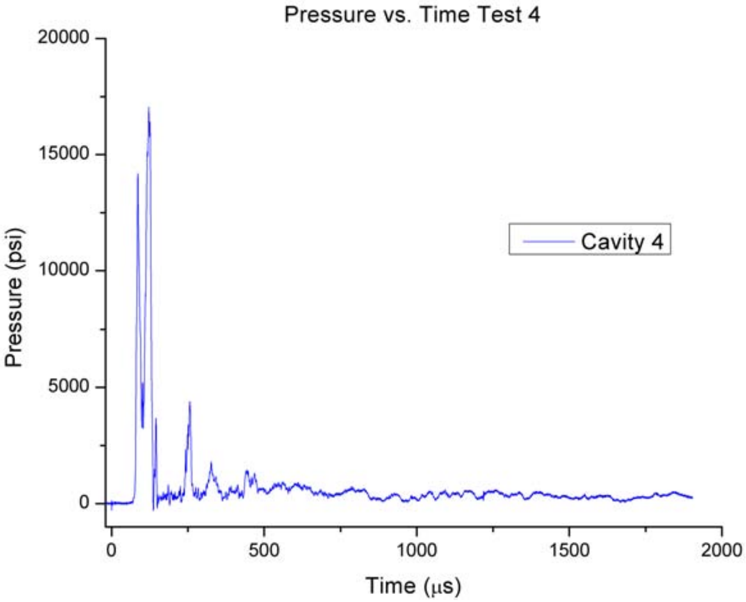

Figure E.19: Test 4 pressure data

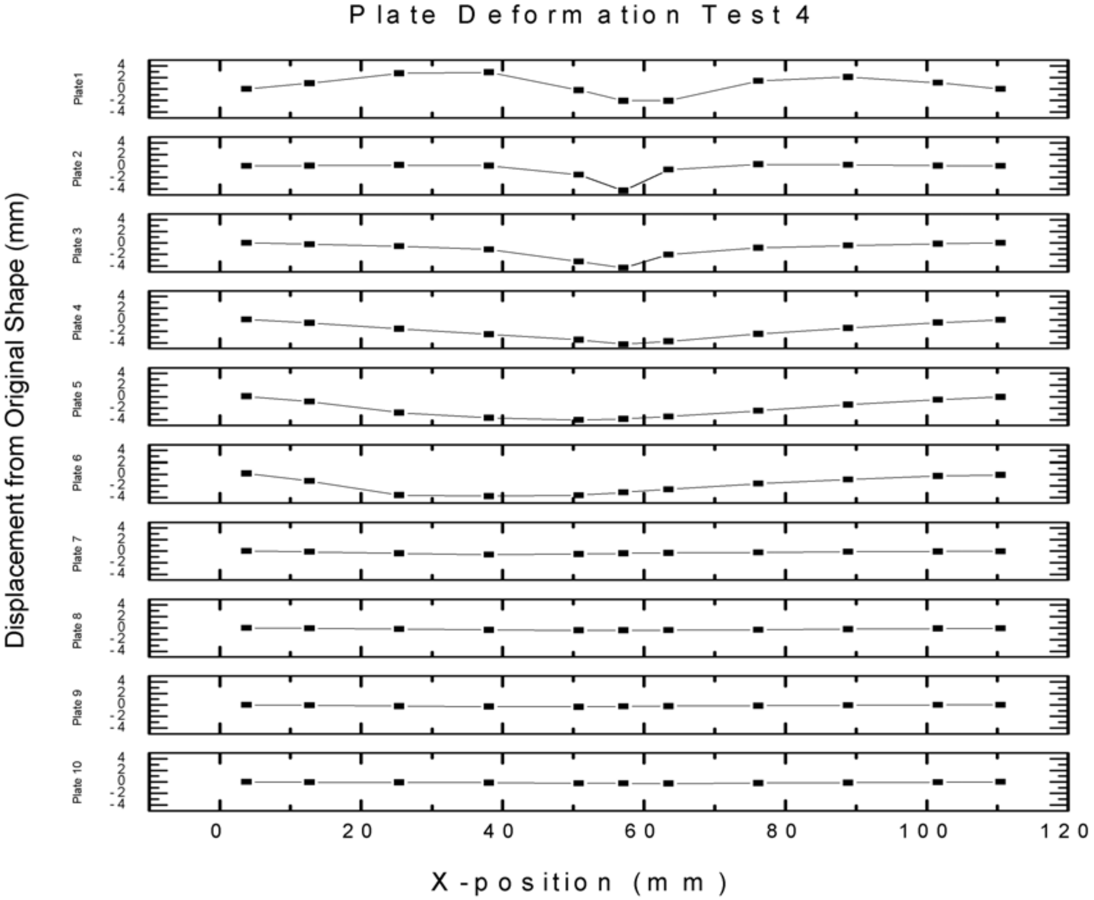

Figure E.20: Test 4 plate deformation

E.5 Test 5

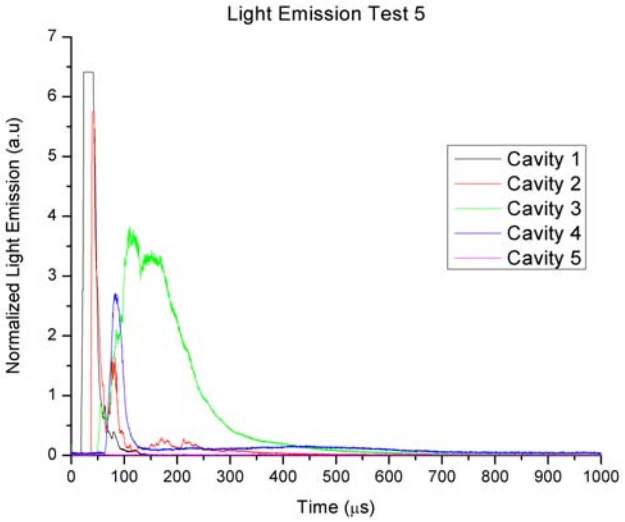

Figure E.21: Test 5 light emission

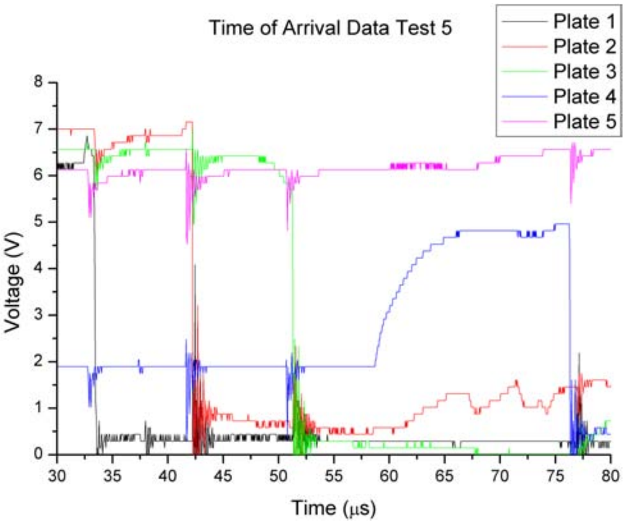

Figure E.22: Test 5 time of arrival

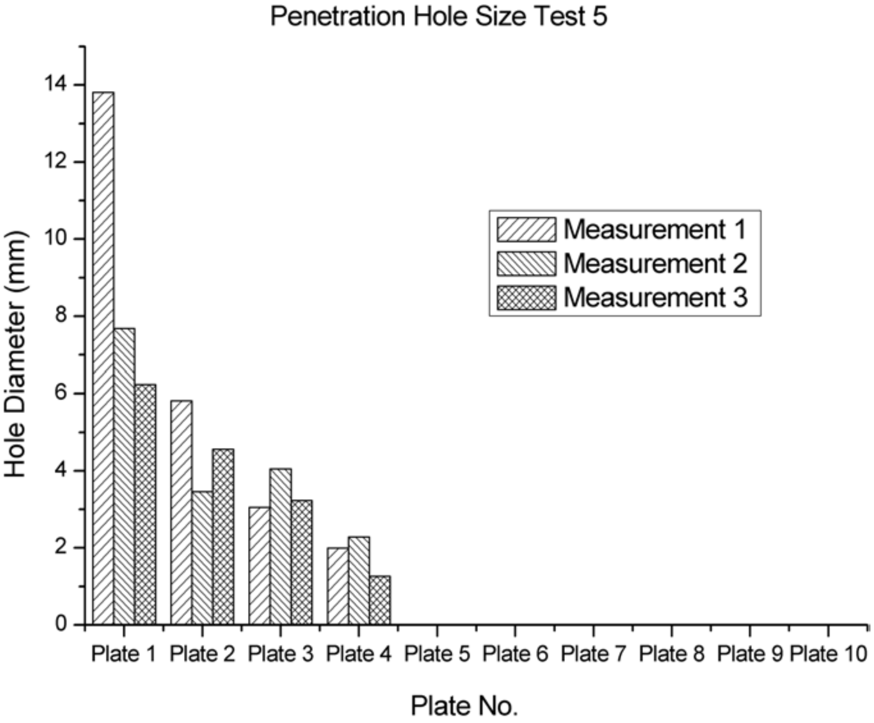

Figure E.23: Test 5 hole size

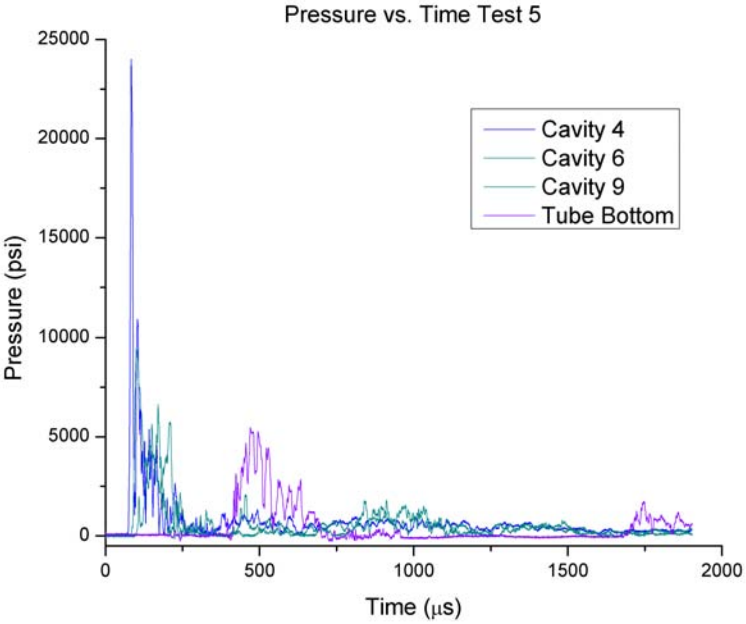

Figure E.24: Test 5 pressure data

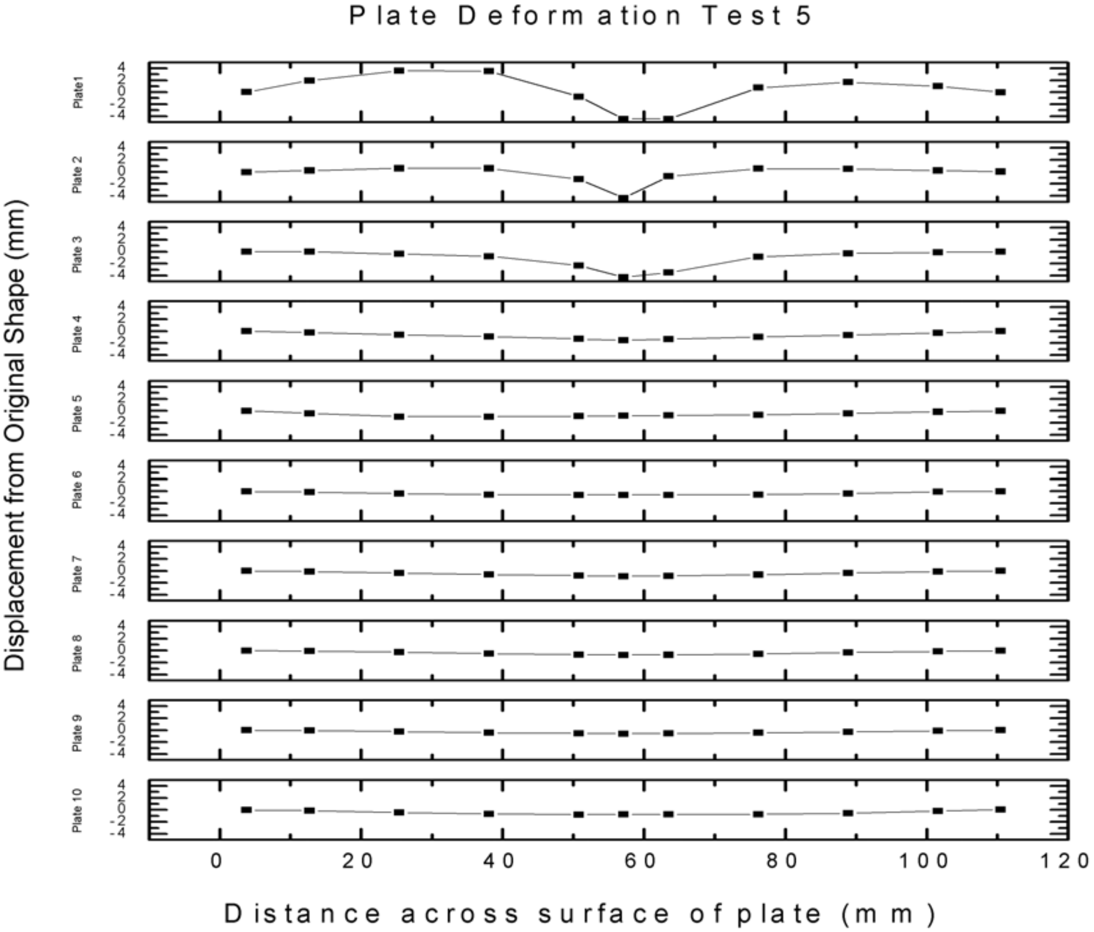

Figure E.25: Test 5 plate deformation

E.6 Test 6

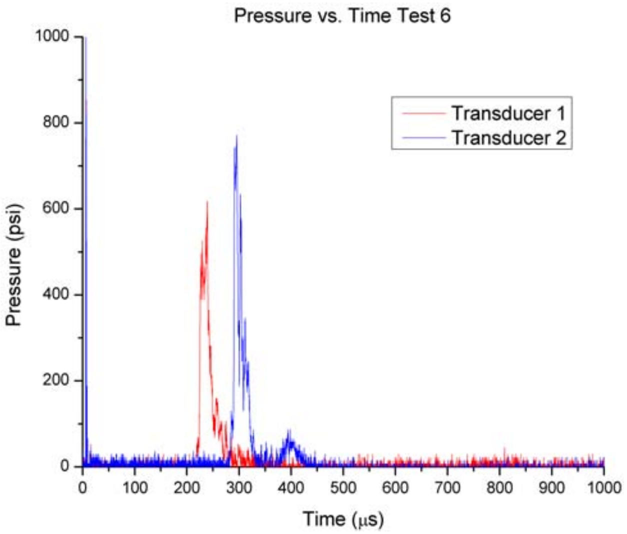

Figure E.26: Test 6 pressure

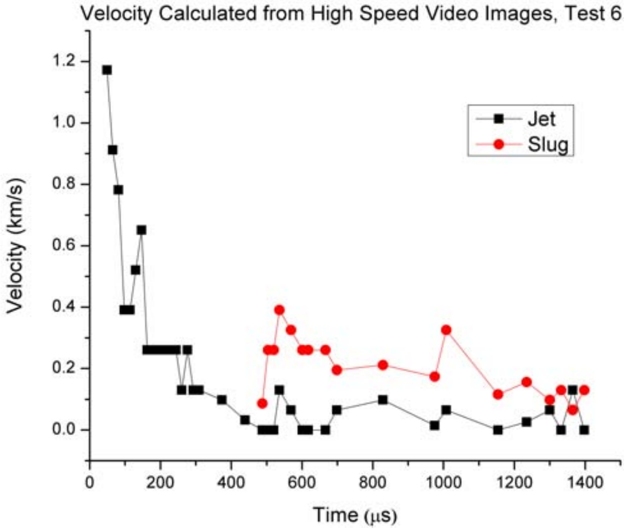

Figure E.27: Test 6 velocity from high speed video

E.7 Test 7

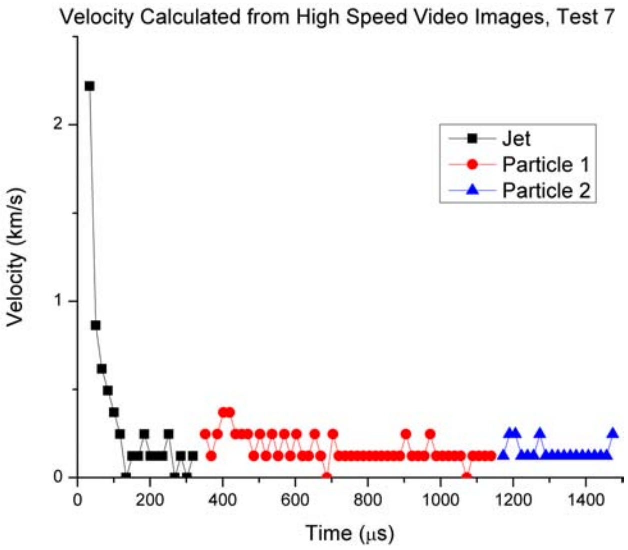

Figure E.28: Test 7 velocity from high speed video

E.8 Test 8

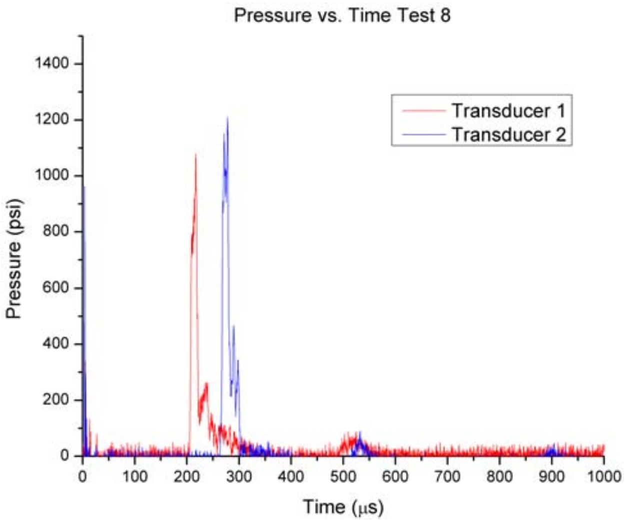

Figure E.29: Test 8 pressure

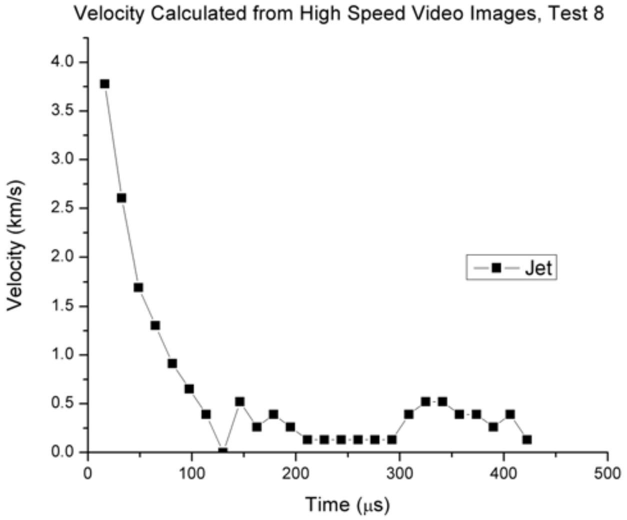

Figure E.30: Test 8 velocity from high speed video

E.9 Test 9

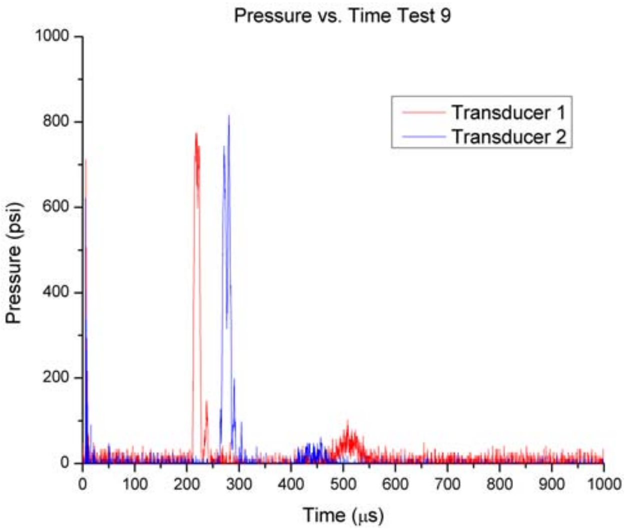

Figure E.31: Test 9 pressure

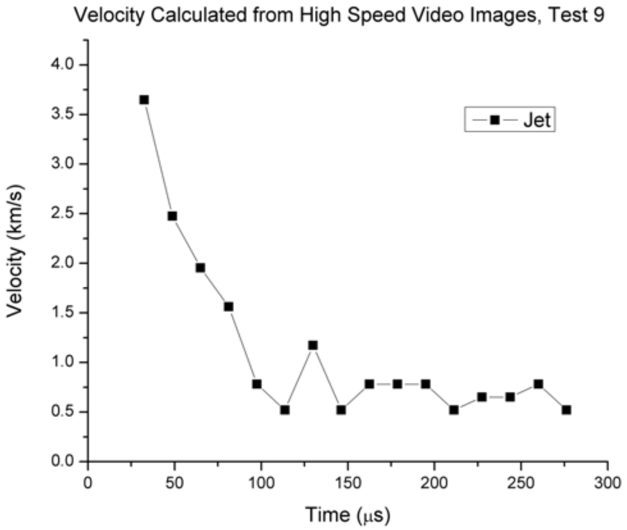

Figure E.32: Test 9 velocity from high speed video

E.10 Test 10

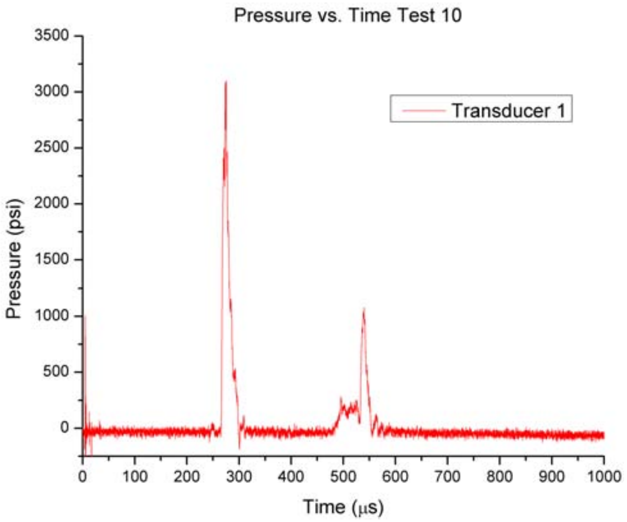

Figure E.33: Test 10 pressure data

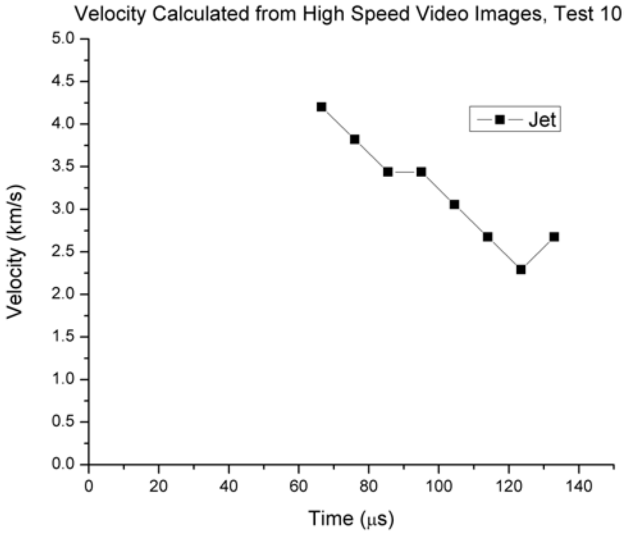

Figure E.34: Test 10 velocity from high speed video

E.11 Test 11

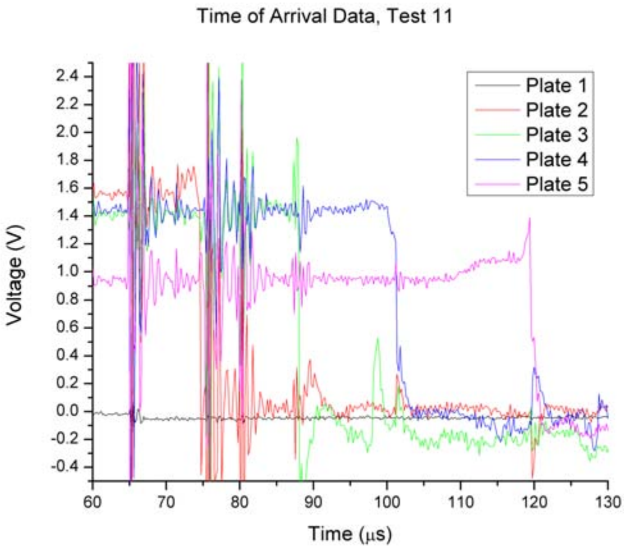

Figure E.35: Test 11 time of arrival data

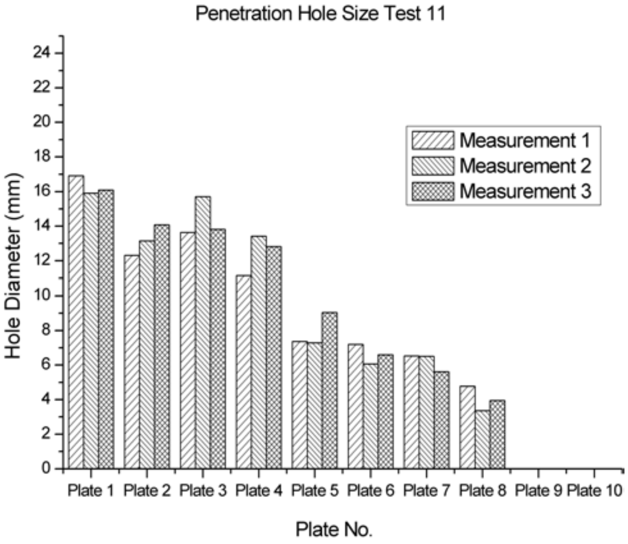

Figure E.36: Test 11 hole size

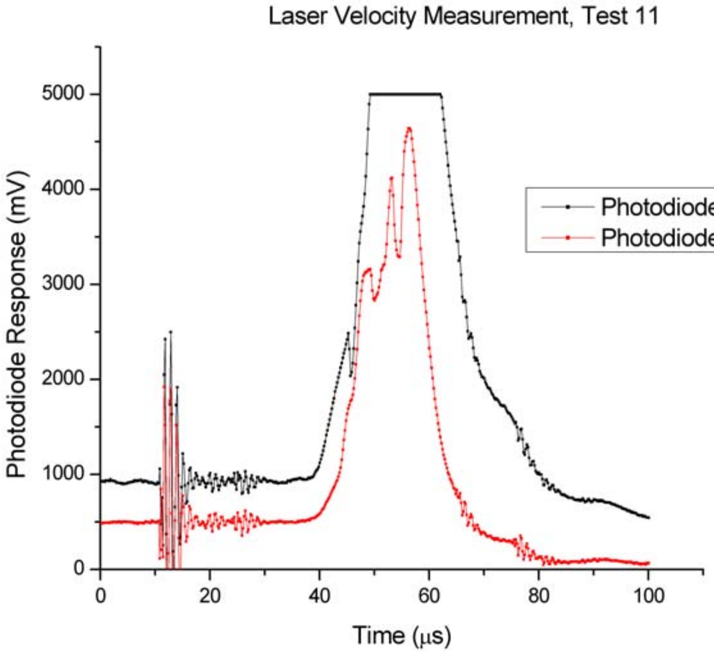

Figure E.37: Test 11 photodiode data for laser velocity measurement

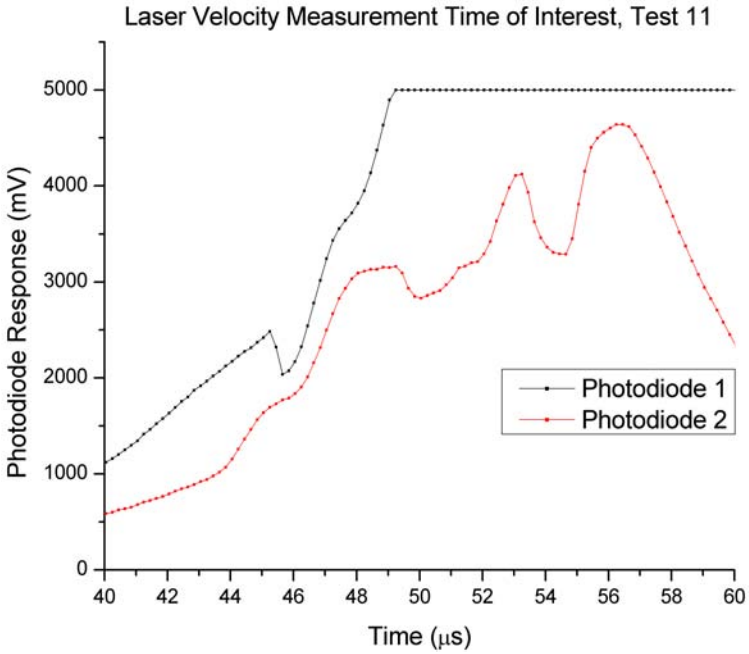

Figure E.38: Test 11 photodiode data for laser velocity measurement (time of interest)

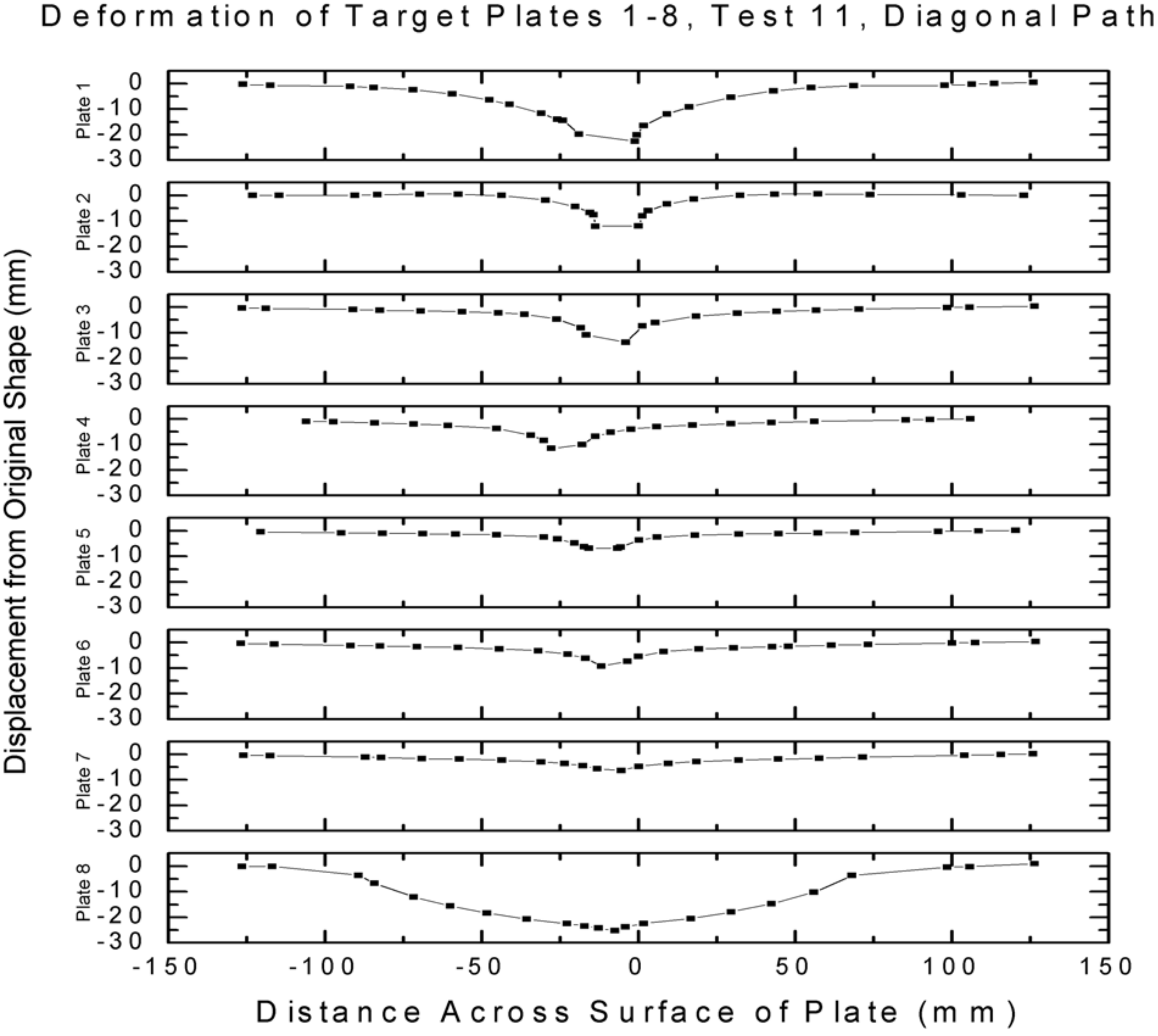

Figure E.39: Test 11 plate deformation data, diagonal path, plates 1 - 8

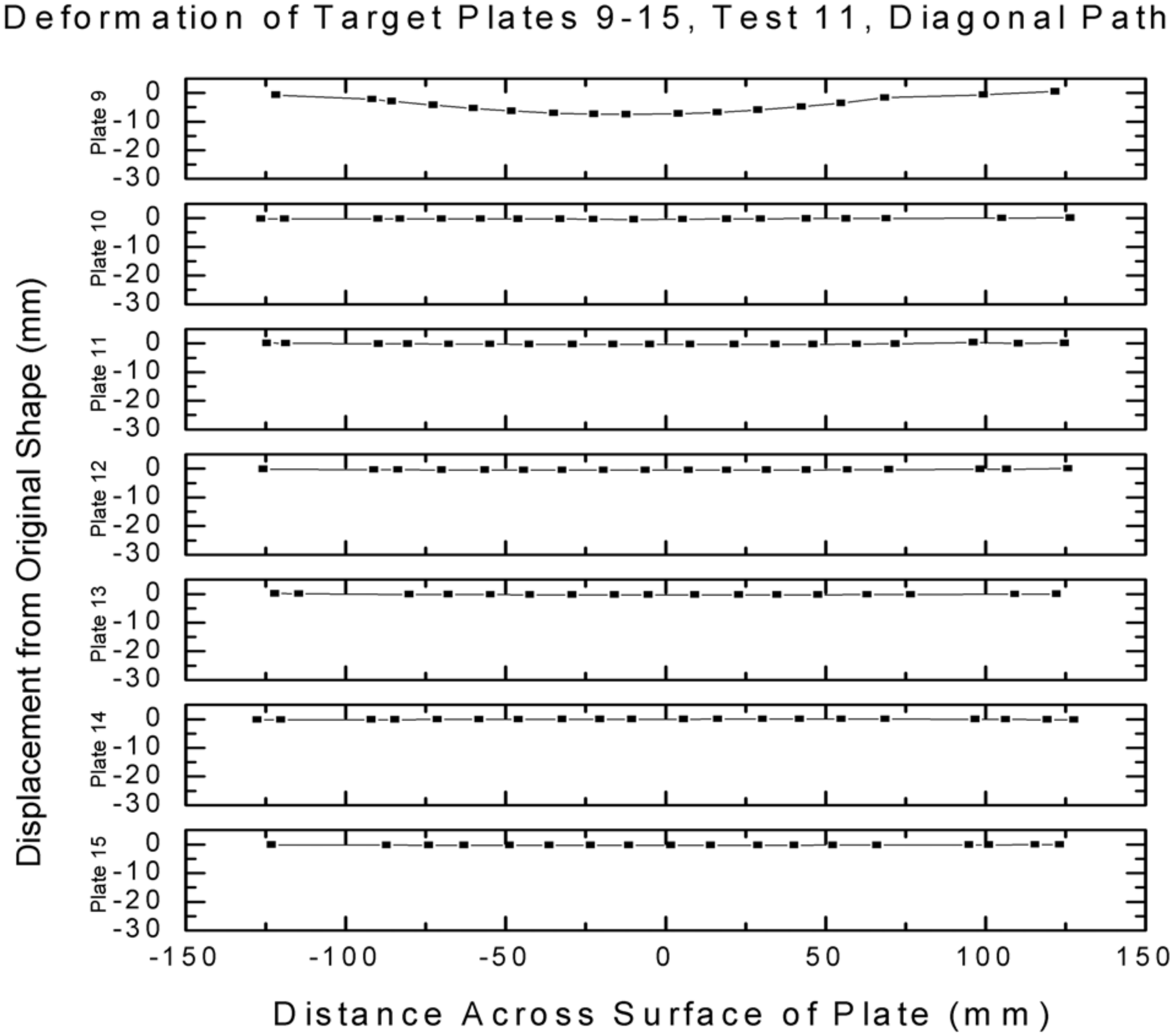

Figure E.40: Test 11 plate deformation data, diagonal path, plates 9 - 15

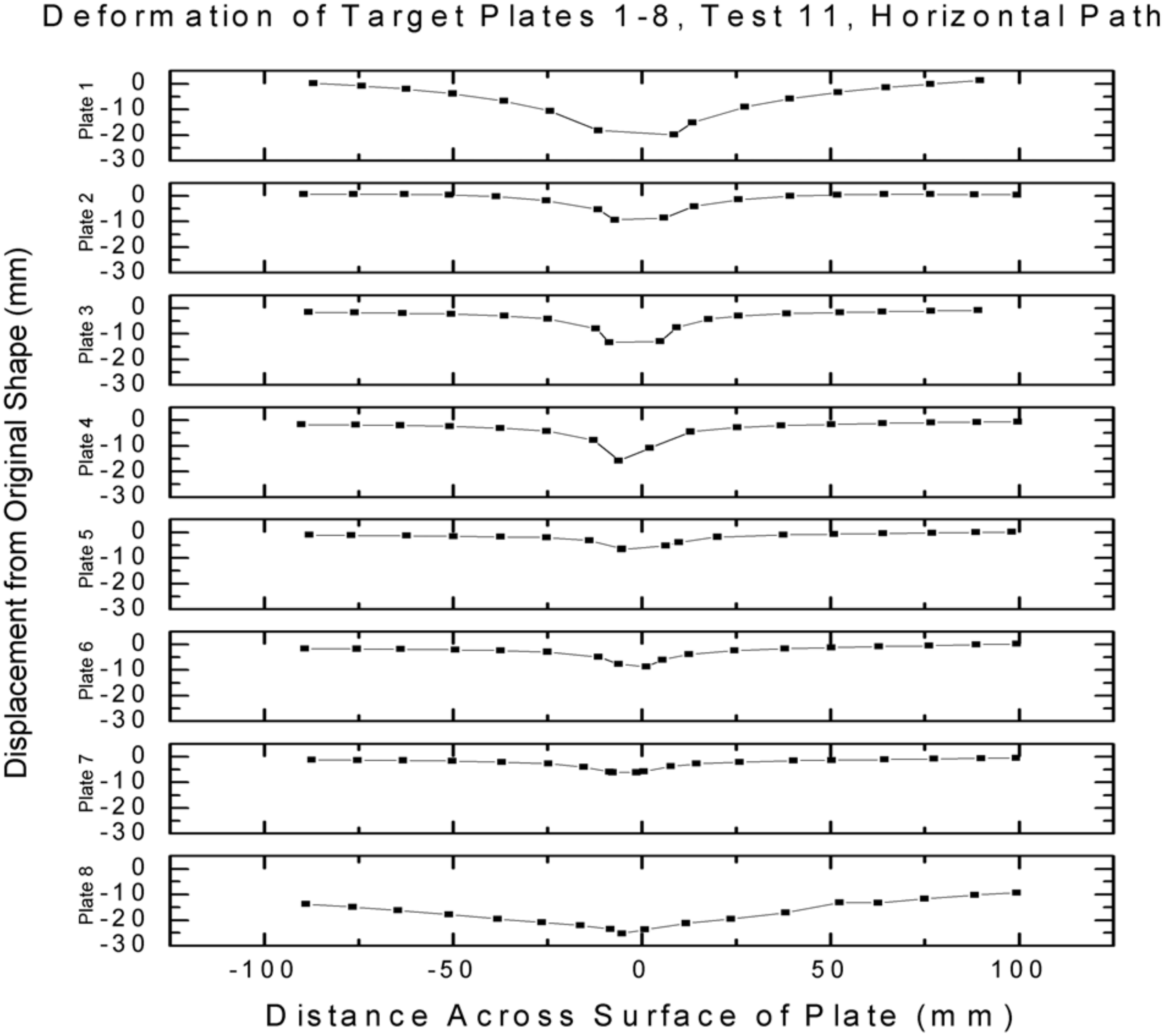

Figure E.41: Test 11 plate deformation data, horizontal path, plates 1 - 8

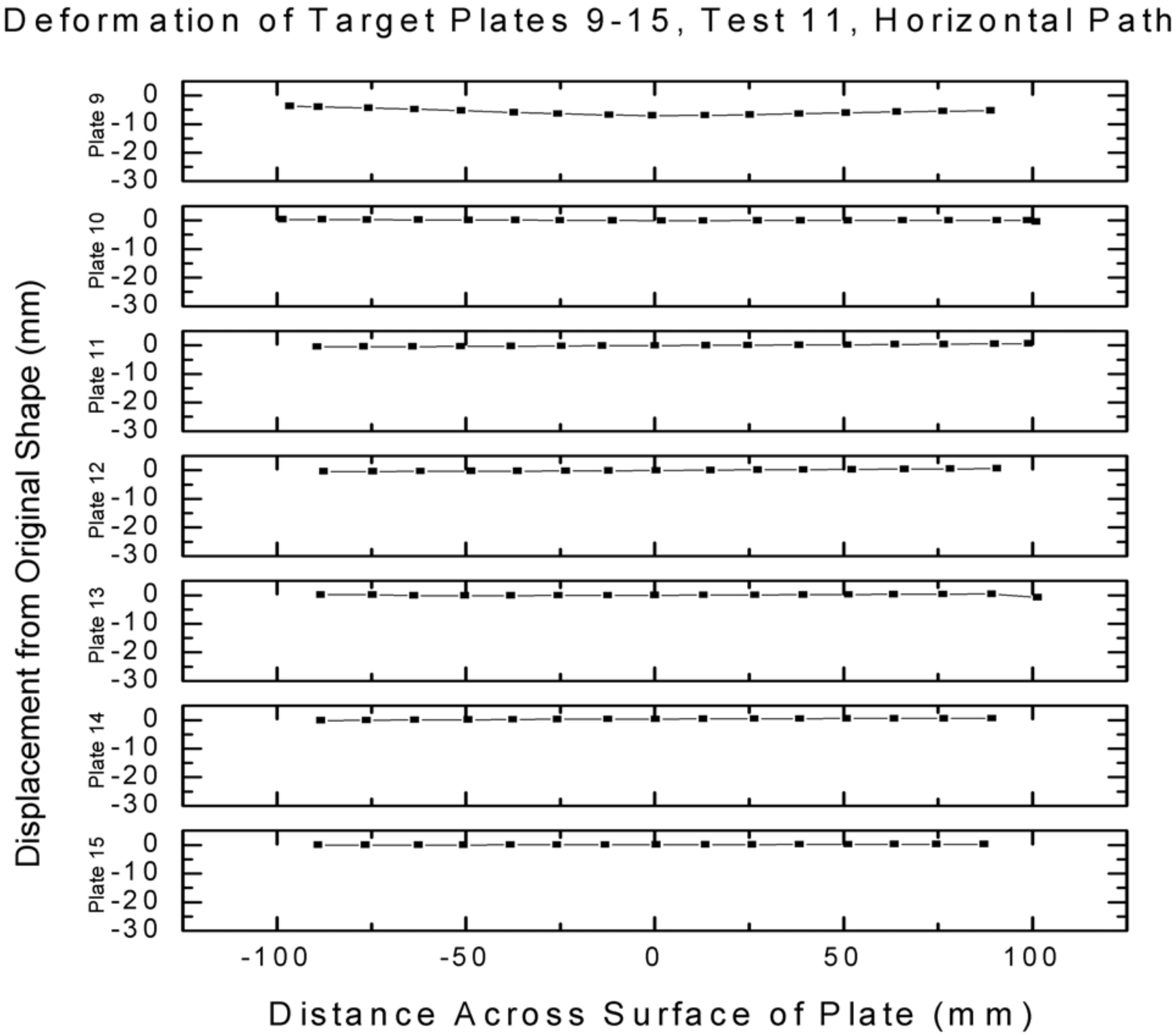

Figure E.42: Test 11 plate deformation data, horizontal path, plates 9 - 15

E.12 Test 12

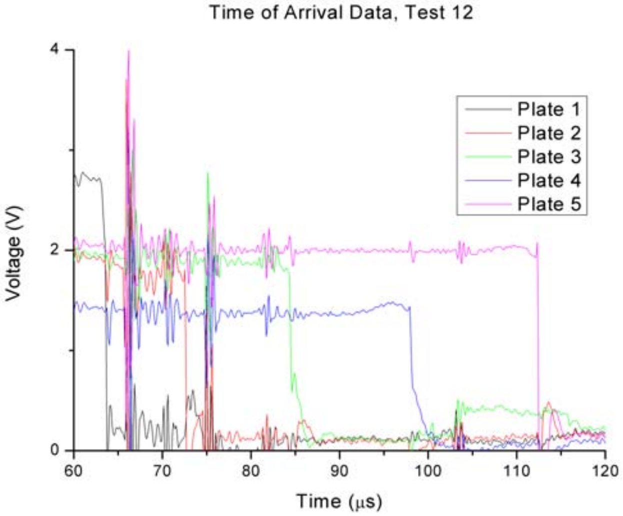

Figure E.43: Test 12 time of arrival data

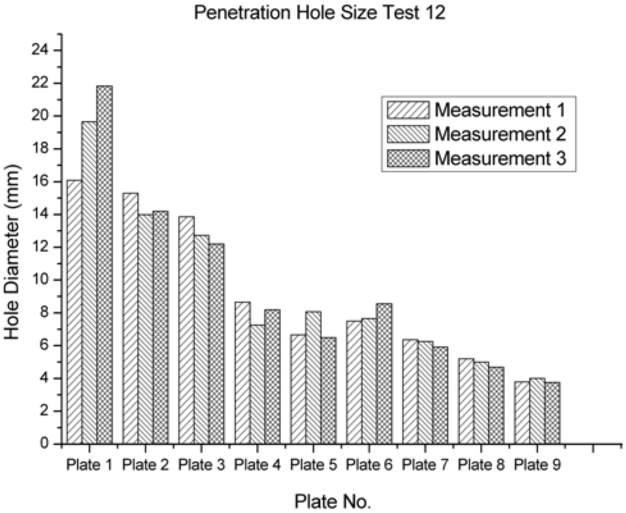

Figure E.44: Test 12 hole size

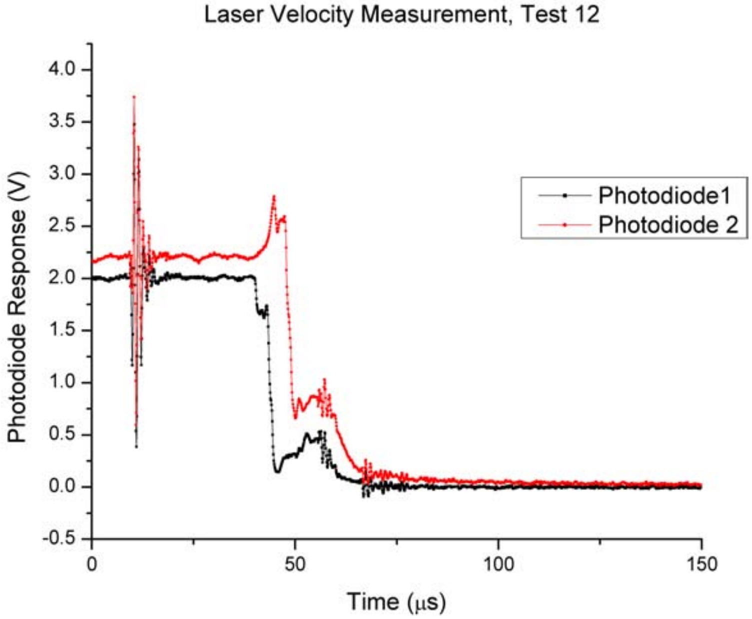

Figure E.45: Test 12 photodiode data for laser velocity measurement

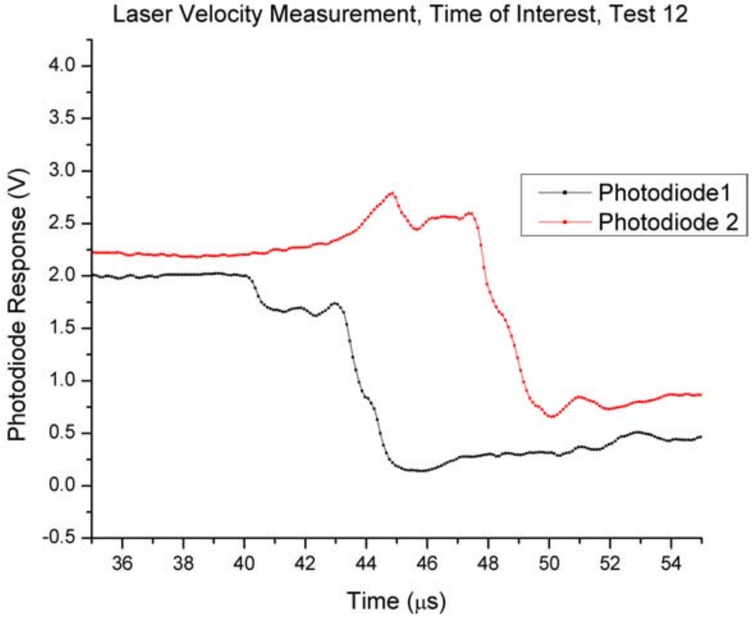

Figure E.46: Test 12 photodiode data for laser velocity measurement (time of interest)

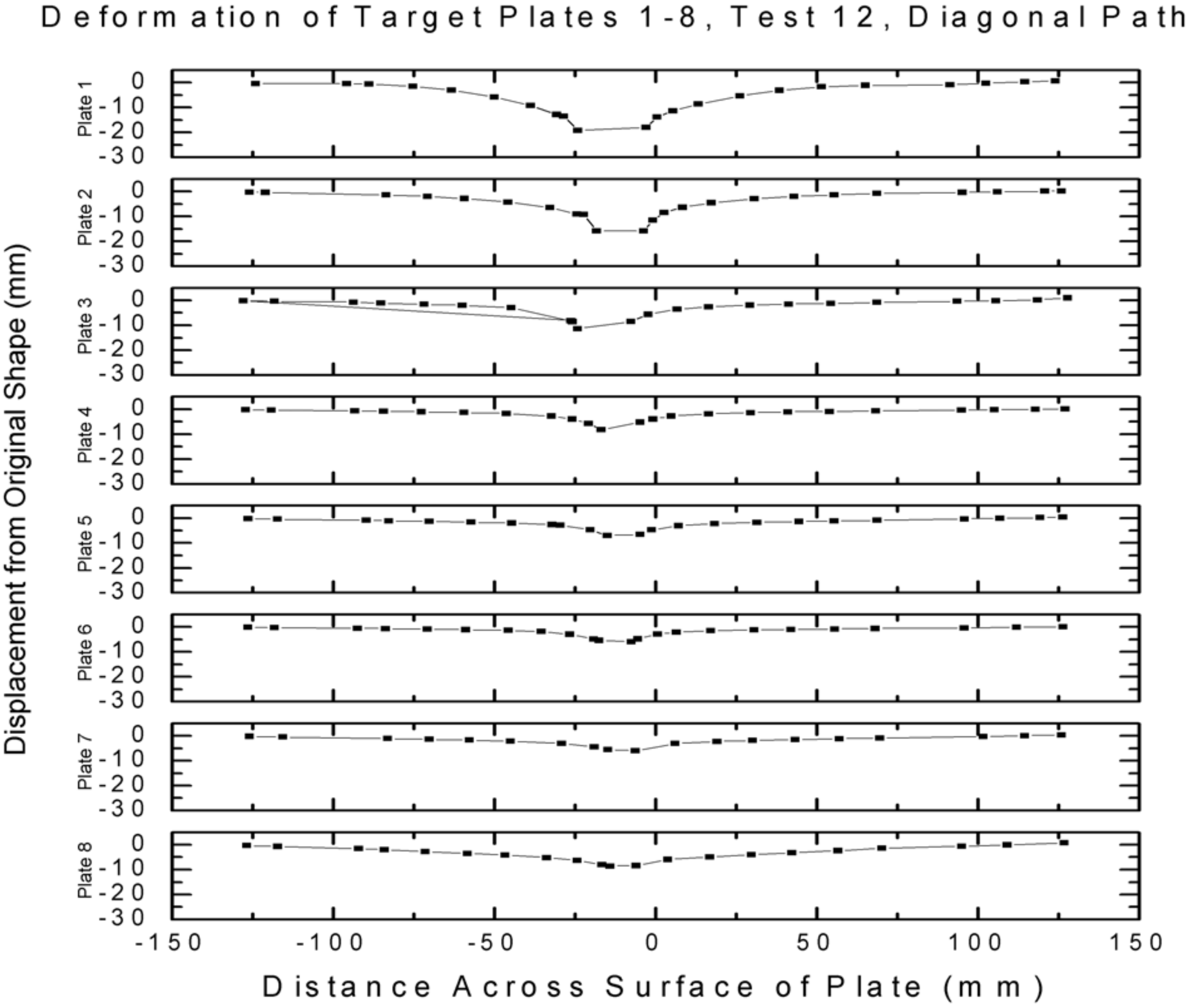

Figure E.47: Test 12 plate deformation data, diagonal path, plates 1 - 8

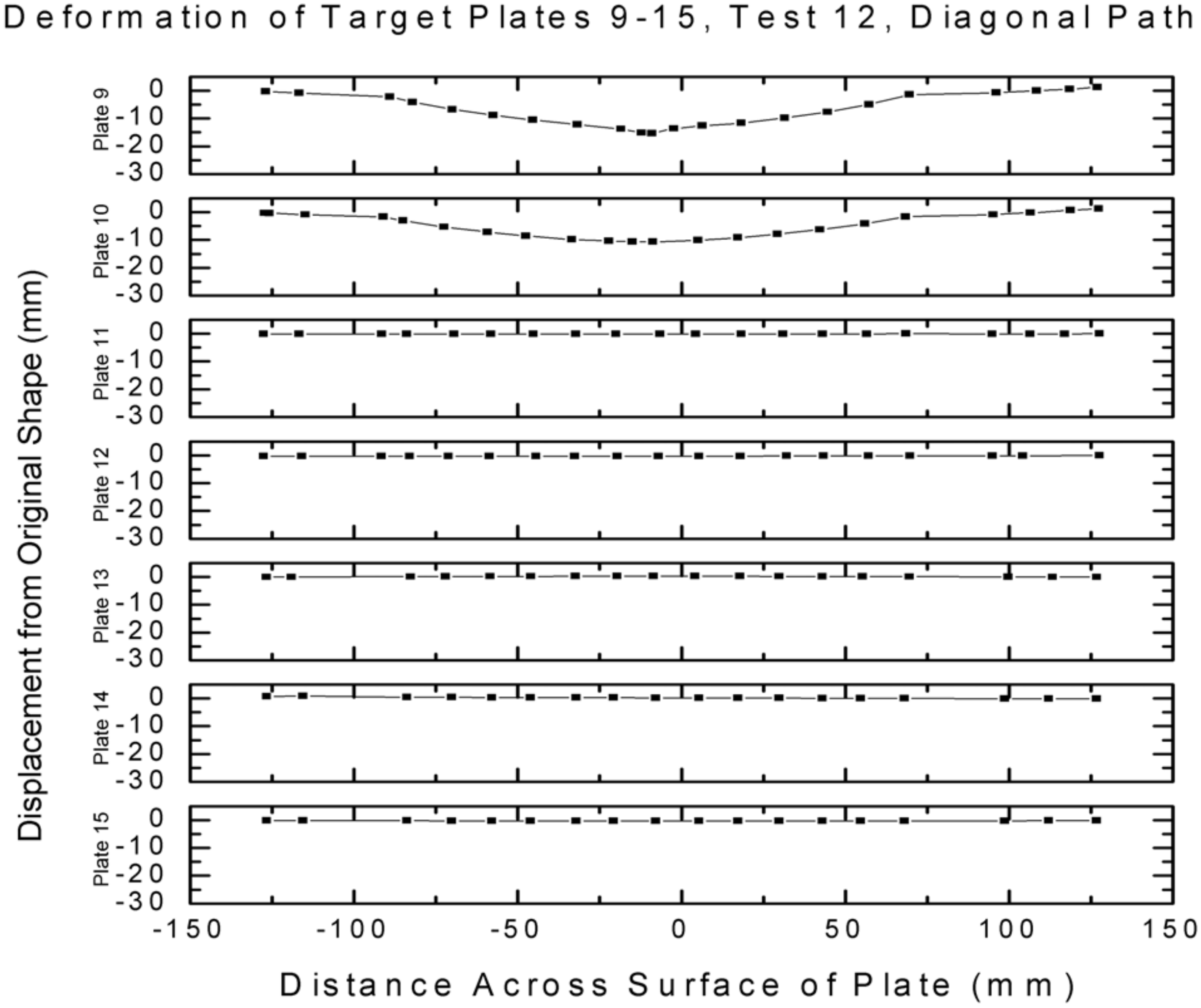

Figure E.48: Test 12 plate deformation data, diagonal path, plates 9 - 15

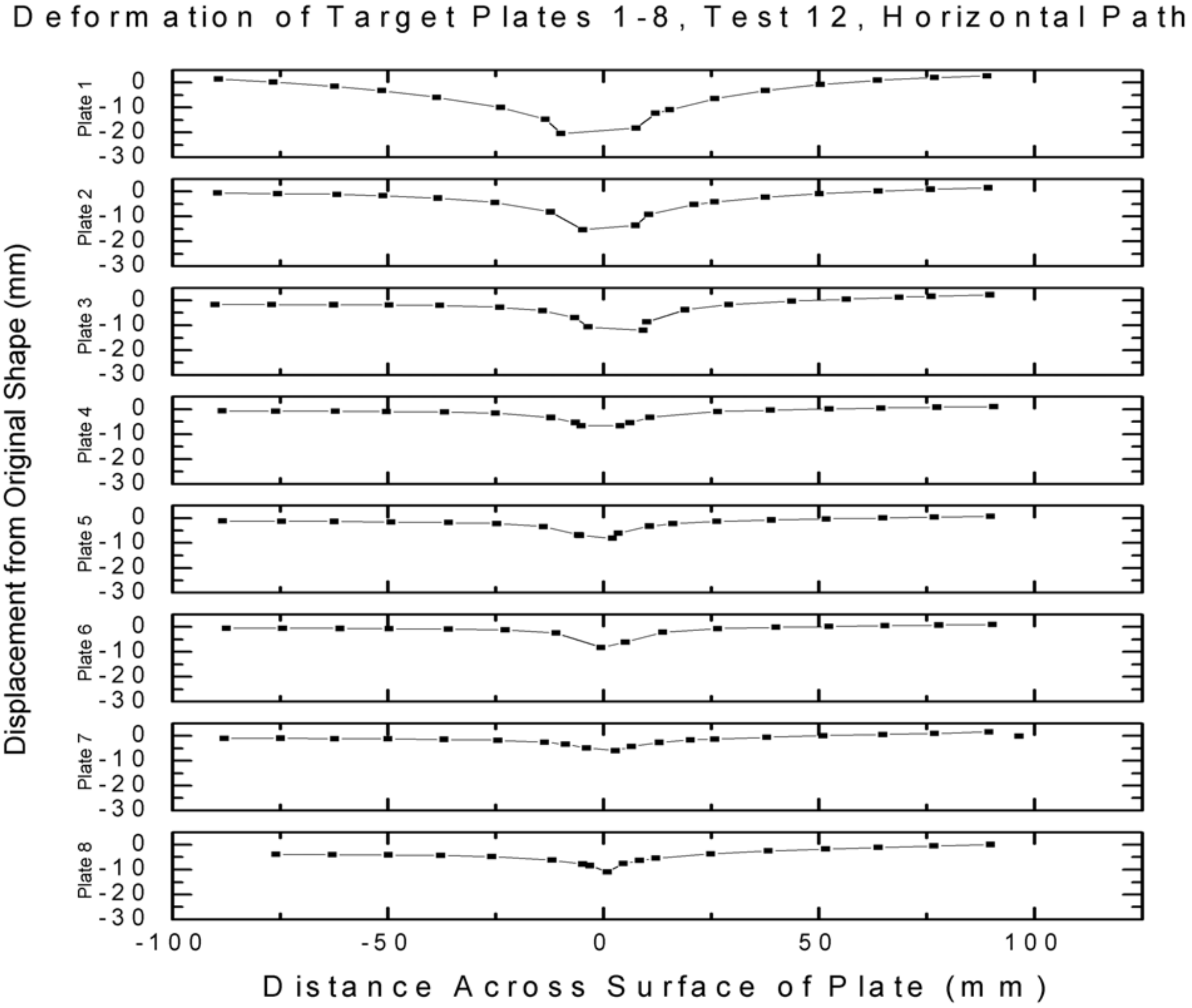

Figure E.49: Test 12 plate deformation data, horizontal path, plates 1 - 8

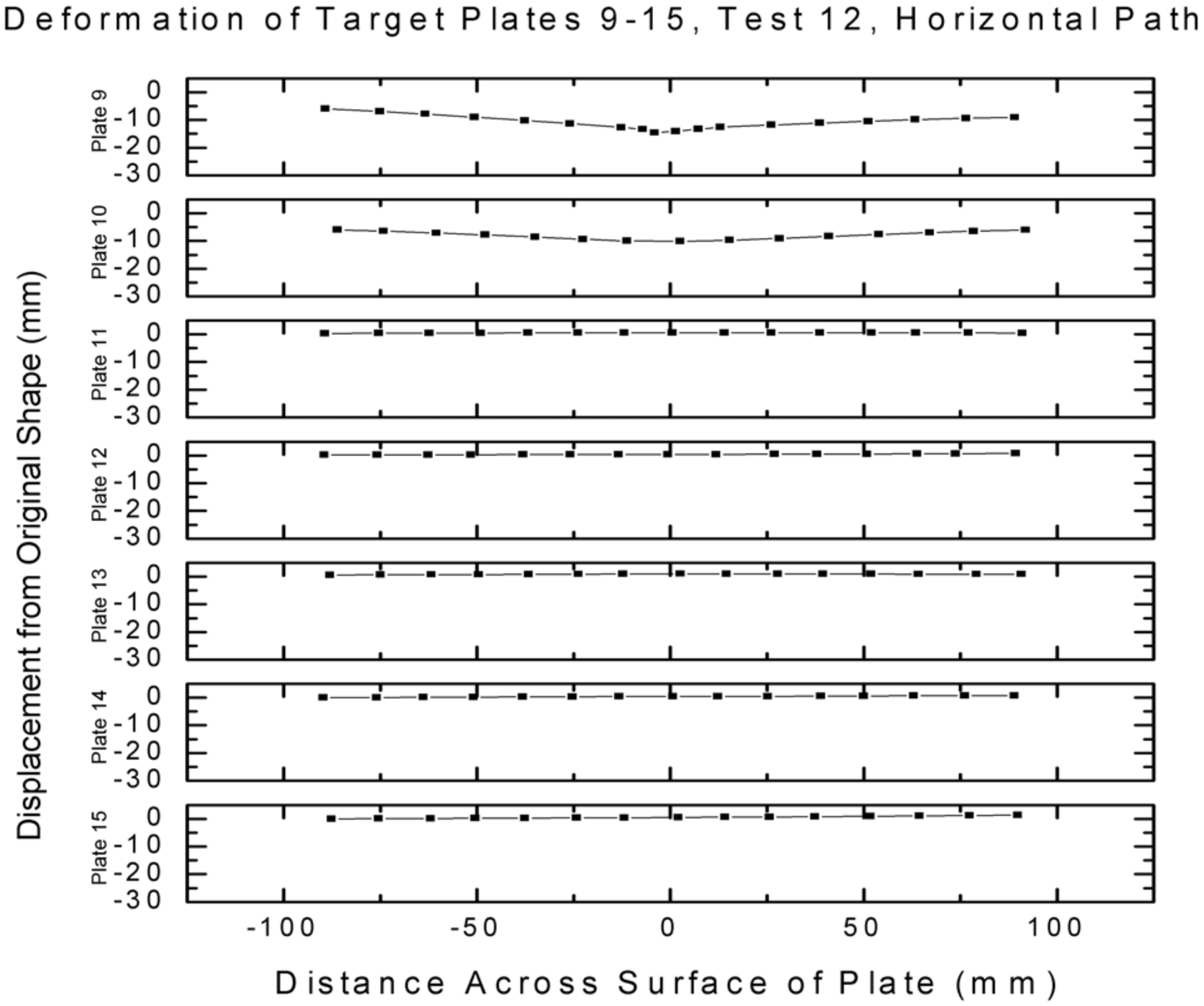

Figure E.50: Test 12 plate deformation data, horizontal path, plates 9 - 15

E.13 Test 13

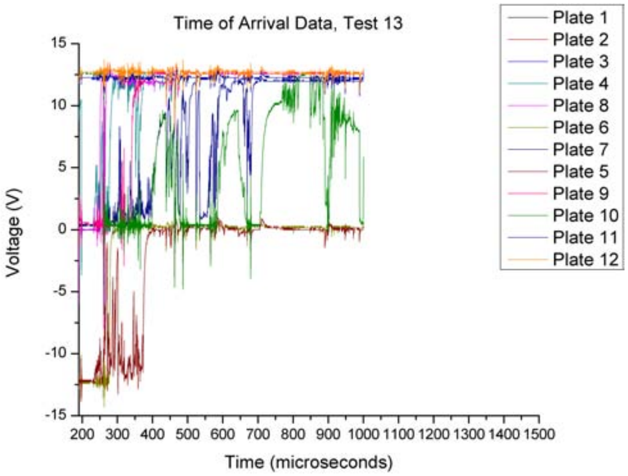

Figure E.51: Test 13 time of arrival data

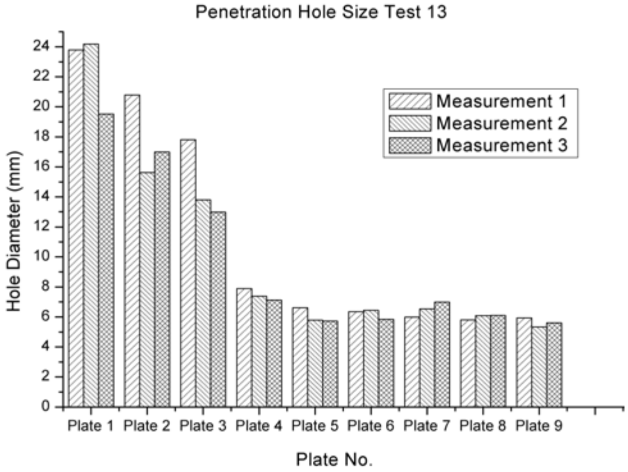

Figure E.52: Test 13 hole size

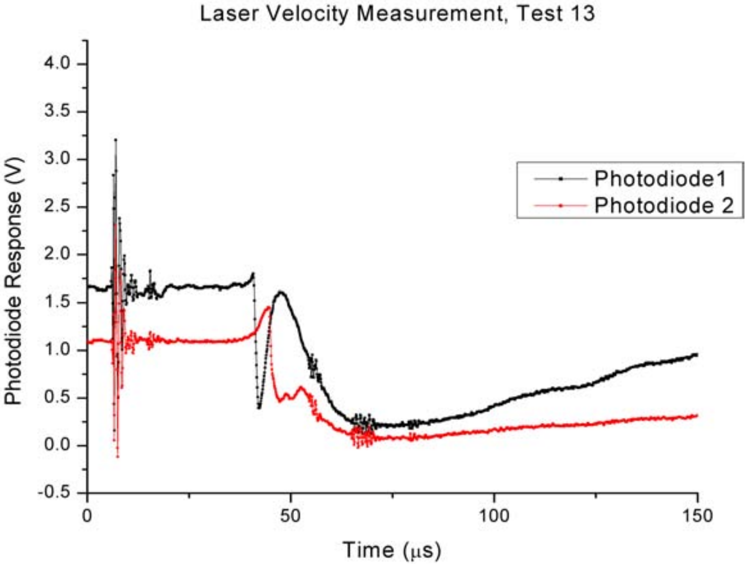

Figure E.53: Test 13 photodiode data for laser velocity measurement

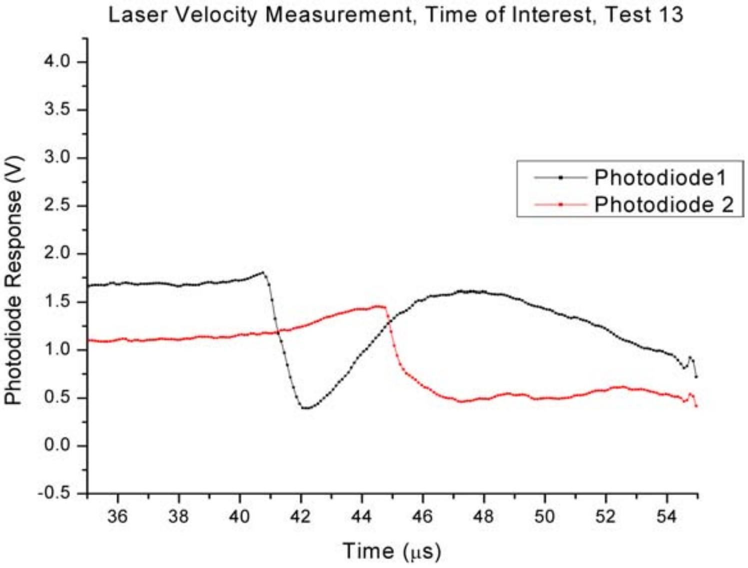

Figure E.54: Test 13 photodiode data for laser velocity measurement (time of interest)

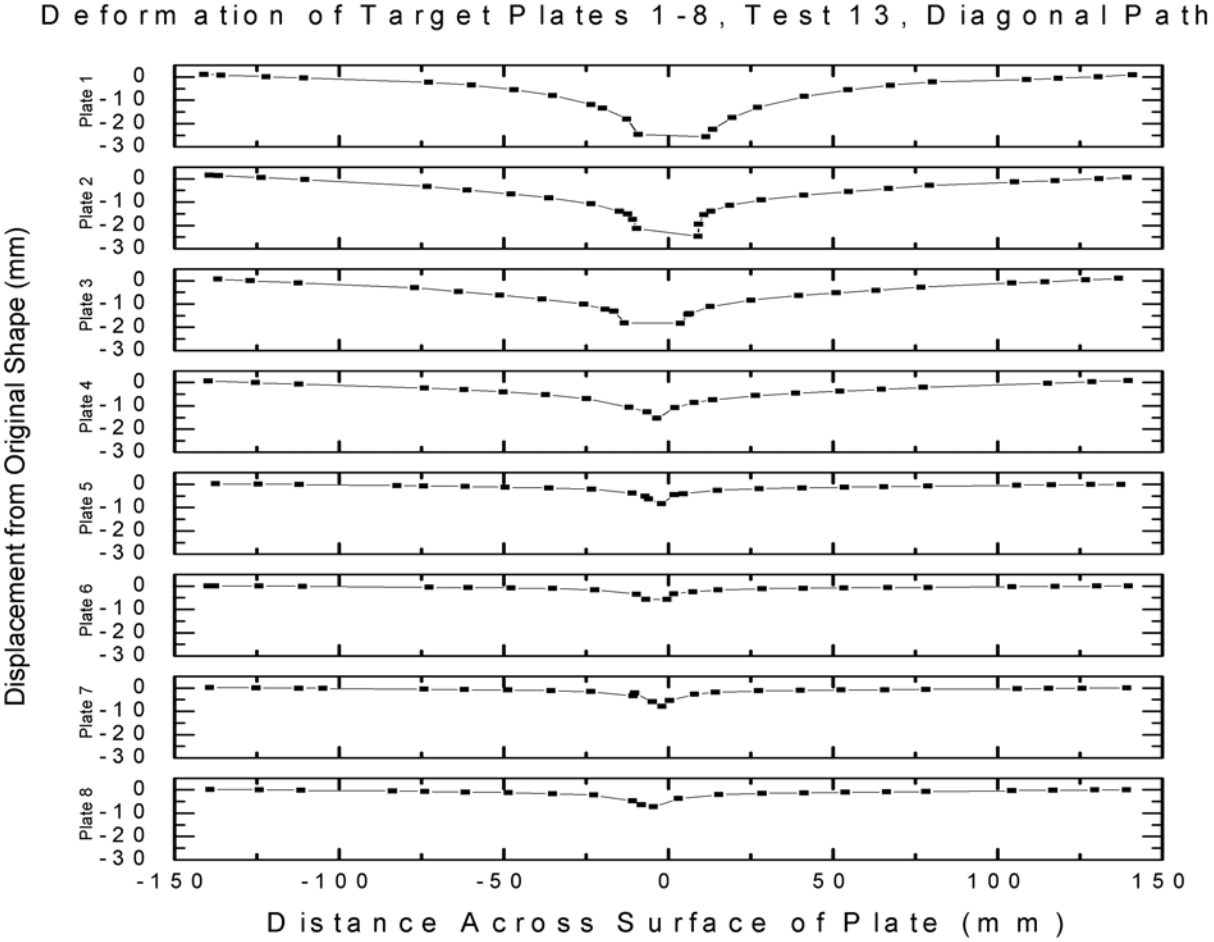

Figure E.55: Test 13 plate deformation data, diagonal path, plates 1 - 8

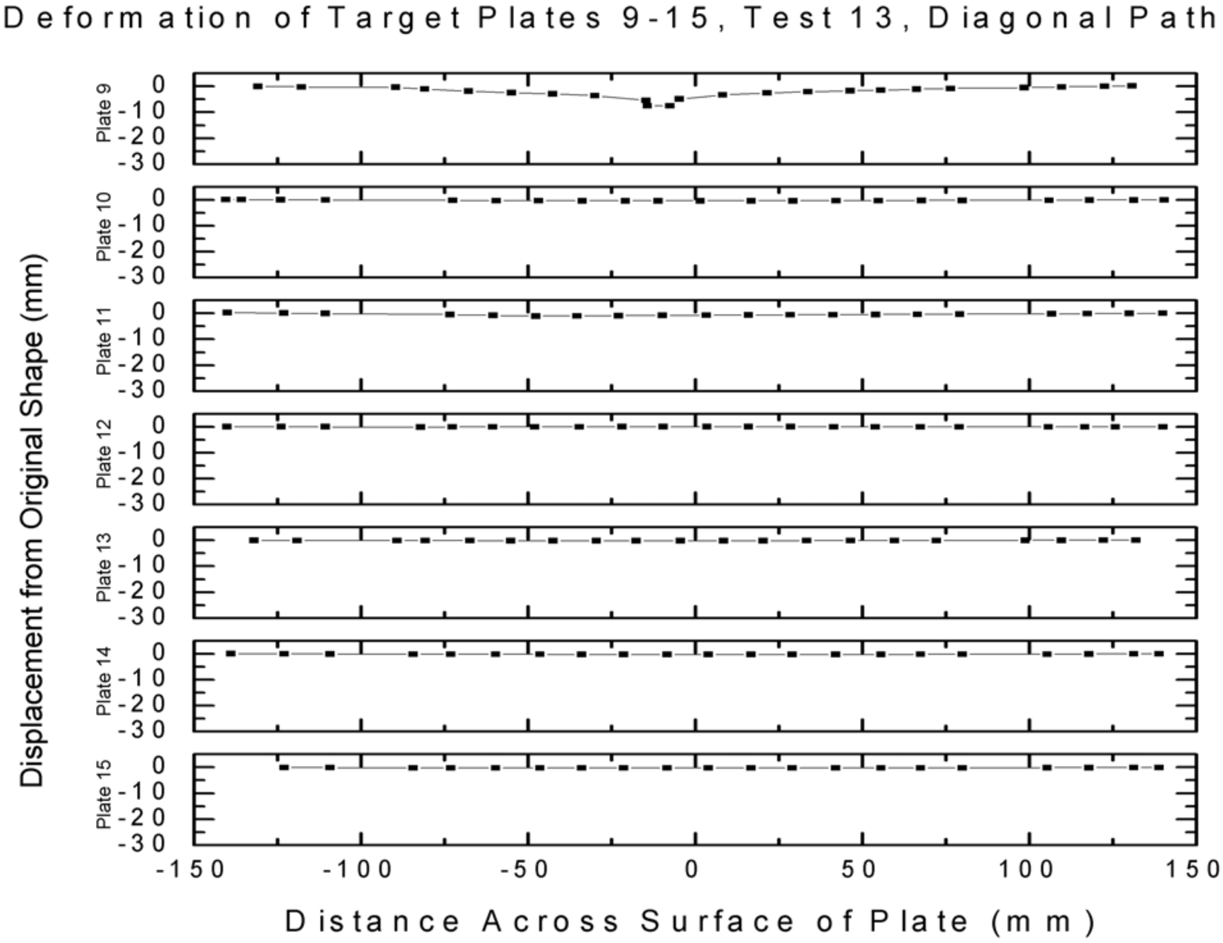

Figure E.56: Test 13 plate deformation data, diagonal path, plates 9 - 15

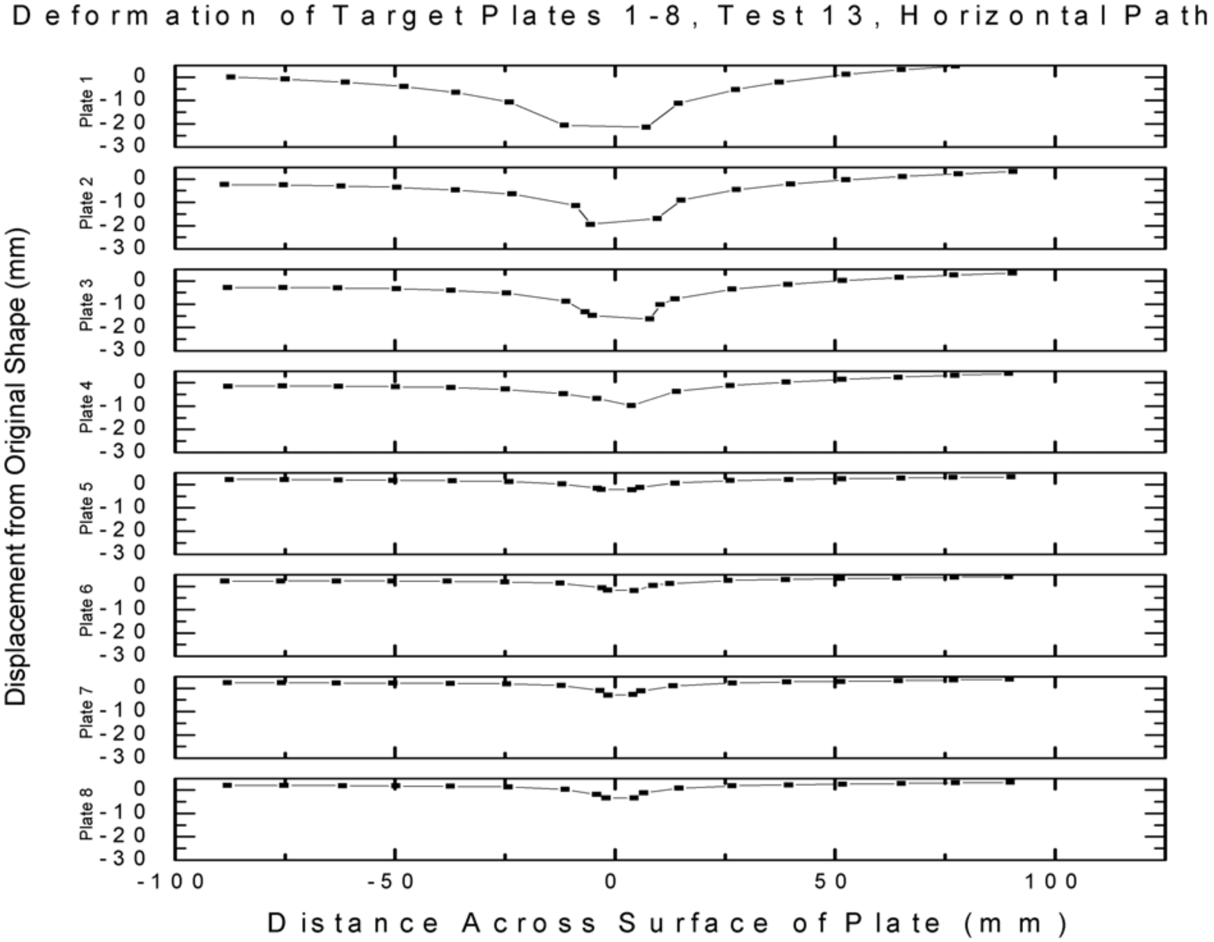

Figure E.57: Test 13 plate deformation data, horizontal path, plates 1 - 8

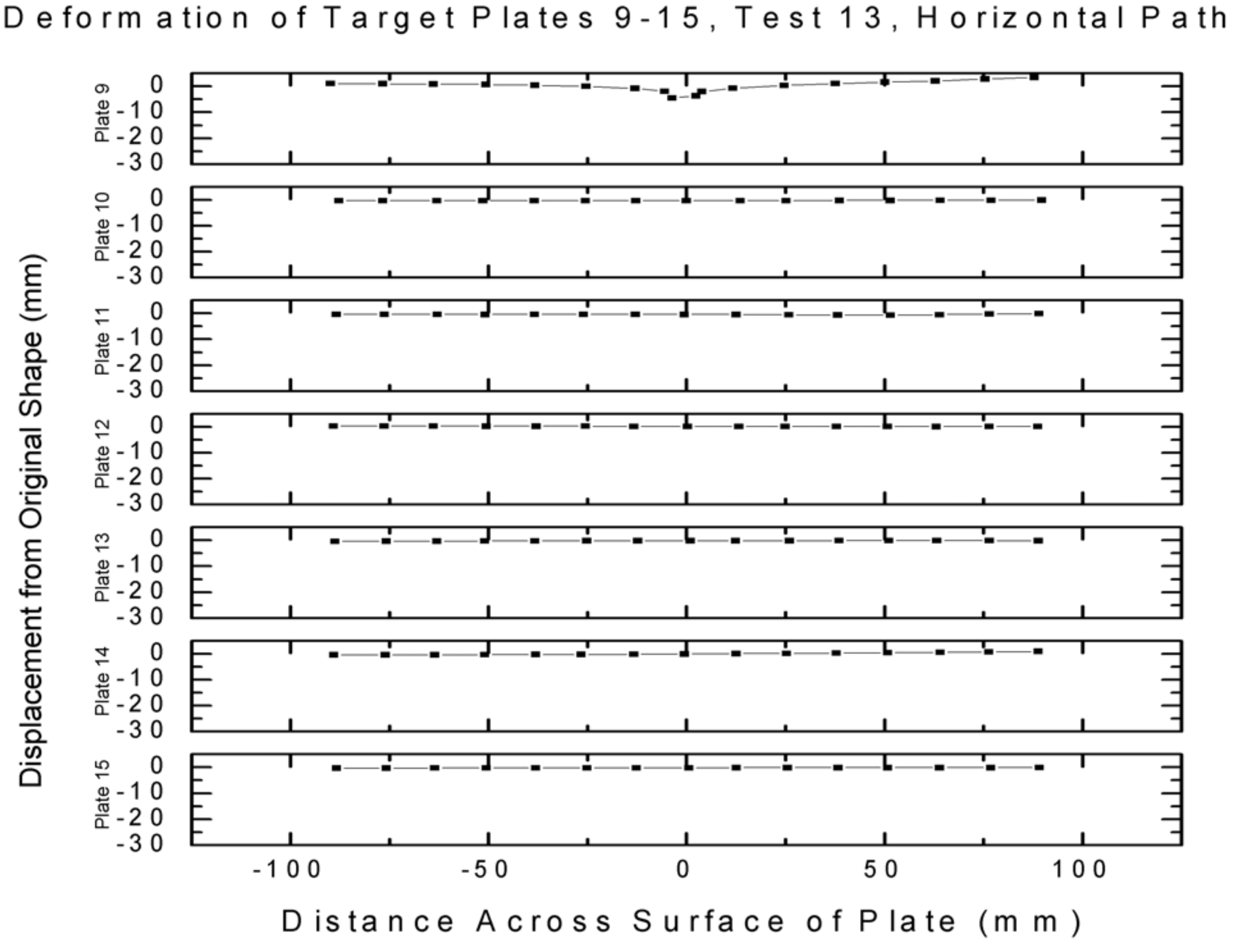

Figure E.58: Test 13 plate deformation data, horizontal path, plates 9 - 15

APPENDIX F

LINER PHOTOS AND DIMENSIONS

Figure F.1: Pictures of solid copper 20.02 mm liner

Table F.1: Thickness of liner at various points (height is the diagonal distance from the base to the point of measurement) - test 11

Liner thickness (in.) - test 11								
	angle of measurement around liner							
	0	45	90	135	180	225	270	315
Base	0.0599	0.06	0.0599	0.0599	0.0597	0.0598	0.0597	0.06
1/2 in high	0.0595	0.0597	0.0596	0.0597	0.0593	0.0587	0.0588	0.0585
1 in high	0.0587	0.0583	0.0589	0.0587	0.0588	0.0587	0.0588	0.0585

Figure F.2: Pictures of Cu/Al insert design liners

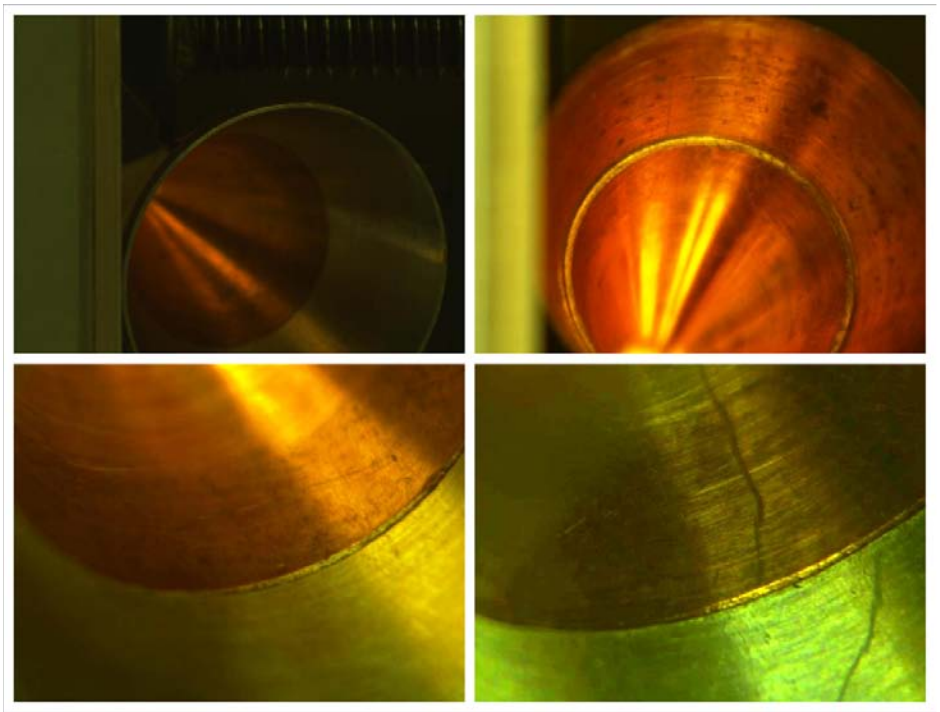

Figure F.3: Close up pictures of fitment between aluminum insert and copper cone

Figure F.4: Pictures of solid copper liner, 50.75 mm diameter, test 10

Figure F.5: Pictures of solid aluminum liner, 50.75 mm diameter, test 11

Table F.2: Thickness of liner at various points (height is the diagonal distance from the base to the point of measurement) - test 12

Liner thickness (in.) - test 12								
	angle of measurement around liner							
	0	45	90	135	180	225	270	315
Base	0.0605	0.0605	0.0605	0.0605	0.0606	0.0607	0.0607	0.0606
1/2 in high	0.0602	0.0602	0.0603	0.0603	0.0605	0.0606	0.0606	0.0603
1 in high	0.0594	0.0593	0.0596	0.0599	0.0599	0.0600	0.0600	0.0597

Figure F.6: Pictures of solid copper liner, 50.75 mm diameter, test 12

Table F.3: Thickness of liner at various points (height is the diagonal distance from the base to the point of measurement) - test 13

Liner thickness (in.) - test 13								
	angle of measurement around liner							
	0	45	90	135	180	225	270	315
Base	0.0609	0.0608	0.0609	0.0614	0.0613	0.0611	0.061	0.0609
1/2 in high	0.0608	0.0609	0.061	0.0611	0.0611	0.0611	0.0609	0.0607
1 in high	0.0603	0.0603	0.0603	0.0605	0.0605	0.0605	0.0603	0.0602

REFERENCES

[1] W. P. Walters and S. K. Golaski, "Hemispherical and conical shaped charge liner collapse and jet formation," Ballistic Research Laboratory, Tech. Rep. ARBRL-TR-2781, 1987.

[2] P. Y. Chanteret and A. Lichtenberger, "Bimetallic liners and coherence of shaped charge jets," in *15th International Symposium on Ballistics*, vol. 2, 1995, pp. 143–148.

[3] A. C. Robinson, "Multilayered liners for shaped charge jets," Sandia National Laboratories, Tech. Rep. SAND85-2300, 1985.

[4] W. P. Walters and J. A. Zukas, *Fundamentals of Shaped Charges.* New York: John Wiley and Sons, 1989.

[5] D. R. Kennedy, "The history of the shaped charge effect, the first 100 years," presented at MBB Schrobenhausen, West Germany, September 20-22, 1983, Tech. Rep. AD-A220 095, 1983.

[6] E. M. Pugh, R. J. Eichelberger, and N. Rostoker, "Theory of jet formation by charges with lined conical cavities," *Journal of Applied Physics*, vol. 23, no. 5, pp. 532–536, 1952, cited By (since 1996): 18.

[7] G. Birkhoff, D. P. Macdougall, E. M. Pugh, and G. I. Taylor, "Explosives with lined cavities," *Journal of Applied Physics*, vol. 19, no. 6, 1948.

[8] R. Engelke, S. A. Sheffield, H. L. Stacy, and J. P. Quintana, "Reduction of detonating liquid nitromethane's chemical reaction-zone length by chemical sensitization," *Physics of Fluids*, vol. 17, no. 9, pp. 1–6, 2005, cited By (since 1996): 3.

[9] L. E. Murr, C. S. Niou, E. P. Garcia, E. T. Ferreyra, J. M. Rivas, and J. C. Sanchez, "Comparison of jetting-related microstructures associated with hypervelocity impact crater formation in copper targets and copper shaped charges," *Materials Science and Engineering A*, vol. 222, no. 2, pp. 118–132, 1997, cited By (since 1996): 18.

[10] W. P. Walters and D. R. Scheffler, "A method to increase the tip velocity of a shaped charge jet using a hollow cavity," vol. 45. Affiliation: U.S. Army Research Laboratory, Weapons and Materials Research Directorate, United States, 2007, pp. 99–108.

[11] P. Y. Chanteret, "Considerations about the analytical modelling of shaped charges," *Propellants, Explosives, Pyrotechnics*, vol. 18, no. 6, pp. 337–344, 1993, cited By (since 1996): 1.

[12] J. Carleone, R. Jameson, and P. C. Chou, "Tip origin of a shaped charge jet." *Propellants Explos*, vol. 2, no. 6, pp. 126–130, 1977, cited By (since 1996): 1.

[13] B. Haugstad, "On the break-up of shaped charge jets," *Propellants, Explosives, Pyrotechnics*, vol. 8, no. 4, pp. 119–120, 1983, cited By (since 1996): 5.

[14] P. Y. Chanteret and A. Lichtenberger, "About varying shaped charge liner thickness," in *17th International Symposium on Ballistics*, vol. 2, 1998, pp. 2–365–2–372.

[15] C. L. Aseltine, "Analytical predictions of the effect of warhead asymmetries on shaped charge jets," Ballistic Research Laboratory, Tech. Rep. ARBRL-TR-002214, 1980.

[16] D. J. Leidel, "A design study of an annular-jet charge for explosive cutting," 1978.

[17] W. M. Evans, "The hollow charge effect," *Bulletin of the Institution of Mining and Metallurgy*, vol. 520, 1950.

[18] D. T. Inc., "Warhead applications of intermetallic reactive materials," Proposal DET-P-99-115, 1999.

[19] D. T. Inc., "Warhead applications of intermetallic reactive materials," Presentation given to Office of Naval Research and NSWC - Indian Head, 2002.

[20] J. E. Felts, "Experimental investigations for initiating reaction of high speed aluminum in gaseous and liquid h2o," 2006.

[21] N. Glumac, H. Krier, T. Bazyn, and R. Ever, "Temperature measurements of aluminum particles burning in carbon dioxide," *Combustion Science and Technology*, vol. 177, no. 3, pp. 485–511, 2005, cited By (since 1996): 21.

[22] R. K. Bill, "Experimental investigation of reactive shaped charge liners for underwater applications," 2007.

[23] B. R. Fant, "Experimental investigation of enhanced aluminum steam explosions for improving reactive underwater shaped charges," 2008.

[24] J. J. Rudolphi, "Experimental investigations of reactive aluminum shaped charge liners alloyed with lithium and gallium," 2009.

[25] J. A. Moore, "Potential effects of asymmetric shock interactions and hydro-reaction during hypervelocity impact," 2006.

[26] W. W. Craig, "Experimental and computational investigations of the effects of hydro-reaction during hypervelocity impact," 2007.

[27] P. H. Belnap, "Experimental and computational investigations of the hypervelocity impact of hydro-reactive shaped charge jets," 2007.

[28] H. Kolsky, C. I. Snow, and A. C. Shearman, "A study of the mechanism of munroe charges part i - charges with conical liners," *Research Supplement*, vol. 2, no. 2, pp. 89–95, 1949.

[29] J. D. Walker and S. R. Institute, "Incoherence of shaped charge jets," in *American Institute of Physics Conference Proceedings*, vol. n 309, 1994, pp. 1869–1872.

[30] T. J. Schilling, "Reactive-injecting follow-through shaped charges from sequent-material conical liners," *Propellants Explos Pyrotech*, vol. 32, no. 4, pp. 307–313, 2007.

[31] J. P. Curtis and R. Cornish, "Formation model for shaped charge liners comprising multiple layers of different materials," *Proc. 18th Int. Symp. Ballistics*, vol. 1, pp. 458–465, November 1999 1999.

[32] W. Walters, 2009.

[33] A. C. on Finishing of Copper and C. Alloys, *Section IX: Cleaning and Finishing*, 8th ed., ser. Metals Handbook, Vol. 2. Ohio: American Society of Metals, 1964, pp. 170–171.

[34] I. Manna and J. D. Majumdar, "Enhanced kinetics of diffusion coating of aluminium on copper by boundary diffusion," *J Mater Sci Lett*, vol. 12, no. 12, pp. 920–922, 1993, cited By (since 1996): 3.

[35] B. S. Kang, B. M. Son, and J. Kim, "A comparative study of stamping and hydroforming processes for an automobile fuel tank using fem," *International Journal of Machine Tools and Manufacture*, vol. 44, no. 1, pp. 87–94, 2004, cited By (since 1996): 9.

[36] M. Dussing, T. Piraino, D. Rennecker, and J. Sunich, "Team 3: Design and construct a test facility to study hot hypersonic metal jets penetrating into water," Unpublished, Tech. Rep., 2005.

[37] W. E. Baker, P. S. Westine, F. T., and Dodge, *Similarity Methods in Engineering Dynamics*. Rochelle Park, NJ: Spartan Books, Hayden Book Company, 1973.

[38] R. DiPersio, W. H. Jones, A. B. Merendino, and J. Simon, "Characteristics of jets from small caliber shaped charges with copper and aluminum liners," Ballistic Research Laboratory Memorandum Report, Tech. Rep. BRL-MR-1866, 1967.

[39] S. Gorosin, D. L. Frost, J. Levine, A. Yoshinaka, and F. Zhang, "Optical pyrometry of fireballs of metalized explosives," *Propellants, Explosives, Pyrotechnics*, vol. 31, no. 3, pp. 169–181, 2006.